Proteomic Analysis and Long Term Live Cell Imaging of Primary Human Cells in Culture

by

Erica J. Murray

A thesis
presented to the University of Waterloo
in fulfillment of the
thesis requirement for the degree of
Doctor of Philosophy
in
Chemical Engineering

Waterloo, Ontario, Canada, 2011

Author's Declaration

I hereby declare that I am the sole author of this thesis. This is a true copy of the thesis, including any required final revisions, as accepted by my examiners.

I understand that my thesis may be made electronically available to the public.

Abstract

Regenerative medicine is a rapidly developing field, merging engineering and biological life sciences to create biological replacements for damaged tissue and organ function. Development of cellular based therapies has the potential of curing present untreatable diseases and conditions, such as diabetes. The identification of protein expression patterns, that guide undifferentiated cells to different lineages, can provide important information about the progression of cellular differentiation at various stages.

This research project utilizes proteomics and *in vitro* live-cell microscopy to investigate two distinct cellular systems: (1) the signaling pathways of calmodulin (CaM) in the differentiation of a human glioblastoma cell line; and (2) the effect of islet neogenesis associated protein (INGAP) on human islet-derived progenitor cells (hIPCs). Using a proteomic readout with a long term live-cell imagining approach, **it was hypothesized that highly specific binding proteins of a CaM-mutant, and proteins in hIPCs perturbed by INGAP, could be identified and studied *in vitro*, characterizing specific signaling pathways which control the function of CaM in brain tumour cells and the mechanism(s) of INGAP in islet-derived progenitor cells.**

This thesis presents the utility of a proteomics and an *in vitro* cell microscopy approach to investigate therapeutic proteins, such as INGAP, on cell culture systems. The results have established the limitations and the utility of DIGE, differential binding of a CaM-mutant versus calcium-CaM, and the cell specific uptake feasibility of using the TAT-binding domain. In the hIPC system, proteomic, phenotypic, motility, proliferation and nuclear effects of INGAP were determined. Specifically, hIPCs exposed to INGAP had 50% decrease in average nuclear speed, the translocation of two identified proteins caldesmon and tropomyosin and INGAP was found to bind specifically to hIPCs. However, hIPCs had no changes in insulin specific hormone expression.

Acknowledgements

I would like to acknowledge, above all, my supervisor Professor Eric Jervis and my co-supervisor Professor Guillemette, for their belief in my scientific abilities, continuous guidance, patience and support. I am grateful to have been mentored by such understanding and committed individuals.

I would like to also acknowledge my colleagues without whom this research would not have been possible. Thank you Julien Verneau for your help with imaging, the introduction to law as a career and for being such a great colleague. Thank you Bredon Crawford for your passion for statistical analysis, Sasha Avreline for your technological support and Ilia Droujinine for all your hard work. Your comic relief, motivation and most of all your friendships throughout this journey will always be appreciated.

This work would not have been possible without the work of my predecessors, Duane Moogk, Darik Gamble, April Blaylock, Andrea Dupont and Geneviève Labbé. Thank you for all your hours of hard work spent designing, implementing and troubleshooting the equipment I would later use to complete my degree.

I would like to thank the members of my examination committee from the University of Waterloo – Professor Christine Moresoli for always being available, Professor Marc Aucoin for the use of his RNA free lab, Professor Brendan McConkey for the use of the Typhoon and for his insightful discussions of my proteomic data. Lastly, thank you Professor Heather Sheardown from McMaster University for her time and travels serving as the external committee member.

Dedication

To my loving husband Jeff. Thank you for supporting and encouraging me through to the end. I would have not been able to complete this degree without you. I love you.

To my son Tyler. You were the greatest gift of my PhD. You gave me the motivation to complete this degree. I wish for you a life of happiness complete with a prosperous education and career. I promise to do everything I can to make all of your dreams come true. Mommy loves you.

To all of my family in Newfoundland. Thank you for instilling in me the passion to strive, the ambition to chase and the dedication to graduate. I love and miss you all very much.

To Beckie Sauder. Without you I never would have been able to stay in Waterloo for nine years. Thank you for being such an amazing woman and friend.

Table of Contents

List of Figures

List of Tables

List of Abbreviations

2D DIGE	2D differential in gel electrophoresis
2D PAGE	two-dimensional polyacryladmide gel electrophoresis
ABPs	actin binding proteins
apo-CaM	apo-calmodulin
APTS	aminopropyl trimethoxy silane
BPs	binding proteins
CaM	calmodulin
CaMBPs	CaM binding proteins
CK-19	cytokeratin-19
CsA	cyclosporine A
DIC	differential interference contrast
DTT	dithiothriotol
EGF	epidermal growth factor
EMT	epithelial-mesenchymal transition
FACS	fluorescence-activated cell sorting analysis
FDR	false discovery rate
GAGs	glycosaminoglycans
GLP-1	glucagon-like peptide-1
GLU	glucagon
GVHD	graft-versus-host disease
HAECs	human aortic endothelial cells

hfNSCs	human fetal neural stem cells
hIPCs	human islet-derived progenitor cells
HIV-1	human immunodeficiency virus 1
HIV	human immunodeficiency virus
HSP 90	heat shock protein 90
HUVECs	human umbilical vein endothelial cells
INS	insulin
INGAP	islet neogenesis associated protein
INGAP-PP	islet neogenesis associated protein pentadecapeptide
IPCs	islet-derived progenitor cells
IPG	immobilized 24-cm linear pH 3-10 gradient
MALDI	matrix assisted laser desorption/ionization
mES	mouse embryonic stem
MS	mass spectroscopy
MSCs	mesenchymal stem cells
NHS	N-hydroxysuccinimide
pMSCs	pancreatic mesenchymal
PPY	pancreatic polypeptide genes
qRT-PCR	quantitative reverse transcriptase polymerase chain reaction
rINGAP	recombinant INGAP
RT	reverse-transcribed
SEM	standard error of the mean

TAT	transactivator of transcription

Chapter 1 Introduction

Since the publication of the complete human genome in 2001, analyzing the expression of many genes has become a focus of drug screening and development. The publication was molecularly historic and it has provided scientists with vast amounts of data at the genomic level. However, genes are simply blueprints for the construction of proteins, whereas protein interactions determine cellular functions. Therefore, understanding the 'gene products' and their associated proteomes is essential to reveal critical signaling pathways involved in cellular responses.

Currently, the evaluation of protein expression levels and the identification of the proteins are most commonly determined using two-dimensional gel electrophoresis coupled with mass spectroscopy (MS). With this approach, proteins are separated in the first dimension by their isoelectric point, followed in the second dimension by their mass. Each protein localizes specifically, creating a spot pattern for each protein separated. Proteins of interest can then be selected for MS analysis, with proteins identified based on their peptide fragments and cross-referencing with the proteome database. However, the nature of these techniques requires collecting destructive results at various time points, followed by extrapolation to translate and infer the non-observed cellular activities. Often such interpretations assume a linear order of events between the experimented time points, however certainly more complex interrelations are occurring. As a result, the benefits to be obtained from real-time dynamic studies of cells in culture are becoming increasingly more evident.

Live-cell imaging and cell tracking techniques enable the direct observation of cells in real-time on the single cell level. The technology provides opportunity for detailed analysis of the fundamentals of cell biology, such as: division, apoptosis, migration, and phenotype classification. Adaptability, sensitivity, resolution and non-invasiveness are but a few of the advantages of *in vitro* live-cell imaging and tracking. Proteomics is vital to understanding the molecular basis of cell signaling, and live-cell imaging enables real-time observation on the single cell level. Therefore, proteomics coupled with live-cell imaging was employed to study two cellular systems:

1) Calmodulin (CaM) in the differentiation of a human glioblastoma cell line
2) Human islet-derived progenitor cells (hIPCs) treated with islet neogenesis associated protein (INGAP)

1.1 Calmodulin (CaM) in the differentiation of a human glioblastoma cell line

The first cellular system is focused around the protein calmodulin (CaM) and its associated bindome; the bindome includes all binding proteins of CaM. CaM is the primary receptor of calcium, playing an essential role in calcium signaling. CaM is the fifth most highly conserved protein in eukaryotes and is responsible for regulating numerous intracellular processes, such as: cell motility, growth, proliferation, and apoptosis (Yokouchi, Numaguchi et al. 2006; Bennett, Mauer et al. 2007; Colomer and Means 2007). As it is a primary receptor for calcium and an allosteric activator of several protein kinases, the Ca^{2+}/CaM dependent signaling cascades are essential to many intracellular processes, including but not limited to: the immune system, the inflammatory response, the activation of T lymphocytes and hematopoietic stem cell maintenance (Braun and Schulman 1995). Although CaM

dependent signaling cascades are still not yet fully understood, it is clear that the mis-regulation of CaM signaling can lead to many diseases (Colomer and Means 2007), emphasizing the importance of developing methods to mediate and study CaM signaling in the cell.

Studying CaM-dependent signaling cascades using proteomics coupled with long term live-cell imaging is a means to dissect CaMs cellular functions. CaM regulates protein binding activity based on intracellular levels of calcium, in its calcium bound and calcium free states. Protein interactions were characterized using calcium-CaM and a CaM-mutant which had mutated calcium binding sites rendering the protein unable to bind calcium. Identifying the binding proteins of CaM was first achieved by probing the bindome of calcium-CaM in comparison to that of the CaM-mutant using affinity chromatography and 2D differential in gel electrophoresis (2D DIGE). By comparing the binding proteins of the calcium free form to the calcium bound form of CaM, **it was hypothesized that a subset of proteins would be identified which bind specifically to the mutant.** Once the specific binding proteins of the CaMs were identified, *in vitro* characterization of the protein interactions using fluorescent microscopy during brain tumour cell differentiation was proposed. Using these methods, **it was hypothesized that the CaM-mutant would selectively control (up regulate or down regulate) critical signaling pathways involved in cell differentiation.** To test this hypothesis, the following were the proposed objectives and milestones of the experimental plan:

1.1.1 Objective 1: Proteomic analysis of calcium-CaM vs. CaM-mutant binding proteins

Milestone 1. Affinity Chromatography

Optimal affinity chromatography conditions were first determined. Once determined, several affinity runs were completed by passing porcine brain extract through calcium-CaM and CaM-mutant columns. The columns were first eluted with EDTA (calcium chelator), followed by NaOH (strong base). The isolation of a sufficient quantity of the binding proteins specifically bound to either calcium-CaM or the CaM-mutant in a calcium independent manner (NaOH elution fraction) was the central aim of this milestone.

Milestone 2. Proteomic Analysis

Once isolated, a proteomic analysis was completed using DIGE to compare the two bound protein populations. Prior to performing DIGE, optimal separation conditions were determined using two-dimensional polyacryladmide gel electrophoresis (2D PAGE) and silver staining. Subsequent to the protein populations being optimally separated, a design of experiments for DIGE was completed considering biological and technical replication to achieve acceptable statistical significance between affinity chromatography runs.

1.1.2 Objective 2: *In vitro* characterization of CaM delivery into cells

Milestone 3. TAT-CaM Uptake into a Human Glioblastoma Cell Line

Once the specific CaM-mutant binding proteins had been identified *in vitro*, the second aim of the project was the delivery of CaM into brain tumour cells. The CaM-mutant and calcium-CaM proteins were fluorescently labeled using different fluorophores and introduced into cells using a cell penetrating peptide: HIV-derived TAT. Achieving TAT uptake into various cell types was required prior to performing TAT-CaM uptake experiments. It was anticipated that the method of TAT uptake would not be straightforward. Therefore, this milestone was understood to require optimization of culture conditions and trials using several primary cell types. The final aim of this milestone was the successful delivery of TAT-CaM and the effective release of CaM into the cytoplasm.

Milestone 4. Live-Cell Imaging and the Characterization of CaM Uptake

Once TAT-CaM uptake had been confirmed, the aim of this milestone was to perform live-cell imaging and cell tracking of cells treated with the fluorescently labeled CaMs. Fluorescently labeled TAT-CaM was delivered to the cytoplasm of human glioblastoma cells. Time course imaging would allow observation of cell phenotype (differentiation state) and the relative distributions of the two labeled forms of CaM.

1.2 Effects of islet neogenesis associated protein (INGAP) on human islet-derived progenitor cells (hIPCs)

It is well known that long term *in vitro* culture of islets of Langerhans results in a population of proliferative fibroblast-like islet hormone-negative cells (Schmied, Ulrich et al. 2001), which have been termed islet-derived progenitor cells (IPCs). The second cellular system is focused around the protein INGAP and studying its proteomic and phenotypic effects on human islet-derived progenitor cells (hIPCs). INGAP is a protein believed to initiate duct cell proliferation and islet neogenesis (Rafaeloff, Pittenger et al. 1997). The mechanism of INGAP action, including cellular specificity and receptor, and the therapeutic potential of hIPCs are unknown. **It was hypothesized that a clinically relevant understanding of INGAPs mechanistic and phenotypic effects will be determined by studying hIPCs treated with INGAP using 2D DIGE and long term live-cell imaging.**

To test this overall hypothesis, the following objectives and milestones for the experimental plan were identified:

1.2.1 Objective 1: Proteomic analysis of hIPCs treated with rINGAP

Milestone 1. Long Term Live-Cell Imaging and rINGAP Treatment of hIPCs

Obtaining islets, followed by culturing them into hIPCs while imaging the proliferation and rINGAP treatment, were the primary aims of this milestone. Established live-cell imaging techniques were used to study isolated human islets proliferating from islets into hIPCs, followed by rINGAP treatment. The imaging

allowed for the comparison of rINGAP-treated cells to untreated cells, the classification of the observed phenotype(s), analysis of the cell cycle times, and analysis of hIPC migration rates.

Milestone 2. Proteomic Analysis-DIGE

Separating and identifying proteins influenced by rINGAP at the various treatment times was the aim of this milestone. Following the rINGAP treatments (or non-treatment controls) cells were lysed and both protein populations were separated and compared using 2D DIGE. Once the protein populations were separated using 2D PAGE and silver staining, a design of experiments for DIGE was completed considering biological and technical replication to achieve acceptable statistical significance. With the correct design of experiments, proteomic effects of rINGAP on the hIPCs were determined.

1.2.2 Objective 2: Endpoint *in vitro* characterization of INGAP's effect on hIPCs

Milestone 3. Protein Validation and Aggregate Formation using rINGAP

The primary aims of this milestone were to identify and validate the proteins determined through DIGE and mass spectrometry (MS). Based on the MS results, two proteins of most interest (proteins identified at multiple treatment times) were validated using immunofluorescence staining. The DIGE results represented the average protein expression of all the cells. Endpoint immunofluorescent staining for the specific proteins of interest was used to validate protein expression and the protein distributions on an individual cell basis. These methods were semi-

quantitative, therefore, quantitative real-time PCR, were employed to further validate the rINGAP effect. Lastly, it was determined that aggregation of the hIPCs treated with rINGAP had additional cellular organization effects.

Milestone 4. INGAP-PP effects on hIPCs

The primary aim of this milestone was to evaluate the effects of the peptide form of INGAP on hIPCs. To understand the specificity of binding of INGAP on hIPCs, the cells were treated with fluorescently labeled islet neogenesis associated protein pentadecapeptide (INGAP-PP) and fluorescent scrambled-INGAP-PP. hIPCs were analyzed for phenotypic effects and significant nuclear effects were observed. Therefore, flow cytometry was utilized to analyze INGAP-PPs effect on cell cycle.

1.3 Justification and Overall Hypothesis

The overall goal of this research was to utilize proteomics and long term live-cell imaging to develop clinically relevant understandings of CaMs bindome and its effects on signaling in differentiation and INGAPs mechanistic and phenotypic effects on hIPCs. CaM dependent signaling cascades are still not fully understood and it is clear that their mis-regulation can lead to many diseases. Furthermore, although there are many issues surrounding the implementation of standard medical practices for the transplantation of organs and tissues, one of the primary challenges related to islet transplantation is islet supply. An available source of insulin-secreting cells is required to improve the quality of life of diabetes patients. hIPCs may offer a scalable supply of human derived cells which given the correct stimuli can be differentiated into insulin producing cells for diabetes transplantation. Therefore,

investigating the effects of INGAP on hIPCs ultimately would determine potential mechanisms of INGAP as a drug in the treatment of type 1 and type II diabetes.

The underlying overall hypothesis of this thesis is:

Live-cell imaging and proteomics can be collectively employed to systematically image and identify regulatory cellular changes, such as phenotypic variations and protein expression differences, which guide undifferentiated cells to different lineages; providing important information about the progression of cellular signaling at various stages of its development, having an impact in the fields of drug discovery and regenerative medicine.

Chapter 2 Literature Review

2.1 Calmodulin (CaM)

CaM is a small 17kDa calcium binding protein found in all eukaryotic cells. It is a ubiquitous protein composed of two lobes: an N- and a C-terminal domain connected by a flexible central linker region. Each domain consists of two EF-hand calcium binding motifs. In its unbound state, the protein structure is a small dumbbell shape, consisting of 148 amino acids. CaM regulates cellular activity based on intracellular levels of calcium. Calcium is an essential intracellular secondary messenger that is able to regulate numerous physiological processes. Calcium concentrations can rise intracellularly from influxes from outside the cell or from internal calcium stores found in the endoplasmic and sarcoplasmic reticulum within the cell (Clapham 1995). For example, calcium can influx through channels which span the plasma cell membrane, such as through voltage-gated calcium channels found in excitable cells (Dolphin 2009).

Upon calcium signaling, the calcium ions bind to CaMs EF-hand motifs causing a conformational change in the protein to a calcium bound form of CaM, termed calcium-CaM. The conformational change upon calcium binding, results in the exposure of hydrophobic patches which bind and control the activity of hundreds of proteins (Weljie, Yamniuk et al. 2003). Calcium-free calmodulin (apo-CaM) also plays an important intracellular role in the regulation of target proteins and numerous signaling pathways (Jurado, Chockalingam et al. 1999), however it is much less understood. Apo-CaM differs from calcium-CaM in its tertiary structure (Yamniuk and Vogel 2004). It has an overall more compact structure, in

comparison to calcium-CaM which has an open "relaxed" structure. In addition, the hydrophilic nature of apo-CaM allows it to bind its target proteins differently, utilizing IQ binding motifs and noncontiguous binding sites (Jurado, Chockalingam et al. 1999; Vogel, Brokx et al. 2002; Houdusse, Gaucher et al. 2006).

Differentiation, effector function and gene transcription are but a few cellular functions dependent on calcium and therefore also upon calcium-CaM (Oh-hora and Rao 2008). As a result, there are several drugs which target calmodulin-binding proteins to interfere with protein signaling required for cell function. For example, cyclosporine A (CsA) is a potent immunosuppressive drug which deregulates part of a calcium-CaM signaling cascade. Initially CsA was used to extend kidney allograft survival, however CsA was also shown to be partially effective in preventing graft-versus-host disease (GVHD) in bone marrow transplantation (Pai, Fruman et al. 1994). CsA binds to intracellular cyclophilin receptors, which combine to form a complex to target and inhibit calcineurin, a CaM dependent binding phosphatase whose activity is required for the induction of T-cell lymphokine production and proliferation (Hayden-Martinez, Kane et al. 2000). Although CsA has proven to be somewhat effective in the treatment of GVHD, chronic administration can lead to resistant acute GVHD, which is not yet fully understood (Pai, Fruman et al. 1994). As an alternative, CaM with mutated calcium binding sites can potentially be used as inhibitors of proliferation that do not act by direct inhibition, such as CsA, but as a drug to simultaneously selectively control (up regulate or down regulate) critical signaling pathways involved in CaM signaling, including differentiation.

CaM binds specifically to a large number of proteins, termed CaM binding proteins (CaMBPs) and binding is precisely controlled within the cell. Elucidating CaMs binding to its numerous target proteins is essential to understanding the many CaM-signaling cascades in which several physiological processes are dependent. The binding of calcium-CaM to its target proteins has been studied extensively over the past several decades, rising from a reported 30 target proteins in 1995 to a reported potential 300 target proteins which have been reported using protein software packages and databases which recognize calcium-CaM binding motifs (Crivici and Ikura 1995; Ikura and Ames 2006). Tremendous progress has been made, however a large number of these target proteins remain to be functionally characterized.

One of the most interesting characteristics of CaM is its diversity in binding proteins between the calcium-dependent and calcium-free forms. It is known that certain CaMBPs bind only to calcium-CaM, while other proteins bind preferentially to apo-CaM and less commonly to other forms of CaM (Jurado, Chockalingam et al. 1999). Apo-CaM has roles in the cell that have been suggested essential for life (Yamniuk and Vogel 2004). In 1999, 15 apo-CaM binding proteins were classified and discussed. The report consisted of a diverse group of proteins, including: enzymes, actin-binding proteins, as well as cytoskeletal and other membrane proteins, including receptors and ion channels (Jurado, Chockalingam et al. 1999). In comparison, it has already been systematically shown that calcium-CaM binds to over 120 proteins (Jang, Guo et al. 2007) and mediates vital processes including memory, immune

response and the cell cycle (Li, Heim et al. 1999; Limback-Stokin, Korzus et al. 2004; Colomer and Means 2007). Furthermore, calcium-CaM has been implicated in many diseases, including, Alzheimer's and some cancers (Murray, Gall et al. 1994; Bartolome, de Las Cuevas et al. 2007; Shigeri, Ishida et al. 2008). Although much less understood, apo-CaM and its binding proteins are equally vital to our understanding of cell signaling and disease, however it is believed that many remain to be identified.

2.2 TAT-Mediated Protein Delivery

TAT is a peptide of the human immunodeficiency virus 1 (HIV-1) cell targeting capsid used to deliver functional cargo proteins intracellularly in an efficient and controlled manner when added exogenously to cultured cells (Schwarze, Ho et al. 1999). Twenty years ago, Frankel and Pabo discovered a short basic segment at amino acids 48-60 of the human immunodeficiency virus (HIV) transactivator of transcription (TAT) protein which was capable of penetrating cell membranes to activate HIV-specific genes (Frankel, Bredt et al. 1988; Frankel and Pabo 1988). Ten years later, in 1999, it was reported that the TAT protein was used to deliver the active enzyme β-galactosidase to all tissues in the mouse, including the brain, following intraperitoneal injection (Schwarze, Ho et al. 1999). Subsequent to this study, several other groups reported using TAT to transduce many other cell types, including human T cells, primary astrocytes, rat cortical neurons, PC12 cells and human aortic endothelial cells (HAECs) (Nagahara, Vocero-Akbani et al. 1998; Matsushita, Tomizawa et al. 2001; Asoh, Ohsawa et al. 2002; Cao, Pei et al. 2002). Besides the fact that these early reports revealed that TAT could penetrate a large variety of cell types, it was reported that uptake was at nearly 100% efficiency (Nagahara, Vocero-Akbani et al. 1998; Matsushita,

Tomizawa et al. 2001; Asoh, Ohsawa et al. 2002; Cao, Pei et al. 2002). However, since these publications, several groups have reported conflicting results surrounding the penetration to every cell type, as well as its efficiency.

Wunderli-Allenspach 2003 and Violini et al. 2002 reported TAT was not capable to permeate intact plasma membranes of MDCK cells (Violini, Sharma et al. 2002; Kramer and Wunderli-Allenspach 2003). Similarly, TAT-mediated cargo delivery was unsuccessful in colonic carcinoma cells (Violini, Sharma et al. 2002) and muscle cells *in vivo* (Caron, Torrente et al. 2001). Richard et al. 2003 demonstrated that both fixation prior to fluorescent microscopic analysis and lack of trypsinization before flow cytometric analysis, which the previous 'successful' TAT-mediated studies employed, produce erroneous results of TAT-mediated uptake (Richard, Melikov et al. 2003; Vives, Richard et al. 2003). Following these results, Cai et al. 2006 using the same constructs as the original reports by Schwarze et al. 1999 and Cao et al. 2002 could not successfully repeat the *in vivo* results from these respective groups; ultimately, questioning the ability of TAT to penetrate plasma membranes of different cell types under diverse conditions (Cai, Xu et al. 2006).

As with many scientific advancements, the first two years of TAT-mediated protein delivery proved to be successful, demonstrating uptake into various cell types and at high efficiencies. The next generation of reports, however, demonstrated inconsistencies in achievability of using TAT to transduce many of the reported cell types. Since, determining the mechanism of TAT-mediated uptake has been central to its application. As a result, the mechanism of

TAT-mediated transduction has been investigated in many cell lines, as well as in primary cells. The controversy of transduction extends from results of required receptors, transporters, endocytosis and/or required electrostatic interactions. In the literature, all possible mechanisms have each been proven, disproven and proven over, with the current consensus being a combination of mechanisms.

In 2001, Tyagi et al. 2001 reported internalization of the TAT protein through electrostatic interactions with cell surface heparin sulphate proteoglycans. Using 20 different recombinant TAT mutants, it was discovered that the arginines in the basic domain of the TAT protein interact with heparan sulphate, a member of the cell surface glycosaminoglycans (GAGs) family of carbohydrates (Tyagi, Rusnati et al. 2001). Since then, using various cell lines, several groups confirmed these results (Tyagi, Rusnati et al. 2001; Vives 2003; Wadia, Stan et al. 2004; Wadia and Dowdy 2005; Bugatti, Urbinati et al. 2007; Duchardt, Fotin-Mleczek et al. 2007; Kumarasuriyar, Dombrowski et al. 2007; Nakase, Tadokoro et al. 2007; Poon, Chang et al. 2007). A more recent study extended the previous results on the cell lines to TAT-mediated protein delivery in primary brain cells, also revealing a dependence on GAG expression. In this study, it was hypothesized through observation of variability in reported TAT-mediated transduction efficiencies that the amount of cell surface proteoglycan may contribute to some of the observed variability. Proteoglycan expression was increased through treatment of astrocytes with ascorbic acid and TAT-uptake efficiencies were evaluated. The increase in proteoglycan content resulted in a significant increase in TAT-mediated transduction, whereas trypsinizing the cells resulted in a 30% decrease in GAG

expression and a significant decrease in TAT-mediated transduction. It was therefore concluded that TAT protein delivery is strongly dependent on the cell type, as well as the growth environment.

The mechanism of endocyotosis was proposed in one of the first studies of TAT uptake. Frankal et al. 1991 demonstrated TAT-mediated uptake through endocytosis by performing fluorescence pulse-chase experiments, in which rhodamine conjugated with TAT was found on the cell surface, followed by localization to the cytoplasm and nucleus (Mann and Frankel 1991). However, following these results, it was demonstrated that internalization was not significantly inhibited by incubation at low temperatures, by depletion of the cellular ATP pool or by inhibitors of endocytosis (Suzuki, Futaki et al. 2002), concluding endocytosis was not the mechanism of TAT-mediated uptake. In 2005, Chernomordik et al. demonstrated that cellular uptake of unconjugated TAT peptide involved clathrin-dependent endocytosis and heparan sulfate receptors (Richard, Melikov et al. 2005). Using different primary cells and inhibitors of clathrin-dependent endocytosis, they demonstrated that TAT uptake was ATP and temperature dependent, as well as partially dependent on the clathrin endocytosis pathway and heparan sulfate receptors (Richard, Melikov et al. 2005). However, uptake was only partially inhibited by clathrin and heparan sulfate inhibitors, therefore it was concluded that internalization of the TAT peptide may be through a combination of several unidentified receptors and endocytic pathways (Richard, Melikov et al. 2005).

In 2009, Yezid et al., summarized nicely a proposed 'endosomal translocating mechanism' of TAT-mediated protein delivery: "*Tat first binds to several cellular receptors such as CD26, CXCR4, heparan sulfate proteoglycans, and the low-density lipoprotein receptor-related protein. Tat is then endocytosed, essentially by the clathrin-coated pit pathway. Once in the endosome, Tat crosses the membrane to enter the cytosol. This translocation step is triggered by endosome low pH (pH 5.3-5.5) and is facilitated by the cytosolic chaperone Hsp90. Hence, Tat enters cells using a "conventional" endosomal translocating toxin strategy, just like diphtheria toxin, which is the best characterized example of this type of toxin."* (Yezid, Konate et al. 2009). It remains to be proven whether this is the precise and complete step by step mechanism of TAT translocation across the plasma membrane or if additional receptors and mechanisms will be proposed and identified.

Although the exact mechanism of TAT-mediated protein delivery remains somewhat ambiguous, over the past five years there has been significant demonstration of the diversity of cellular uptake made using a TAT-based delivery system. The TAT-mediated delivery system has been extended from proteins to a large variety of cargoes such as oligonucleotides, imaging agents, low molecular mass drugs, nanoparticles, micelles and liposomes (Gump and Dowdy 2007). Its delivering potential has been described as almost unlimited. However, for a given drug or protein to be considered successfully delivered, it must be transported across the plasma membrane and efficiently released into the cytoplasm. The plasma membrane of mammalian cells has been a barrier to effective delivery of potential drug candidates into the cell for decades. Several other methods have been

employed to facilitate delivery across the plasma membrane, such as electroporation, microinjection or macromolecular systems. However, these strategies often do not yield sufficient delivery, while comprising the cells and frequently resulting in cell death. Although perhaps not perfectly understood on a mechanistic level, TAT-mediated delivery has overcome many of the obstacles surrounding other therapeutic delivery systems. As a result, future investigations which attempt to utilize TAT as a delivery mechanism are warranted.

2.3 Islets of Langerhans and Diabetes

The pancreas is a multi-function gland organ. It acts as both an endocrine gland, secreting vital hormones directly into the blood and as an exocrine gland by secreting and transporting 22 digestive enzymes such as lipases, proteases and amylases through the branched ductal network to the small intestine (Slack 1995). The majority of the pancreas mass is comprised of exocrine cells, with less than 2% of its mass consisting of endocrine cells. The endocrine cells are located throughout the organ primarily in clusters, termed islets of Langerhans or islets. A healthy adult human pancreas has approximately one million islets, with a combined mass of only 1 gram. Islets are composed of four cells types: alpha, beta, delta and pancreatic polypeptide secreting cells. Each cell type is responsible for producing the hormones glucagon, insulin, somatostatin and pancreatic polypeptide, respectively, which work together as complex micro-organs to regulate blood glucose levels. Beta cells are the most prevalent cell type, comprising 65-85% of an islet and are solely responsible for the secretion of insulin, the major hormone which maintains glucose homeostasis.

Type I and type II diabetes are both characterized by the impairment of islet secretary function of insulin. Specially, type I diabetes is associated with the autoimmune destruction of insulin producing beta cells and type II diabetes by an insulin resistance. One of the most widely used current treatment strategies requires administration of exogenous insulin, which ultimately can lead to unstable blood glucose control, resulting in the risk of hypo- or hyperglycemic episodes. As well, there are many associated long-term effects of insulin use, including: cardiovascular disease, nephropathy, retinopathy, and neuropathy (Shamoon, Duffy et al. 1993; Steffes, Chavers et al. 2003). In attempts to achieve independence from insulin therapy, clinical trials have demonstrated promise of islet transplantation (Ryan, Lakey et al. 2001; Shapiro, Ryan et al. 2001); however, up to three islet transplants are needed to achieve insulin independence. Furthermore, often five years post-transplantation patients require insulin injections due to the decline in graft function related to the immune response to the transplanted islets (de Kort, de Koning et al. 2011). Besides the poor long-term results of islet transplantation, there remains a short supply of donor pancreata in which the islet cells are isolated (Noguchi 2009).

The regenerative potential of islets of Langerhans has been demonstrated in animal models of decreased beta cell mass (Montana, Bonner-Weir et al. 1993). In these *in vivo* studies however, it has proven difficult to implicate specific cell phenotypes, while clearly identifying the mechanisms involved in the regeneration process. Although some studies have implicated the pancreatic ductal region as the site of islet regeneration (Bouwens and Pipeleers 1998), others have implicated stem or progenitor cells which reside within the islet

as the source of regeneration (Guz, Nasir et al. 2001; Zulewski, Abraham et al. 2001). Additionally, one group has suggested that insulin-producing β-cells self-duplicate to expand islet cell mass (Dor, Brown et al. 2004). Not only does the mechanism of islet regeneration remain unknown, it is also unclear how similar human islets are to other species. Therefore, it remains to be identified the degree to which animal models can be applied to interpret the human system. This emphasizes the importance of studying human patient derived cells.

2.4 Human Islet-Derived Progenitor Cells (hIPCs)

Isolated islets cultured *in vitro* are a promising source of progenitor cells for islet replacement because they expand exponentially into a large mixed population of proliferative islet hormone-negative cells (Russ and Tobin 1998; Schmied, Ulrich et al. 2000). These proliferative cells have been termed islet-derived progenitor cells (IPCs). The characterization of origin of IPCs however, has not yet been determined. Several groups have attempted to characterize the origins of IPCs, debating β-cell origin versus non-β-cell origin. Dedifferentiated human β-cells have been implicated as a source of IPCs (Gershengorn, Hardikar et al. 2004; Bar, Russ et al. 2008), but appear to require soluble factors from other non-β cells. Conversely, using a mouse model, several groups (Chase 2007, Atouf 2007 and Morton 2007) have demonstrated that the proliferative IPC populations from dedifferentiated islets were not of β-cell origin (Atouf, Park et al. 2007; Chase, Ulloa-Montoya et al. 2007; Morton, Geras-Raaka et al. 2007). Mesenchymal stromal cells present within islets or the pancreas have also been suggested as a source of IPCs (Davani, Ikonomou et al. 2007; Gallo, Gambelli et al. 2007). Despite the lack of scientific consensus on IPC origin, IPCs hold promise in cell replacement therapies for the treatment of diabetes, by potentially providing a

large cell source which ideally can be coaxed to differentiate into functional insulin-producing cells.

Epithelial-mesenchymal transition (EMT) has been shown to be critical in embryogenesis, in which epithelial cells lose their mature characteristics (i.e. gap junctions) and acquire characteristics of mesenchymal cells (i.e. vimentin expression) (Vicovac and Aplin 1996). Studies have suggested that pancreatic beta-cells undergo EMT and dedifferentiate into IPCs. However, it is argued that these results may be flawed, since the harvested islet fractions studied are never pure endocrine cell populations (Atouf, Park et al. 2007). Therefore, those studies cannot definitively prove that the IPCs are not derived from, for example exocrine cells, and as a result are not definitively of beta-cell origin (Atouf, Park et al. 2007). Chase 2007, demonstrated using genetic-based lineage-tracing models that IPCs were not derived from beta-cells undergoing EMT, but that the IPCs are a population of MSCs from within the pancreas (Chase, Ulloa-Montoya et al. 2007). However, it was unclear if the observed differences of EMT hypothesis versus MSC origin were due to undetermined animal model and/or cell culture differences (Chase, Ulloa-Montoya et al. 2007).

To date, efforts to dedifferentiate IPCs into insulin-producing cells have demonstrated promising, however, inconsistent results. Gershengorn 2007 reported characterization of human IPCs (hIPCs) as a population of MSCs capable of dedifferentiation into islet-like structures following proliferative expansion. In this study, the hIPCs expressed the MSC surface markers CD73/90/105-positive and CD14/19/34-negative (Davani, Ikonomou et al.

2007). Contrary to Chase 2007, the origin of the hIPCs was described as migrating out *in vitro* from the islets spreading into mono-layers not simply from pancreatic tissue. Following proliferative expansion, cell clusters were generated which were transplanted into a small pocket created under the renal capsule of SCID mice. It was reported that 22 of 35 transplanted clusters differentiated and matured into functional cells which secreted human C-peptide (marker of endogenous insulin production) in response to glucose. However, secretion was only at levels of 1% compared to adult islets (Chase, Ulloa-Montoya et al. 2007).

Melton 2004 demonstrated that beta-cells were formed by self-duplication of pre-existing beta-cells (Dor, Brown et al. 2004), which are results inconsistent with beta-cells arising from stem or progenitor cells. These results were in the context of normal growth of beta-cells; therefore, it remains possible that stem or progenitor cells do participate in beta-cell regenerative repair. It was concluded that beta-cells are the major source of new beta-cells in normal adult life, challenging the view that a stem cell population is responsible for beta-cell homeostasis (Dor, Brown et al. 2004). Later in 2007, Melton et al. published further evidence confirming the capability of beta-cell duplication and maintenance, demonstrating that the beta-cell population is homogeneous with respect to replication capacity. Therefore, suggesting that all beta cells are candidates for *in vitro* expansion (Brennand, Huangfu et al. 2007; Nir, Melton et al. 2007).

In 2008, Melton took a different approach to generating beta-cells for transplantation. Rather than focusing on the previous findings of beta-cell duplication, the focus was shifted to converting adult cells into beta-cells. Examples of adult cell reprogramming are known, such as the discovery of induced-pluriopotent stem cells (Takahashi, Tanabe et al. 2007). However, unknown are controlled methods of intentionally directing one cell type into a specific desired differentiated cell type. Recently, Melton et al. using key developmental regulators *in vitro* (Ngn3, Pdx1 and Mafa), reprogrammed exocrine cells in adult mice into beta-like cells which could ameliorate hyperglycemia. This suggested that beta-cells may regenerate from non-beta-cell origin, such as a stem cell population (Zhou, Brown et al. 2008).

In summary, the identification and confirmation of a pancreatic stem cell population remains elusive. There is strong evidence that isolated human islets contain a distinct population of mesenchymal stem cells (MSCs) (Carlotti, Zaldumbide et al. 2010). Although these transplanted MSCs are reported to express insulin mRNA at low levels, they are indeed capable of differentiating into hormone-expressing cells at levels 1% of adult islets (Davani, Ikonomou et al. 2007). However, it is unclear how and if these cells contribute to islet neogenesis *in vivo*. It is known that during the life of a healthy adult, beta cells are regenerated perhaps from self-duplication or activation of a dormant stem cell population contained in the pancreatic ducts, from within the islets or the bone marrow. It is possible that a combination of several of the proposed cell types may contribute to islet neogenesis. For example, during embryonic induction, islets may arise from cells found within the ductal

network, whereas during adulthood beta cells may self-duplicate or dormant 'MSC like' stem cell populations may differentiate into islets. Lastly, it is important to note that the identification of extrinsic factors and the culture conditions required to promote islet neogenesis is another key required to produce cells for transplantation. Ultimately, continuous and rigorous characterization of the discussed cell types in parallel with the study of important regulatory factors involved in islet neogenesis will result in insulin secreting cells which are adequate for islet transplantation.

2.5 Islet Neogenesis Associated Protein (INGAP)

INGAP is a 17 KDa member of the Reg family of proteins that was first discovered in 1997 by Dr. Aaron Vinik and Dr. Lawrence Rosenberg who identified a gene, islet neogenesis associated protein (INGAP), whose product stimulated the growth of insulin-producing cells in the pancreas of a hamster model (Rafaeloff, Pittenger et al. 1997). Although not conclusive, they postulated that the gene expressed a protein that appeared to initiate cell proliferation in pancreatic ducts but not directly in islets. In this model, animals developed increased beta cell mass that was able to reverse induced diabetes. Initially, a crude protein extract was prepared from the pancreas of the model hamsters, termed ilotropin (Pittenger, Vinik et al. 1992). The protein INGAP was later identified as the active component of the crude hamster extract (Rosenberg, Vinik et al. 1996). Sequencing of the full-length protein identified a region (amino acids 104-118) that was specific in comparison to other Reg proteins. This region, termed INGAP peptide (INGAP-PP), was synthetically produced and proposed to be the region of INGAP which induced islet neogenesis in hamsters (Rafaeloff, Pittenger et al. 1997).

To date, studies of INGAP have focused on evaluating the islet neogenesis effects of INGAP-PP. Jamal et al. were the first to demonstrate the phenotypic plasticity of pancreatic islets using an INGAP-PP treatment. In this study, isolated islets were induced to duct-like structures which displayed the loss of islet-specific hormones and then treated with INGAP-PP. It was reported the reversion of the islet-derived duct/cystic structures back to islet-like structures displaying the expression of islet hormones and glucose responsiveness following INGAP-PP treatment (Jamal, Lipsett et al. 2005). These results suggested that human islets may possess a remarkable degree of morphogenetic plasticity when exposed to INGAP-PP. As a result, since this publication several groups have focused on evaluating the effects of INGAP-PP on various animal islets.

INGAP-PP has been studied extensively in rat islets. In 2006, Barbosa et al. cultured neonatal rat islets for 4 days with INGAP-PP. These islets released significantly more insulin in response to glucose in comparison to islets which were cultured without the peptide. Furthermore, several genes related to islet metabolism, insulin secretion and beta cell mass were modified by INGAP-PP. It was concluded that INGAP-PP enhances the secretion of insulin and the transcription of genes involved with islet neogenesis (Barbosa, Bordin et al. 2006). Following this study, Barbosa et al. attempted to elucidate the mechanistic pathways involved in INGAP-PP signaling in rat islets. Studying both neonatal and adult rat islets, it was observed that INGAP-PP stimulated the up-regulation of cholinergic receptors which suggested the participation of the cholinergic pathway in INGAP-PP mediated effects in rat

islets (Silva, Barbosa et al. 2008). Subsequent to this publication, the group wanted to further understand the mechanisms involved in INGAP-PP effects upon their findings of increased beta cell mass and function. They shifted their focus to working with a complete animal model, the hamster, whereas their previous work had focused on studying isolated rat islets *in vitro*. This study concluded that INGAP-PP promoted a controlled and functionally active increase in beta cell mass *in vivo* and suggested the existence of a negative feedback loop which involved Ngn-3, a transcription factor involved with the specification of endocrine lineage (Madrid, Del Zotto et al. 2009).

In 2009, this group took a different approach to evaluating the effects of INGAP-PP by focusing on islet beta cell differentiation of mouse embryonic stem (mES) cells. Using established mES differentiation protocols with or without the addition of INGAP-PP, gene expression was quantified using qPCR. It was determined that INGAP-PP increased significantly insulin gene expression, while reducing glucagon and somatostatin gene expression. Additionally, PdX-1 gene expression increased by 115% in INGAP-PP treated cells. It was concluded that INGAP-PP promoted stem cell differentiation into beta cell-like phenotype, while simultaneously decreasing mES differentiation towards non-beta cell precursors (Francini, Del Zotto et al. 2009). This significant finding indicated for the first time that INGAP-PP could potentially be useful in the differentiation of stem cells to beta cells.

In addition to rats, hamsters and mice, INGAP-PP has been investigated in dogs by Vinik's group in 2007. Non-diabetic beagle dogs received either a placebo or three different doses of INGAP-PP injections (0.5, 1.5 or 10 mg/kg). It was determined that dogs which were treated with INGAP had a significant ($P < 0.001$) increase in the percentage of insulin-positive cells and insulin gene expression. Additionally, there was a dose dependent trend of increased insulin-positive cells and gene expression (Pittenger, Taylor-Fishwick et al. 2007). It was concluded that INGAP-PP stimulates islet neogenesis in dogs. However, like in other animal models it was not possible to determine with certainty specifically which cells contributed to the neogenesis effect. It was suggested that islet progenitor cells found in the pancreatic duct epithelium of the healthy dogs stimulated islet neogenesis. However, this was based on previous findings from this group in which the duct cells of INGAP-PP treated diabetic mice whose diabetes was reversed had increased PDX-1 expression specifically in the duct cells (Rosenberg, Lipsett et al. 2004).

The mechanism of INGAP is still under debate. However, the evidence presented from a range of groups using several different animal models (rats, hamsters, mice and dogs) demonstrates its potential role in the cure of diabetes. As a result, in 2003 the FDA approved human trials using INGAP-PP as a drug to treat diabetic patients. The first phase 2 clinical trials evaluated INGAP-PP in 200 patients with both type I and type II diabetes. Patients received INGAP-PP treatment for 90 days and overall INGAP-PP was found to increase C-peptide secretion in Type 1 diabetic patients and improve glycemic control in Type 2 diabetic patients (Dungan, Buse et al. 2009). Clear trends of efficacy were demonstrated, however,

evaluating the effects of a refined formulation, delivery regimen, appropriate dosage, site of administration, as well as the duration of therapy were concluded as necessary considerations in future clinical trials.

Although the original work of cloning and sequencing INGAP concluded that both the peptide and the protein demonstrated effects of islet neogenesis, it was noted that INGAP protein appeared to have a more potent effect in comparison to the peptide (Rafaeloff, Pittenger et al. 1997). Recently, the production and characterization of full-length recombinant INGAP (rINGAP) has been reported to facilitate studies of the mechanism(s) of INGAP action (Assouline-Thomas, Pilotte et al. 2009). Importantly, rINGAP exhibited 100 times the bioactivity in comparison to INGAP-PP using an *in vitro* assay (Assouline-Thomas, Pilotte et al. 2009). To date, there have been no subsequent publications which study the effects of rINGAP on islet neogenesis.

In summary, since INGAP's discovery, several groups have attempted to determine its mechanism and role in islet neogenesis, as well as its been investigated as a drug in phase two human clinical trials for the treatment of type I and type II diabetes. It is believed that in the animal pancreas, INGAP differentiates islet progenitor cells or stem cells into insulin secreting islet-like cells; and/or that INGAP induces a reversion of proliferative duct-like epithelial cells of non-β cell origin to insulin secreting cells; and/or that INGAP acts on existing islets by increasing insulin secretion (Yuan, Rosenberg et al. 1996; Jamal, Lipsett et al. 2003; Lu, Gu et al. 2005). Evidence suggests that hIPCs may represent an important adult

precursor or stem cell population. If so, it is conceivable that when expanded and cultured *in vitro*, hIPCs could offer a useful supply of cells which, given the right factor(s), could be coaxed into islet-like cells and used for transplantation. To date, studies using only INGAP to dedifferentiate hIPCs into insulin-producing islet-like cells have yet to be published. As a result, investigating INGAP's effect on hIPCs at the proteomic, behavioral and phenotypic levels, will further characterize both INGAP and hIPCs therapeutic potential in the treatment of diabetes.

2.6 Proteomics

Like the human genome work, there is valuable information to be obtained from studying protein-protein interactions. Proteomics focuses on the identification and function of proteins in the cell. The proteins in a cell change with the conditions of the cell including: the stage of cell cycle, the age of the cell, and with external or internal signaling. As a result, the amount and complexity of the data obtained from the sequencing and mapping of every organism's proteome is several times greater than that of the same organism's genome. Unfortunately, because of the quantity and complexity of the data required to elucidate a proteome, proteomic technology has not advanced at the same rate as that of the genome. The current and most commonly used laboratory technique for expression proteomics is separation using two-dimensional polyacrylamide gel electrophoresis (2D PAGE), in which an electric current is applied to a gel matrix to separate an entire protein population. There are several variations to the technique, such as the dimensions of separation, the composition of the polyacrylamide gel, as well as the pH range utilized. To achieve quantitative analysis, two-dimensional

differential in gel electrophoresis (2D DIGE) uses fluorescent dye labeling in combination with 2D PAGE, allowing statistical analysis of the protein abundances. Once the lysate mixture of cell-derived proteins has been separated, they are identified primarily by mass spectrometry (MS). Finally, after the proteins have been identified, bioinformatic analysis is used to elucidate the protein interaction networks.

2.6.1 Two-Dimensional Gel Electrophoresis (2D PAGE)

In 2D PAGE, proteins are separated in the first dimension based on their isoelectric point, followed in a second dimension by mass. Each protein localizes differently throughout the gel, creating individual spots based on their unique size and charge. After the proteins have been separated and stained, spots can then be cut out from the gel, digested into short peptides and analyzed using MS. For over three decades 2D PAGE has been used as a powerful tool for the analysis of large protein sample populations. However, there are several limitations which render this technique more of a qualitative tool. 2D PAGE requires significant preparation and consideration of the protein sample being analyzed. A significant amount of hydrophobic proteins, such as transmembrane receptors and alkalines, are underrepresented on the gel as they cannot be integrated into the aqueous buffer system (Cho 2007). Additionally, 2D PAGE is a time-consuming, labour-intensive process, requiring skilled and trained operators. Depending on the optimal voltage for separation, the process can take up to 60 hours before the gels can be stained and visualized. Proteins present at low concentrations in the protein sample are generally not detected on the stained gels, even when using highly sensitive stains such as Deep Purple™ (Xie, Goldys et al. 2007).

Furthermore, a resolved protein spot on a 2D gel can represent more than one protein, as often some proteins cannot be completely resolved within a single gel.

Conceivably the biggest limitations of 2D PAGE are reproducibility and variability. Experimental or technical variability can be introduced by: heterogeneities in the gel polymerization, incomplete protein uptake into the isoelectric focusing strips, deficient migration of the proteins during isoelectric focusing and incomplete protein transfer from the first to second dimension (Smith 2006). The unavoidable introduction of these experimental errors results in gel-to-gel technical variation that can potentially mask the biological variation between protein samples, therefore resulting in erroneous results (Smith 2006). Lastly, in order to compare protein samples and protein populations, different samples have to be separated using individual gels. The individual gels are then visually aligned to compare spot patterns or differences in intensities from one gel to another. As there are many explicit experimental steps in 2D PAGE, there is tremendous potential for the introduction of gel-to-gel variability and the mis-match of proteins across gels.

2.6.2 Two-Dimensional Differential In Gel Electrophoresis (2D DIGE)

Over the past three decades, 2D PAGE coupled with MS has been one of the only methods of high resolution protein separation and identification (Issaq and Veenstra 2008). However, as the study of proteomics advances, the limitations of 2D PAGE have driven the development of a quantitative technique. 2D DIGE builds on the principles of separation in 2D PAGE by adding an accurate quantitative dimension that allows simultaneous separation and comparison of two protein samples on a single gel (Marouga, David et al. 2005). This is

achieved by first labeling each protein sample with specifically engineered fluorescent Cy dyes: Cy2, Cy3 and Cy 5. The Cy dyes are charge matched with the residues they bind and have the same molecular weights (0.5kDa). The size and charge matching of the three dyes results in the labeling having an equal impact on protein migration in the gel, allowing for accurate comparison of the fluorescent intensities (Karp, Kreil et al. 2004). Digital protein spot images of each labeled sample within a gel is created through sequential excitation of the three fluorophores. Following a similar three day separation process as 2D PAGE (with the addition of fluorescent labeling), the proteins are visualized using a fluorescence scanner (GE Healthcare) and a computer software package, such as DeCyder (GE Healthcare), which provides analysis of the protein abundances between populations.

An additional advantage of the DIGE technology is the use of an internal standard. The internal standard is a pooled sample loaded on all gels in the experiment, containing equal amounts of the protein samples. The internal standard assists with inter-gel alignment, which allows for a relative measurement between the same protein spot in different gels. While viewed as advancement, the dependence of DIGE on fluorescent labeling for quantification is costly, as well as it introduces new technical concerns. 2D DIGE was designed to reduce the main limitations of 2D PAGE, which are gel-to-gel variation and quantification. Although 2D DIGE does reduce gel-to-gel variation, through the use of an internal standard to align the gels, gel-to-gel variation is not eliminated and therefore several issues remain which limit the use of the technology. Besides the introduction of fluorescent dye labeling, the technology is based on 2D PAGE, therefore limitations, such as: heterogeneities in the gel polymerization, incomplete protein uptake into the isoelectric focusing strips, deficient migration of the

proteins during isoelectric focusing and incomplete protein transfer from the first to second dimension, all remain significant in 2D DIGE.

2.6.2.1 2D DIGE Quantification and Statistical Analysis

Although there remain issues surrounding the 2D DIGE technology, its development has permitted the multiplexing of samples and the quantification of protein spots across a gel series. This is achieved by the internal standard and by protein labeling with the fluorescent Cy Dyes. Since these dyes have different system gains based on differences in fluorescence, to account for these differences the measured spot volumes from the gels are first normalized. The software co-detects the spots from the digital images, performs normalization and compares the spot volumes (fluorescent intensities). Normalization in DeCyder is based on the assumption that the majority of proteins are not differently expressed (Karp, Kreil et al. 2004). Normalization adjusts the primary spot volumes ($v1$) by a scaling factor (a) so that the frequency histogram of the log volume ratios centres on zero, resulting in a calculated normalized spot volume ($nv1$):

$$nv1 = v1 \times a \quad (1)$$

To determine the scaling factor (a), a normal distribution is fitted to the main peak of the frequency histogram and the mean of the fitted normal distribution is shifted to zero by the factor (a). Shifting the mean of the fitted normal distribution to zero is done because of the assumption that most proteins are not differently expressed. However, depending on the biological system being analyzed this assumption is not always accurate. Therefore, DeCyder's normalization method is not always ideal (Karp, Kreil et al. 2004).

Once the spot volumes have been normalized by a factor (a), DeCyder calculates a log volume ratio (R) of the primary spot volume in the secondary image ($v2$) over the normalized spot volume ($nv1$):

$$R = \log\left(\frac{v2}{nv1}\right) \quad (2)$$

Using the log volume ratio (R), an expression ratio (E), is calculated based on if R is less than or greater than zero:

$$E = \left(\frac{v2}{nv1}\right) for\ R > 0,\ \frac{v2}{nv1} > 1 \quad (3)$$

$$E = -\left(\frac{nv1}{v2}\right) for\ R < 0,\ \frac{nv1}{n2} > 1 \quad (4)$$

The expression ratio (E) is reported to the user as the measurement of fold change and is greater than one or less than minus one (Karp, Kreil et al. 2004).

In addition to the reported fold change of a protein spot between the two samples (E), a p-value is also reported to the user. The p-value is a measure of significance of the fold change in terms of the false positive rate (Karp, McCormick et al. 2007). A Student's *t*-test is used to calculate the statistical significance of an abundance change between the two groups, considering both the within group variance and the between group variance. For example, a large p-value indicates that the within group variance is large compared to the between group variance, hence the reason why gel-to-gel variation has such an immediate effect on the statistical analysis. The null hypothesis being tested in the Student *t*-test is that there is no significant change in the protein abundance between the two experimental groups (Storey

and Tibshirani 2003). The Student's *t*-test assumes a normal distribution of protein abundances and a frequency distribution of the p-values is used to estimate the proportion of features that are unchanging (Karp, McCormick et al. 2007). P-values reflect the probability that the observed change has occurred from random chance alone, supporting the null hypothesis. In other statistical analyses, probability values less than 0.05 from a Student *t*-test are generally used to determine a statistically significant difference from the null hypothesis. However, when evaluating 1000 proteins, for example, a p-value cut off of 0.05 would represent potentially 50 false-positives. As a result, it is argued that stringent confidence intervals in the 99^{th} percentile ($p<0.001$), are more valid for DIGE applications (Storey and Tibshirani 2003).

Although a prescribed significance threshold of, for example 0.001, is more stringent than 0.05, a substantial number of false positives may still accumulate. For example, often protein systems studied have greater than 2000 proteins detected, resulting in potentially 20 false-positives out of a list of 50. This accumulation of false-positives at even low p-value cut-offs is due to the lack of consideration of multiple testing in the Student *t*-test. Thousands of statistical Student *t*-tests are being conducted, however on an individual spot basis, without taking into account that the spots being simultaneously tested have between-feature dependence (Storey and Tibshirani 2003). For example, often in 2D-gel proteomics, proteins can be represented multiple times in a charge train (Karp, McCormick et al. 2007). As a result, Benjamini and Hochberg recognized this multiple testing phenomenon and defined the false discovery rate (FDR) as the proportion of changes identified as significant that are

actually false (Hochberg and Benjamini 1990). As an extension to the FDR, Storey et al. developed a q-value, which is a measure of FDR in comparison to the p-value.

In summary, Student *t*-tests control the rate in which unchanging features are indicated as significant, whereas the FDR test controls the rate of those significant features being actually false (Storey and Tibshirani 2003). As a result, the q-values are calculated directly from the p-values using the FDR feature within the DeCyder software. The exact algorithm is confidential, however a frequency distribution of the p-values is used to determine the number of features which are unchanging. If there were no changes in protein expression, a uniform distribution of the p-values is expected because it is assumed through testing thousands of features that p-values of all ranges to one will be obtained by chance. However, proteins which change in expression will have low p-values (<0.05) and stand out above the unchanging proteins which contribute to a uniform frequency distribution. A q-value is then calculated for each protein using the corresponding p-value and through estimating the proportion of false positives within the total number of proteins considered initially significant (Karp, McCormick et al. 2007).

2.6.2.2 DIGE Experimental Design

The development of the spectrally resolvable Cy Dye's permits quantification across many gels, which ultimately allows for statistical analysis, such as the Student's *t*-test and the FDR analysis. However, both the Student's *t*-test and the FDR approach rely on the use of a correct experimental design. The design of any experiment is critical to a hypothesis being successfully answered and to the validity of the results obtained. To maximize the

information gained from a DIGE experiment one must consider replication type, replication number and overall design. The replication type affects what can be concluded from the experiment. There are two types of replicates: biological and technical. Biological replicates are different biological samples from the same treatment group (Karp, Spencer et al. 2005). Technical replicates are repeated measures on the same biological sample (Karp, Spencer et al. 2005). For example, biological replication of a brain would consist of each replicate being from a different brain, whereas technical replication would be replicate samples from the same brain. Biological variability is inherent between all organisms, arising from genetic and/or environmental factors (Karp, Spencer et al. 2005). Without the consideration of biological replicates, false conclusions which assume there is no biological variability will be drawn. Including biological replication into an experimental design considers the natural variation within a sample population. In summary, false deductions may be made in the absence of biological replication. On the other hand, in experiments with only biological replication in which technical replication is not included, the uncertainty about the true reading for a given sample is reduced (Karp, Spencer et al. 2005). Technical replicates are essentially repeat measurements on the sample and therefore reduce experimental noise and/or measurement error.

Replication allows experimentally collected data to be analyzed statistically. Therefore, considering both biological and technical replication in the experimental design is critical to allowing more vigorous data analysis and interpretation. The power of a DIGE experiment is the probability that a true positive will be detected (Horgan 2007). Ideally both replicate

types should be employed to achieve sufficient power of analysis in an experiment, however depending on the experimental circumstances incorporation of both replicate types into the experimental design may not be feasible. Particularly, in experiments with low sample yields and/or experiments with cost restrictions, using both types of replication is not always possible or practical. For example, when performing proteomic analysis on human samples, which are often a highly-limited resource and availability cannot be guaranteed, biological replication is directly dependent on availability of independent biological samples. In comparison, in studies with cost and equipment restrictions, a large number of technical replicates may not be reasonable. Overall, it is important to be aware of the fact that the number of replicates (gels) is directly related to the power of the experiment for the size of expression changes detected (Horgan 2007). Therefore, maximizing the replication within an experimental design increases the power of the experiment.

Sample pooling is an alternative to using several individual organisms through reducing the number of independent biological samples (Karp and Lilley 2009). Individually prepared biological samples are combined using equal contributions from each to form a pooled sample. If the material is available, a sub-pooling design can be employed, in which additional biological pools can be formed, each representing a biological replicate. Technical replicates of the pooled samples can then be measured through repeat measurements on the pools. Changes in protein expression will not be identified if the biological variability of the population is greater than the protein expression changes, therefore sample pooling is especially favorable when biological variability is high (Karp and Lilley 2009). When sample

pooling is utilized, identified protein expression changes are changes in the average biological pooled sample detected above the technical noise. It is important to consider that sample pooling should not be incorporated into the design of experiments if the intention of the experiment is to show a relationship between the detected protein expression changes and the biological subjects which were pooled (Karp and Lilley 2009). As information about variables at the biological subject level is lost in the pooling process.

In summary, sample pooling reduces biological variability by minimizing individual biological variation. Sample pooling, however, assumes biological averaging; that the measurements taken on the pooled sample are equal to the average of the individual samples which contributed to the pool (Karp and Lilley 2009). In other words, pooling assumes that the biological mean equals the mathematical mean. However, in biological samples with a large degree of variation, Jensen's inequality effect, in which the mean of the individuals is less than the mean of the pool, may apply and therefore this assumption may not hold (Karp and Lilley 2009). The average of the pool must be greater than or equal to the average of the individuals when outliers in the individual samples are attenuated through the log transformation and then averaged (Karp and Lilley 2009). Karp et al 2009 demonstrated that the Jensen's inequality effect may be significant for some biological systems, but not for all. For example, the biological variation between human brains is much greater than mouse and therefore there is balance between biological variation, technical variation and sample pooling. Thus, sample pooling is beneficial when there is large biological variation, however

to avoid systematic biasing, the correct design of experiments needs to be employed (Karp and Lilley 2009).

Depending on the biological variability of the samples, the technical variability of the process, the availability of financial and equipment resources, as well as the overall aim of the experiment, an indefinite number of experimental designs can be considered. **Figure 2-1** represents four different possible experimental designs for comparing a treatment group versus a controlled group. The first option is an experiment with only technical replication (**figure 2-1i**). All that can be concluded from this experiment is that one biological sample is different from the other, however no broader application to the entire biological populations can be made. The second option is an experiment with only biological replication (**figure 2-1ii**). Biological changes will be detected above the technical variability and no conclusions within each of the biological populations can be drawn. A third design of experiments represents an ideal, largely funded and supported experiment, incorporating both technical and biological replication (**figure 2-1iii**). Lastly, the fourth experimental design is a sub-pooling design, in which two biological replicates are pooled and three independent pools are compared (**figure 2-1iv**). In conclusion, there are many factors to consider when designing a 2D DIGE experiment. With the proper consideration of the ultimate goal of the experiment and the correct experimental design, the obtained results can serve to answer the original hypothesis.

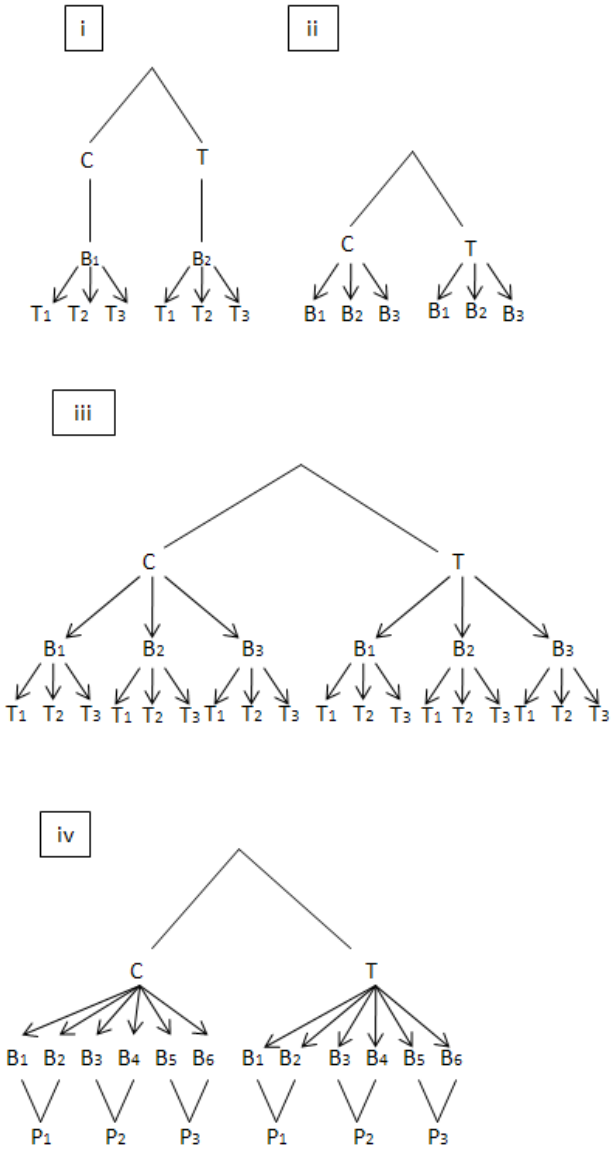

Figure 2-1: Representation of possible experimental DIGE designs when comparing control (C) versus treated (T). (i) Represents an experiment with only technical replication. (ii) Represents an experiment with only biological replication. (iii) Represents an ideal, largely funded and supported experiment, incorporating both technical and biological replication. (iv) Depicts an ideal sub-pooling design of experiments, in which two biological replicates are pooled and three independent pools are compared. B is biological replicate. T is technical replicate. P is pooled replicate. Image adapted from Karp and Lilley 2009.

2.6.3 Mass Spectrometry (MS)

Mass spectrometry (MS) is an analytical technology that generates a mass spectrum of the peptides in the sample. The mass spectrometer scans the population of eluting ions, measures the mass to charge ratio, fragments the peptides through collision and then obtains a mass spectrum from the fragment patterns. The generated mass spectrum is compared to model spectrums in databases to identify the protein originally separated using 2D PAGE (Webb-Robertson and Cannon 2007). Over the past three decades, 2D PAGE and 2D DIGE coupled with MS has been the preferred approach of global protein profiling. MS has provided an essential analytical component to the process of understanding biology from a systems level. The process of computational peptide identification, although fundamental to MS, provides limitations to the technology (Webb-Robertson and Cannon 2007). Computational peptide identification compares generated mass spectrums to model spectrums, created from predicted peptides of a sequenced genome. However, these computational database searches can return false-positives. Additionally, to allow for the expected experimental variation between the generated mass spectrums and the model spectrums, a normal mass error distribution is used in the computational process which can ultimately also result in proteins being falsely identified (Webb-Robertson and Cannon 2007).

2D PAGE is the main technique used to separate proteins of interest prior to MS analysis. However, although widely used it poses problems for high-throughput MS sample preparation. Specifically, it is time-consuming to pick protein spots and it is often difficult to detect low abundant proteins on the 2D gels. Therefore, rendering the identification of low

abundant proteins unreliable and/or infeasible. As a result, over the past five years companies have been focusing on technology developments which automate many of the steps involved in 2D-PAGE. One method has been transferring the protein samples from 2D gels onto matrix assisted laser desorption/ionization (MALDI) targets. This novel technology supports micro-scale digestion of proteins using pico to nanoliter volumes of reagents and delivers the proteins directly to the mass spectrometer from the 2D gels (Sommerer, Centeno et al. 2007).

2.7 Long Term Live Cell Imaging and Cell Tracking

Over the past two decades, cell biology has developed into an integrative discipline which combines areas such as genetics, proteomics and molecular biology to understand the many complex mechanisms of living cells. However, these disciplines employ techniques, such as 2D PAGE and immunohistochemistry, which require destroying cells to obtain results. Furthermore, time-course analysis is frequently applied to these techniques which require collecting destructive results at various time points, followed by the interpolation of the data to infer non-measured cellular activities. Regularly, such interpretations assume a linear order of events between the experiment time points, however further complex interrelations are occurring in real-time which ultimately are not detected with these destructive techniques. In general, this means that events which occur at interim time points can go undetected, ultimately potentially leading to the publication of incomplete cellular information. Although these will remain critical to understanding the molecular basis of the cell, it is becoming increasingly more evident that there are numerous benefits to be obtained from real-time dynamic studies of cells in culture.

Time course imaging and cell tracking techniques enable the direct observation in real-time on the single cell level. This provides opportunity for detailed analysis of the fundamentals of cell biology, such as: differentiation, apoptosis, migration rates, morphological and phenotype classifications. Adaptability, sensitivity, resolution and non-invasiveness are but a few of the advantages of the technique. Adapting long term live-cell imaging and cell tracking techniques to study the fundamentals of disease is essential to advancing our ability to investigate and monitor disease mechanisms in experimental degeneration models (Weissmann and Brandt 2008). Non-invasive cell tracking in combination with fluorescent markers has permitted, for example, tracking the long-term dynamics of transgene expression to investigate the timing and expression patterns leading to transgene variegation (Ramunas, Montgomery et al. 2007).

Time course imaging and cell tracking are not recently invented techniques; however some of their recent applications are innovative, with further advancement allowing for studies with an increasingly higher level of complexity. Time course cell imaging techniques were originally developed in the 1960s and were initially employed to study the generation times of monolayer cell cultures (Hsu and Kellogg 1960; Earle 1962; Froese 1964). Over the past decade, the improvements to the microscope in combination with a computer technology revolution and new engineering innovations, have facilitated tracking single cell movements through three-dimensional substrates (Demou and McIntire 2002; Rabut and Ellenberg 2004). In our lab, Moogk et al. 2007 described a novel imaging chamber engineered to facilitate long-term three-dimensional imaging of human islets in culture. The imaging chamber enables the high resolution imaging of three-dimensional islets while maintaining

the structure of the islet cells and intercellular matrix components (Moogk, Hanley et al. 2007).

Ultimately, it is essential to be proficient at analyzing in real-time cell behavior and growth on a single cell level. This data can be correlated and connected with genetics, proteomics and other molecular biology techniques. Genome sequencing projects were intended to answer global biological questions, however with the reality of post-transcriptional modifications, such projects have resulted in endless amounts of convoluted experimental data which often cannot be directly understood and applied to cellular function. Combining more conventional cell biology techniques, such as proteomics, with long term live-cell imaging and cell tracking, allows for the identification of cellular changes in real-time that guide undifferentiated cells to different lineages.

Chapter 3 Proteomic analysis of calcium-CaM versus CaM-mutant binding proteins (BPs) and the *in vitro* characterization of CaM

3.1 Preamble

This chapter presents the findings from the study of the first proposed cellular system: calmodulin (CaM) in the differentiation of a human glioblastoma cell line. Specifically, this chapter outlines CaM affinity chromatography optimization, 2D DIGE design of experiments considerations and results, as well as the feasibility of delivering CaM into a brain tumour cell line.

3.2 Overview

Transient rises in intracellular calcium levels initiate most signaling cascades essential for processes such as cell motility, proliferation, differentiation and apoptosis. Calmodulin (CaM) is the major intracellular receptor of calcium and in all organisms in which the CaM gene was deleted, it was found to be essential. CaM regulates signaling through its binding to a diverse population of protein targets, called calmodulin-binding proteins (CaMBPs). Although known to be essential, it is believed that there are many CaMBPs which remain to be identified and understood at the cellular level. Here, CaM protein interactions are characterized by probing the binding proteome of calcium-CaM in comparison to the binding proteome of a CaM-mutant that mimics apo-CaM, a calcium-free-CaM. Affinity chromatography and 2D DIGE was used to compare the respective bindomes. Furthermore, using live-cell imaging and a cell penetrating peptide, trans-activating transcriptional activator (TAT), protein trafficking experiments were performed on calcium CaM to evaluate

the feasibility of CaM cellular delivery; which if accomplished, would extend the current knowledge of CaMs role in mammalian cells.

3.3 Introduction

CaM is a small ubiquitous calcium binding protein found in all eukaryotic cells. The protein features two lobes, an N- and a C-terminal domain connected by a flexible central linker region and each domain consists of two EF-hand calcium binding motifs. CaM is an essential regulator of cellular activity mediated by intracellular levels of calcium. Upon calcium signaling, the calcium ions bind to CaM causing a conformational change in the protein to a calcium bound form, termed calcium-CaM. The conformational change upon calcium binding results in the exposure of hydrophobic patches that bind hundreds of proteins, termed CaM binding proteins (CaMBPs), which control the activity of numerous cellular processes (Weljie, Yamniuk et al. 2003).

Apo-CaM is the calcium unbound form of CaM, therefore its protein binding is not dependent on calcium. The protein plays an important intracellular role in numerous signaling pathways and has several unknown target proteins (Jurado, Chockalingam et al. 1999). It was discovered much later than calcium-CaM, as a result its binding proteins (BPs) and its cellular role is much less well understood. Apo-CaM differs from calcium-CaM in its tertiary structure (Yamniuk and Vogel 2004). It has a more compact structure overall, in comparison to calcium-CaM that has an open, "relaxed" structure. Due to its hydrophilic nature, apo-CaM binds its BPs differently than calcium-CaM, utilizing IQ binding motifs and

noncontiguous binding sites (Jurado, Chockalingam et al. 1999; Vogel, Brokx et al. 2002; Houdusse, Gaucher et al. 2006).

For a complete literature review on CaM and its BPs see section 2.1 Calmodulin (CaM).

Studying CaM-dependent signaling cascades using proteomics coupled with live-cell imaging was proposed as a means to dissect CaMs cellular functions. Protein interactions were characterized using a purified calcium-CaM and a CaM-mutant, which had the four calcium binding sites mutated rendering it incapable of binding calcium to mimic apo-CaM. The identification of the relevant CaMBPs was performed by comparing the BPs of calcium-CaM to the BPs of the CaM-mutant using affinity chromatography and 2D DIGE. It was proposed that once the differentially bound CaMBPs were determined by 2D DIGE and identified using MS, an *in vitro* characterization of the two forms of CaM and their protein interactions would be completed using live-cell imaging and fluorescent microscopy.

Here, HPLC elution protocols were created and optimized, followed by affinity chromatography runs which confirmed protocol, technique and elution profiles. Preliminary 2D DIGE experiments were performed to understand a suitable design of experiments in which statistically valid results could be achieved through the use of this technology. Furthermore, preliminary i*n vitro* cell microscopy experiments were performed to evaluate the feasibility of cellular uptake of the CaM-TAT constructs. In these studies, calcium-CaM (labeled red) was introduced into various cells using the HIV-derived TAT-binding domain.

It was proposed that following uptake of the labeled CaM, the cells would be tracked over time using live-cell fluorescent video microscopy to record and study cell phenotype. Specifically, analysis of the relative distributions of the labeled forms of CaM was proposed, as well as CaMs cellular effect. ***The hypothesis behind this experimental plan was that mutations to the calcium binding sites of CaM would identify a new sub-population of CaMBPs which bind to the CaM-mutant at high affinities and upon cellular delivery, the CaM-mutant would perturb critical signaling pathways involved in cellular function.***

3.4 Experimental Materials and Methods

3.4.1 Affinity Chromatography

3.4.1.1 CaM expression, purification and mutation

Calcium-CaM and the CaM-mutant were provided by Dr. Guy Guillemette in the Department of Chemistry at the University of Waterloo. Calcium-CaM was purified following a previously published protocol with a few minor modifications (Gopalakrishna and Anderson 1982). The CaM-mutant, which was defective in calcium binding at all four of the calcium binding EF hands in both the C-terminal and N-terminal lobes was also purified following a previously published protocol (Sienaert, Nadif Kasri et al. 2002).

3.4.1.2 Porcine brain extraction

The fetal porcine brains were isolated by Dr. Douglas Wey at the University of Guelph. The brains, each weighing approximately 30g, were flash frozen and kept at -80C until the extract was prepared. Porcine brains were homogenized on ice in 200 mL of a solution containing

50mM Tris-HCl pH 7.5, 0.15M NaCl, 1mM DTT and protease inhibitor. Once the brains were homogenized until approximately 90% liquid, the homogenate was centrifuged at 20 000 rpm for 20 minutes. The supernatant was collected and sonicated on ice for 20 seconds three times. The sonicated solution was then clarified by centrifugation at 20 000 rpm for 30 minutes. After centrifugation, the supernatant was filtered through a 0.45 um filter, and protein concentrations were quantified using the standard Lowry method and aliquoted at approximately 10 mg/mL.

3.4.1.3 Packing

Following purification of the CaM proteins, the protein was coupled to N-hydroxysuccinimide (NHS) activated Sepharose 4 Fast Flow resin following the recommended standard procedures from GE Healthcare. Briefly, the proteins to be coupled (approximately 15 mg/mL resin) must be Tris free, therefore the CaM proteins were dialysed overnight against three changes of 0.1M $NaHCO_3$, 0.5M NaCl and 1mM $CaCl_2$. After dialysis and immediately before use, the NHS-activated resin was washed with 10-15 column volumes (60 mL) of cold 1mM HCl. The purified and dialysed CaMs were then mixed individually with the resin and rotated overnight at 4^oC. Following coupling overnight and prior to blocking non-reacted groups on the resin, the resin was left to settle and the supernatant removed. The supernatant protein concentration was promptly quantified using the Lowry method to confirm coupling efficiency. The coupling efficiency was determined as the ratio between the concentration of CaM in the supernatant before and after coupling with the resin overnight. Once the coupling was completed and confirmed, any non-reacted groups were blocked by adding 0.1M Tris-HCl pH 8.5, 0.5M NaCl for three hours. This resin

slurry was then washed four times with three column volumes (20 mL) of alternating between high and low pH buffers: 0.1M Tris-HCl buffer, 0.5M NaCl pH 8.5 and 0.1M acetate buffer, 0.5M NaCl pH 4.5. Prior to packing the columns, two additional washes of 0.1M Tris-HCl buffer, 0.5M NaCl pH 8.5 were performed and the pH was verified to be approximately 8.5. Once the resin was coupled to the protein, Bio Rad Bio-Scale MT5 Columns were packed using the manufacturers' slurry packing method. Briefly, the column was assembled without the upper end cap or upper bed support. Placing the column vertically, the slurry was slowly poured into the column and allowed to settle. The high pH buffer (0.1M Tris-HCl buffer, 0.5NaCl, pH 8.5) was first de-gassed and continuously used to keep the column wet while packing. When the columns were filled to the top with resin (approximately 5.7 mL total volume each) the upper assembly of the column was attached. When not in use, the columns were stored in 20% ethanol at 4^{o}C to prevent bacterial contamination.

3.4.1.4 Elution

Prior to use, the columns were equilibrated with 5 column volumes of 50mM Tris-HCl pH 7.5, 0.15M NaCl, 1mM $CaCl_2$. Affinity chromatography was performed by diluting approximately 150mg of porcine brain extract to 50 mL using 50mM Tris-HCl pH 7.5, 0.15M NaCl, 1mM $CaCl_2$, 1mM DTT and protease inhibitor. The extract was loaded using an external sample loop at 0.05 mL/min, allowing overnight incubation at 4^{o}C. Prior to the elution of the interacting proteins, the column was washed at 0.3 mL/min for ten column volumes with 50mM Tris-HCl pH 7.5, 0.15M NaCl, 1mM $CaCl_2$. Once washed, there were

two elution steps, a subsequent wash, a final elution step and a stripping step, each three column volumes at 0.5 mL/min. The first step was a calcium dependent elution using EDTA (50mM Tris-HCl pH 7.5, 0.15M NaCl, 5mM EDTA). EDTA is a calcium chelator therefore in the case of calcium-CaM, EDTA will chelate the calcium ions bound to CaM resulting in a reversal of the conformational change of CaM and elution of the bound interacting proteins. The next elution step was with 1M KCl. Any charge-charge interactions will be broken and proteins bound through electrostatic interactions are eluted. To avoid compromising the column following the KCl elution, the column was washed with 50mM Tris-HCl pH 7.5, 0.15M NaCl, 1mM $CaCl_2$. Once washed, the final elution step was performed using 0.1M NaOH. NaOH is such a strong base such that any proteins which were hydrophobically bound to CaM and therefore were not eluted by the EDTA or KCl elution steps, would be eluted. Lastly, to ensure there were no remaining bound proteins, the columns were stripped with 1M NaOH, washed with 50mM Tris-HCl pH 7.5, 0.15M NaCl, 1mM $CaCl_2$ and then water, followed by storage in 20% ethanol at 4^oC.

3.4.2 Differential In Gel Electrophoresis (DIGE)

3.4.2.1 Sample preparation

Protein samples of interest which were eluted from the CaM columns were quantified using the 2-D Quant Kit (GE Healthcare) and aliquoted into 50µg or 25µg. To remove urea and salt, the samples were cleaned-up using PlusOne 2-D Clean-Up Kit (GE Healthcare) and re-suspended in 10µl of DIGE lysis buffer.

3.4.2.2 Cy dye labeling

Protein samples were labeled using fluorescent Cyanine dyes 2, 3 and 5 developed by GE Healthcare for DIGE. Fifty micrograms of the two protein populations to be compared were each labeled with 200 pmol of amine reactive cyanine dye 3 or 5 freshly dissolved in anhydrous DMF. As a standard, twenty-five micrograms of the two protein populations to be compared, were combined and labeled with 200 pmol of amine reactive cyanine dye 2 freshly dissolved in anhydrous DMF. The three labeling reactions were incubated at room temperature in the dark for 30 min. The reactions were then terminated by the addition of 10 nmol lysine to each sample for 10 min in the dark. Rehydration buffer (8M Urea, 2M Thiourea, 2% CHAPS, 0.5% IPG Buffer 3-10, 13 mM DTT and bromophenol blue) was then used to mix the three labeled samples to a final volume of 450 µl prior to rehydration and iso-electric focusing.

3.4.2.3 Protein separation

In-gel sample rehydration was performed at room temperature for 20 hours using immobilized 24-cm linear pH 3-10 gradient (IPG) strips. The rehydrated strips were focused using an Ettan IPGphor II (Amersham Biosciences) for approximately 67 000 VhrT with a gradual voltage ramp to a maximum of 8000V for 18 hours. Focused strips were immediately equilibrated in two steps, reduction followed by alkylation, each for 15 min on a shaker in 15mL of 50mM Tris-HCl pH 8.8, 6M Urea, 30% (v/v) glycerol, 2% (w/v) SDS and 1% DTT (reduction) or 2.5% iodoacetamide (alkylation). Equilibrated strips were then loaded between 1mm thick 18x20cm 12.5% polyacrylamide poured gels with low fluorescence glass plates.

The strips were then overlaid with 0.5% (w/v) agarose in 1X running buffer (25 mM Tris, 0.2M glycine, 0.1% (w/v) SDS, pH 8.3) with 0.002 mg of bromophenol blue on a shaker. The gels were run in an Ettan Dalt 6 apparatus (GE Healthcare) at 5 W/gel for 30 min and then 20 W/gel at 15^{o}C until the dye front had reached the bottom of the gels.

3.4.2.4 Gel imaging and analysis

Gels were visualized using a Typhoon 9410 imager (Amersham Biosciences). For optimal resolution the gels were scanned at 100 μm pixel size. The photomultiplier tube was set to ensure maximum pixel intensity, 40 000-60 000 units. Once the gels were scanned, the scanned images were then cropped using ImageQuant 5.2 (GE Healthcare) to remove the boarder of the gels. The cropped images were analyzed using DeCyder 6.5 software (GE Healthcare). The estimated number of spots for detection was set to 2000. No area, volume or peak height exclusion filters were applied.

3.4.3 CaM-TAT coupling and cell culture treatment

The TAT-FITC peptide was purchased from ANASPEC (Fremont, California, USA). The CaM proteins (calcium-CaM and CaM-mutant) were coupled with the TAT-FITC peptide by Odi Israel, a master's student in Professor Guillemette's lab in the Chemistry Department, University of Waterloo. To achieve a reported 100% coupling efficiency the CaM proteins were devoid of Dithiothriotol (DTT) and Tris buffer were removed by gel filtration using a Sephadex G-25 PD-10 column (Amersham Biosciences) with a coupling buffer of 100 mM Phosphate buffer and a pH of 6.3. The CaMs (calcium-CaM and CaM-mutant) were then reacted with 4 fold excess TAT-FITC to CaM protein to ensure maximum coupling. The

reaction was carried out at room temperature on a shaker flask for 12 hours. The samples were then washed three times with deionized water using a 10 kDa cut-off spin column (Pall Scientific, USA) to remove excess unbound FITC-TAT. MS was performed on the samples to confirm FITC-TAT labeling of the CaM proteins. Human glioblastoma cells were obtained from the Peter Dirks laboratory University of Toronto, Ontario. The cells were adhered to the surface of poly-ornathane treated glass chambers which contained 500 μL of DMEM/F12 media. Each chamber was then incubated with one of the following constructs: TRITC, TAT-FITC, CaM-TRITC or FITC-TAT-CaM-TRITC, each with a concentration of 20 μM for 2 hours at 37°C. Following incubation, the cells were washed three times with 500 μL of media and imaged using 40X or 63X objective lens on a fluorescence microscope (Zeiss Axiovert 200M).

3.5 Results

In attempts to identify the CaMBPs of calcium-CaM and the CaM-mutant, CaM was coupled to resin and packed into columns at various densities. HPLC elution protocols were created and optimized, followed by numerous affinity chromatography experiments which confirmed protocol, technique and the expected elution profiles. Following the affinity chromatography optimization described next, several 1D gels were then completed, as well as 2D PAGE separation methods and conditions were established. Preliminary 2D DIGE experiments were completed to determine DIGE capabilities and limitations. Lastly, TAT-CaM mediated uptake into human glioblastoma cells was performed with inconclusive results.

3.5.1 CaM Affinity Chromatography Column Optimization

To understand the diversity of the porcine brain protein population to be loaded to the columns, a 400 µg preparative 2D gel was performed. **Figure 3-1** confirmed a large and diverse protein population to pass through the columns.

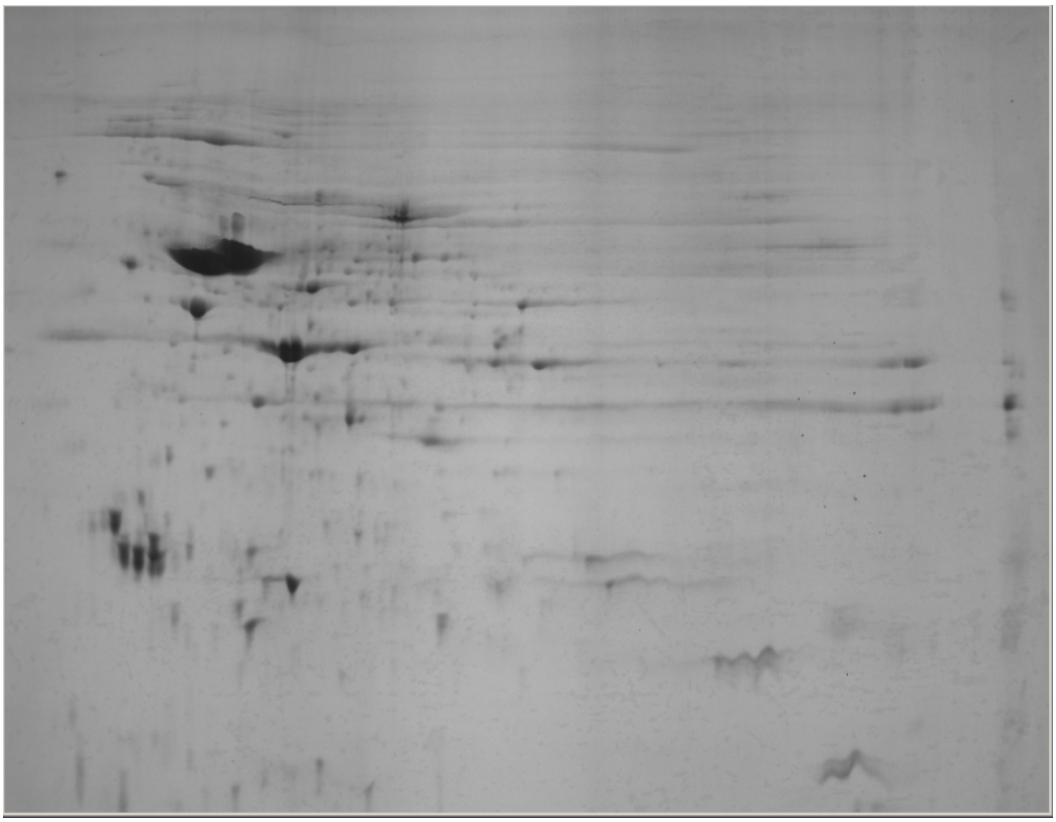

Figure 3-1: 2D gel of 400 µg of porcine brain extract pH range 3-10

Three column packings were studied, each with different experimental conditions which included increasing the amount of porcine brain loaded to the columns and increased concentrations of CaM coupling to the resin. **Table 3-1** outlines the conditions of each column packing.

Table 3-1: Summary of the three packing conditions

Packing Number	Porcine Brain Extract (mg)	CaM Coupling (mg/mL)
1	38	2.5
2	76	5
3	200	14

Establishing the techniques and protocols of the affinity chromatography was the focus of the first packing experiment. As outlined in **table 3-1**, a CaM coupling density of 2.5 mg/mL was evaluated with a loading 38 mg of porcine brain extract to each column. Following the elution protocol described in section 3.3.1.4, two fractionation peaks were obtained (a calcium-dependent and independent). **Figures 3-2** and **3-3** are the HPLC run profiles of the loading and elution of the calcium-CaM and CaM-mutant columns, respectively. Depicted is the porcine brain being continuously loaded into the column (0-50 mL on the x-axis), followed by a buffer wash (50-100 mL), an elution with EDTA at 105 mL, an elution with 0.1M NaOH at 130 mL and lastly a stripping elution with 1M NaOH at 155 mL. Each run was then terminated with a buffer wash followed by an ethanol wash prior to storage at 4^{o}C.

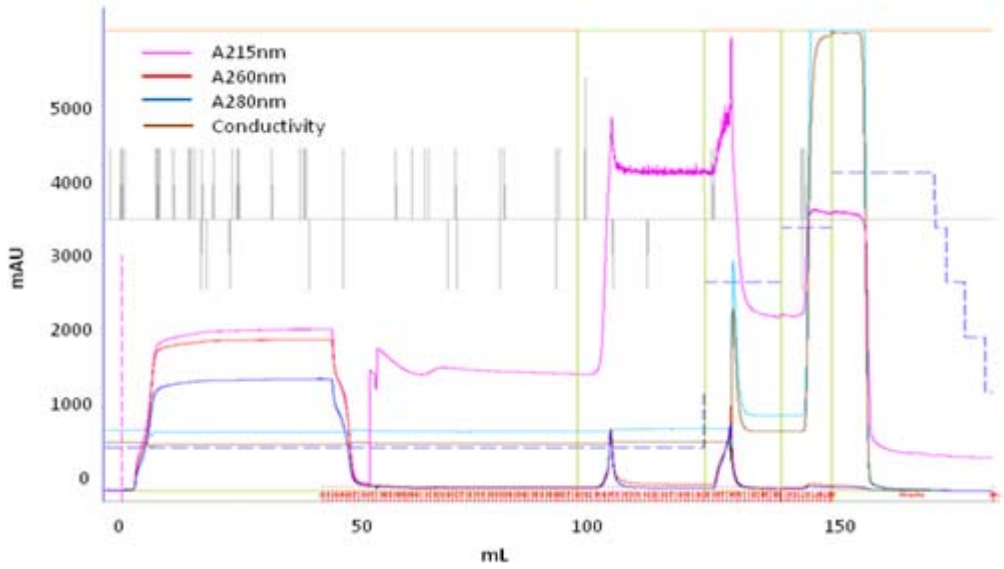

Figure 3-2: calcium-CaM first loading and elution profile using the elution sequence: EDTA, Buffer, NaOH. The blue line is A280nm and the pink line is A215nm. The first peak is calcium-dependent binding proteins. The second peak represents non-specific calcium-CaM binding proteins.

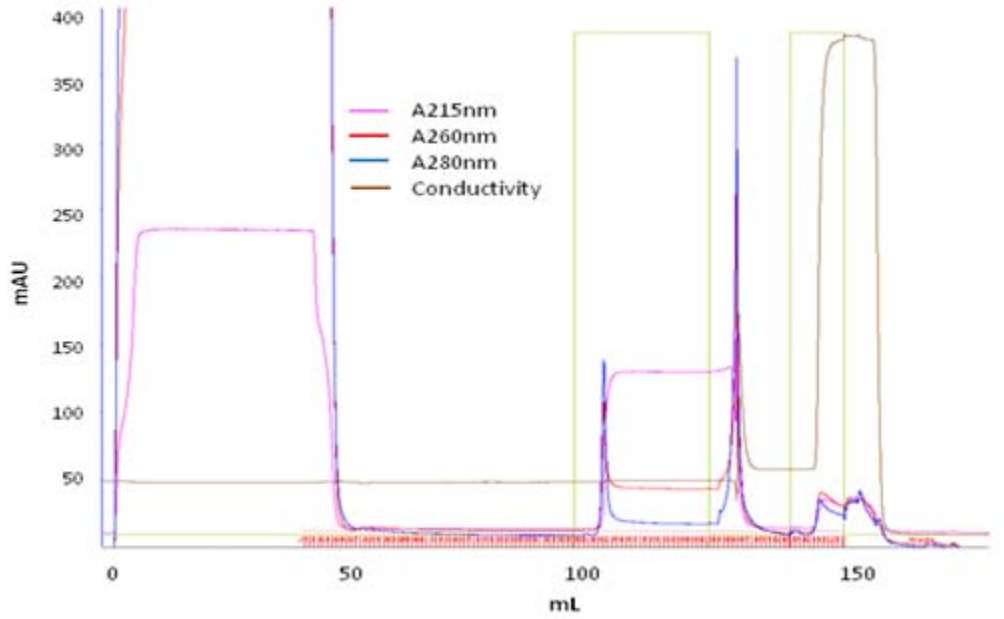

Figure 3-3: CaM-mutant first loading and elution profile using the elution sequence: EDTA, Buffer, NaOH. The blue line is A280nm and the pink line is A215nm. Two small peaks are evident, representing proteins bound to the CaM-mutant non-specifically and CaM-mutant binding proteins, respectively.

Comparison of the two HPLC profiles (**figures 3-2** and **3-3**) indicated that overall less protein had bound to the CaM-mutant column. To clearly show the peak heights, the absorbance scale on the y-axis in **figure 3-3** is much smaller than in **figure 3-2**. In specifically evaluating the two fractionation peaks at 105 mL and 130 mL in both figures, the magnitude of the calcium-CaM column peaks were both at approximately 750 mAU. However, both of the elution peaks from the CaM-mutant column were much less in magnitude in comparison to the calcium-CaM column. The EDTA peak of the CaM-mutant column was 150 mAU and the 0.1M NaOH elution peak was 375 mAU, 2.5 less than the EDTA peak of calcium-CaM. Although every attempt was made to couple and load equivalent amounts of CaM and porcine extract to both columns, these findings suggested that the CaM-mutant was coupled at a lower efficiency than the calcium-CaM column or that less porcine brain had been loaded to the CaM-mutant column or that the CaM-mutant has few CaMBPs in comparison to calcium-CaM.

Protein quantification of the 0.1M NaOH elution peaks of interest, further confirmed the difference between column runs. Approximately 350 μg and 75 μg of protein were eluted from each of the calcium-CaM and CaM-mutant 0.1M NaOH elution peaks, respectively. In evaluating the loading of the 50 mL of porcine brain in **figures 3-2** and **3-3**, the absorbance reading during loading of calcium-CaM column was near 1500 mAU. However, the absorbance reading during loading of CaM-mutant column was less than 1000 mAU. Although both runs were performed using the same protocol, this indicated that an inaccuracy had occurred in which less porcine brain was loaded onto the CaM-mutant

column. To determine if there were qualitative proteomic differences between the calcium-CaM and CaM-mutant binding protein populations, the EDTA and 0.1M NaOH elution peaks were separated using 1D gel electrophoresis, **figures 3-4** and **3-5** below. In order to optimize the number of lanes to be compared, no molecular standard was run. Comparison of the gels at both elution peaks (calcium-dependent and calcium-independent), revealed protein bands which were unique between columns (indicated by the small black arrows in **figures 3-4** and **3-5**). To determine if the 0.1M NaOH elution removed the majority of bound proteins after the EDTA elution, the final stripping elution of 1M NaOH was also evaluated using 1D-gels, **figure 3-6**. Both of the column gels showed a minimal amount of protein bands, indicating the two initial elution steps were effective at releasing the bound proteins.

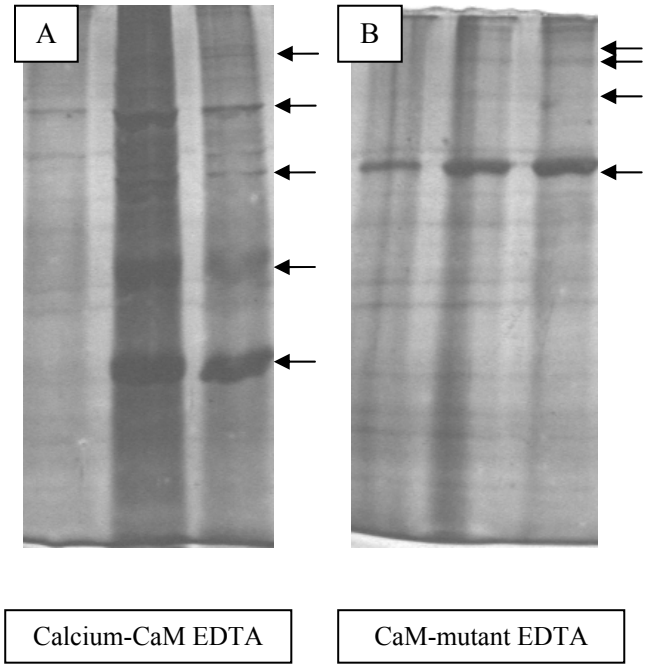

Figure 3-4: 1-D 12% SDS-PAGE analysis of EDTA peaks with arrows indicating differences in protein populations (A) Calcium-CaM column (B) CaM-mutant column. Each lane represents 10 µL from a 1mL collection sample during the elution peak.

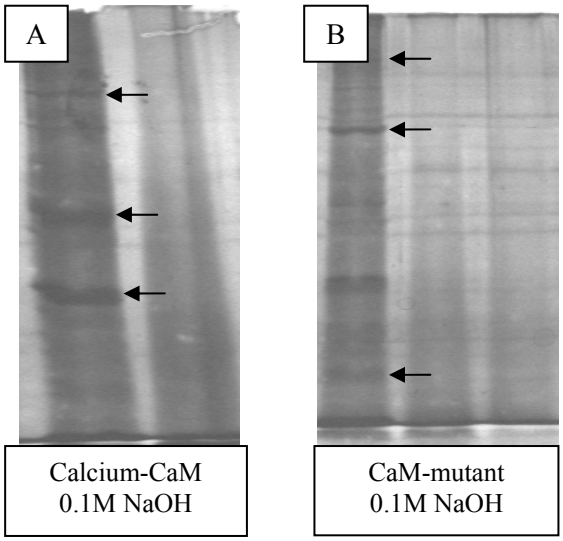

Figure 3-5: 1-D 12% SDS-PAGE analysis of 0.1M NaOH peaks with arrows indicating differences in protein populations (A) Calcium-CaM column (B) CaM-mutant column. Each lane represents 10 µL from a 1mL collection sample during the elution peak.

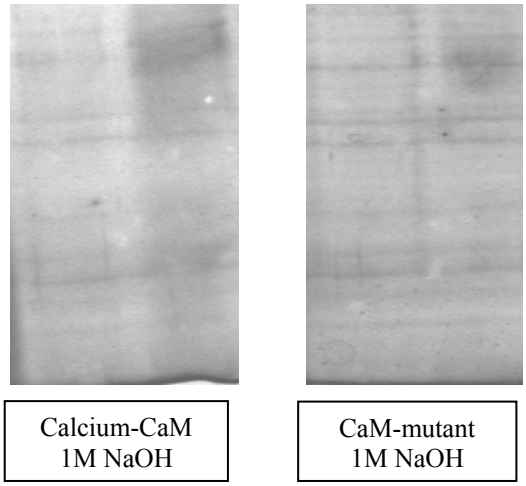

Figure 3-6: 1-D 12% SDS-PAGE analysis of 1M NaOH wash peaks. Comparable clear gels indicated the columns were effectively eluted using the previous EDTA and 0.1M NaOH steps. (A) Calcium-CaM column (B) CaM-mutant column. Each lane represents 10 µL from a 1mL collection sample during the elution peak.

The elution sequence of EDTA, 0.1M NaOH and 1M NaOH was confirmed to be an effective protocol for separating CaMBPs. However, the coupling conditions were not optimized to achieve sufficient yields of eluted protein to complete a comprehensive proteomic analysis which would include trials of 2D gel separation, followed by a 2D DIGE analysis. A combined 425 µg of total protein was eluted during the two 0.1M NaOH elution peaks, and the majority of this eluted protein was used in the 1D-gel analysis presented above. Based on this 1D-gel analysis it was concluded that there appeared to be proteomic differences in BPs to calcium-CaM in comparison to the CaM-mutant. However, to improve protein yields, re-coupling the columns at a higher CaM density in combination with ensuring that accurate and excess porcine brain extract was passed through the column, was necessary to complete a proteomic analysis.

Packing 2

In the second packing experiment, calcium-CaM and the CaM-mutant were coupled to the resin at two times the concentration (5 mg/mL) of the first packing experiments. Additionally, to ensure greater protein yields, the amount of porcine brain passed through the columns was increased by two times to 76 mg. **Figures 3-7** and **3-8** below are the overnight loadings of the porcine brain at 0.05 mL/min. Unlike during the first packing experiment, the loading profiles between both columns were consistent, with the absorbance remaining constant at approximately 2700 mAU.

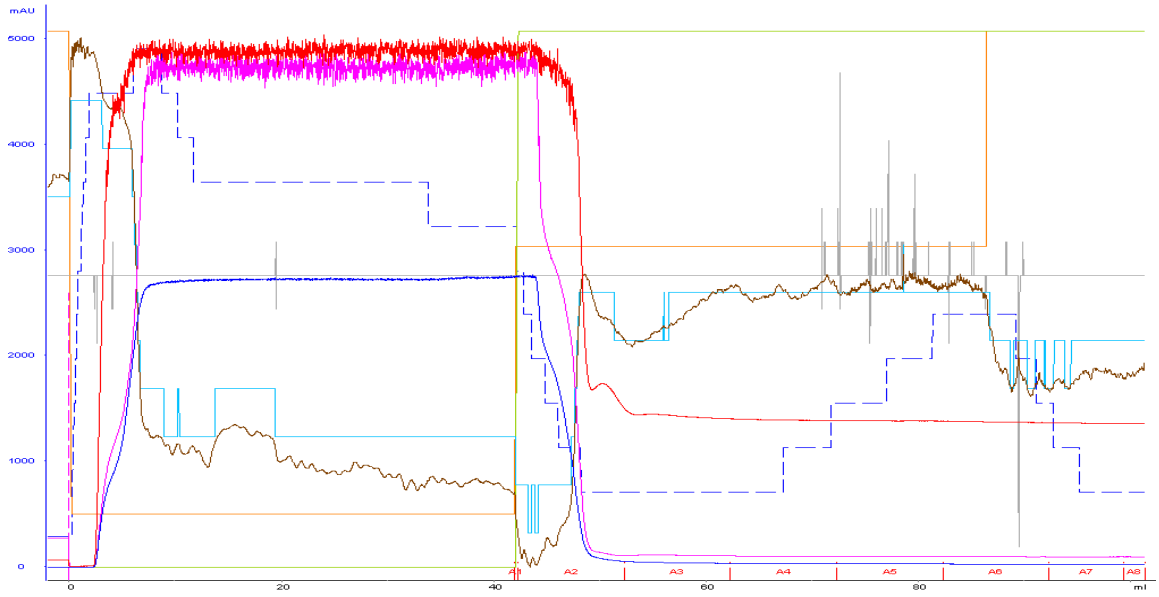

Figure 3-7: Second packing, calcium-CaM column loading. The blue line is A280nm, the red line is A260nm and the pink line is A215nm.

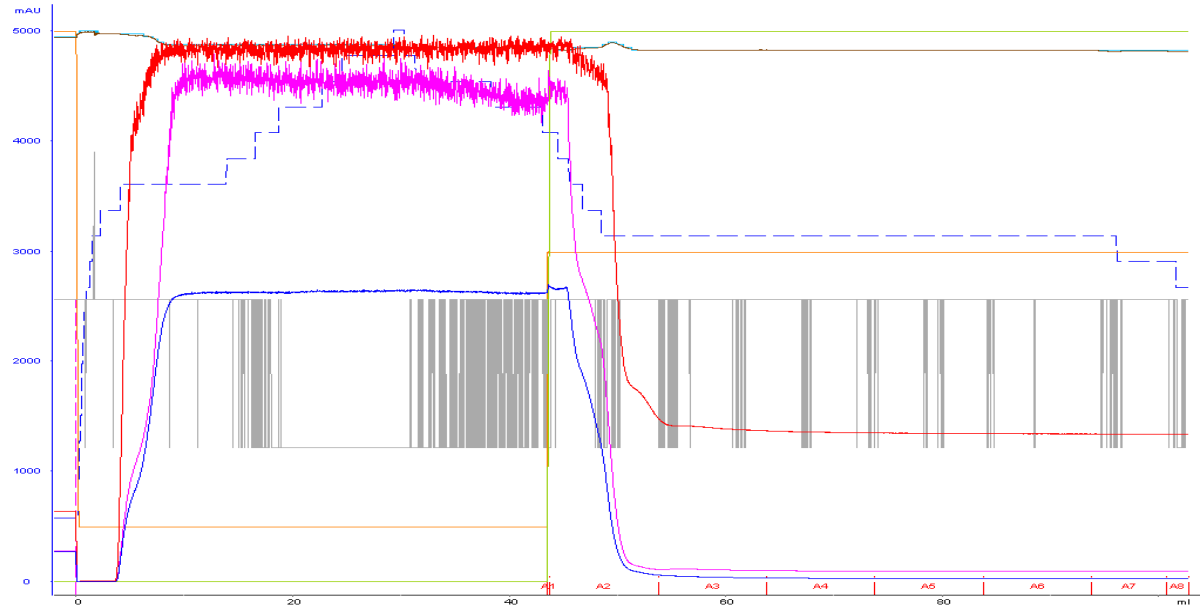

Figure 3-8: Second packing, CaM-mutant column loading. The blue line is A280nm, the red line is A260nm and the pink line is A215nm.

It was anticipated that increasing the CaM coupling density in combination with increasing the amount of porcine brain to be loaded to the columns, would ultimately result in greater protein elution for a proteomic analysis. **Figures 3-9** and **3-10** are the elution profiles for calcium-CaM and the CaM-mutant with the second packing conditions outlined above in **table 3-1**. Comparison of these two elution profiles with first two (**figures 3-2** and **3-3**), illustrated smaller elution peaks, qualitatively suggesting that increasing the amount of porcine brain to be loaded to the columns, in combination with an increased CaM coupling density, did not achieve greater protein yields. Quantification of the calcium-CaM and the CaM-mutant 0.1M NaOH elution peaks, revealed only 230 μg and 65 μg of protein was eluted from each column, respectively. This eluted protein (295 μg) was combined and used to determine optimal 2D-gel separation conditions. A 2D-gel with a pH range of 4-7 was first performed, however this range did not achieve clear protein separation, **figure 3-11**.

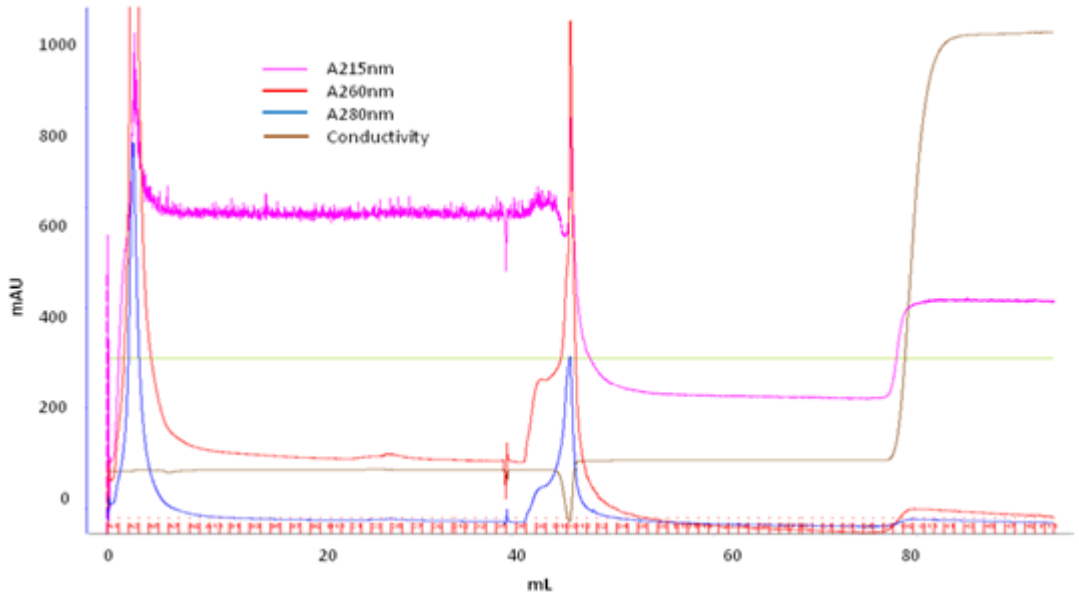

Figure 3-9: calcium-CaM second packing elution profile using the elution sequence: EDTA, Buffer, NaOH. The blue line is A280nm and the pink line is A215nm. The first peak is calcium-dependent binding proteins. The second peak represents non-specific calcium-CaM binding proteins.

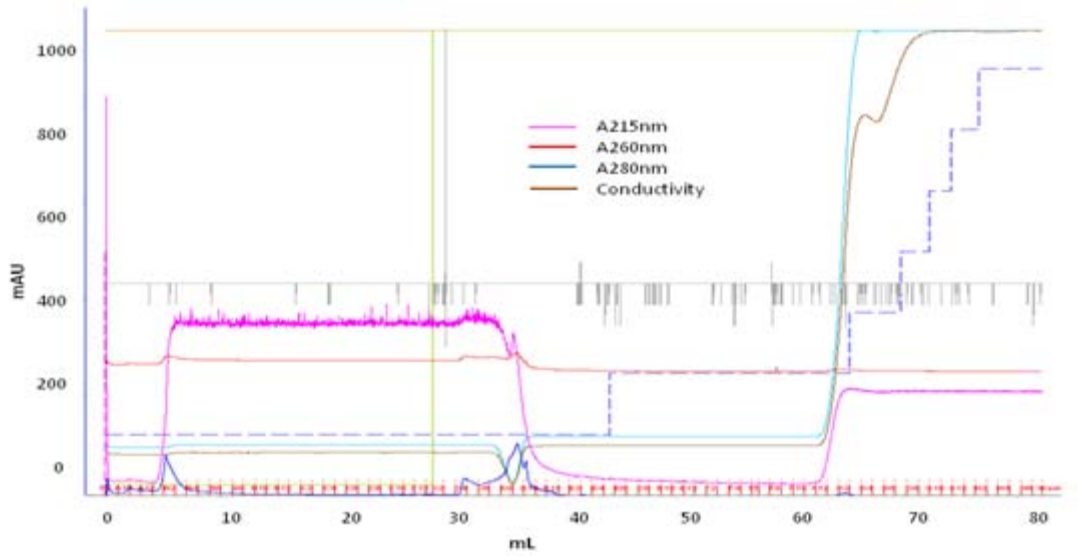

Figure 3-10: CaM-mutant second packing elution profile using the elution sequence: EDTA, Buffer, NaOH. The blue line is A280nm and the pink line is A215nm. Two small peaks are evident, representing proteins bound to the CaM-mutant non-specifically and CaM-mutant binding proteins, respectively.

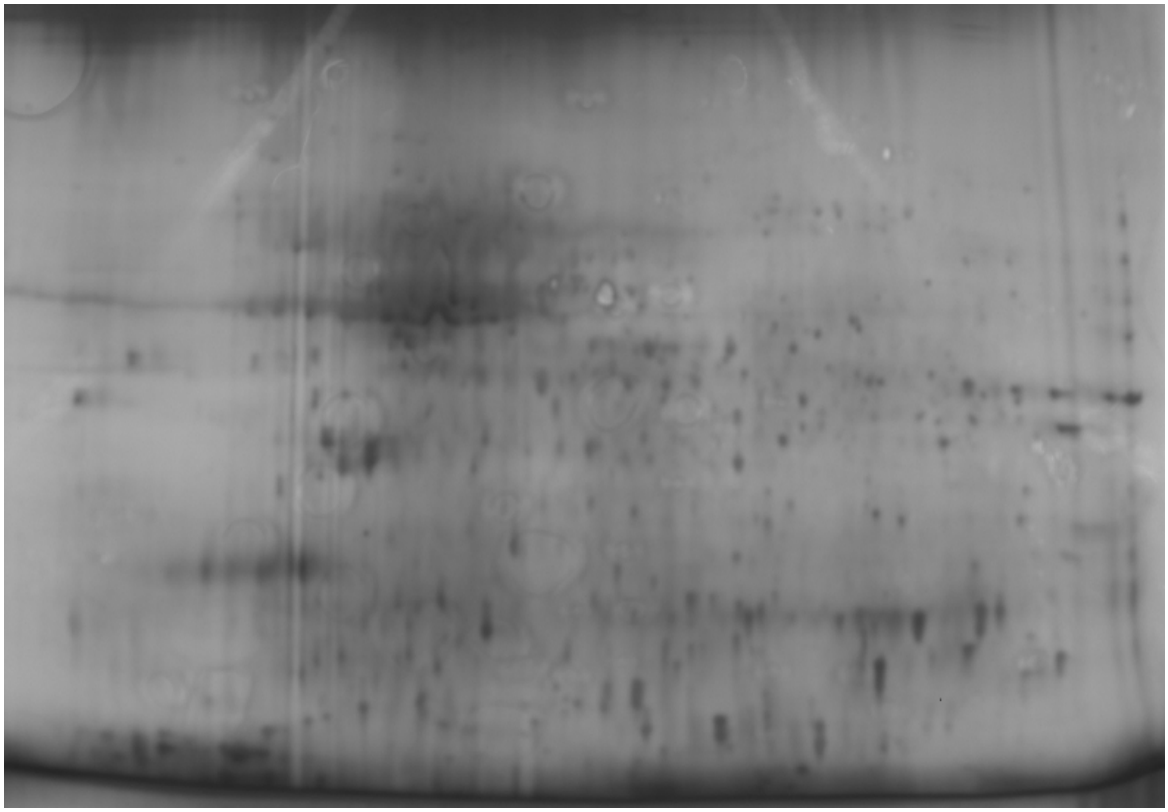

Figure 3-11: 2D 12% gel pH 4-7 of protein eluted during second packing of 0.1M NaOH peaks

Packing 3

The overall objective of the third packing was to increase the quantity of CaMBPs. This was achieved by increasing the coupling density of CaM and through loading excess porcine brain extract. Calcium-CaM and the CaM-mutant were coupled to the resin at approximately three times the concentration (14 mg/mL) of the second packing experiment. In addition, the amount of porcine brain passed through the columns was increased by five times, to 200 mg. **Figure 3-12** and **figure 3-13** show the overnight loadings of the third packing (200 mg of porcine brain at 0.05 mL/min). In comparing these absorbance readings during loading to the

second packing experiments, it was evident that twice the amount of porcine brain was loaded. In the second experiments (CaM packing 5 mg/mL, porcine brain loading 76 mg) the absorbance during loading was 2700 mAU. In comparison, in the third (packing 14mg/mL, porcine brain loading 200 mg) the absorbance during loading for both columns was 4700 mAU.

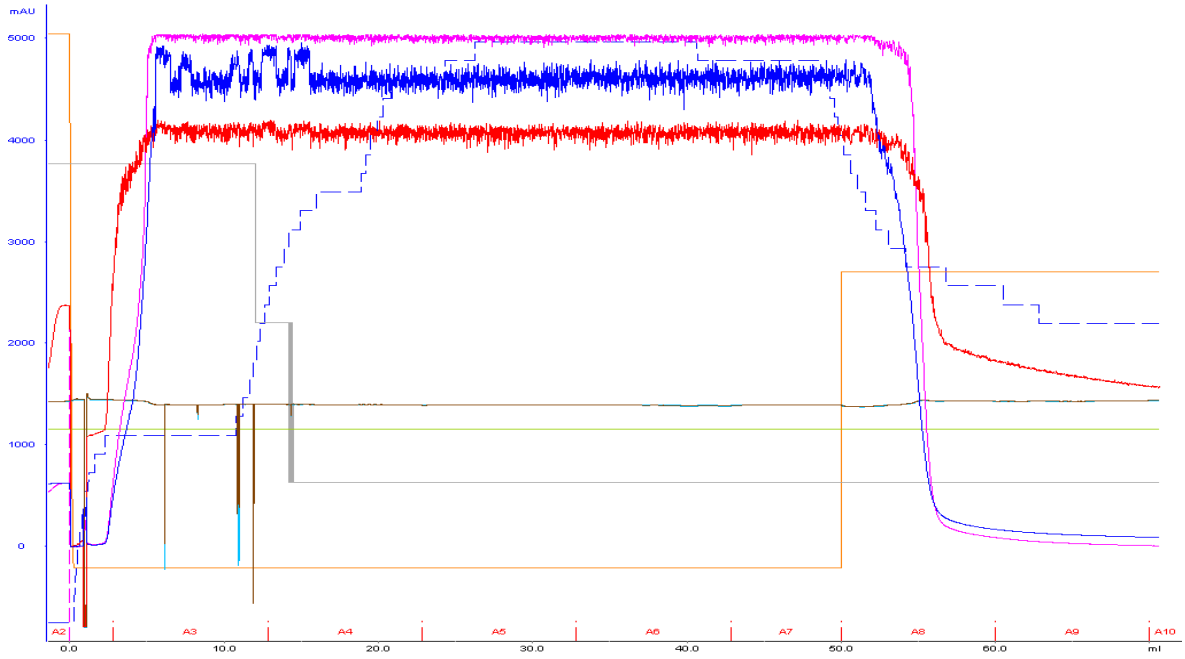

Figure 3-12: Third packing, calcium-CaM column loading. The blue line is A280nm, the pink line is A260nm and the red line is A215nm.

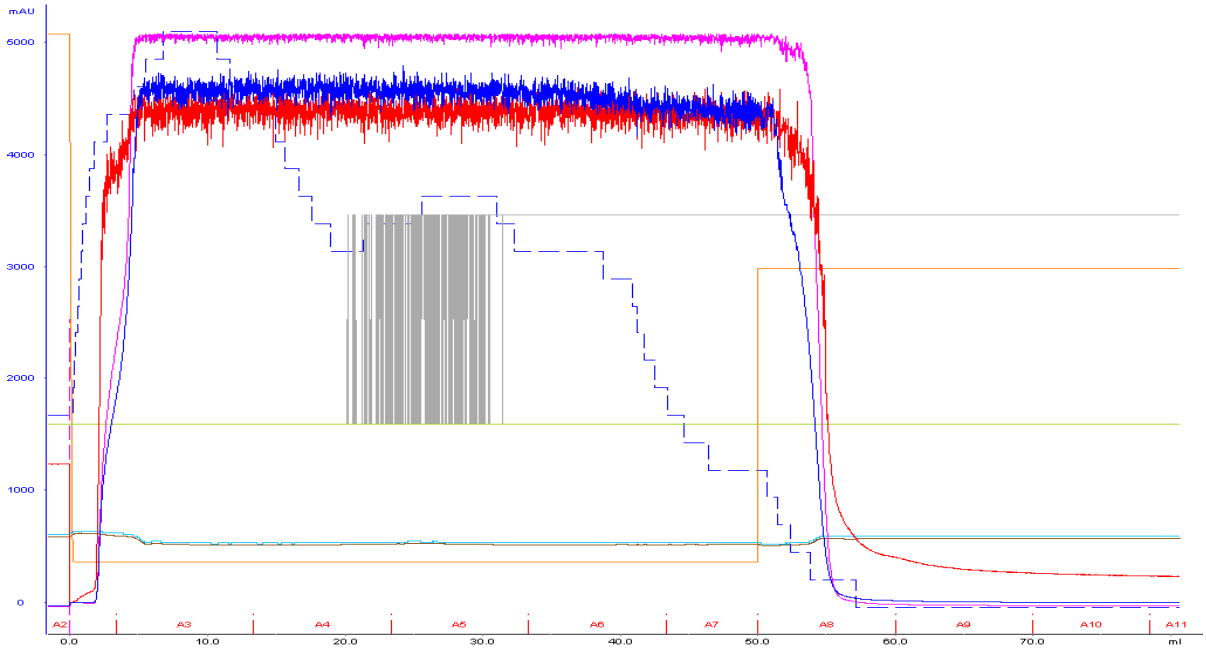

Figure 3-13: Third packing, CaM-mutant column loading. The blue line is A280nm, the pink line is A260nm and the red line is A215nm.

Following loading of the columns, the columns were eluted to fractionate and collect the CaMBPs. Although the EDTA followed by 0.1M NaOH elution sequence was found to be effective in the preliminary packing trials, an additional KCl elution step followed by a buffer wash was introduced in between the EDTA and 0.1M NaOH elution's to break any charge-charge interactions. To avoid compromising the column following the KCl elution, the column was first washed in Tris buffer and the final elution step was performed using 0.1M NaOH. **Figure 3-14** and **figure 3-15** are the elution profiles for calcium-CaM and the CaM-mutant with the third packing conditions.

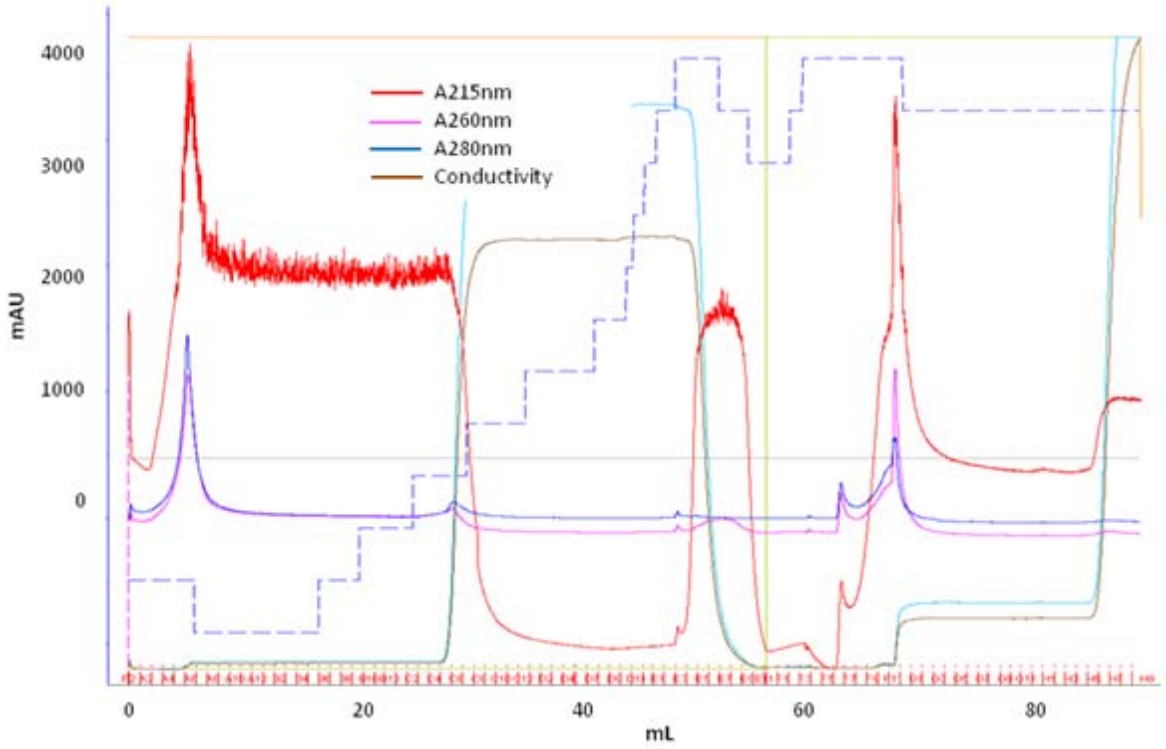

Figure 3-14: Calcium-CaM third packing elution profile using the elution sequence: EDTA, KCl, Buffer, NaOH. The blue line is A280nm and the red line is A215nm. The first peak is calcium-dependent binding proteins. At the introduction of the KCl, as well as at the introduction of the wash step which follows, two small peaks are evident, representing proteins bound to CaM by charge-charge interactions. The last peak represents non-specific calcium-CaM binding proteins.

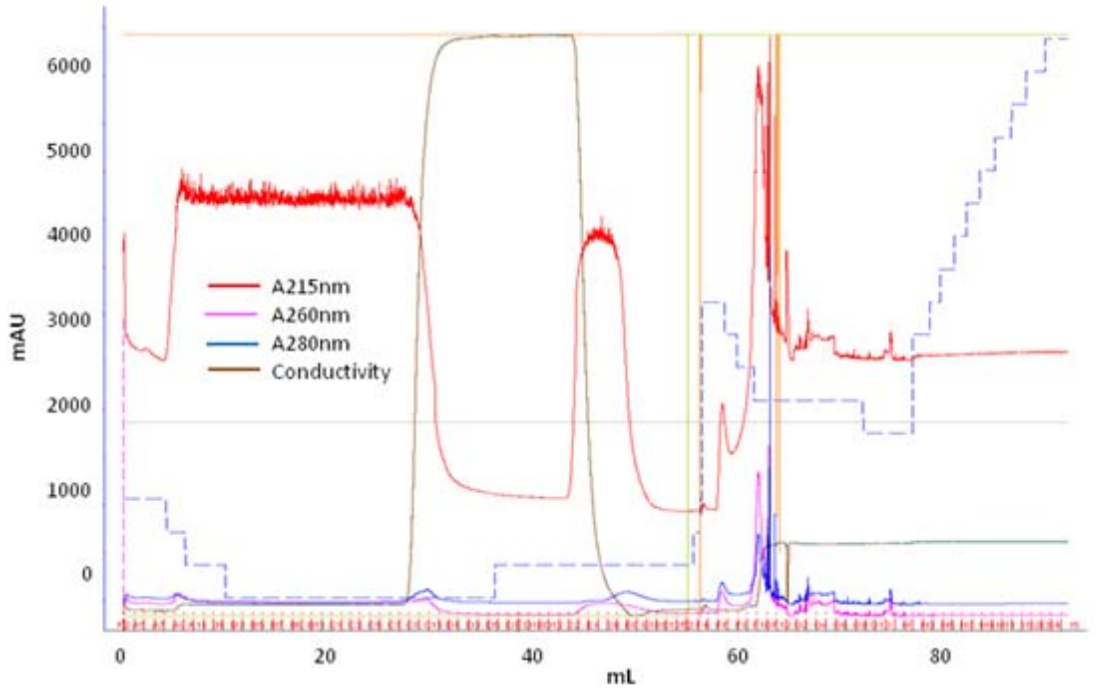

Figure 3-15: CaM-mutant third packing elution profile using the elution sequence: EDTA, KCl, Buffer, NaOH. The blue line is A280nm and the red line is A215nm. Three small peaks are evident, representing proteins bound to CaM-mutant non-specifically or by charge-charge interactions. The last larger peak represents specific CaM-mutant binding proteins.

It was anticipated that the introduction of the KCl elution step would further fractionate the interacting proteins based on the nature of binding. In evaluating the elution profiles at the introduction of KCl, as well as at the introduction of the wash step which follows, two small peaks were evident, representing proteins which were bound to CaM by charge-charge interactions. Furthermore, comparison of these two elution profiles with the previous (**figures 3-2, 3-3, 3-9, 3-10**) indicated similar elution profiles. However, illustrated are much larger elution peaks. Quantification of the calcium-CaM and CaM-mutant 0.1M NaOH elution peaks of interest, determined that 1550 µg and 350 µg of protein was eluted from

each column, respectively. Approximately six times more protein than the two previous run series was eluted, however the CaM-mutant column achieved much lower yields in comparison to the calcium-CaM column. This suggested that calcium-CaM binds a larger protein population than the CaM-mutant. Analysis of the affinity chromatography elution profiles and protein quantification of the elution peaks from all three packing experiments, concluded that the addition of the KCl elution step followed by buffer wash in between the EDTA and 0.1M NaOH elutions, was an effective protocol for further fractionating the CaM BPs. In addition, the CaM coupling density of 14 mg/mL, in combination with loading 200mg of porcine brain, resulted in the necessary yields to perform a 2D DIGE analysis. A summary of the three column packing results is found in **Table 3-2** and **3-3**.

3.5.2 Analysis of Re-Using the CaM Affinity Chromatography Columns

Once the CaM coupling density, quantity of porcine brain extract and elution method were optimized to yield quantities of protein which would be adequate to complete a 2D DIGE analysis, the columns were re-loaded and re-used for two additional runs. It was theorized that these optimally packed columns could be re-used to establish three replicates, the minimum replicate requirement for a 2D DIGE analysis. Once the two columns were re-used three times each with the same elution sequence, a comparison of the calcium-CaM run elution profiles, **figure 3-16** below, revealed the column performed repeatability, however the non-specific binding increased with column use. Similarly, comparison of the three

Table 3-2: Summary of the elution's (mAU) for each packing experiment. The 280 absorbance of the peaks (relationship to quantity of protein) increased as the porcine brain extract and CaM coupling densities were optimized.

			Loading Abs (mAU)		EDTA Peak 280 Abs (mAU)		0.1M NaOH Peak 280 Abs (mAU)	
Run Series	Loaded Porcine Brain Extract (mg)	CaM Coupling (mg/mL)	Calcium-CaM	Apo-CaM	Calcium-CaM	Apo-CaM	Calcium-CaM	Apo-CaM
1	38	2.5	1500	1000	750	750	140	350
2	76	5	2700	2700	725	300	100	100
3	200	14	4700	4700	1500	500	100	750

Table 3-3: Summary of eluted protein (µg) for each packing experiment and the end use of the protein. A CaM coupling density of 14 mg/mL, in combination with loading 200 mg of porcine brain, resulted in sufficient yields to perform a DIGE analysis.

			0.1M NaOH Eluted Protein (µg)		End Use
Run Series	Porcine Brain Extract (mg)	CaM Coupling (mg/mL)	Calcium-CaM	Apo-CaM	
1	38	2.5	350	75	1-D Gels
2	76	5	230	65	2-D Gels
3	200	14	1550	350	DIGE

elution profiles from re-using the CaM-mutant column, **figure 3-17**, indicated the same trend. In both figures, the 0.1M NaOH elution peak increased with use, perhaps due to degradation from the harsh 1M NaOH wash stripping step used at the end of each run. The EDTA elution peaks on the CaM-mutant column were ten times smaller than the calcium-CaM EDTA peaks and less BPs were eluted since its protein binding is calcium independent.

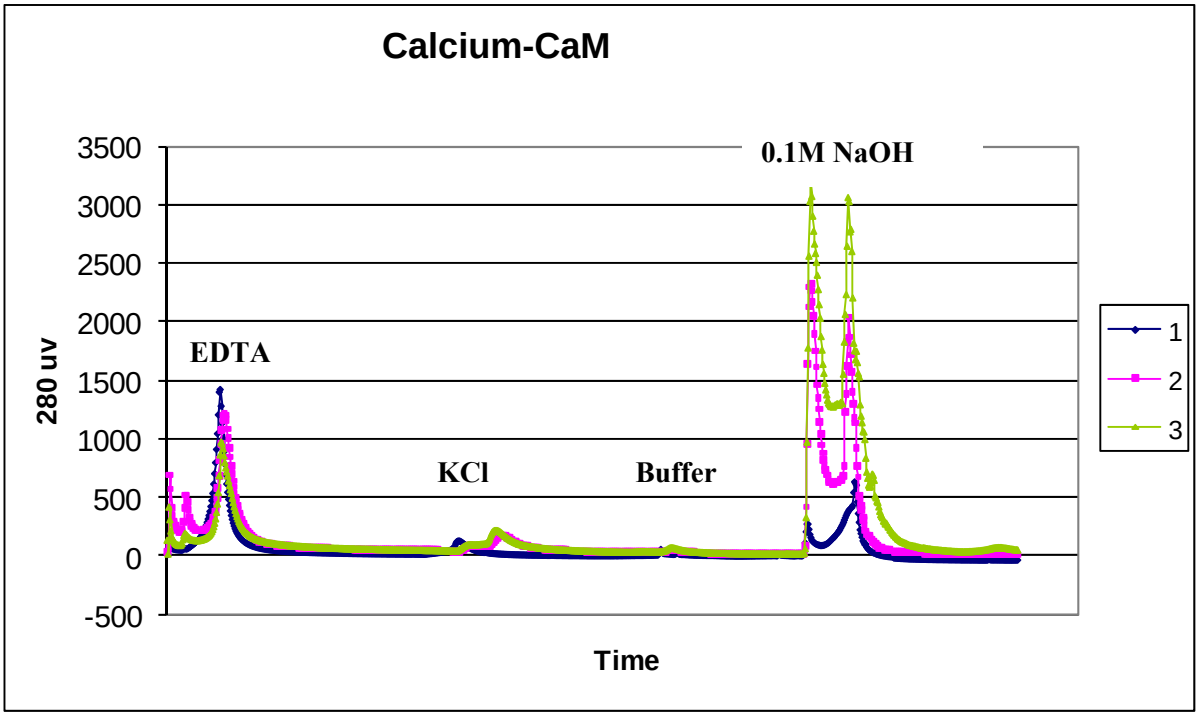

Figure 3-16: Analysis of re-using the calcium-CaM column once optimized. The elution profiles of three successive runs are overlaid for comparison. The column performed repeatability however the non-specific binding increased (0.1M NaOH peak) as the column was used.

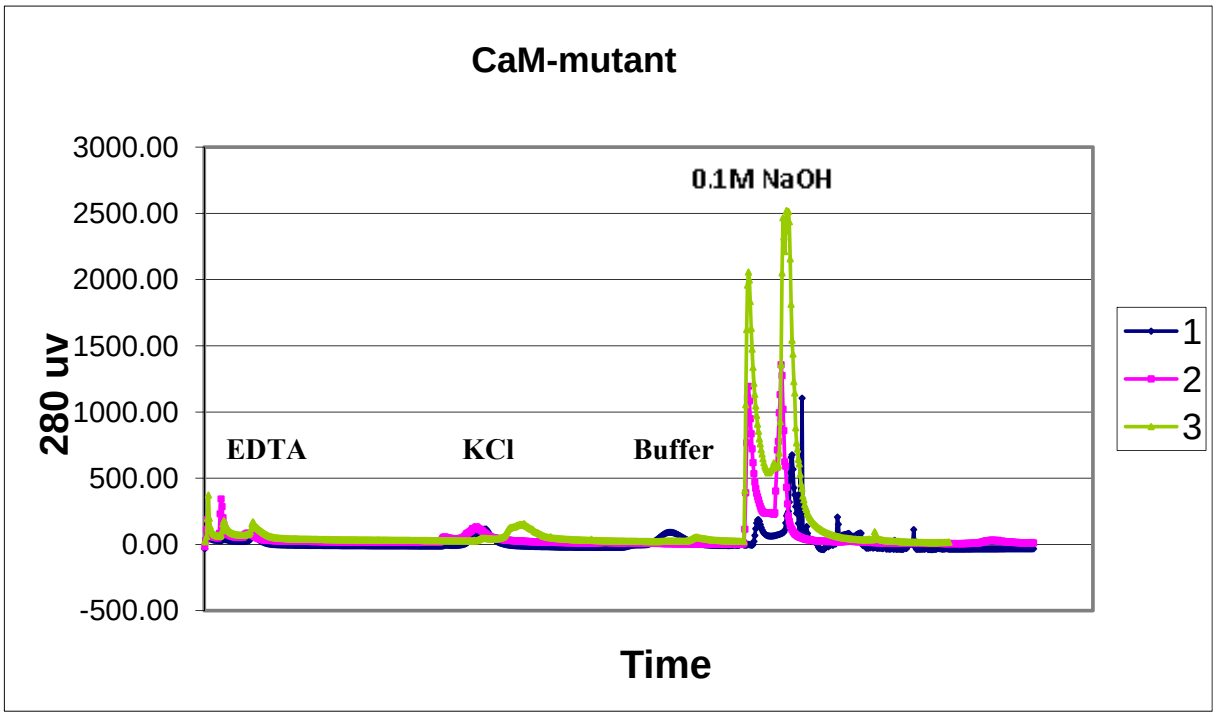

Figure 3-17: Analysis of re-using the CaM-mutant column once optimized. The elution profiles of three successive runs are overlaid for comparison. The column performed repeatability however the non-specific binding increased (0.1M NaOH peak) as the column was used.

3.5.3 DIGE Analysis of Eluted CaM binding proteins

To achieve statistical inference from 2D DIGE, a minimum of three gels are required. Therefore, if obtaining replicates is limited, either three technical replicates could be incorporated into the design of experiments, or three biological replicates. When initially designing the experiment, it was thought that through re-using the columns to achieve replication, technical replicates would be obtained. However, comparative analysis of the three elution profiles for each column, determined that the 0.1M NaOH peak of interest

increased substantially with each run (**figures 3-16 and 3-17**). As discussed in the previous section, it is believed that this was due to an increase in the non-specific binding of the porcine brain proteins to the columns. Since technical replicates are considered to be repeat measurements on the same biological sample, the repeat column runs did not represent technical replicates as the elution's (measurements) were not repeatable. Technical replicates ideally have small variation between samples, however based on the elution comparative analysis, the non-specifically bound BP expression levels and perhaps overall protein populations would have large variation between column runs.

Biological replicates are different biological samples from the same treatment group. Although each elution peak was obtained from loading the columns with the same pooled sample of porcine brain, the column replicates represented more similar to biological replicates than technical replicates. Biological replicates have greater variability within the same treatment group, similar to the columns having variation between runs on the same column. Using a replicate design of experiments discussed in Section 2.6.2.2 DIGE Experimental Design, three 2D DIGE gels were processed in which each column run represented a replicate. The replicates however did not represent a true technical or a true biological replicate. **Figure 3-18** shows a schematic of the design of experiments. One of the main limitations of this experimental design was the limited number of replicates. As there are many technical challenges (discussed previously) related to 2D gel separation and protein transfer, there is potential to not obtain statistically valid results. For example, in this 2D

DIGE experiment, one gel ran unsuccessfully, therefore only two gels were analyzed and no statistical inference was possible.

The two gels analyzed (runs 1 and 2) identified a proteomic difference between the BPs of the CaM-mutant and calcium-CaM with a large fold change range of 2-10. However, these results have no statistical confidence associated with the findings since they are based on only two column runs. Therefore, no proteins were chosen for MS identification. **Figure 3-19** shows a 2D DIGE ImageQuant gel with separation of the CaM binding proteins. As an example, **figure 3-20** is a protein spot comparative representation from the DeCyder analysis of a protein detected with an approximate 2 fold change. Thirteen proteins were detected (highlighted in pink) with a proteomic difference between the BPs of the CaM-mutant and calcium-CaM columns, however of the 13 spots detected, only 6 would be feasible to pick for MS identification if proven to be statistically valid.

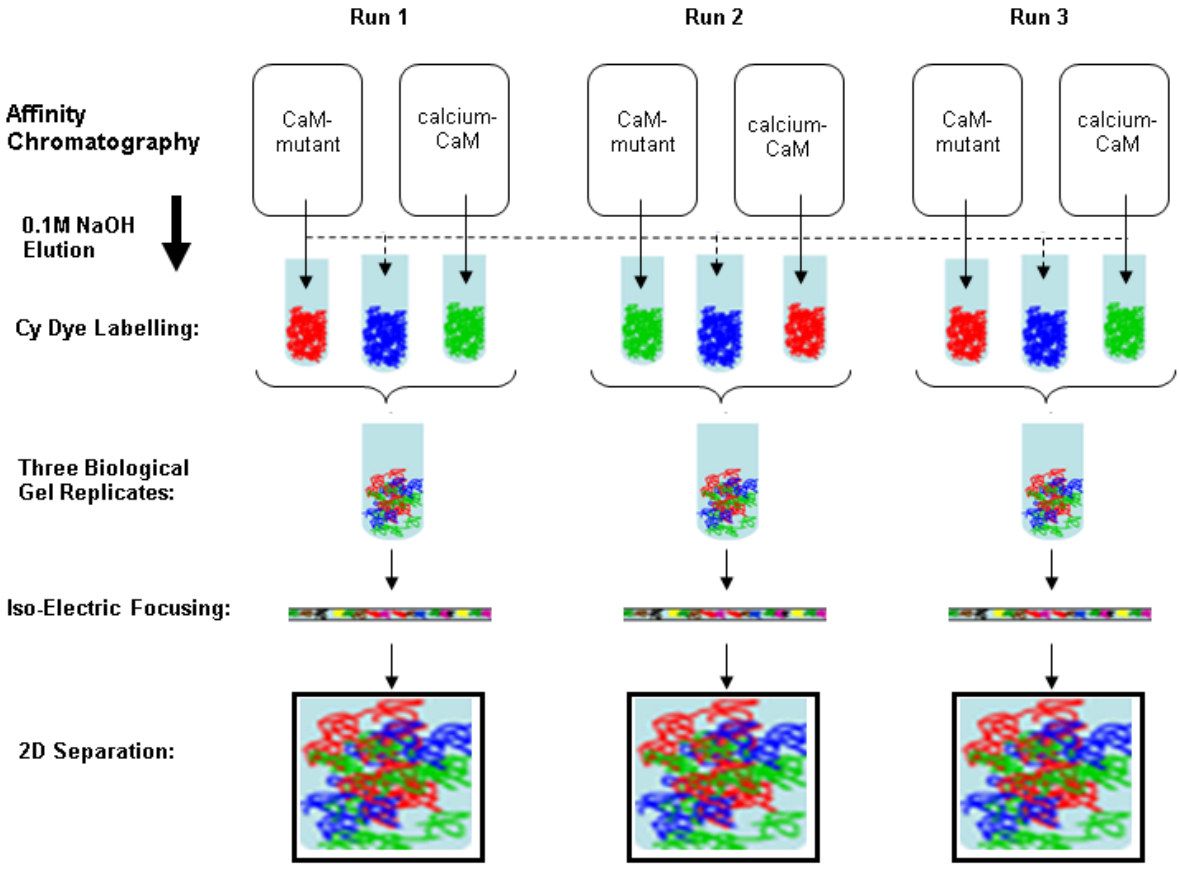

Figure 3-18: CaM Affinity Chromatography DIGE Design of Experiments. 3 DIGE gels were processed in which three different column packings represented a biological replicate.

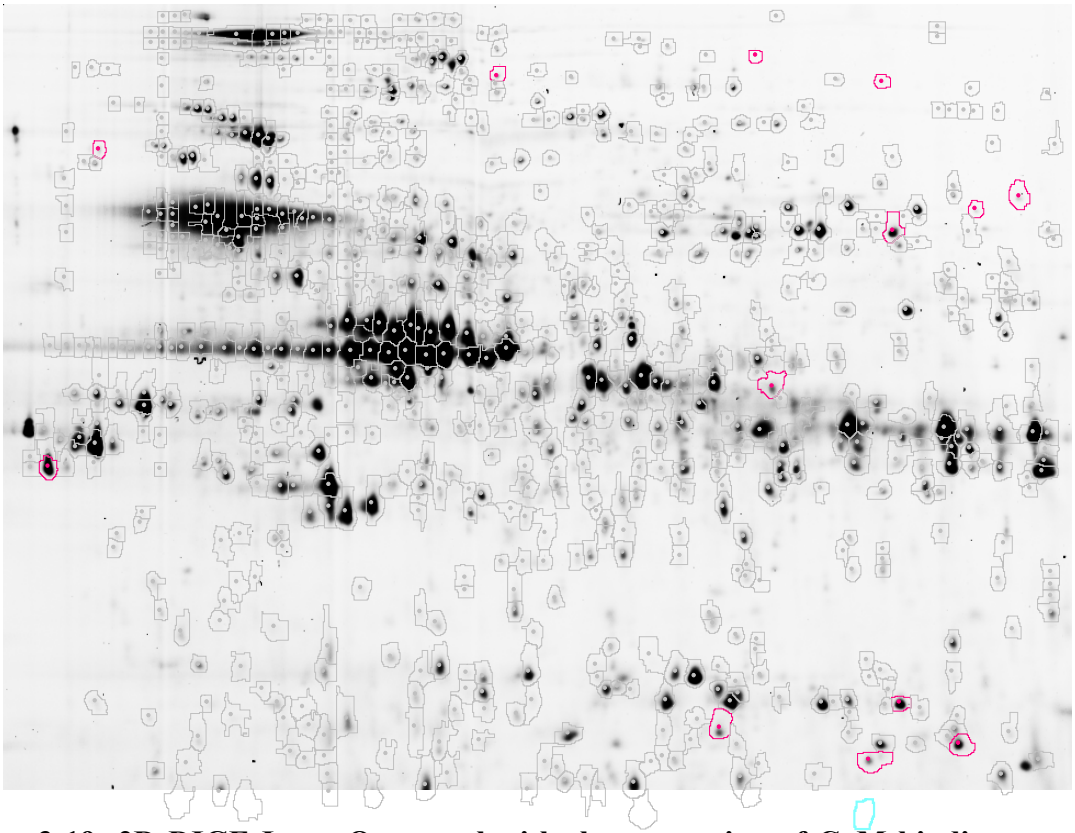

Figure 3-19: 2D DIGE ImageQuant gel with the separation of CaM binding proteins. Thirteen proteins outlined in pink had a fold range of 2-10 between the two columns.

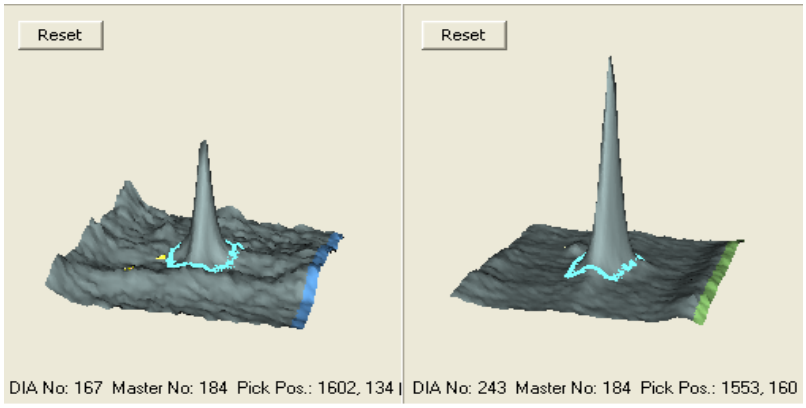

Figure 3-20: Protein spot comparative representation from DeCyder of a CaM binding protein detected with an approximate 2 fold change.

3.5.4 CaM-TAT Mediated Uptake

Following the affinity chromatography and DIGE experiments, TAT-CaM mediated uptake into human glioblastoma cells was studied using fluorescent microscopy. These preliminary i*n vitro* cell microscopy experiments were performed to evaluate the feasibility of cellular uptake of the CaM-TAT construct. In these studies, the calcium-CaM was labeled with TRITC (red) and disulfide bond linked to the HIV-derived TAT cell penetrating peptide which was labeled with FITC (green). It was proposed that following up-take of the labeled CaMs, the cells would be tracked over time using live-cell fluorescent video microscopy to record and study cell phenotype, specifically the state of differentiation of the human glioblastoma cells, and the cellular distribution of CaM.

Prior to evaluating the full TAT-CaM construct, TAT-FITC, FITC and TRITC were imaged in separate chambers after two hours of incubation with 20 μm of each sample (**figures 3-21 and 3-22**). The TAT-FITC signal was punctate and observed on every cell. This initially suggested that TAT had penetrated the cell membrane and was internalized. As discussed in the literature review, although TAT has been established as a cell penetrating peptide capable of penetrating various cell types, there has been an emergence of evidence suggesting that the peptide is not capable of penetrating many cell types. It is proposed that differing membrane compositions interfere with TAT uptake (Fonseca, Pereira et al. 2009). It is important we acknowledge that it was not confirmed with certainty if the TAT-FITC construct was internalized or if the observed signal was an artifact of nonspecific interactions between TAT-FITC and cell membrane constituents as confocal microscopy was not employed. It was

however confirmed that the detected green punctate signal was not due to excess non-specific FITC interaction or excess free FITC (**figure 3-21**). As an additional control, TRITC, the fluorophore used to label CaM was also evaluated for non-specific binding. Despite the notion that TRITC is impermeable to the cell membrane, non-specific emission was detected even after three wash steps in PBS (**figure 3-21**).

Although TRITC was found to bind non-specifically to the human glioblastoma cells, the full CaM-TRITC-TAT-FITC construct was incubated with the cells for 2 hours at 37^{o}C to evaluate the distribution and co-localization of TAT and CaM. Both fluorophores were colocalized with punctate emission signals (**figure 3-22**). This suggested that the disulfide bond used to link the TAT-FITC and CaM-TRITC constructs was not broken and that the full construct was bound to the cell membrane, as the disulfide bond would have been reduced once inside the cell. It has been reported that thiol/disulfide exchange reactions can occur between cell penetrating peptide residues and thiols on the cell-surface (Aubry, Burlina et al. 2009). Therefore, it is possible that the TAT-FITC peptide used in this study may be interacting with cell membrane thiol groups via a cysteine residue, leading to its binding to the cell membrane.

Overall, the results of cellular uptake of the full CaM-TAT construct into the human glioblastoma cells was inconclusive. Although punctate cellular signal was detected, it was not confirmed if the construct was intracellular or membrane bound. Additionally, the

detected non-specific TRITC signal in the TRITC only control rendered all obtained results disputable since CaM localization could not be confirmed.

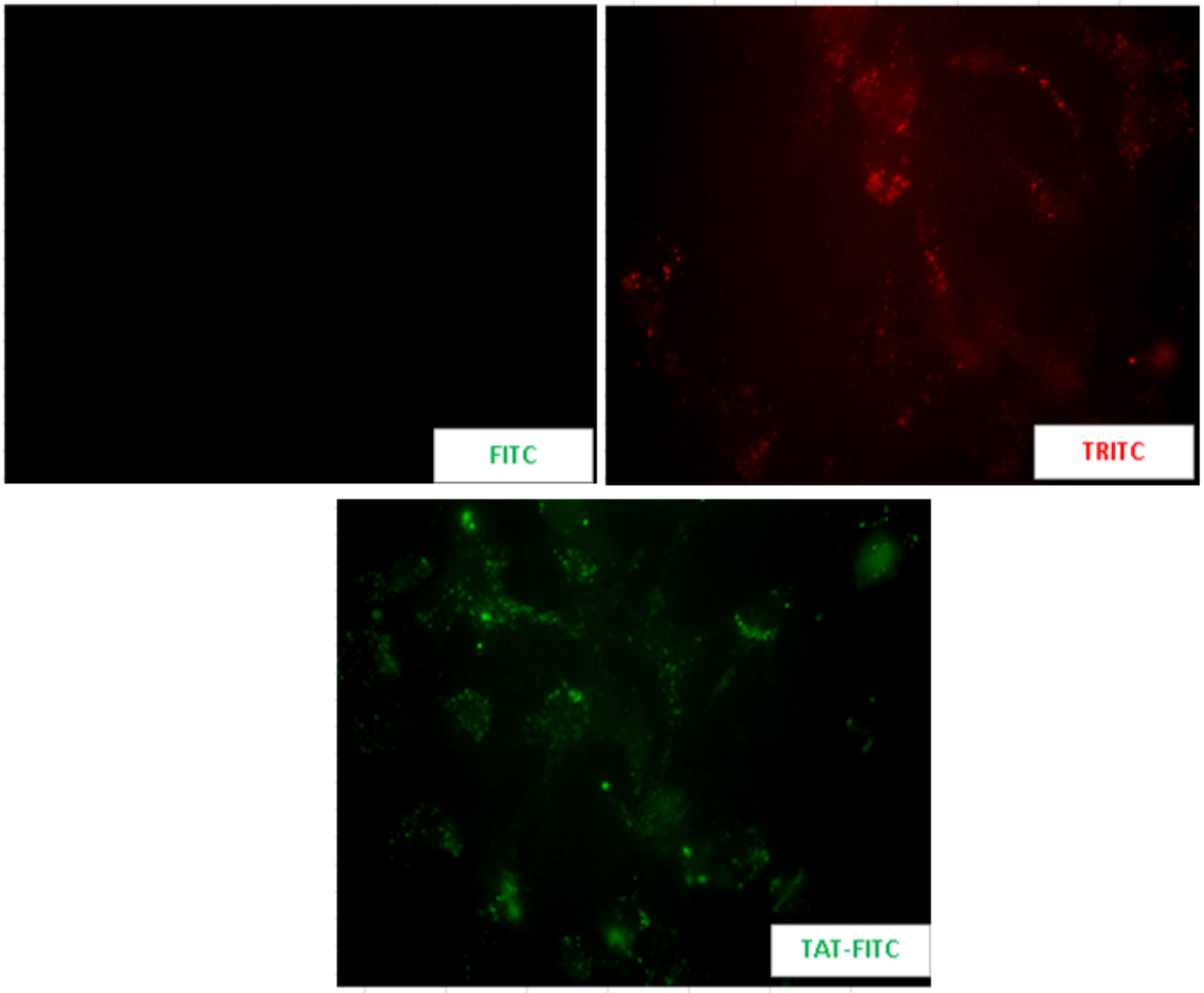

Figure 3-21: 40X fluorescent images two hours after 20µm FITC-TAT, FITC and TRITC incubation.

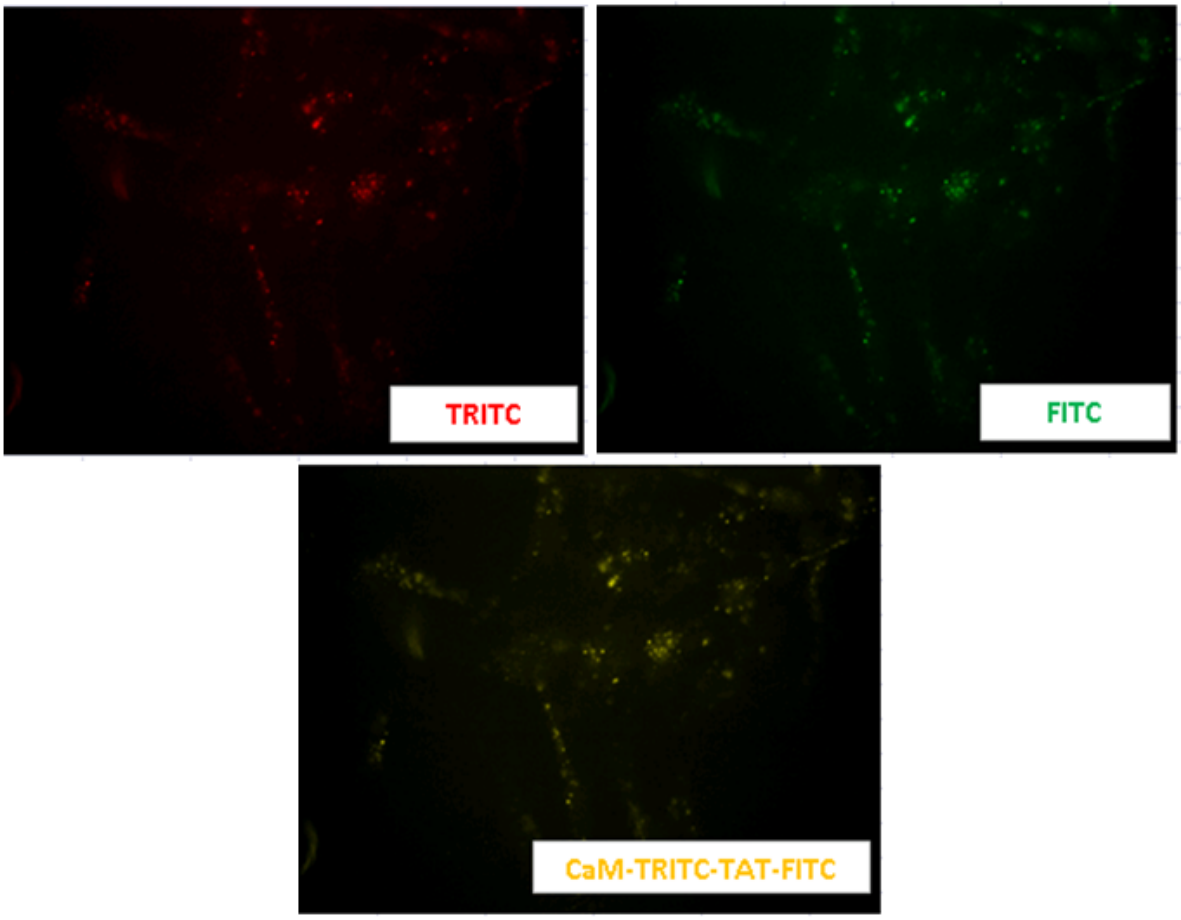

Figure 3-22: 40X fluorescent images two hours after 20µm CaM-TRITC, TAT-FITC and CaM-TRITC-TAT-FITC incubation.

3.6 Discussion and Conclusions

CaM cycles between its calcium-bound and calcium-free states binding different proteins based on its conformation. The BPs of the two primary forms of CaM, calcium- bound and apo-CaM, were studied using purified calcium-CaM and a purified CaM which was mutated to mimic apo-CaM. CaM protein interactions were isolated and characterized by comparing calcium-CaM BPs to the CaM-mutants using affinity chromatography and 2D DIGE. Eluting

sufficient protein from the columns to perform proteomic techniques, including 1D and 2D gel electrophoresis followed by 2D DIGE, was an initial constraint in completing a successful proteomic analysis. Three affinity chromatography packing trials were performed with increasing CaM coupling densities and amount of porcine brain extract passed through the columns.

In the first set of affinity chromatography experiments, the NHS-resin and CaMs were coupled and packed effectively, however at a low packing density of 2.5 mg/mL. Although two fraction peaks were obtained (**figures 3-2 and 3-3**), a limited quantity of protein was eluted. A 1D-gel analysis (**figures 3-4, 3-5, 3-6**) consumed all of the eluted protein and qualitatively confirmed proteomic differences between calcium-CaM and the CaM-mutant BPs. In contacting the supplier, it was recommended that the ligand density for CaM to the NHS-resin be 5 mg/mL. Therefore, in the second series of runs a packing density of 5 mg/mL was employed and double the amount of porcine brain was loaded to the columns. The results remained promising, as the elution peaks were greater than the first run series (**figures 3-9 and 3-10**), as well as the coupling, packing, elution and collection methods were determined to be repeatable. However, the eluted protein was consumed performing a 2D gel optimization which was necessary to achieve clear separation to perform a 2D DIGE analysis.

It is believed that the insufficient amounts of CaMBPs eluted from the columns was due to either not all the CaM being coupled efficiently to the resin, or since theoretically only the

proteins which interact with CaM will bind and be eluted, this may have been a small quantity of protein in the mg's of porcine brain extract being loaded to the columns. Consequently, for the third run three times the CaM coupling density was utilized and five times the amount of porcine brain extract was loaded. These packing conditions eluted the necessary CaMBP yields to perform one 2D DIGE gel. Each column was loaded and eluted three times to obtain three replicates; the minimum number of replicates required to perform a 2D DIGE analysis. Unfortunately, one gel ran unsuccessfully therefore no statistical analysis could be performed. Analysis of the two successful gels confirmed the proof of concept that the CaM affinity chromatography method of isolating and fractionating CaM binding proteins could be analyzed using 2D DIGE. There were 13 proteins detected with expressions differences between the CaM-mutant and calcium-CaM populations. However, in order to make quantitative proteomic conclusions, statistical analysis is necessary before proteins can be identified and reported as significantly changed. As a result, no proteins were chosen for mass spec identification.

The DIGE technique simultaneously separates two fluorescently labeled protein populations and achieves statistical inference through replication. Although DIGE is a very powerful proteomics technique, it has several associated technical limitations, including achieving the separation of sufficient replicates to determine statistically valid protein differences. Analysis of re-using the columns determined that the non-specific binding to CaM increased as the columns were re-used, therefore re-using the affinity columns to obtain replicates for the 2D DIGE analysis was concluded to be a poor design of experiments. Alternatively, using the

determined affinity chromatography elution conditions and perhaps a column sub-pooling 2D DIGE design of experiments which incorporates at least six gels (either through technical replication or biological like replication or a combination of both) would be necessary to achieve quantitative DIGE results. This experiment would require a minimum of twelve accurate and successful column packings in which the resin is coupled in batch in attempts to achieve negligible column to column variation. However, this large scale experiment was not undertaken due to time and resource limitations.

The second objective of the proposed experimental plan, the cellular uptake of the TAT-TRITC-CaM-FITC construct, overall, gave inconclusive results. The TAT-FITC construct which was used as a control to confirm TAT cellular uptake independent of CaM, emitted a punctate cellular signal however it was not confirmed if TAT was indeed internalized or if TAT was actually bound to the cellular membrane. It was confirmed that there was no non-specific interactions between FITC and the human glioblastoma cells, as no signal was detected in the FITC only control. It is therefore concluded that FITC is a suitable fluorophore to be utilized to label TAT for fluorescent cellular analysis. On the other hand, the TRITC fluorophore used to label CaM is concluded to be unsuitable for cellular analysis. Although the CaM-TRITC construct was punctate and appeared to be specific, the TRITC only control revealed a similar punctate signal, providing evidence that TRITC is not a suitable fluorophore to be used in cellular specificity experimentation. It is suggested that a different fluorophore be utilized to label CaM and recommended that the chosen fluorophore be evaluated for non-specific cellular interaction prior to being labeled with CaM and di-

sulfide bond linked to the TAT-FITC construct. The observed fluorescent results suggested that the disulfide bond link between TAT and CaM was not broken as both of the respective fluorescent signals were co-localized. However, due to the negative results of the CaM-TRITC control, it is inconclusive if the observed co-localized punctate signal was indeed the TAT-CaM construct interacting with the cell membrane or an artifact of TRITC non-specific interactions with the cells.

In conclusion, although the outlined experimental design did not give conclusive results, there is valuable cell signaling information to be obtained from studying CaM protein interactions. Besides the apo-CaM 'mutant' which was studied, various other CaM-mutants which have different combinations of the 1,2,3,4-mutated calcium binding sites had already been generated in collaboration with Professor Guy Guillemette in the Chemistry Department at the University of Waterloo. Therefore, there was great promise in elucidating a wide spectrum of CaM binding interactions and cell signaling using the proposed methods and purified CaM proteins. With the correct design of affinity chromatography and DIGE experiments, potentially new CaMBPs would have been identified and then studied at the cellular level using the TAT cell penetrating peptide. Unfortunately, time did not allow for such large scale experimental modifications and further analysis.

Chapter 4 Proteomic Analysis of Human Islet-Derived Progenitor Cells Treated with rINGAP

4.1 Preamble

This chapter shifts focus from the study of calmodulin to the second proposed cellular system: human islet-derived progenitor cells (hIPCs) treated with islet neogenesis associated protein (INGAP). Specifically, this chapter investigates recombinant INGAPs (rINGAP) affect on hIPCs at the proteomic and mRNA levels.

4.1.1 Objective and Justification

The main objective of this chapter was to identify the differential expression of proteins as a result of recombinant INGAP (rINGAP) induction of human islet-derived progenitor cells (hIPCs). Additionally, the effects of rINGAP on mRNA expression by real time quantitative reverse transcriptase polymerase chain reaction (real time qRT-PCR) was performed. This research is of importance because revealing mechanistic clues of INGAPs cellular affects on hIPCs may prove to be critical for the clinical development of INGAP and the treatment of diabetes.

4.2 Publication Title and Authors

The results presented in this chapter have been prepared for publication for the Journal of Proteomics Clinical Applications. The results have not yet been submitted for publication because additional real time qRT-PCR is currently being completed on genes of the proteins (caldesmon and tropomyosin) identified by the DIGE analysis.

Title: Proteomic Analysis on Differentially Expressed Proteins of Human Islet-Derived Progenitor Cells Treated with Recombinant Islet Neogenesis Associated Protein

Authors:

Erika Murray[1], Ilia Droujinine[1], Julia Makhlin[3], Guy Guillemette[2], Lawrence Rosenberg[3], Eric Jervis[1]

[1]Department of Chemical Engineering, University of Waterloo, Waterloo, Ontario, Canada; [2]Department of Chemistry, University of Waterloo, Waterloo, Ontario, Canada; [3]Department of Surgery, McGill University, Montreal, Quebec, Canada

4.3 Statement of clinical relevance

Islet neogenesis associated protein (INGAP) is a protein first discovered for its pancreatic regeneration effects in hamsters. In diabetic animal model studies INGAP has demonstrated beta-cell regenerating effects with an evident increase in beta-cell mass in animals treated with INGAP peptide. Additionally, recent phase-two human clinical trials concluded INGAP peptide increased C-peptide secretion in type 1 diabetics and improved glycemic control in type 2 diabetics. Although studies have demonstrated an increase in beta-cell mass in animal models, the precise mechanism of INGAP action remains unknown, including active transcription pathways and the identification of a potential cellular receptor. Long-term expansion of isolated human islets in culture results in a population of islet-derived progenitor cells (IPCs), which have been characterized as pancreatic mesenchymal stem cells (pMSCs) by several groups. When transplanted with minimal pancreatic islet cell mass, pMSCs have demonstrated restoration of normoglycemia in mice. To our knowledge, to date, no proteomic analysis of INGAP on any cell type has been performed. The present work

investigates the differential expression of proteins and pancreatic genes as result of recombinant INGAP (rINGAP) stimulation of human islet-derived progenitor cells (hIPCs). These proteomic findings in combination with the PCR results provide insight into INGAPs mechanistic affects on hIPCs.

4.4 Overview

We applied 2-D difference gel electrophoresis (2-D DIGE) to compare recombinant INGAP (rINGAP) treated hIPCs with non-treated cells to determine at the proteomic level hIPCs responses to rINGAP. Analysis was performed using hIPCs derived from three donors at three different time points (24 hrs, 48 hrs and 96 hrs) of rINGAP exposure. The differential proteome analysis revealed 35 statistically significant affected proteins (between -1.2 – 1.95 fold change), in which rINGAP altered protein levels. Of the 10 proteins identified by mass spectrometry, 5 are cytoskeletal proteins involved in process formation, migration and differentiation. Specifically, the identification of the proteins caldesmon, transgelin, tropomyosin, STRN and cofilin-1, revealed major regulation of the hIPC cytoskeleton at 48 hours of rINGAP induction. Our results provide, for the first time, mechanistic clues for an understanding of proteins that may be clinically relevant to INGAP's action on hIPCs and the treatment of diabetes.

Keywords

Islet neogenesis associated protein / Islet-derived progenitor cell/ Pancreatic mesenchymal stem cell / 2-D difference gel electrophoresis / Cytoskeleton / Differentiation

4.5 Introduction

Diabetes is a disease manifested by the destruction of beta-cell mass in the pancreas. Type 1 diabetes mellitus is the result of a progressive autoimmune-mediated destruction of beta-cells (Halban 2004). Similarly, beta-cell mass is decreased in Type 2 diabetes mellitus cases and the mechanism is increased beta-cell apoptosis (Butler, Janson et al. 2003). This decrease in β-cell mass, results in a decline of insulin production and loss of glucose homeostasis; requiring often as a treatment option regular insulin injections which can result in long term complications. Currently, diabetes researchers focus on islet cell regeneration both *in vivo* and *in vitro. In vivo*, therapeutic molecules, such as INGAP, are being administered into animal models as well as humans, and studied for inducing islet cell neogenesis, C-peptide secretion and glycemic control.

INGAP is a 17 kDa protein that was first discovered to be a constituent of ilotropin (Pittenger, Vinik et al. 1992), an islet-specific growth factor, which is expressed during islet neogenesis. Further sequencing determined a region of the protein consisting of 15 amino acids (104-118) to induce similar islet neogenesis effects (Rafaeloff, Pittenger et al. 1997). This active region of INGAP was synthetically produced and named INGAP-PP or $INGAP^{104-118}$. Since its discovery, the synthetically produced INGAP peptide has been extensively investigated for its islet neogenesis affects in diabetic animal models, as well as in human clinical trials. In type 1 diabetic mice INGAP-PP reversed hyperglycemia and further dissection of the mice pancreata demonstrated that INGAP-PP increased beta-cell mass (Rosenberg, Lipsett et al. 2004). *In vivo*, studies of normoglycemic rodents and dogs

who received intramuscular injections of INGAP-PP showed a dose-dependent expansion of beta-cell mass (Pittenger, Taylor-Fishwick et al. 2007). At the genomic level, INGAP-PP enhances the transcription of genes implicated in islet metabolism, β-cell mass, islet neogenesis and specifically, the release of insulin in rats (Barbosa, Bordin et al. 2006). Of the greatest clinical significance, are the results of phase 2 clinical trials in which INGAP-PP was concluded to increase C-peptide secretion in type 1 diabetics and improved glycemic control in type 2 diabetics (Dungan, Buse et al. 2009).

Although there is sufficient evidence to conclude INGAP-PP holds therapeutic potential in the cure of diabetes, there remains limited information about a potential INGAP cellular receptor or its signal transduction pathways. In the original publication of the cloning and sequencing of INGAP it was concluded that both the peptide and the protein were capable of initiating cell proliferation, a prerequisite for islet neogenesis, though it was noted that the full length recombinant protein appeared to have an even more potent proliferative effect (Rafaeloff, Pittenger et al. 1997). To date, however, studies of INGAP have focused on evaluating the islet neogenesis effects of the synthetic peptide, not the full length recombinant protein (rINGAP). The production and characterization of rINGAP has recently been reported in hopes to facilitate the delineation of the INGAP mechanism(s) (Assouline-Thomas, Pilotte et al. 2009). Of importance, it was concluded using an *in vitro* assay of human islet regeneration, that rINGAP exhibits 100-times the bioactivity of the INGAP-PP on a molar basis (Assouline-Thomas, Pilotte et al. 2009).

During fetal development, new endocrine cells appear to arise from progenitor cells in the pancreatic ducts. Many researchers have maintained these progenitor cells are islet stem cells residing within the ductal cell population which give rise to endocrine cells as the fetus develops. If this is accurate, it is hypothesized that the pancreata stem cell population would require stimulation from extrinsic factor(s), such as INGAP, which initiate and terminate their differentiation into functional insulin producing cells. The long term culture of islets on tissue culture-treated surfaces results in a population of proliferative fibroblast-like islet-derived precursor cells (Gallo, Gambelli et al. 2007), which were shown to be mesenchymal stromal cells that were capable of differentiating into hormone-expressing cells (Davani, Ikonomou et al. 2007). Recently, it was demonstrated that the cells outgrowing from isolated islets are pancreatic mesenchymal stem cells (pMSCs) which had the capacity to improve transplanted islet function, through facilitating the restoration of normoglycemia and neovascularization of the graft in mice (Sordi, Melzi et al. 2010).

Although it remains unknown if the pMSCs expanded from human islets in culture are representative of an *in vivo* pancreata stem cell population, characterization of potential extrinsic factors, such as INGAP, which may induce pMSC differentiation and the identification of activated transcription pathways are necessary. In this study, we isolated and expanded human islet cells from three different donors into a population of islet-derived progenitor cells (hIPCs). After positively evaluating the hIPCs for established mesenchymal pMSC markers using immunocytochemistry, the hIPCs were cultured in media supplemented with rINGAP for 24, 48 and 96 hours. A two-dimensional differential in-gel electrophoresis

(2D DIGE) analysis was then performed in order to identify differentially expressed proteins that characterize rINGAPs mechanistic effects on hIPCs. Furthermore, the effect of rINGAP on mRNA expression by real time quantitative reverse transcriptase polymerase chain reaction (real time qRT-PCR) was performed.

4.6 Materials and Methods

4.6.1 Cell Culture and rINGAP treatment

Human islet isolation protocols were first approved by the Institutional Review Board of McGill University, Montreal, QC. Human islets were isolated according to established protocols (Shapiro, Lakey et al. 2000) from three healthy cadaveric donor pancreases through an organ procurement organization at the Montreal General Hospital, as previously described (Jamali, Emmerson et al. 2005). Upon isolation, the islets were washed and re-suspended in CMRL-1066 medium with penicillin, streptomycin, and amphotericin B (Antibiotic-Antimycotic (100X) liquid; Gibco, Burlington, ON, Canada) and 10% fetal bovine serum (MBI, Amherst, NY, USA). The islet cells were then shipped on ice overnight in a polypropylene container without airspace from Montreal, QC to Waterloo, ON.

The hIPCs were derived from the isolated human islets as previously described (Gershengorn, Hardikar et al. 2004; Gallo, Gambelli et al. 2007; Sordi, Melzi et al. 2010), with minor modifications. Briefly, the islets were plated in 75cm^2 tissue culture-treated flasks at a density of approximately 1 islet/mm^2 in modified RPMI-1640 medium (11.1 mM glucose) (Invitrogen, Burlington, ON), supplemented with 10% FBS (Invitrogen, Burlington,

ON). The flasks were incubated at 37°C, 5% CO_2 and 95% humidified air, and after 24 hours non-adherent cells were removed and 12.5 mL of fresh media was replenished. The media was then replaced every 3 days for the remainder of the culture. At day 15 of culture the islets which were spread into a monolayer were detached from the surface with 2.5 g/L trypsin with 0.38 g/L EDTA (Invitrogen, Burlington, ON) and reseeded as single cells at a density of $1.2x10^4$ cells/cm^2, followed by subsequent passaging at $4x10^3$ cells/cm^2 once 90% confluence had been obtained, approximately every 10 days. After 6 passages, half of the flasks were treated with rINGAP which was supplemented in the media. The rINGAP was provided by Dr. Rosenberg's lab from the Montreal Diabetes Research Center, QC, which was produced and purified as previously described (Assouline-Thomas, Pilotte et al. 2009). The hIPCs were treated with 10 nM of rINGAP at various treatment times (24, 48 and 96 hours). After culturing hIPCs in media supplemented with and without rINGAP for the respective treatment times, the cells were detached from the flask surfaces with 0.25% Trypsin EDTA, transferred to 1.5 mL eppendorf tubes and washed three times in PBS. The hIPCs were then frozen in liquid nitrogen as a pellet in PBS until protein extraction.

4.6.2 Protein extraction and preparation

hIPC cell pellets were lysed in 1mL of DIGE lysis buffer containing 30mM Tris-HCl pH 8.5, 8M Urea, 2M Thiourea, 4% CHAPS and 13 mM DTT. Lysing the pellets efficiently was critical. The DIGE lysis buffer was added to the pellet, vortexed and left to sit on ice for 10 min. The samples were then sonicated in a small bath sonicator for 30 seconds, three times and then homogenized by passing through a 25-gauge needle five times. The minimal insoluble material was removed by centrifugation at 13 000 rpm for 15 min at 4^0C. The

proteins of interest were then quantified using 2-D Quant Kit (GE Healthcare) and aliquoted into 50 ug or 25 ug samples. To remove urea and salt, the samples were cleaned-up using PlusOne 2-D Clean-Up Kit (GE Healthcare) and re-suspended in 10ul of DIGE lysis buffer.

4.6.3 CyDye labeling

Protein samples were labeled using fluorescent Cyanine dyes 2, 3 and 5 developed by GE Healthcare for 2-D DIGE. Fifty micrograms of the two protein populations to be compared, were each labeled with 200 pmol of amine reactive cyanine dye 3 or 5 freshly dissolved in anhydrous DMF. As a standard, twenty-five micrograms of the two protein populations to be compared, were combined and labeled with 200 pmol of amine reactive cyanine dye 2 freshly dissolved in anhydrous DMF. The three labeling reactions were then incubated at room temperature in the dark for 30 min. The reactions were terminated by the addition of 10 nmol lysine to each sample for 10 min in the dark. Rehydration buffer (7M Urea, 2M Thiourea, 2% CHAPS, 0.5% Triton X-100, Pharmalyte 3-10 for IEF, 0.1% NP-7, 13 mM DTT and bromophenol blue) was then used to mix the three labeled samples to a final volume of 450 µl prior to rehydration and iso-electric focusing.

4.6.4 Isoelectric focusing and two-dimensional SDS-PAGE electrophoresis (2D-gels)

In-gel sample rehydration was performed at room temperature for 20 hours using immobilized 24-cm non-linear pH 3-10 gradient (IPG) strips (GE Healthcare). The rehydrated strips were focused using an Ettan IPGphor II (Amersham Biosciences) for approximately 56 000 VhrT with a gradual voltage ramp to a maximum of 8000V for 12.5 hours. Focused strips were then immediately equilibrated in two steps, reduction followed by

alkylation, each for 15min on a shaker in 15mL of 50mM Tris-HCl pH 8.8, 6M Urea, 30% (v/v) glycerol, 2% (w/v) SDS and 1% DTT (reduction) or 2.5% iodoacetamide (alkylation). Equilibrated strips were then loaded between 1mm thick 18x20cm pre-cast gradient 8-16% polyacrylamide poured gels with low fluorescence glass plates (Jule Inc.). The strips were then overlaid with 0.5% (w/v) agarose in 1X running buffer (25 mM Tris, 0.2M glycine, 0.1% (w/v) SDS, pH 8.3) with 0.002 mg of bromophenol blue on a shaker. The gels were run in an Ettan Dalt 6 apparatus (GE Healthcare) at 5 W/gel for 30 min and then 20 W/gel at 15^0C until the dye ran off the bottom of the gels.

4.6.5 Scanning, image processing and statistical analysis

Gels were visualized using a Typhoon 9410 imager (Amersham Biosciences), scanned at 100 μm pixel size. The photomultiplier tube was set to ensure maximum pixel intensity at 40000-60000 pixel units. Scanned images were cropped using ImageQuant 5.2 (GE Healthcare) to remove the border of the gels. The cropped images were analyzed using DeCyder 6.5 software (GE Healthcare). The estimated number of spots for detection was set to 2000. No area, volume or peak height exclusion filters were applied.

4.6.6 In-gel tryptic digestion and protein identification by mass spectrometry

Preparative gels were made using 450 μg of protein separated using the same rehydration, iso-electric focusing and SDS-PAGE procedures described above. Total protein was detected by post-staining with 500 mL of 1% Coomassie Blue G-250 (GE Healthcare) overnight at room temperature on a shaker. Excess dye was removed by washing the gels three times in excess water, followed de-staining over night in water. Protein spots of interest were cut from

the stained preparative gel and the proteins were excised from the gel using in-gel trypsin digestion. The digested proteins were sent for mass spectrometry analysis and protein identification performed by the Mass Spectrometry Facilities at McMaster University, Hamilton, Ontario and Queen's University, Kingston, Ontario.

4.6.7 RNA isolation and quantitative real time RT-PCR

Total RNA was isolated using the Trizol reagent, according to the instructions of the company (Invitrogen). Briefly, cells were centrifuged, resuspended in Trizol, vortexed, and frozen. After thawing and standing at room temperature for 5 min, 17% (v/v) chloroform was added, and tubes were shaken by hand. After centrifugation at 12000g for 15 min at 4°C, the upper aqueous phase was transferred to isopropanol, incubated for 10 min at room temperature and centrifuged at 12000g for 10 min at 4°C. The RNA precipitate was then washed with 70% EtOH, and centrifuged at 7500g for 5 min at 4°C. The pellet was air-dried briefly, resuspended in ddH_2O, and frozen at -80°C. The RNA was reverse-transcribed (RT) using SuperScript III RT (Invitrogen). Up to 2 μg of RNA (equal among samples) was mixed with 2.5 μM $Oligo(dT)_{20}$ primer, without prior DNAase digestion, heated at 70°C for 5 min and quick-chilled on ice. This was added to a master mix, giving final concentrations of 1x first strand buffer, 20 mM DTT, and 200 units of RT enzyme. The reaction was then carried out at 50°C for 60 min, followed by inactivation of enzyme at 70°C for 15 min. Real time PCR reactions were performed by Julia Makhlin (Department of Surgery, Research Institute of the McGill University Health Center) using SYBR Green method and exon-boundary-spanning forward and reverse primers. The conditions of reaction were 95°C for 3 min, and

40 cycles of 95°C for 10 sec, 58°C for 30 sec, and 72°C for 30 sec. Islet cDNA was used as control and a melting curve analysis confirmed the nature of the products.

4.7 Results and Discussion

4.7.1 rINGAP Treatment Alters Protein Expression of hIPCs

To identify specific protein expression changes following rINGAP treatment of hIPCs in culture, we analyzed protein lysates from hIPCs cultured in media supplemented with rINGAP in comparison to control hIPCs which were cultured in standard media. It was of interest to evaluate rINGAPs temporal effects on hIPCs in attempts to gain mechanistic clues vital for the clinical development of INGAP and the treatment of diabetes. The hIPCs were derived from three healthy donors and each population received a different rINGAP treatment time. Three independent proteomic analyses were performed at 24, 48 and 96 hrs of rINGAP exposure in comparison to the control hIPCs. Lastly, it was determined that a sub-pooling design of experiments was necessary to complete the DIGE analysis of treated hIPCs in culture.

To determine if there were preliminary apparent proteomic differences between the rINGAP treated cells and the non-treated controls, proteins were first analyzed using 1D gels, comparing INGAP treated and non-treated flasks of the same and different donors. The 1D gel analysis using various molecular weight ranges revealed no proteomic differences between rINGAP treated hIPCs (results not shown). Therefore, separation into the second dimension was necessary. To date, there is no published data of 2D gel analysis on hIPCs. As

a result, determining optimal 2D gel separating conditions was required before performing a DIGE analysis. Three pH ranges (4-7, 3-10 and 3-10NL) were evaluated in combination with five rehydration buffers, which had different combinations of detergents to improve protein solubilization. Several iso-electric focusing programs, incorporating different voltages and rates of separation, in combination with using a reducing agent (DTT) in the wicks during separation, were studied to determine ideal iso-electric focusing conditions. Lastly, various concentrations of acrylamide gels (8%, 12% and 8-16% gradient) were also tested to determine optimal molecular weight range. The final 2D separation conditions were listed in section 4.6 Material and Methods.

Proteomic analysis at 24 hours of rINGAP treatment with no pooling

Following the 2D gel optimization, the optimized separating conditions were used in an un-pooled 2D DIGE analysis with a 24 hour rINGAP treatment. The experiment was designed with each protein flask representing a replicate (4 treated and 4 non-treated flasks) (**figure 4-1**). Subsequent to the 2D DIGE experiment and analysis performed in DeCyder, the distribution of the obtained p-values was compiled. As discussed in section 2.6.2.1, DIGE Quantification and Statistical Analysis, the p-values reflect the probability that the observed change has occurred from random chance alone. Therefore, a frequency histogram of the distribution of obtained p-values is expected to be uniform when comparing two identical protein populations, towards 1 when there is a biased or large inter-treatment variability, and towards 0 when there are significantly changed proteins between the two compared protein populations (Karp, McCormick et al. 2007). The un-pooled DIGE experimental design at 24 hours resulted in a bias in the p-values towards 1 (**figure 4-2**). This indicated that an

underlying assumption of the Student's t-test was not being met, leading to a distortion in the obtained p-value distribution (Karp, McCormick et al. 2007). This effect was postulated to arise from large flask to flask variability between the same treatment group. In other words, it was believed that the protein expression levels of the non-treated flasks (and/or the rINGAP-treated flasks) had high inter-flask variability and therefore no valid statistical inference was made.

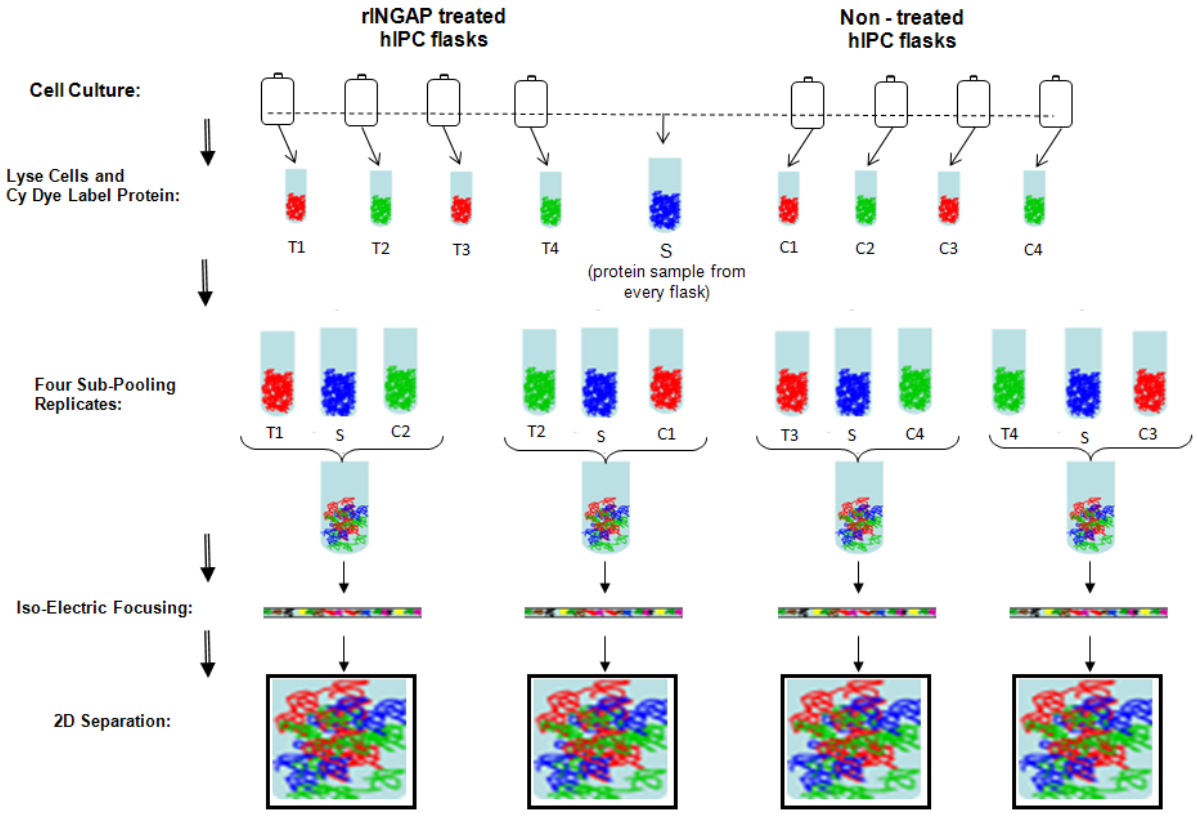

Figure 4-1: Representation of DIGE hIPC Non Pooling Design of Experiments. 4 DIGE gels were processed to compare the overall proteomic effect of rINGAP on individual flasks of hIPCs from one biological replicate (donor). T is treated. C is control. S is standard.

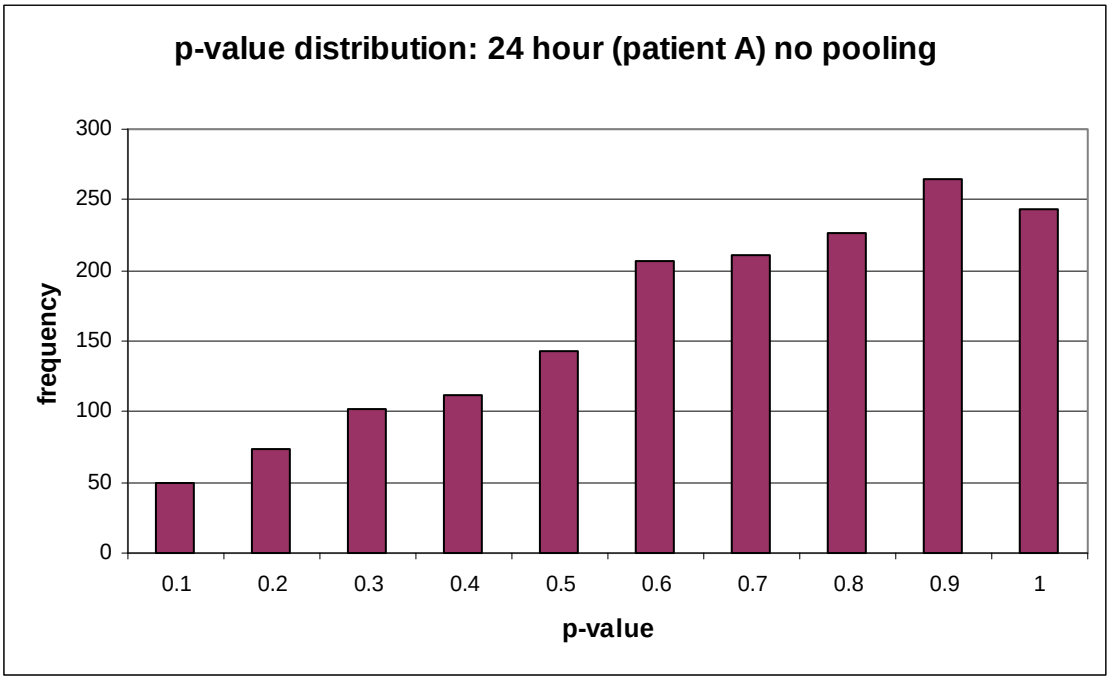

Figure 4-2: Frequency distribution of the p-values obtained from the 24 hour rINGAP treatment using a non-pooled experimental design. A distribution towards 1 was obtained and therefore no valid statistical inference was made from this experiment.

Proteomic analysis at 24 hours of rINGAP treatment: with pooling

To reduce the flask to flask variability, the DIGE analysis at 24 hours of rINGAP treatment was repeated using a sub-pooling design of experiment. Specifically, it was of interest to determine if a suitable p-value distribution towards $p<0.05$ could be obtained. A sub-pooling DIGE design of experiments described in Section 2.6.2.2 DIGE Experimental Design was performed. In short, resolved proteins of hIPCs treated with rINGAP for 24 hours were compared to proteins of hIPCs that received no treatment using four sub-pooled replicates in

which two flasks from each treatment group were combined to create a replicate. **Figure 4-3** shows a representation of the sub-pooled design of experiments, which considered the objective of studying the overall proteomic effect on all flasks, and the fact that the hIPCs were derived from one biological replicate. Subsequent to the DIGE experiment and statistical analysis, the distribution of the obtained p-values was compiled. The frequency histogram revealed a distribution of p-values towards 0 (**figure 4-4**), indicating that there were significantly changed proteins between the rINGAP-treated and non-treated hIPC protein populations (Karp, McCormick et al. 2007).

A total of 910 proteins were detected and 527 proteins were matched. Statistically significant differences were found between 16 protein spots using a stringent Student t-test and false discovery rate cut-offs of $p<0.05$ and $q\leq0.15$, respectively. A significant but small fold-change range was determined for the 16 proteins between -1.10 to 1.25. Furthermore, rINGAP both up-regulated and down-regulated proteins compared to the untreated control. **Figure 4-5** shows a 2D gel with proteins which were found down-regulated by rINGAP in blue and up-regulated by INGAP in red. As further representation of the analysis performed in DeCyder, **figure 4-6** shows a workspace page with a protein identified as significantly changed being evaluated. Since the average fold change range was found to be small at 24 hours of rINGAP treatment, no proteins were chosen immediately for MS identification. An extended treatment time of 48 hours was proposed to determine if the overall detected protein fold change would be increased with a longer rINGAP exposure.

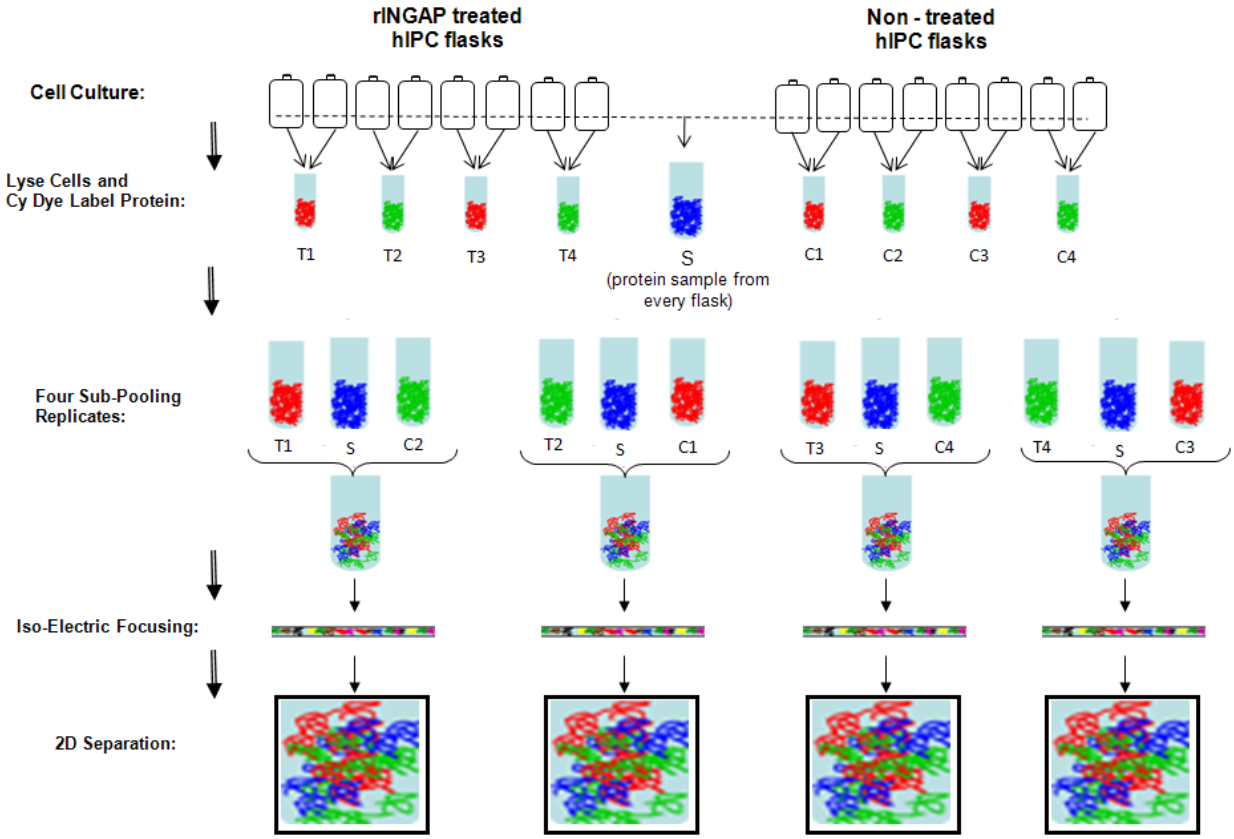

Figure 4-3: Representation of DIGE hIPC Sub-Pooling Design of Experiments. 4 DIGE gels were processed to compare the overall proteomic effect of rINGAP on two pooled flasks of hIPCs from one biological replicate (donor). T is treated. C is control. S is standard.

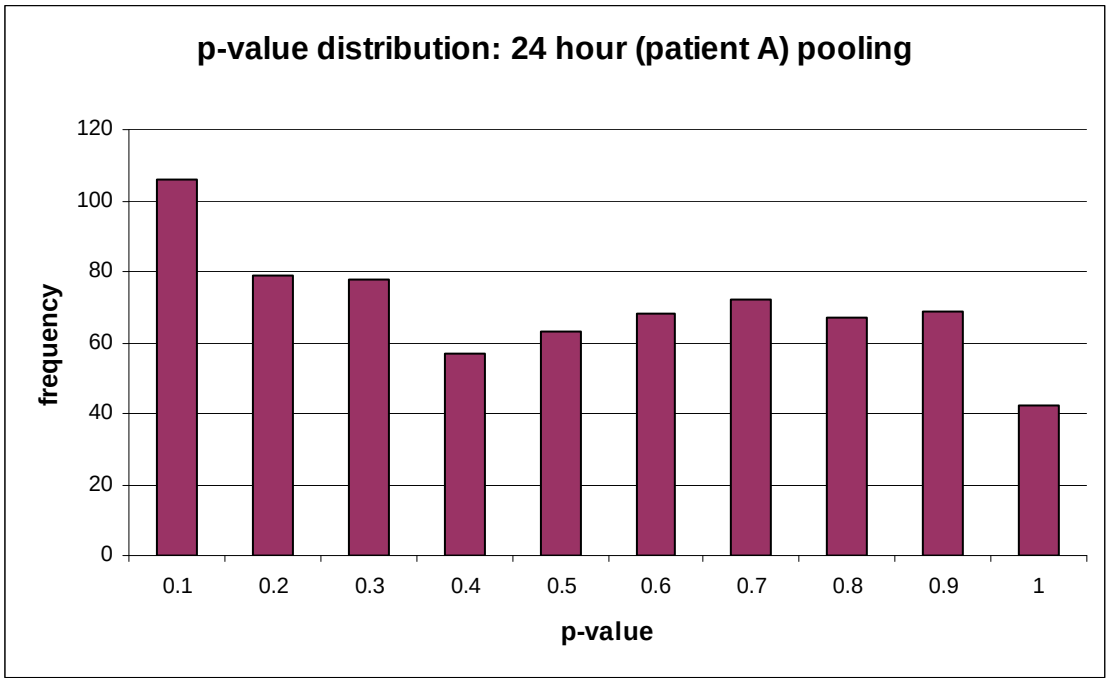

Figure 4-4: Frequency distribution of the p-values obtained from the 24 hour rINGAP treatment using a sub-pooled experimental design. A distribution towards 0.1 was obtained and therefore valid statistical inference could be drawn from this experiment.

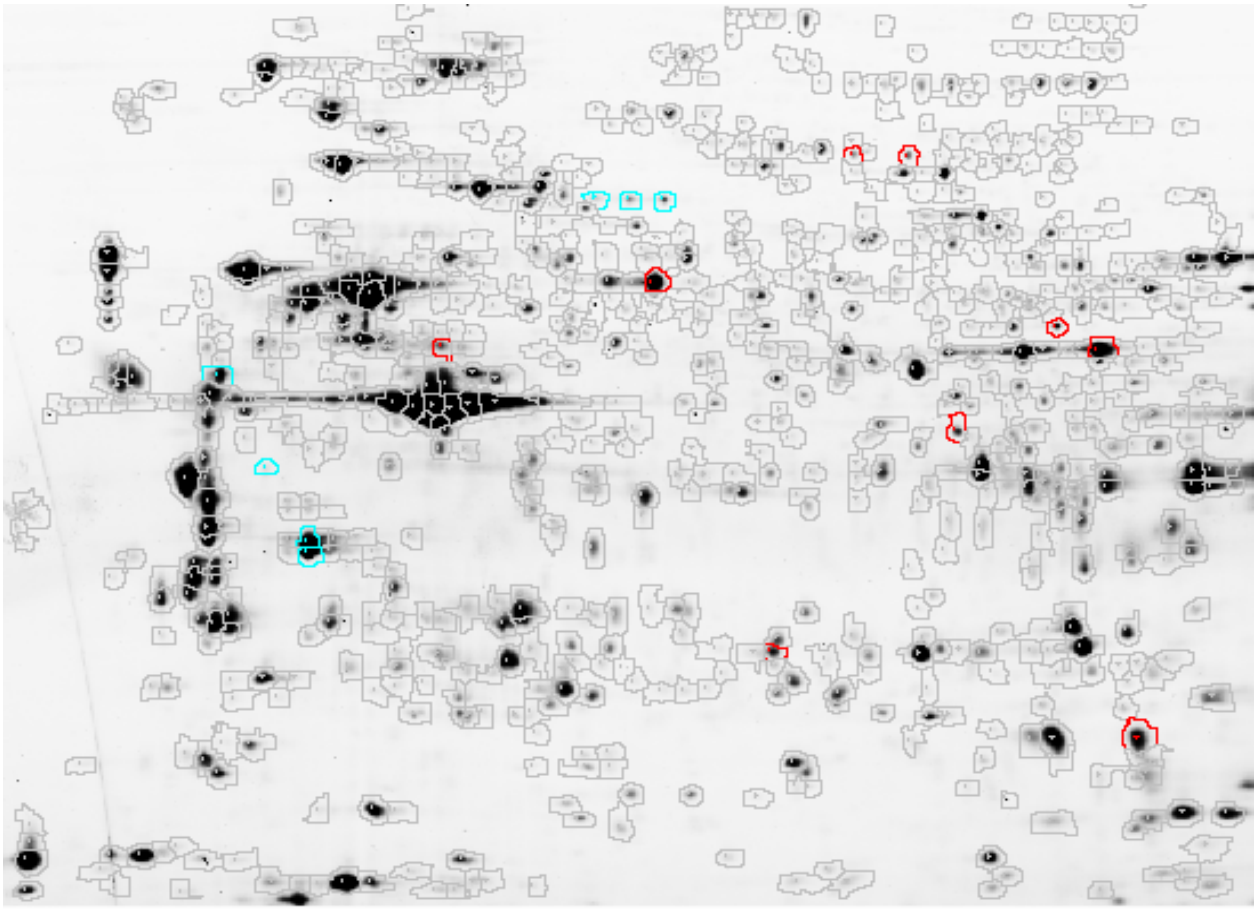

Figure 4-5: 2D pH 3-10NL DIGE gel of 24 hour rINGAP treatment. Proteins outlined in red represent up-regulated proteins identified as significantly changed ($p<0.05$, $q<0.15$). Proteins outlined in blue represent down-regulated proteins identified as significantly changed ($p<0.05$, $q<0.15$).

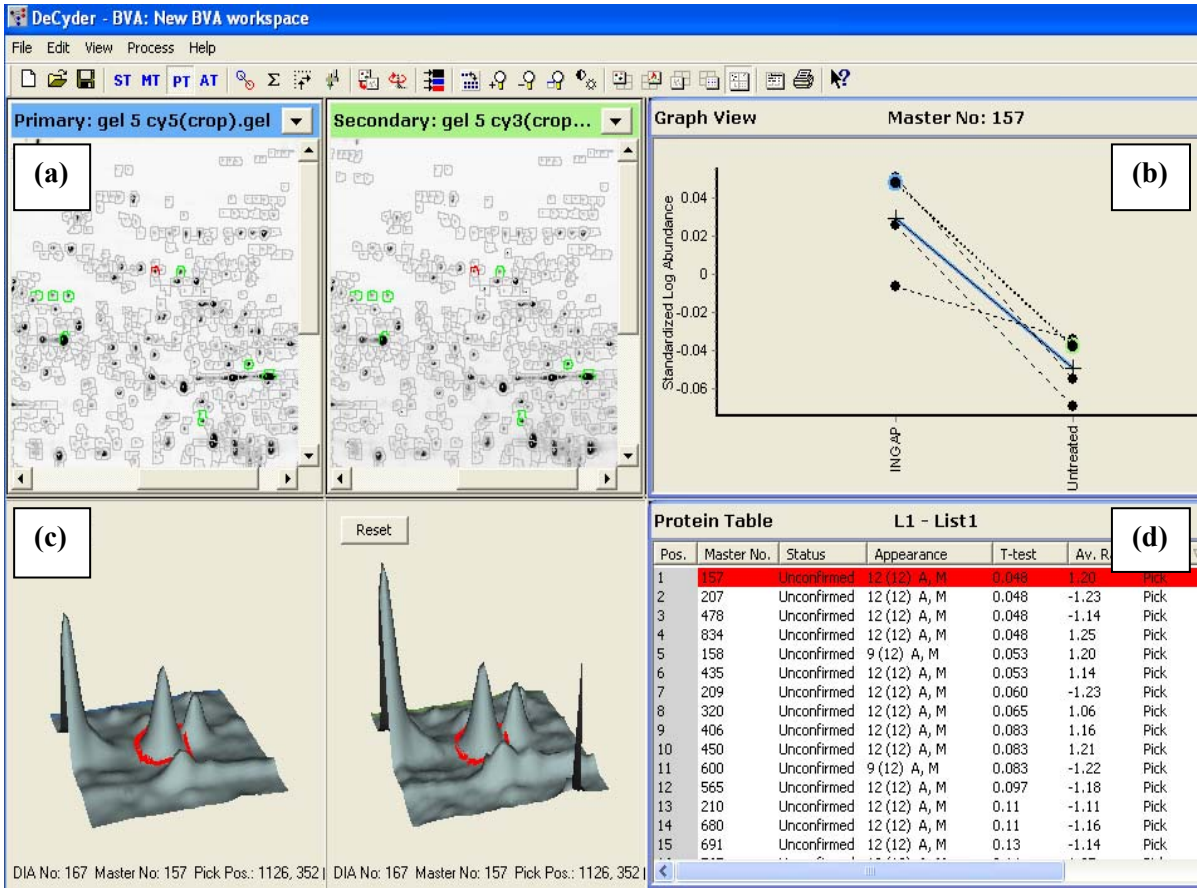

Pos.	Master No.	Status	Appearance	T-test	Av. R	
1	157	Unconfirmed	12 (12) A, M	0.048	1.20	Pick
2	207	Unconfirmed	12 (12) A, M	0.048	-1.23	Pick
3	478	Unconfirmed	12 (12) A, M	0.048	-1.14	Pick
4	834	Unconfirmed	12 (12) A, M	0.048	1.25	Pick
5	158	Unconfirmed	9 (12) A, M	0.053	1.20	Pick
6	435	Unconfirmed	12 (12) A, M	0.053	1.14	Pick
7	209	Unconfirmed	12 (12) A, M	0.060	-1.23	Pick
8	320	Unconfirmed	12 (12) A, M	0.065	1.06	Pick
9	406	Unconfirmed	12 (12) A, M	0.083	1.16	Pick
10	450	Unconfirmed	12 (12) A, M	0.083	1.21	Pick
11	600	Unconfirmed	9 (12) A, M	0.083	-1.22	Pick
12	565	Unconfirmed	12 (12) A, M	0.097	-1.18	Pick
13	210	Unconfirmed	12 (12) A, M	0.11	-1.11	Pick
14	680	Unconfirmed	12 (12) A, M	0.11	-1.16	Pick
15	691	Unconfirmed	12 (12) A, M	0.13	-1.14	Pick

Figure 4-6: DeCyder analysis workspace page. A protein identified as significantly changed is presented. (a) Overall depiction of gel area of the protein. The protein spot circled in red is being analyzed and the other significant proteins are circled in green. (b) Graphic representation of standardized log abundance detected differences in 4 gels. (c) Abundance representation of the spot in 2 gels. (d) Protein table with list of matched proteins. Protein of interest highlighted in red.

Proteomic analysis at 48 hours of rINGAP treatment: with pooling

Using the same sub-pooling design as the above 24 hour treatment analysis (**figure 4-3**), hIPCs treated with rINGAP for 48 hours were lysed and their protein expression levels were compared to hIPCs which received no treatment. Following the DIGE experiment of separation and data analysis (which included p-value calculations for every detected spot matched across the gels), a frequency histogram of p-values towards 0 was obtained (**figure 4-7**). This distribution was comparable to the p-value distribution obtained in the 24 hour sub-pooling experiment and confirmed that there were significantly changed proteins between rINGAP-treated and non-treated hIPC protein populations at 48 hours (Karp, McCormick et al. 2007). Of noted interest, in comparison to the 24 hour p-value distribution, the p-value distribution at the 48 hours had a greater number of proteins distributed at low p-values and an overall smaller background distribution.

A total of 802 proteins were detected and 369 proteins were matched. Statistically significant differences were found between 27 protein spots using stringent Student *t*-test and false discovery rate cut-offs of $p<0.05$ and $q\leq0.15$, respectively. Compared to the 24 hour fold change range of 1.10 to 1.25, a greater fold change range of -1.2 to 1.95 was determined for the 27 proteins. rINGAP was found to both up-regulate and down-regulate proteins in comparison to the untreated control. **Figure 4-8** is a 2D-gel showing proteins which were down-regulated by rINGAP in blue and up-regulated by rINGAP in red at 48 hours.

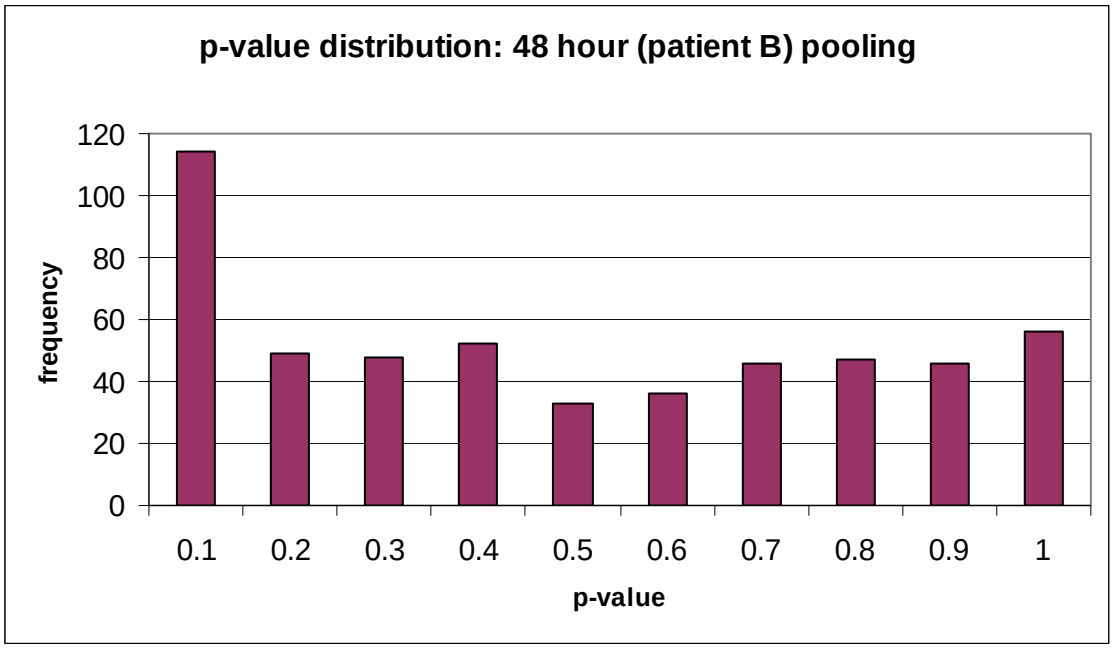

Figure 4-7: Frequency distribution of the p-values obtained from the 48 hour rINGAP treatment using a sub-pooled experimental design. A distribution towards 0.1 was obtained and therefore valid statistical inference could be drawn from this experiment.

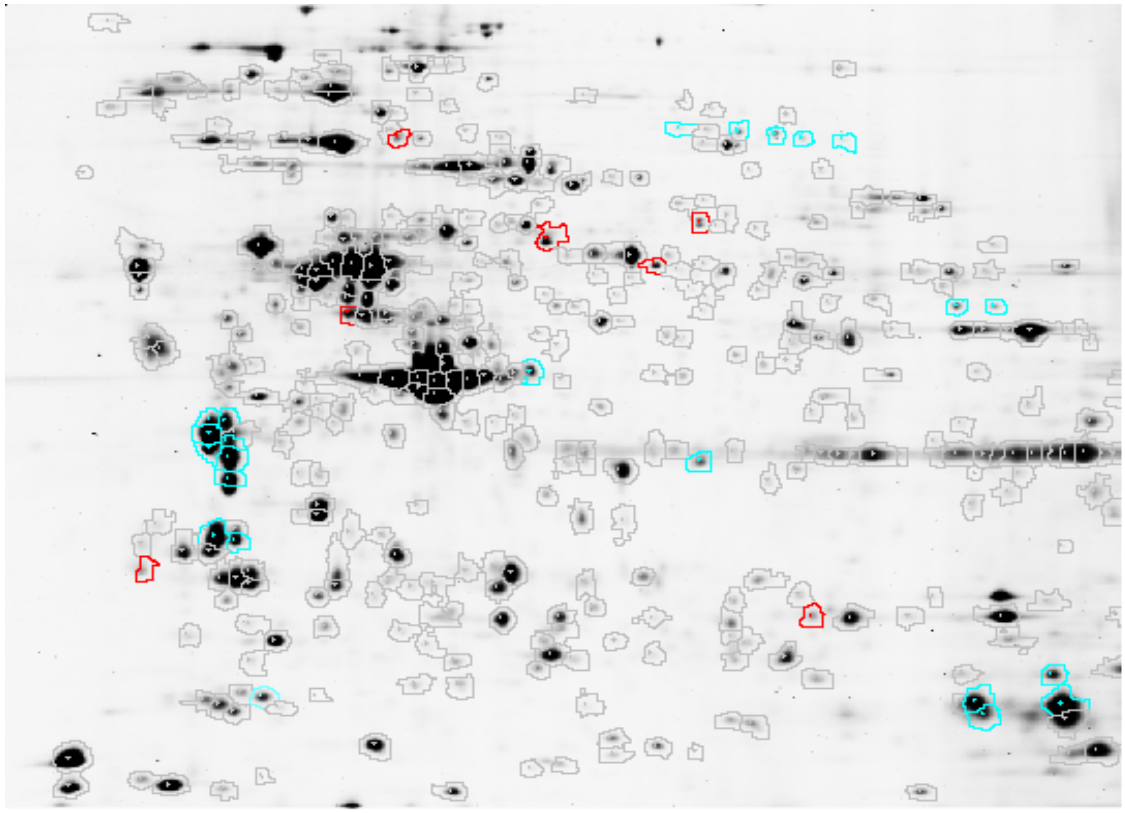

Figure 4-8: 2D pH 3-10NL DIGE gel of 48 hour rINGAP treatment. Proteins outlined in red represent up-regulated proteins identified as significantly changed ($p<0.05$, $q<0.15$). Proteins outlined in blue represent down-regulated proteins identified as significantly changed ($p<0.05$, $q<0.15$).

Comparison of 24 hour vs. 48 hour rINGAP treatments with pooling

To determine the treatment time dependent proteomic effect of rINGAP on hIPCs, a comparative analysis of the p-value distributions, fold change range and analysis of any proteins which were detected as significantly changed in both treatment times was completed. It was determined that in the 24 hour analysis, 6% of the total proteins were detected above the background noise as changing with a p-value < 0.05. In comparison, it

was determined that in the 48 hour analysis, 13% of the total proteins were detected above the background noise as changing with a p-value <0.05. However, through applying a q-value cutoff of q $\leq$0.15, a large number of the spots detected with a p-value of < 0.05 were removed from the analysis. This included spots with q >0.15, spots not found in all gels, as well as gel imperfections which were detected as spots. After removing these spots, it was concluded that in the 24 hour treatment experiment, 2% of the total proteins detected above the background noise were statistically significant and valid for further analysis. In comparison, in the 48 hour analysis 5% of the total proteins were detected above the background noise as signifcant and valid with a p-value <0.05 and q $\leq$0.15. **Table 4-1** highlights the overall dectected differences between the 24 and 48 hour rINGAP treatment analyses. Only four of the spots were found to be significantly changed at both treatment times. Interesting, all four proteins were up-regulated in the 24 hour treatment analysis, and down-regulated in the 48 hour treatment analysis. **Table 4-2** is a list of the 4 proteins significant at both treatment times and the corresponding calculated fold changes, p-values, and q-values.

No proteins were immediately chosen for identification, due to the resources associated with identifying proteins excised from gels. Based on the non-pooled DIGE analysis at 24 hours and the two sub-pooling analyses of hIPCs at 24 and 48 hours of rINGAP treatment, it was concluded that the sub-pooling design of experiments on one biological donor's cells was most ideal for detecting small proteomic differences between cultured flasks. rINGAP had a proteomic effect at both 24 and 48 hours of treatment, however INGAP had an increased

proteomic effect at the longer treatment time of 48 hours. Prior to choosing spots for MS identification, it was of interest to evaluate the proteomic response after 96 hours of rINGAP treatment.

Table 4-1: Comparison of 24 hour vs. 48 hour rINGAP treatments

INGAP Treatment Time:	**24 hours**	**48 hours**
# of proteins detected as significantly changed ($p<0.05$, $q \leq 0.15$)	14	27
Fold Change Range	1.10-1.25	1.2-1.95
% of proteins with significant change ($p<0.05$)	6%	13%
% of proteins with significant change and are real spots ($p<0.05$, $q \leq 0.15$)	2%	5%

Table 4-2: Comparison of the four proteins which were found to be significantly changed at both treatment times. All four spots were up-regulated with the 24 hour treatment, and down-regulated with the 48 hour treatment.

Master No.		**q-value**		**p-value**		**Fold Change**	
24 hours	48 hours	24 hours	48 hours	24 hours	48 hours	24 hours	48 hours
157	55	0.048	0.11	0.0023	0.0038	1.2	-1.81
158	56	0.053	0.065	0.0035	0.0018	1.2	-1.6
406	249	0.083	0.022	0.01	0.0003	1.16	-1.37
834	689	0.048	0.15	0.0028	0.0084	1.25	-1.41

Proteomic analysis at 96 hours of rINGAP treatment: with pooling

Using the same sub-pooling design employed for the 24 and 48 hour treatments (**figure 4-3**), lysed proteins of hIPCs treated with rINGAP for 96 hours were compared to proteins of hIPCs which received no treatment. However, a uniform frequency histogram of p-values was obtained (**figure 4-9**). A frequency histogram of the distribution of obtained p-values is expected to be uniform when comparing two identical protein populations (Karp, McCormick et al. 2007). Therefore, the p-value distribution suggested that there were no significant differences between the untreated and the 96 hour rINGAP treated hIPC protein populations. A total of 701 proteins were detected and 313 proteins were matched. Although a uniform p-value distribution was obtained, statistically significant differences were found between 18 protein spots using stringent Student *t*-test and false discovery rate cut-offs of $p<0.05$ and $q\leq0.15$, respectively. A fold change range of -1.18 to 1.34 was determined for the 18 proteins. **Figure 4-10** is a 2D gel showing proteins which were found to be significantly changed.

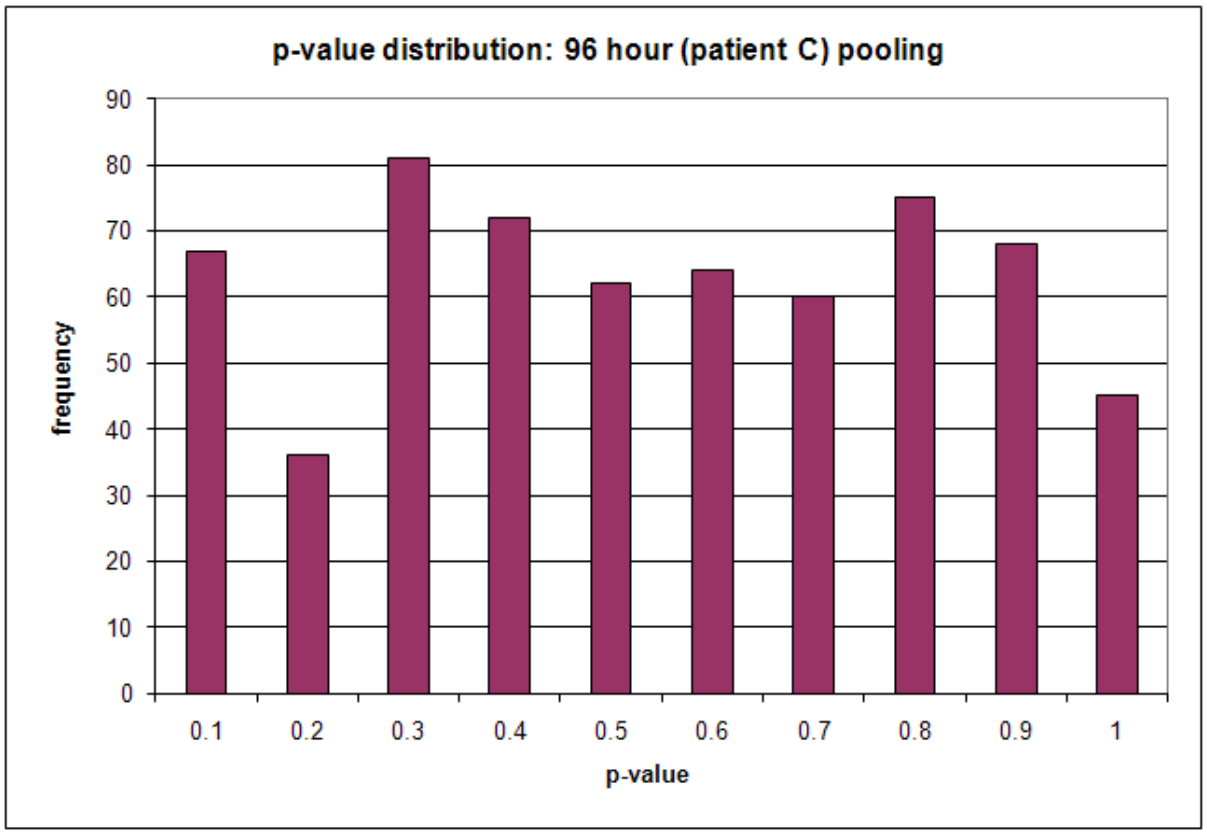

Figure 4-9: Frequency distribution of the p-values obtained from the 96 hour rINGAP treatment using a sub-pooled experimental design. A uniform distribution was obtained which suggested there were no significant differences between the untreated and the 96 hour rINGAP treated hIPC protein populations.

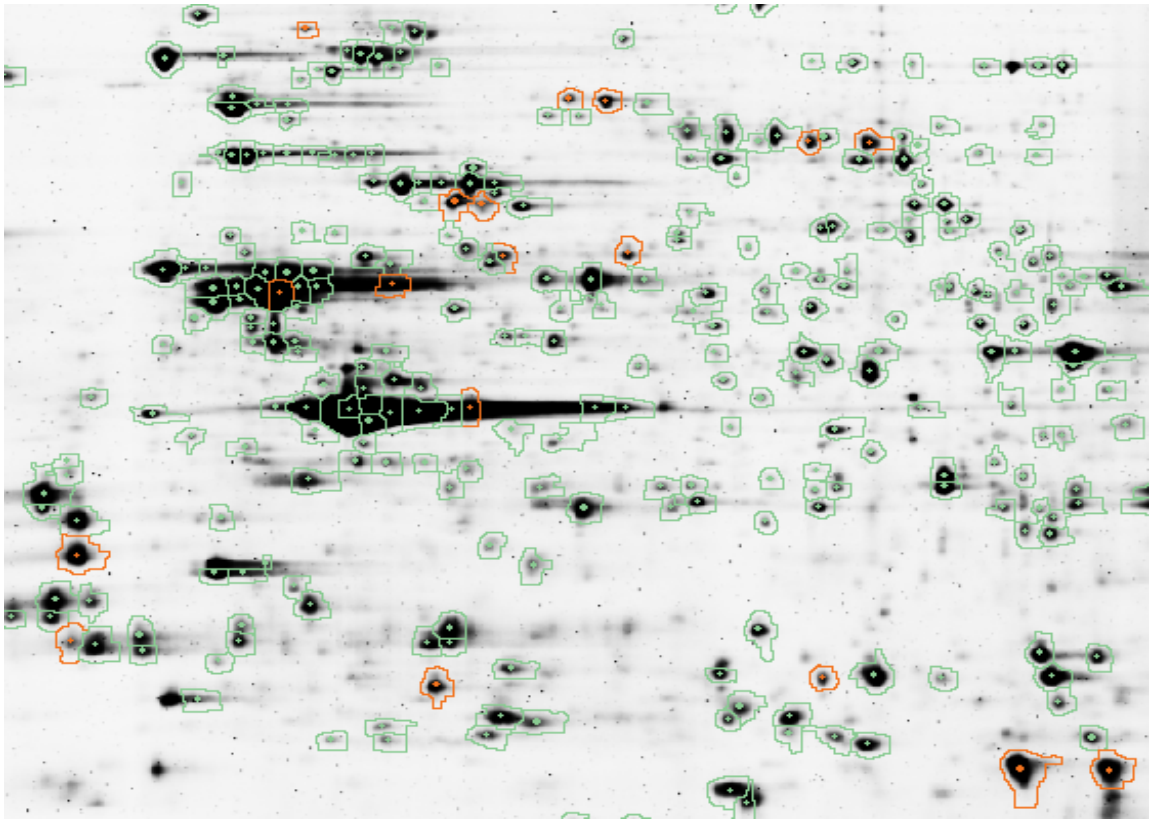

Figure 4-10: 2D pH 3-10NL DIGE gel of 96 hour rINGAP treatment. Proteins outlined in red are up-regulated and down-regulated proteins identified as significantly changed ($p<0.05$, $q<0.15$).

Comparison of 24 hour, 48 hour, and 96 hour rINGAP Treatments and Mass Spectrometry Identification

The first non-pooled design of experiments in which each hIPC culture flask represented a replicate, no statistical inference could be made. To reduce the variability between the replicates of the same treatment group (non-treated flasks and rINGAP-treated flasks), the DIGE analysis was completed based on a sub-pooling design of experiments in which the lysed protein from two flasks of the same treatment group were pooled to form a replicate.

This experimental design resulted in a suitable p-value distribution towards $p<0.05$ at both 24 and 48 hours of rINGAP treatment. However, the 96 hour p-value distribution was uniform, suggesting that there were no significant differences between the untreated and the rINGAP treated hIPC protein populations.

Table 4-2 outlines the number of proteins detected as signifcantly changed ($p<0.05$, $q \leq 0.15$) at each treatment point (24, 48 and 96 hours) and the respective fold change ranges. The greatest proteomic effect (in terms of largest fold change range and number of detected signifcant proteins) was at 48 hours of rINGAP treatment (**figure 4-11**). To achieve a general analysis into the types of proteins in which rINGAP up and/or down-regulated, these proteins were evaluated to determine which proteins would be of greatest interest for identification. Thirteen protein spots were manually excised from a preparative gel and were identified by MS. The ten spots were chosen to include proteins from various positions on the gels, as well as both up and down regulated proteins. Specifically, it was of interest to identify the proteins which had the greatest fold changes and/or were detected at several timepoints and/or were detected as significantly changed protein charge trains in multiple experiments. A complete list of the proteins identified by MS, including the treatment time in which they was detected, as well as the associated p and q-values are presented in **table 4-3**. Furthermore, a brief description of each protein is provided in **table 4-4** and a complex protein interaction network map analysis was made in Navigator, University of Toronto (**figure 4-12**).

Table 4-2: Comparison of 24, 48 and 96 hours of rINGAP treatment

Treatment Time:	24 Hours	48 Hours	96 Hours
Number of Proteins Significantly Up or Down Regulated:	14	27	18
Log Fold Change Range:	-1.10 – 1.25	-1.20 – 1.95	-1.18 – 1.34

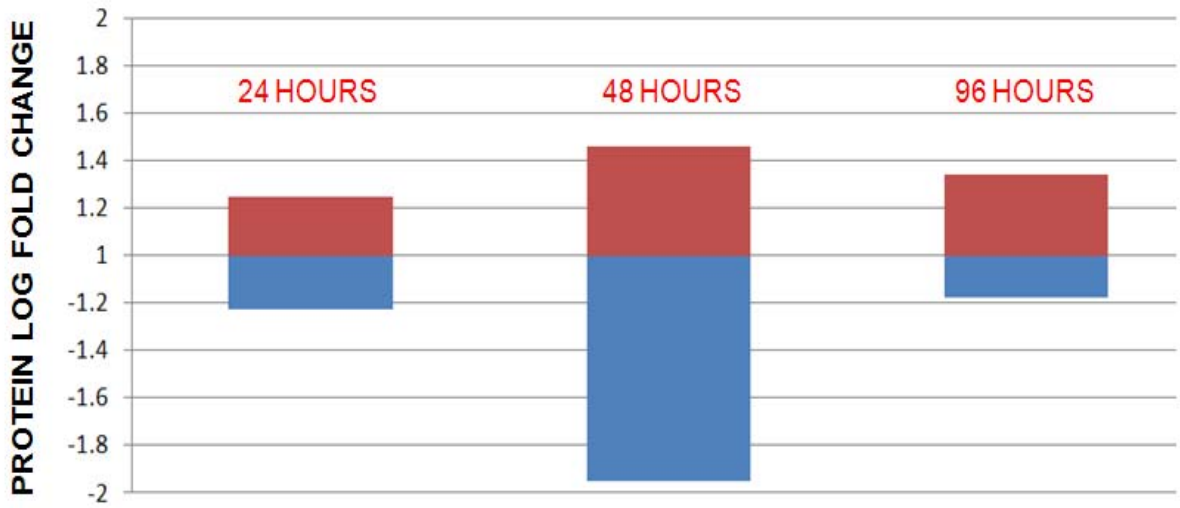

Figure 4-11: Comparison of the detected protein log fold change range at each treatment point ($p<0.05$, $q<0.15$). 48 hours of rINGAP had the greatest change in protein expression.

Table 4-3: Summary of the identified proteins

Hours of rINGAP Treatment	DIGE Protein Number	Protein MS Identification	Fold Change	p-value	q-value
24	157	Caldesmon	1.2	0.0023	0.048
24	158	Caldesmon	1.2	0.0035	0.053
48	45	Caldesmon	-1.46	0.0084	0.15
48	47	Caldesmon	-1.7	0.000039	0.0084
24	834	Transgelin	1.25	0.0028	0.048
48	688	Transgelin	-1.72	0.00092	0.044
48	689	Transgelin	-1.36	0.0084	0.15
24	406	Straitin (STRN)	1.16	0.01	0.0003
48	249	Straitin (STRN)	-1.37	0.083	0.022
48	555	Tropomyosin	-1.36	0.0043	0.11
48	336	Plasminogen Activator Inhibitor	-1.68	0.00005	0.0084
24	680	Annexin V	-1.16	0.019	0.11
24	450	Alpha-enolase	1.21	0.0097	0.083
48	62	Heat Shock Protein 90 (HSP 90)	1.46	0.0062	0.13
48	669	Cofilin 1	-1.38	0.0097	0.15

Table 4-4: List of the MS identified proteins and brief descriptions

Protein Name	Description
Caldesmon	A calmodulin, actin, myosin and tropomyosin-binding protein that plays an essential role in the regulation of smooth muscle and nonmuscle contraction.
Transgelin	A transformation and shape-change sensitive actin binding protein found in fibroblast and smooth muscle cells.
STRN	A calmodulin-binding protein which may function as scaffolding or signaling protein.
Tropomyosin	An actin-binding protein that regulates actin mechanics.
Plasminogen Activator Inhibitor	Inhibits proteases and controls proteolytic cascades
Annexin V	A calcium-dependent phospholipid-binding protein associated with many cellular functions, including: vesicle trafficking, cell division, apoptosis, calcium signaling, and growth regulation
Alpha-enolase	A glycolytic enzyme expressed in most tissues.
Heat Shock Protein 90 (HSP 90)	A member of the heat shock protein family which is upregulated in response to stress.
Cofilin 1	An actin-binding protein which disassembles actin filaments.
Homeobox protein HOX-C8	A transcription factor that plays an important role in morphogenesis in all multicellular organisms.

Identified Proteins

Thirteen proteins were chosen for MS identification and ten proteins were identified. One digested protein spot was undetectable and several spots were isoforms of the same protein. Six of the ten proteins were actin binding, calmodulin binding and/or calcium-dependent proteins. These proteins included caldesmon, straitin, transgelin, tropomyosin, annexin and cofilin 1. Of the greatest significance, the actin-binding proteins caldesmon, transgelin and tropomyosin were both found be to significantly changed at multiple time points. Actin, the cytoskeleton of cell, is vital for a diverse number of critical cellular processes, including, cell motility, cell division and cell surface receptor movement. Actin-binding proteins regulate actin organization both individually and cooperatively to control these cellular processes.

Caldesmon is a large 87 kDa multifunctional protein which binds specifically to calmodulin, tropomyosin, myosin, actin and tropomyosin (Smith, Pritchard et al. 1987; Ikebe and Reardon 1988). In nonmuscle cells, caldesmon differs in its structural organization as it serves as an important cross-linker between actin and myosin (Marston 1989). The functions of nonmuscle caldesmon, which include: the assembly and stability of microfilaments as well

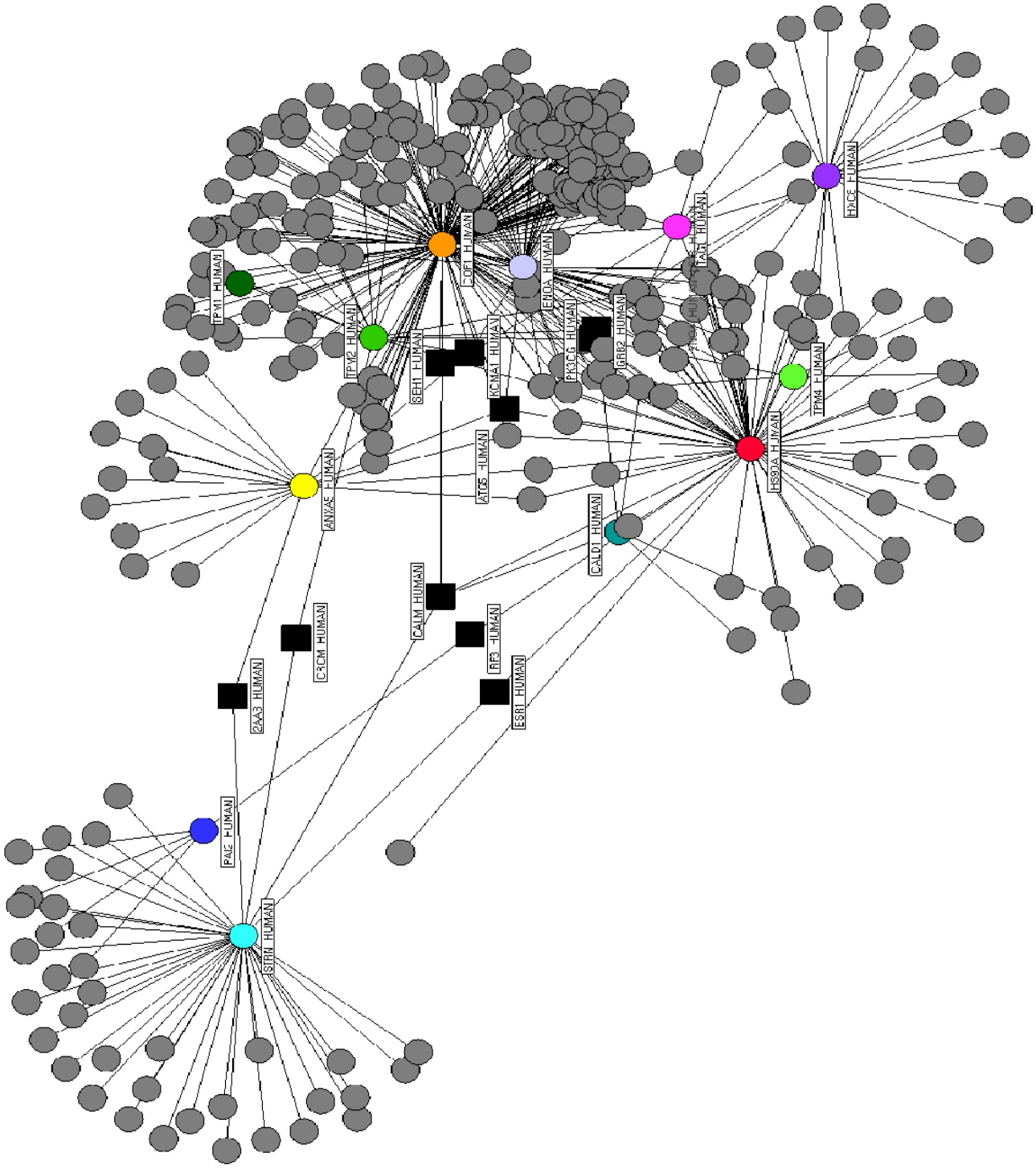

Figure 4-12: Complex protein network of identified up or down-regulated proteins (shown in colours). Black squares are proteins which interacted with the identified proteins with 2-5 degrees of interaction.

as the regulation of cell contraction and intracellular motility processes, are controlled by calcium-calmodulin binding or caldesmon phosphorylation (Dabrowska, Kulikova et al. 2004). Interestingly, in this study, a caldesmon protein-charge train was detected as significantly changed at every time point. Although not fully understood, after 24 hours of rINGAP exposure the charged forms of caldesmon were found to be up-regulated, however at the 48 hour time point all of these caldesmon spots were detected to be down-regulated. This suggests that since rINGAP is affecting every form of caldesmon, the mRNA expression of caldesmon may also be perturbed in hIPCs following rINGAP treatment. Caldesmon has been linked to both type 1 and type 2 diabetes (Imperatore, Hanson et al. 1998; Fogarty, Moczulski et al. 1999). The chromosome in which the caldesmon gene is located (7q35), is associated with type two diabetes (Imperatore, Hanson et al. 1998; Fogarty, Moczulski et al. 1999). Furthermore, caldesmon has been linked to diabetic nephropathy in type 1 diabetic patients and an important role of the actin cytoskeleton in the pathogenesis of diabetes was suggested (Conway, Maxwell et al. 2004).

Transgelin is a 22kDa actin-binding, gelling and transformation sensitive protein found in smooth muscle and non-muscle cells (Shapland, Hsuan et al. 1993). Transgelin is localized in the cytoplasm where it binds actin (Shapland, Hsuan et al. 1993), however it has also been reported to be localized in the nuclear compartment (Bregant, Renzone et al. 2009). The protein plays important roles in the circulatory, genitourinary, respiration and digestive systems (Li, Li et al. 2008). Transgelin expression is lost in several cancers, including: prostate, breast and colon (Shields, Rogers-Graham et al. 2002; Prasad, Stanton et al. 2010).

Therefore, it has been suggested that transgelin acts as a tumour suppressor and may be used as a diagnostic marker of cancer development (Assinder, Stanton et al. 2009). Similar to caldesmon, transgelin was up-regulated at the 24 hour treatment point and down-regulated at 48 hours of rINGAP treatment. Significantly, the protein was detected as changed in two spots on the gel, which indicated that both transgelin isoforms were affected from rINGAP exposure. The physiological diabetes significance of the down-regulation of transgelin is unclear, however transgelin expression has been strongly associated with cell transformation and differentiation (Li, Li et al. 2008; Shapland Hsuan et al. 1993). Its expression is one of the first markers of smooth muscle differentiation during embryogenesis (Li, Li et al. 2008). In a 2D DIGE study of cultured human fibroblast cells from type 1 diabetics in comparison to healthy subjects, transgelin was found to be significantly down-regulated (Puricelli, Iori et al. 2006). Furthermore, several other 2D DIGE analyses have identified the protein as significantly down-regulated during the transition from proliferative to differentiated cellular states (Roche, Provansal et al. 2006; Bregant, Renzone et al. 2009; Kantawong, Burgess et al. 2009). Therefore, it is possible that this DIGE analysis may begin to establish transgelin as an early marker of hIPC differentiation following rINGAP treatment or as a useful differentiation marker in other INGAP and/or pancreatic cellular studies.

In addition to the actin-binding proteins caldesmon and transgelin, the actin binding protein tropomyosin was down-regulated after 48 hours of rINGAP treatment. Tropomyosin is a 37kDa protein that plays a critical role in regulating the actin filaments in both muscle and nonmuscle cells (Gunning, O'Neill et al. 2008). Multiple isoforms of the protein exist in all

mammalian cells, including alpha-tropomyosin, beta-tropomyosin, gamma-tropomyosin and delta-tropomyosin, also termed tropomyosin 1, 2, 3, 4; respectively (Lin, Hegmann et al. 1988). It is believed that these isoforms play central roles in several, if not all, actin cytoskeleton functions, including: intracellular vesicle movement, cell migration, cytokinesis, cell proliferation and apoptosis (Lin, Eppinga et al. 2008). Tropomyosin and its binding proteins, specifically caldesmon (discussed above), have previously been suggested to be required for the regulation of actin filament stability, cell shape determination, and cytokinesis (Lin, Warren et al. 1997).

The 48 hour 2D DIGE analysis detected an area of the gels consisting of seven protein spots which were localized together and all down-regulated following rINGAP treatment (**figure 4-8**). The preparative gel used for MS spot picking, however, did not resolve the seven protein spots, rather the area appeared to be three stained proteins. As a result, these three protein spots (which were detected by DIGE as 7 spots) were excised from the preparative gel and digested for MS analysis. MS identified three of the four tropomyosin isoforms within each of the digested protein samples, including tropomyosin-1, tropomyosin-2 and tropomyosin-4, as well as homeobox protein HOX-C8. HOX genes code transcription factors, including HOX-C8, which are considered master regulators of embryonic development (Axlund, Lambert et al. 2010). The overall functional roles of HOX proteins have been directly related to body patterning, developmental growth and cellular differentiation (Lewis 1978; Mann and Morata 2000; Pearson, Lemons et al. 2005). However, it is not known which proteins and exactly how each protein controls cellular

development. Little has been published on specifically the HOX-C8 protein which was identified as down-regulated after 48 hours of rINGAP treatment. However, the protein has been directly linked to differentiation of mesenchymal cells into chondrocytes using 2D DIGE (Cormier, Mello et al. 2003). This is of significant interest since the expanded hIPCs have been suggested to represent a pancreatic mesenchymal stem cell population (Sordi, Melzi et al. 2010).

In general, heat shock proteins are known to be molecules which are up-regulated in response to environmental changes, as they function to maintain cellular homeostasis (Yamada, Hashiguchi et al. 2000). Heat shock protein 90 (HSP 90) was the only protein identified at the 48 hour rINGAP treatment point which was up-regulated. This result is confirmation that rINGAP induced a response on hIPCs. Furthermore, HSP90 has been strongly associated with cellular morphogenesis and differentiation. The protein has been suggested to enable morphological evolution at the molecular level (Rutherford and Lindquist, 1998; Lele *et al.*, 1999). Hsp90 homeostasis serves as a cellular thermometer, controlling both the heat shock response and morphological differentiation (Wiesgigl and Clos 2001). Hsp90 has been shown to interact directly with ligand-dependent transcription factors and cell cycle regulators (Rutherford and Zuker, 1994; Scheibel and Buchner, 1998; Buchner, 1999), which then impacts morphological differentiation of multicellular organisms (Wiesgigl and Clos 2001).

Overall, the temporal proteomic analysis revealed perturbation and possible reorganization of the hIPC cytoskeleton following rINGAP treatment. Several of the identified proteins

although directly linked to the actin cytoskeleton, have also been previously linked to diabetes, cell proliferation, as well as cell differentiation (Imperatore, Hanson et al. 1998; Fogarty, Moczulski et al. 1999). While other proteins, specifically plasminogen activator inhibitor and alpha-enolase were also identified as down-regulated, it is unclear how these proteins are involved in INGAPs overall mechanistic affect on hIPCs. No proteins were identified which were directly related to insulin secretion. Therefore, to further evaluate if hIPCs were being differentiated towards insulin secreting islet-like cells following rINGAP treatment, it was of interest to complete a temporal mRNA analysis on islet expressing genes.

4.7.2 rINGAP Treatment Alters mRNA Expression of hIPCs

Gene expression studies were carried out to examine whether short-term exposure to rINGAP alone could alter mRNA expression levels in addition to proteomic levels. Of specific interest was to evaluate whether rINGAP was promoting the *in vitro* differentiation of hIPCs towards an insulin-secreting β-cell lineage. The DIGE results demonstrated that rINGAP treatment changed the global protein expression levels of hIPCs at various treatment times. The most significant result was the down regulation of hIPC actin binding proteins associated with the cytoskeletal platform. In this real-time PCR study, we present two repeat experiments of hIPCs treated with rINGAP. Total RNA samples were derived from one donor's hIPCs and analyzed at 24, 48 and 96 hours of rINGAP exposure (same treatment times as the DIGE analysis). As well, the hIPCs were analyzed after 15 minutes and 1 hour of rINGAP treatment to evaluate immediate mRNA expression.

Similar results were obtained from the two experiments; however, in the second experiment insulin was not detected. In the first experiment, after a 15 min of rINGAP treatment, no significant differences were observed between the treated cells and the non-treated controls with respect to cytokeratin-19 (CK-19), glucagon (GLU), insulin (INS), and pancreatic polypeptide genes (PPY) (**figure 4-13i**). Hence, for the second experiment, it was decided not to perform the analysis at the 15 min treatment point. The 1 hour treatment point revealed the most inconsistent results of all time points and the error bars were large. After 1 hour of rINGAP exposure, PPY decreased in both experiments at this time point (**figure 4-13ii**). In the first experiment, CK-19 and GLU increased slightly (**figure 4-13ii**), however in the second experiment both gene expression levels were down at the 1 hour time point (**figure 4-13ii**). At the 24 hour treatment point, the decrease in GLU and CK-19 expression was consistent between the two experiments. However, PPY expression showed inconsistent results (increasing in experiment 1 and decreasing in experiment 2), with large error bars (**figures 4-13iii and 4-14ii**). Significantly, in the second experiment all gene expression levels decreased following rINGAP treatment at 1 hour, 24 hours and 48 hours (**figures 4-14i, 4-14ii, 4-14iii**). In the first experiment, however, PPY increased at 24 and 48 hours (**figure 4-13iv**). Finally, since DIGE analysis was performed after 96 hours of culture, in the second qRT-PCR experiment 96 hour expression levels were evaluated. In comparison to the extent of mRNA expression changes at the earlier time points, no significant expression changes were detected at 96 hours (**figure 4-14iv**).

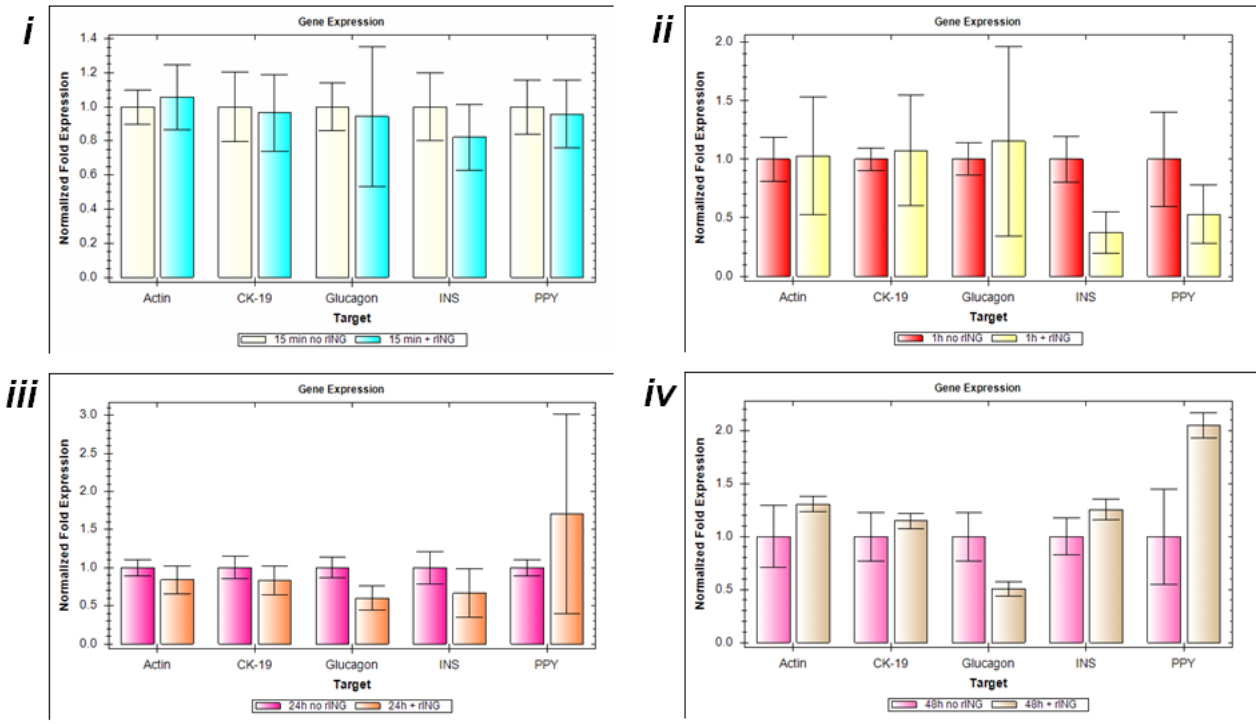

Figure 4-13: First experiment of rINGAP treatment which altered mRNA expression of hIPCs shown by real-time RT-PCR. Treated hIPCs were exposed to 10nM of rINGAP with a media change on day two which included rINGAP supplementation. Shown are mRNA expressions of treated versus non-treated controls at (i) 15 minutes (ii) 1 hour (iii) 24 hours (iv) 48 hours. Error bars correspond to 95% confidence intervals.

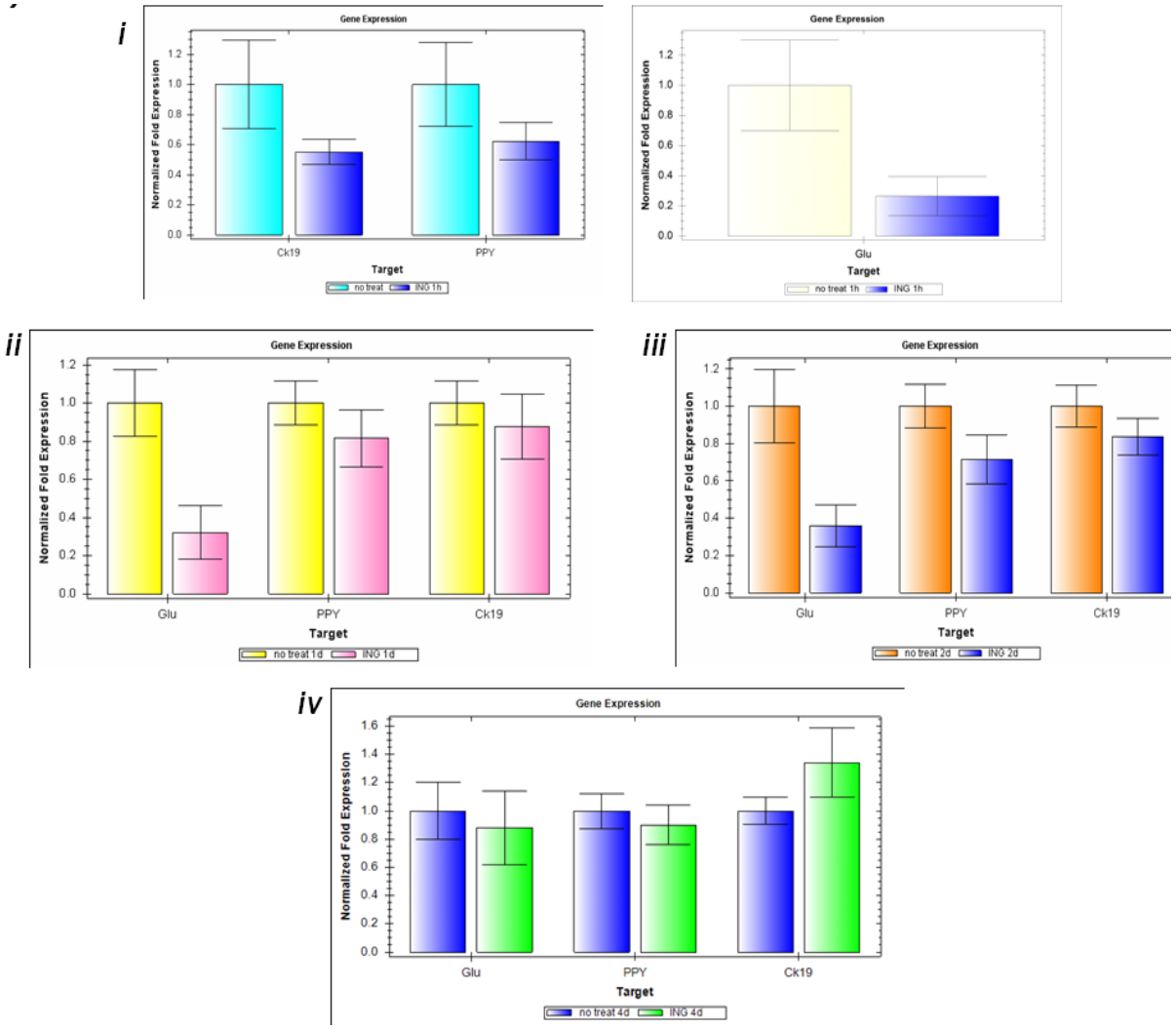

Figure 4-14: Second experiment of rINGAP treatment which altered mRNA expression of hIPCs shown by real-time RT-PCR. Treated hIPCs were exposed to 10nM of rINGAP with a media change on day two which included rINGAP supplementation. Shown are mRNA expressions of treated versus non-treated controls at (i) 1 hour (ii) 24 hours (iii) 48 hours (iv) 96 hours. Error bars correspond to 95% confidence intervals.

Overall, it was observed that rINGAP exposure altered the mRNA expression of hIPCs. These results complement the DIGE analysis. Decreases in islet associated gene expression was the main trend observed in the PCR analysis, and a similar trend was determined by DIGE with many of the protein changes having decreases in expression level. The first PCR analysis had large or overlapping error bars and overall no statistically conclusive results can be drawn. In the second experiment, all gene expression levels (glucagon, PPY and CK-19) decreased significantly to varying extents from 1 to 48 hours of rINGAP treatment. As the absolute expression levels of some proteins, including: PPY, glucagon and CK-19 are likely low (Davani, Ikonomou et al. 2007), the decrease in their levels may not have been readily detected by DIGE. The DIGE results demonstrated the greatest changes in protein expression at 48 hours of treatment. In the second PCR analysis, immediate and comparable decreases in mRNA levels were seen at 1 through 48 hours of treatment (**figure 4-14i, ii, iii**). This is consistent with development and regeneration, in which growth factors often rapidly influence transcriptional and post-transcriptional regulation, with subsequent altered protein expression (Alberts et al. 2008; Gilbert et al. 2006).

In both experiments, insulin expression was either unchanged or inconsistent (experiment 1) or not detected (experiment 2). Inconsistency in insulin detection may have been observed while decreases in the levels of glucagon were detected because while both insulin and glucagon gene promoters have activation histone marks, the glucagon promoter has fewer repressive marks (Wilson, Wong et al. 2009). Hence, rINGAP may act to suppress basal levels of PPY and glucagon endocrine hormones in hIPCs, possibly leaving insulin

unchanged and hIPCs further poised differentiation. Previous *in vitro* work with neonatal rat islets has shown that INGAP pentadecapeptide 104-108 (INGAP-PP) treatment increases insulin and glucagon mRNA expression levels (Barbosa, Bordin et al. 2006). While species differences may exist, the islets in that study were a complex combination of endocrine, stromal, and vascular endothelial cells (Edlund 2002; Hess, Li et al. 2003; Sordi, Melzi et al. 2010), rather than an enriched population of progenitor cells (Davani, Ikonomou et al. 2007). Alternatively, it has been shown that when human cells are INGAP-PP treated *in vitro* CK-19 is typically seen down regulated from duct-like epithelial cells (Jamal, Lipsett et al. 2005). Similarly, in this study, CK-19 mRNA expression was decreased following rINGAP treatment.

4.8 Conclusions

Evidence suggests that hIPCs may represent an important stem cell population that when expanded and cultured *in vitro* could offer a useful supply of cells for islet transplantation. Although the differentiation of hIPCs into functional insulin producing cells has not yet been achieved in this study or others, the investigation of various differentiation protocols using assorted factors, including INGAP, is warranted. It was proposed that INGAP may be a factor required for islet progenitor cell dedifferentiation *in vitro*, as it is suggested for physiological islet regeneration *in vivo* (Rosenberg, Lipsett et al. 2004; Dungan, Buse et al. 2009). Given the correct culture conditions, INGAP supplementation *in vitro* could induce insulin secretion of islet-derived progenitor cells which then could be aggregated into islets for transplantation.

The proteomics coupled with genomics investigation presented in this chapter, further characterizes at the mechanistic level both INGAP and hIPCs therapeutic potential in the treatment of diabetes. As the field of proteomics advances, proteins will be identified with newly discovered functions. These proteins will serve as new bio-markers and will be vital for deducing the mechanisms and responses of drug treatments and differentiation protocols. Of particular importance for drug effect and differentiation studies is the characterization of temporal protein expression in relation to mRNA expression. In this study, we characterized rINGAPs affect on hIPCs to gain insights into possible mechanisms to explain the observed clinical effects of INGAP. DIGE and PCR analyses on hIPCs at three rINGAP treatment times indicated a time-dependent rINGAP effect with the most significant changes in mRNA levels were from 1-24 hours and with the greatest proteomic perturbation at 48 hours of rINGAP exposure.

We have identified for the first time a series of proteins which rINGAP altered expression. Cytoskeletal proteins, specifically, the actin binding proteins: caldesmon, transgelin, tropomyosin and cofilin-1; a heat shock protein (HSP90); and a glycolytic enzyme (alpha-enolase), a protein possibly involved in glucose metabolism, were among those identified as significantly changed. These proteins and their related binding proteins form complex protein interaction networks which have been previously linked to diabetes, cell proliferation and cell differentiation (Imperatore, Hanson et al. 1998; Fogarty, Moczulski et al. 1999). Overall, the temporal proteomic analysis suggests perturbation and possible reorganization of the

hIPC cytoskeleton following rINGAP treatment. Of significant importance, cytoskeletal reorganization in mesenchymal stem cells and progenitor cells has previously been reported (Rodriguez, Gonzalez et al. 2004; Yourek, Hussain et al. 2007; Hong, Chen et al. 2010), which could indicate hIPCs are undergoing differentiation.

The qRT-PCR data indicated that following rINGAP treatment, glucagon, pancreatic polypeptide and CK-19 expression is decreased from 1 hour to 48 hours after treatment initiation, while insulin expression is largely unchanged or undetected. The insulin gene promoter in hIPCs has shown histone modifications indicative of active genes (Mutskov, Raaka et al. 2007), however repressive modifications have been also observed (Wilson, Wong et al. 2009). We propose that rINGAP may act to suppress basal levels of PPY and glucagon endocrine hormones in hIPCs, possibly further poising hIPCs for differentiation. If INGAP is acting early in the differentiation pathway, similar to embryonic cells where such a phenomenon has been confirmed (Fleming and Rosenberg 2007), additional factors are likely required for the differentiation of hIPCs into functional β-like cells (Wilson, Wong et al. 2009). In studies where streptozotocin was administered to animals and islet regeneration was reported (Fernandes, King et al. 1997; Rosenberg, Lipsett et al. 2004), INGAP with other factors aided or contributed to this regeneration - likely at the early stage (Fleming and Rosenberg 2007). Interestingly, at 96 hours of rINGAP exposure, most of the changes in expression levels were attenuated; that is the levels became similar to the control at the mRNA and proteomic levels. It has been observed in previous studies that INGAP is induced rapidly after pancreatic partial obstruction with cellophane wrapping in hamsters and is

detected for up to 2 days (Rafaeloff, Pittenger et al. 1997). Therefore, it has been hypothesized that INGAP may act early in the islet cell induction cascade (Rafaeloff, Pittenger et al. 1997; Fleming and Rosenberg 2007). The early changes in mRNA profiling of hIPCs followed by the detected down-regulation of the actin cytoskeleton following rINGAP treatment is consistent with this hypothesis (Oliver-Krasinski and Stoffers 2008). However, it is acknowledged that the changes were not large and insulin was either unchanged or not-detected. The genes which were analyzed are expressed or down regulated late in the differentiation pathway to islet cells. Therefore, analyses of earlier genes such as Pdx-1 and Ngn-3 which have been correlated with ductal- and islet-associated progenitor cells (Fernandes, King et al. 1997; Seaberg, Smukler et al. 2004; Xu, D'Hoker et al. 2008), would be of interest to confirm this hypothesis. Moreover, it would be of interest to monitor the genes of the proteins determined through DIGE analysis at the mRNA level, to fully understand the mechanism(s) of INGAP action.

The mechanism of INGAP-mediated repression of proteins and mRNA levels remain to be investigated further. It may include developmental and regenerative mechanisms of differential transcriptional control, chromatin structure, mRNA processing, mRNA stability, RNA interference, and translational control (Alberts et al. 2008; Gilbert et al. 2006). Different cell populations may be required to orchestrate complete differentiation, where one cell population may induce another (Gilbert et al. 2006). Other cells may respond to INGAP to induce hIPC differentiation. Alternatively, INGAP may be acting on hIPCs to induce genes that influence the fate of other cells (Gilbert et al. 2006). Finally, some studies have

proposed that hIPCs may form a stromal population of cells in the islets *in vivo* (Sordi, Melzi et al. 2010), which INGAP may be targeting and inducing islet neogenesis in the treated patients with diabetes.

Chapter 5 Live Cell Imaging Analysis of Human Islet-Derived Progenitor Cells Treated with rINGAP

5.1 Preamble

To further understand the cellular, specifically cytoskeletal effects of rINGAP on hIPCs, this chapter expands the previous mechanistic findings of rINGAP. Long term live-cell imaging was used to study cell motility and proliferation effects and immunofluorescent imaging of two actin binding proteins which were identified in the DIGE analysis in the previous chapter are utilized to understand the cytoskeletal effects of rINGAP on hIPCs.

5.2 Publication Title and Authors

The results presented within this chapter have been prepared for publication to the Journal of Cytoskeleton.

Title: rINGAP Induces Morphological Changes and Cytoskeletal Reorganization in Human Islet-Derived Progenitor Cells

Authors:

Erika Murray[1], Bredon Crawford[1], Julien Verneau[1], Lawrence Rosenberg[2], Eric Jervis[1]

[1]Department of Chemical Engineering, University of Waterloo, Waterloo, Ontario, Canada; [2]Department of Surgery, McGill University, Montreal, Quebec, Canada

Running Headline: Live-cell imaging of hIPCs with rINGAP

5.3 Overview

Expansion of isolated human islets in culture yields a proliferative population of nestin positive human islet-derived progenitor cells (hIPCs) that have been previously characterized as pancreatic mesenchymal stem cells (pMSCs). The therapeutic potential of hIPCs for diabetes treatment is not understood and requires further investigation. Here, we use long term live-cell imaging and immunocytochemistry to characterize the phenotypic effects of a therapeutic protein, islet neogenesis associated protein (INGAP), on hIPCs in culture. In human clinical trials INGAP peptide increased C-peptide secretion in Type 1 diabetic patients and improved glycemic control in Type 2 diabetic patients. The mechanism of INGAP action, including cellular specificity and receptor, is unknown. Live-cell imaging enabled the tracking of nuclear motion every 5 minutes over 76 hours. Analysis revealed a greater than 50% decrease in average nuclear speed and a change in morphology of cells exposed to recombinant INGAP (rINGAP). Furthermore, immunofluorescent labeling of actin binding proteins (ABPs) tropomyosin and caldesmon exhibited perinuclear and extranuclear translocation in rINGAP-treated cells, respectively. These results combined are suggestive of a decreased proliferation potential of hIPCs exposed to rINGAP. We demonstrate rINGAP affects cell morphology, cell motility, cytoskeletal arrangement and propose rINGAP may poise hIPCs for differentiation.

Keywords

Live-cell imaging; lineage analysis; human islet-derived progenitor cells (hIPCs); islet neogenesis associated protein (INGAP); pancreatic mesenchymal stem cells (pMSCs); actin binding proteins (ABPs); caldesmon; tropomyosin

5.4 Introduction

Diabetes is a disease strongly associated with the loss of β-cell mass in the pancreas. Type 1 diabetes mellitus is the result of a progressive autoimmune-mediated destruction of β-cells, and patients with Type 2 diabetes typically have a 50% decrease in β-cells mass (Halban 2004). This decrease in cell mass results in a decline of insulin secretion and contributes to a loss of glucose homeostasis. Although islet transplantation has resulted in improved glucose stability with a significant reduction of insulin dependence, a shortage of pancreas organ donors in combination with engraftment and immunosuppressant toxic effects, limits the therapeutic potential of this approach (Shapiro, Lakey et al. 2000; Ryan, Paty et al. 2005). Islet regeneration is an ideal treatment for this loss of insulin production. *In vivo,* islet neogenesis associated protein (INGAP) is being administered in animal models and clinical trials, and evaluated for islet cell neogenesis, C-peptide secretion, and glycemic control (Rosenberg, Lipsett et al. 2004; Barbosa, Bordin et al. 2006; Dungan, Buse et al. 2009). *In vitro*, a central goal of regenerative diabetes research is the generation of functional islet cells for transplantation (Serup, Madsen et al. 2001; Peck, Cornelius et al. 2002; Baharvand, Jafary et al. 2006; Tateishi, He et al. 2008).

Targeting cells derived from the *in vitro* expansion of pancreatic islets may represent an ideal cell source for islet differentiation, since these expanded cells retain epigenetic marks (Joglekar, Joglekar et al. 2009) and activity of the islet gene modules (Kutlu, Kayali et al. 2009). The expansion of isolated islets results in a proliferative cell population of islet derived progenitor cells (IPCs) characterized as pancreatic mesenchymal stem cells (pMSCs) (Sordi, Melzi et al. 2010), that express insulin mRNA at low levels and are capable of differentiating into hormone-expressing cells at levels 1% of adult islets (Davani, Ikonomou et al. 2007). Additionally, when pMSCs are transplanted with minimal pancreatic islet mass, they facilitate neovascularization of the graft and restoration of normoglycemia in the mice (Sordi, Melzi et al. 2010). Although it is known that pMSCs do not express the insulin gene (Mutskov, Raaka et al. 2007) and express negligible levels of islet-specific genes (Sordi, Melzi et al. 2010), they do possess epigenetic markers that could position them for activation of insulin expression (Mutskov, Raaka et al. 2007).

Activation of insulin expression of IPCs may require one or more factors to induce differentiation into functional insulin producing cells. Several factors have been suggested as inducers of beta-cell mass which may also act on IPCs, including but not limited to a combination of gastrin and epidermal growth factor (EGF) (Brand, Tagerud et al. 2002; Suarez-Pinzon, Lakey et al. 2005; Suarez-Pinzon, Yan et al. 2005), glucagon-like peptide-1 (GLP-1) (Tourrel, Bailbe et al. 2001; Xu, Kaneto et al. 2006), exendin-4 (Xu, Stoffers et al. 1999; Xu, Kaneto et al. 2006) and INGAP (Rafaeloff, Pittenger et al. 1997; Rosenberg, Lipsett et al. 2004; Barbosa, Bordin et al. 2006). INGAP is a 17 kDa protein which was

discovered to be a constituent of ilotropin (Pittenger, Vinik et al. 1992), an islet-specific growth factor, which is expressed during islet neogenesis. Through further sequencing of INGAP, an active region of the protein (amino acids 104-118) was determined to have similar islet neogenesis effects and has been termed INGAP peptide (Rafaeloff, Pittenger et al. 1997). In human clinical trials, INGAP peptide increased C-peptide secretion in Type 1 diabetic patients and improved glycemic control in Type 2 diabetic patients (Dungan, Buse et al. 2009). Furthermore, dissection of mouse pancreata has shown that INGAP peptide increases β-cell mass (Rosenberg, Lipsett et al. 2004), however the precise mechanism of INGAP action, including cell target and receptor is unknown.

To date, studies of INGAP have focused on evaluating the islet neogenesis effects of INGAP peptide. Although the original work of the cloning and sequencing of INGAP concluded that both the peptide and the protein demonstrated effects of islet neogenesis, it was noted that the INGAP protein appeared to have a more potent effect (Rafaeloff, Pittenger et al. 1997). Recently, the production and characterization of full-length recombinant INGAP (rINGAP) has been reported to facilitate studies of the mechanism(s) of INGAP action (Assouline-Thomas, Pilotte et al. 2009). Importantly, rINGAP exhibits 100 times the bioactivity in comparison to the INGAP peptide using an *in vitro* assay (Assouline-Thomas, Pilotte et al. 2009). Mechanistic studies of rINGAPs action on various pancreata cell types require further investigation, including rINGAPs effect on IPCs. Although it is unknown if these cells represent a physiological stem cell population, characterization of an islet neogenesis factor

such as rINGAP is necessary for the clinical development of both INGAP and islet-derived cells in diabetes treatment applications.

Here, we use live-cell imaging to characterize the effect of rINGAP on human islet derived progenitor cells (hIPCs) with a previously reported novel culture system (Ramunas, Illman et al. 2006). The imaging chamber culture system allowed for nuclear tracking using differential interference contrast (DIC) microscopy, lineage tree construction, and phenotypic scoring, to characterize rINGAP-treated hIPCs. Our results reveal rINGAP significantly decreases nuclear speed, indicating that rINGAP affects nucleo-cytoplasmic coupling, a previously unknown cellular consequence of rINGAP. We demonstrate that hIPCs respond immediately to rINGAP and reach an average nuclear speed of 8 μm/hr from an initial average speed of 18 μm/hr within 10 hours of rINGAP addition. Furthermore, two actin binding proteins, tropomyosin and caldesmon, which have been previously associated with cell speed (Bach, Creed et al. 2009; Jiang, Huang et al. 2010), differentiation (Abd-el-Basset, Ahmed et al. 1991) and rINGAP exposure (manuscript in preparation), exhibited perinuclear and extranuclear localization following rINGAP treatment of hIPCs. These results were consistent with the rINGAP cellular motility and nuclear speed effects observed through the live-cell imaging analysis. These observations provide novel mechanistic insights into rINGAPs effect on hIPCs, which include: a decrease in cell speed and directional persistence, a change in tracked morphology, and the cytoskeletal reorganization of hIPCs exposed to rINGAP. These observations suggest a potential mechanism of hIPCs in the therapeutic effect of INGAP, which may prove clinically relevant for the treatment of diabetes.

5.5 Materials and Methods

Human Islet-Derived Progenitor Cell (hIPC) Culture

Human islet isolation protocols were approved by the Institutional Review Board of McGill University, Montréal, QC. A healthy pancreas was obtained from an adult cadaveric donor through an organ procurement organization at Montréal General Hospital. The islets were isolated according to established protocols (Shapiro, Lakey et al. 2000; Jamali, Emmerson et al. 2005). Briefly, islets ranging from 75 to 400 μm were determined to be greater than 90% purity by dithizone staining (Sigma, St Louis, MO), collected, washed and re-suspended in CMRL-1066 medium with penicillin, streptomycin, and amphotericin B (Antibiotic-Antimycotic (100X) liquid; Gibco, Burlington, ON) and 10% fetal bovine serum (MBI, Amherst, NY). Suspended islets were placed in a polypropylene container without airspace and shipped on ice overnight from Montréal, QC to Waterloo, ON.

The hIPCs were derived from the fresh human islets as described previously (Gershengorn, Hardikar et al. 2004; Gallo, Gambelli et al. 2007; Sordi, Melzi et al. 2010) with modifications. Briefly, the islets were plated in 75 cm^2 tissue culture-treated flasks at a density of approximately 1 islet/mm^2 in modified RPMI-1640 medium (11.1 mM glucose) (Invitrogen, Burlington, ON), supplemented with 10% FBS (Invitrogen, Burlington, ON). The flasks were incubated at 37°C, 5% CO_2 and 95% humidified air, and after 48 hours non-adherent cells were removed and 12.5 mL of fresh media was replenished. The media was then replaced every 3 days for the remainder of the culture. At day 15 of culture the islets

which were spread into a monolayer were detached from the surface with 2.5 g/L trypsin with 0.38 g/L EDTA (Invitrogen, Burlington, ON) and reseeded as single cells at a density of $1.2x10^4$ cells/cm^2, followed by subsequent passaging at $4x10^3$ cells/cm^2 once 85% confluence had been obtained, approximately every 10 days.

Live-Cell Imaging

Trypsinized hIPCs were resuspended in media at a concentration of $2x10^7$ cells/mL. Commercial 10 μm size standard beads (Corpuscular Inc., Cold Spring, NY) were used to maintain spacing when loaded under aminopropyl trimethoxy silane (APTS)-treated glass imaging chambers as previously described (Ramunas, Illman et al. 2006; Moogk, Hanley et al. 2007). The chambers were filled with 1.5 mL of RPMI-1640 medium with 10% FBS. Imaging chambers were then cultured under standard conditions for 24 hours to allow for cell attachment before long term imaging on inverted microscopes using DIC (Axiovert 200; Carl Zeiss MicroImaging GmbH, Berlin, Germany). Imaging was performed in a humidified 37°C atmosphere with 5% CO_2 for 76 hours using monochrome high resolution CCD cameras (XCD-SX910/X710; Sony Corporation, Tokyo, Japan) at 5 minute intervals with 20X objective and a 0.5X camera adapter. Image mosaics were compiled using custom-built motorized stages and image software (Moogk, Hanley et al. 2007). After 23 hours of imaging, 1.5 mL of media was replaced with fresh media supplemented with 10nM of rINGAP supplied by the Rosenburg Lab, Montréal, QC, produced and purified as previously described (Assouline-Thomas, Pilotte et al. 2009). In the control population, 1.5 mL of fresh

media was replaced without rINGAP addition. At 48 hours, 10nM of rINGAP was re-supplemented into the media of the rINGAP-treated chamber. Both the rINGAP-treated and control chambers were imaged for 53 hours after the first rINGAP addition.

Cell Tracking

Individual fields of view were combined to create mosaics covering 3.4 mm^2. Time-lapse image mosaics were tracked as previously described (Moogk, Hanley et al. 2007) to capture cell nuclei x-y position using distinct cellular features as references, including: cell membrane, cell cytoplasm, nuclear envelope and nucleoli. Nuclear tracking was performed by manual examination of image frames captured every 5 minutes over the 76 hours of acquisition. The tracker was uninformed of the experimental details to prevent biased tracking. Cell fates, including cell divisions, deaths and loss-of-trackability were recorded and lineage trees were generated. Loss-of-trackability included loss of observable nuclear features, such as: nuclear envelope and nucleoli, and cell migration from the field of view. In total, 24,675 positional data points were recorded for the rINGAP-treated cells and 15,845 positional data points were recorded for the control population. **Figures 5-1 a-c** demonstrates an individual hIPC tracked by nuclear position over 56 hours, using observable nuclear features in the same field of view.

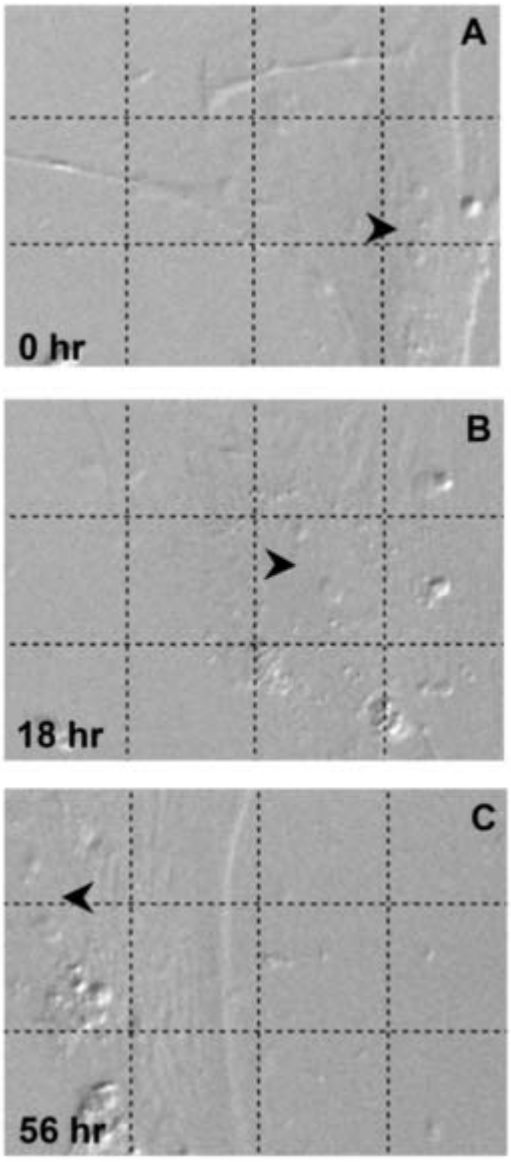

Figure 5-1: Nuclear position was tracked using nuclear features including nuclear envelope and nucleoli. DIC images were taken every 5 minutes. Images are shown at 0 (a), 18 (b), and 56 (c), hours of a typical tracked hIPC. The arrowheads indicate the nuclear position assigned by the tracker. The grid size represents 30µm.

Data Analysis

At the first recorded time-step the nuclear x-y positions were determined and a nearest neighbor distance was calculated for each cell to verify comparable cell loadings between the two chambers, with respect to both cell density and spatial distribution. The cell density (d) was also calculated for the mosaic area. The average nearest neighbor distance ($\bar{r}$) was normalized to the expected value for randomly distributed nuclei, $(r) = \frac{1}{2\sqrt{d}}$, to yield the index of aggregation (Clark and Evans 1954) $R = 2\bar{r} \cdot \sqrt{d}$.

Position data was used to calculate speeds for each cell over time in both rINGAP-treated and control hIPC populations. Trackable motions were determined from consecutive nuclear position measurements, calculating speed as displacement per time-step. Due to human tracking limitations, cells with nuclear motions less than 0.5 μm/hr were considered stationary. These measurements comprised only 0.3% of all tracked movements in comparison to 30% of measurements which were tracked as stationary. Speed and the logarithmic transformation of speed were used to identify trends and to determine statistical significance. Cell movement paths, normalized to an arbitrary origin, were visualized as rose plots using MatLab (MathWorks™).

Statistical Analysis

Error bars on graphs depicting speed correspond to the standard error of the mean (SEM), while error bars on logarithmically transformed speed graphs correspond to 95% confidence intervals. Statistical analysis was performed in Statistica 8 (StatSoft™) and Microsoft Excel 2007™.

Immunostaining and Confocal Microscopy

hIPCs were expanded from isolated human islets and cultured in imaging chambers for 100 hours as described above. The expression of nestin, CD133, vimentin, cytokeratin 19 (CK-19), tropomyosin and caldesmon, were examined with immunofluorescent confocal microscopy. At the end of the image acquisition cells were rinsed twice with PBS, fixed with 4% paraformaldehyde for 20 min, rinsed twice with PBS, permeabilized with 0.5% Triton X-100™ for 45 min, rinsed twice with PBS and blocked with 5% BSA at room temperature overnight. Cells were then rinsed with PBS and incubated with primary antibodies for 4 hours at room temperature. All antibodies were purchased from Abcam Inc. Cambridge, MA or Miltenyi Biotec, Germany. The primary antibodies used were 1:1000 mouse monoclonal anti-nestin (ab22035), 1:11 mouse monoclonal anti-CD133 (MACS 130-090-851), 1:150 rabbit polyclonal anti-vimentin (ab15248), 1:4 rabbit polyclonal anti-cytokeratin 19 (ab15464), 1:50 mouse monoclonal anti-tropomyosin (ab7785) and 1:250 rabbit monoclonal anti-caldesmon (ab32330). Following primary antibody staining, cells were rinsed with PBS and blocked with 1% BSA overnight. Secondary antibodies were then incubated overnight at 4°C and comprised 1:2000 goat polyclonal to mouse IgG FITC (ab6785) and 1:800 goat

polyclonal to rabbit IgG Cy5 (ab6564). The cells were rinsed twice with PBS, nuclear stained using DAPI with antifade (Vector Laboratories Inc., Burlington, ON) for 20 min and imaged sequentially on a laser scanning confocal microscope (FV1000; Olympus Canada Inc., Markham, ON).

5.6 Results

Human Islet-Derived Cells Express Mesenchymal Markers (Nestin$^+$ and Vimentin$^+$)

Phenotype was evaluated using immunocytochemistry of mesenchymal (nestin, vimentin) and epithelial (CK19, CD133) markers to verify that the outgrowth cells from expanded human islets were characteristic of a mesenchymal cell population. These results showed the entire population to be nestin$^+$, vimentin$^+$, CK19$^-$, and CD133$^-$ at passages four, six, and eight (figures 5a-c). This was in agreement with previous characterization of IPCs as pMSCs in which nestin$^+$ pMSCs were found to completely replace the non-proliferative highly apoptotic epithelial (CD133$^+$) cells from expanded islets (Sordi, Melzi et al. 2010).

Cell Tracking, Scoring and Lineage Analysis Demonstrates a Change in Morphology Following rINGAP Treatment

Wide field live-cell DIC microscopy was employed to image 3.4 mm^2 areas at high spatial and temporal resolution for 76 hours using mosaics of 20X magnification collected every 5 minutes. To confirm comparable hIPC loadings of the imaging chambers, cells were counted in each mosaic element 24 hours after cell seeding. The distribution of loadings was evaluated using the Clark-Evans nearest-neighbor statistic (Clark and Evans 1954). Cells

were counted in the control mosaic (N=387) and in the chamber to be treated with rINGAP (N=400). Clark-Evans R-statistic values for the control and rINGAP chamber, were calculated and determined to be comparable (R=1.02 and 1.07, respectively). A value of R=1 represents complete spatial randomness (Clark and Evans 1954), indicating hIPC loadings were randomly distributed in both chambers at the beginning of the imaging run. Of the 400 cells in the mosaic of the rINGAP chamber, 32 hIPCs were randomly selected to be tracked, with 7 of these cells remaining trackable for the entire 76 hours of imaging. In comparison, 25 cells were randomly selected to be tracked in the control chamber with 9 remaining trackable to the end of the experiment.

Cell lineages were produced by manual nuclear tracking of x-y positions, cell divisions and deaths (**figures 5-2 a,b**). In the lineage trees, an 'X' indicates cell death in which cells typically spontaneously rounded up and burst. A 'Δ' indicates that the cell left the imaging field of view and therefore became untrackable. An 'O' indicates that the cell lost DIC imaged nuclear features, such as distinct nuclear envelope and nucleoli, and therefore became untrackable. 6 of the 32 tracked cells divided in the rINGAP chamber, which included 4 cells that divided before and 2 cells that divided after the rINGAP addition. In comparison, none of the 25 randomly-selected tracked cells divided in the control. A one-sided Fishers exact test showed poor evidence of a difference in proliferation frequency between the two chambers prior to rINGAP addition (p=0.1054). Additionally, examination of randomly-selected fields of view from each chamber (n=8), failed to demonstrate a significant difference in the number of division events during the first 10 hours of imaging (p=0.2359).

These results reveal that both chambers were proliferating at comparable rates prior to the addition of rINGAP. Based on the reported doubling time of pMSCs (84±16 hours (Sordi, Melzi et al. 2010)), doubling time was evaluated and no cells divided more than once in the 76 hours of imaging in either the rINGAP or control chambers.

We determined through the live-cell tracking and scoring a change in cellular morphology following rINGAP addition. The rINGAP-treated hIPCs exhibited a transition from an adherent state in which the nuclear membrane and nucleoli were visible to partial losses of attached phenotype and observable nuclear features, which rendered a significant proportion of hIPCs untrackable at the 5 min time-steps following rINGAP addition. Live-cell imaging analysis of the control versus the rINGAP-treated chamber revealed only one cell of 25 tracked hIPCs in the control population was found to become permanently untrackable (**figure 5-2a**). In comparison, 12 of 32 tracked cells in the rINGAP-treated chamber were scored as having a permanent loss of trackable nuclear features with the described morphological changes (**figure 5-2b**), consistent with the cytoplasmic retraction of the plasma membrane. These untrackable cells were confirmed to exhibit features of live cells, such as cytoplasmic activity and vesicular movement, and to retain their untrackable morphology until the end of the imaging run (**figures 5-2c,d**). It is concluded that the loss of trackable nuclear features especially the loss of distinct nucleoli, combined with morphological changes, was a morphogenetic response of hIPCs induced by rINGAP. Of importance, the observed morphological changes, including cell rounding,

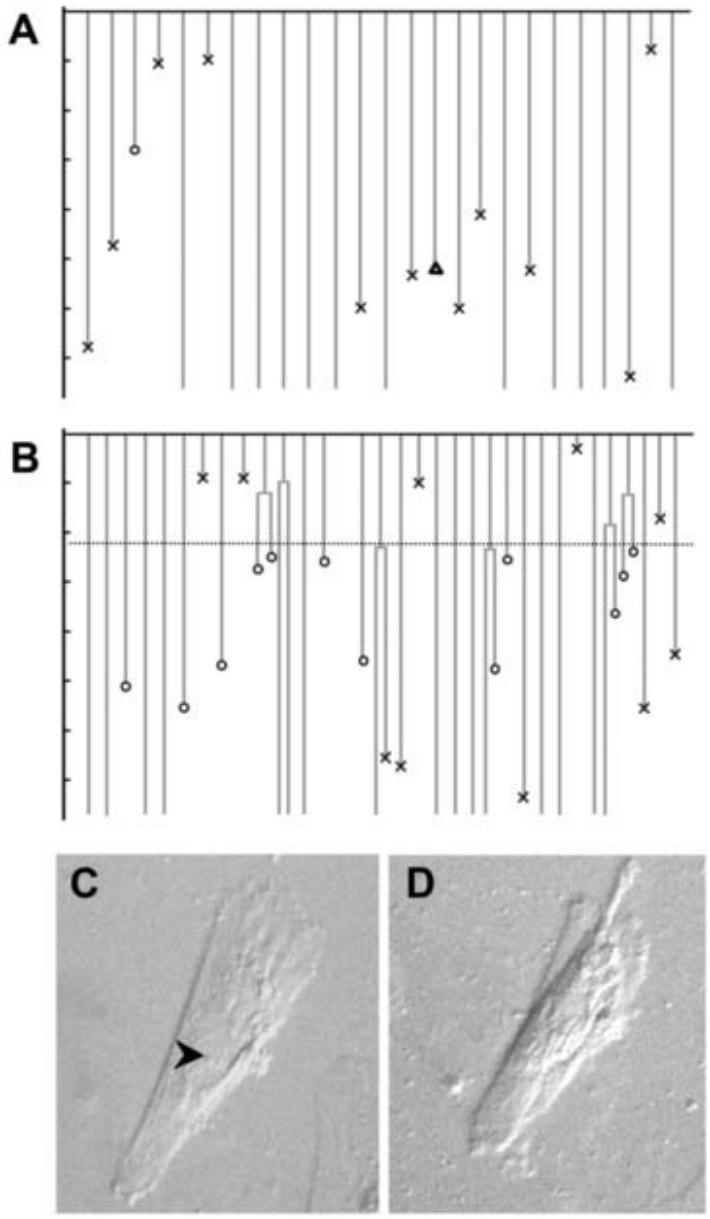

Figure 5-2: Lineage trees of randomly selected hIPCs tracked every 5 minutes over 76 hours, with a representative cell shown. (a) Control lineage with 25 randomly selected tracked cells. (b) rINGAP-treated lineage with 32 randomly selected tracked cells. rINGAP was added at 23 hours indicated by the dotted horizontal line. X, ∆, and O indicate cell death, cell migration from the imaging field of view and a loss of trackable nuclear features, respectively. A typical cell in which the nucleus was visible for tracking for the first 30 hours of imaging (c) followed by a loss of trackable nuclear features and change in cell morphology after rINGAP addition (d) this cell was scored with an O.

membrane ruffling, and cytoplasmic retraction have been associated with cell motility (Okamoto, Kajiya et al. 2004; Fackler and Grosse 2008), as well as the differentiation of MSCs and other stem cells (Worster, Nixon et al. 2000; Wenisch, Trinkaus et al. 2006; Rowlands, George et al. 2008).

rINGAP Reduces Cellular Movement and Nuclear Speed

To determine if rINGAP had an effect on hIPC motility, the 76 hours of x-y nuclear position data was used to generate rose plots to visualize the migration paths of the tracked hIPCs in culture (**figure 5-3**). Two rose plots were generated for each of the control and rINGAP chambers; at 0-20 hours of imaging (before rINGAP addition) and at 50-70 hours (27 hours after rINGAP addition) (**figures 5-3 a,b,d,e**). For the first 20 hours of imaging, the rose plots of 20 randomly selected cells in the control chamber and in the chamber to be treated with rINGAP, revealed the cells migrated approximately the same distance over time (80 μm over 20 hours) and with similar migratory trajectories before rINGAP was supplemented in the media (**figures 5-3 a,d**). Following the addition of rINGAP, comparison of the rose plots revealed an overall decrease in directional persistance at 50-70 hours in both the control and the rINGAP-treated hIPC populations (**figure 5-3**). It was concluded that although the cells were incubated for 24 hours to allow for cell attachement prior to imaging, during the first 20 hours of imaging the cells were not fully attached therefore resulting in increased cell motion at the beginning of the run in both chambers. Most importantly, closer evaluation of the rose plots following rINGAP addition (**figures 5-3c,f**) revealed a reduced density of nuclear paths

in the rINGAP-treated chamber relative to the control. In summary, the rose plots demonstrated qualitatively that the hIPCs in both chambers were migrating over comparable distances with similar trajectories prior to the addition of rINGAP, however the rINGAP-treated hIPCs significantly decreased migration in response to rINGAP. Since cell migration is dependent on both cell direction and speed, it was unclear from the qualitative observations of the rose plots if rINGAP affected both, or just one parameter. To accurately evaluate the distance the cells travelled over the 76 hours of imaging, nuclear paths were analyzed in terms of cumulative distance. Average cumulative distance plots for both the control and the rINGAP-treated hIPCs revealed that prior to rINGAP induction (0-23 hours) both chambers hIPCs had comparable cumulative distance trajectories, consistent with the rose plots, however at 23 hours of rINGAP addition rINGAP-treated hIPCs show a reduction in distance travelled over time (**figure 5-4a**).

We next determined the average speed of the hIPCs over 70 hours (**figure 5-4b**). Following rINGAP addition, rINGAP-treated hIPCs exhibited a significant decrease in average nuclear speed, from 17.9±0.5 to 8.0±0.4 μm/hr (SEM), which persisted for the remaining 2 days of

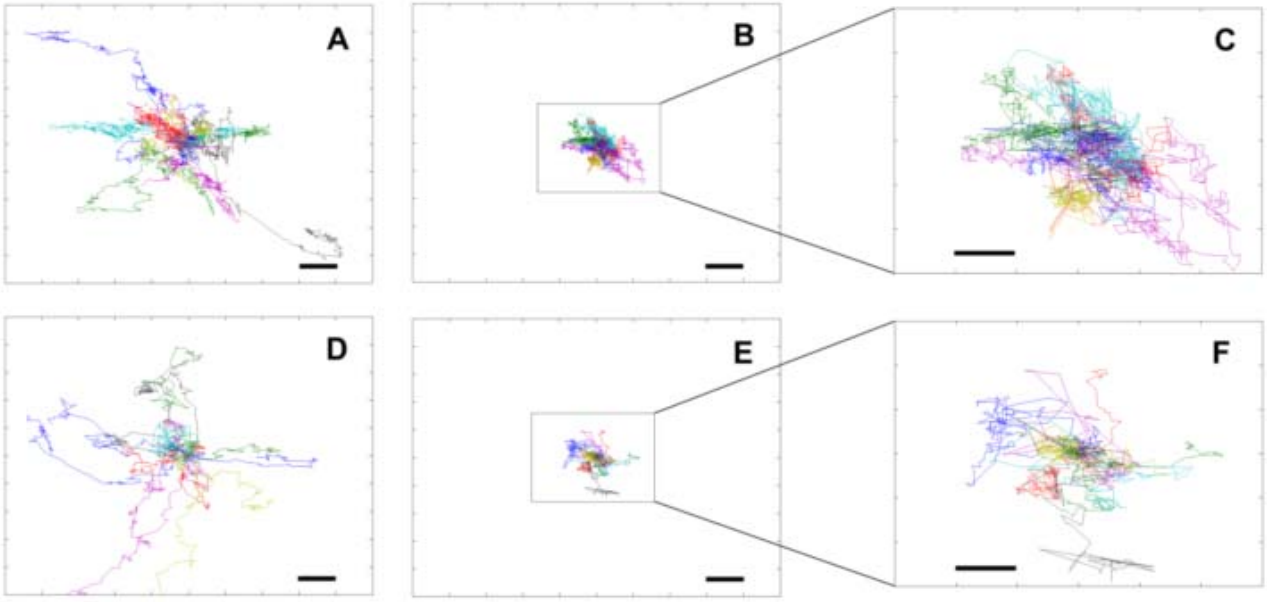

Figure 5-3: Rose plots of control and rINGAP-treated hIPCs. Each line represents the migration path of a tracked nucleus, normalized to the origin. Control (a) and rINGAP-treated cells (d) are shown at 0-20 hours (n=20 cells), and at 50-70 hours (n=14 cells) (b,e respectively). (c,f) Enlarged rose plots of b,e (respectively). Scale divisions correspond to 20µm (a,b,d,e) and 10µm (c,f). Prior to rINGAP addition both cell populations are migrating over the same distances with comparable cellular movements (a,d). Comparison of 0-20 hours versus 50-70 hours reveal both cell populations exhibit a decrease in overall migration attributed to increased cell attachment (a-b,d-e). Comparison of control versus rINGAP-treated cells at 50-70 hours shows decreased nuclear movement relative to the control population (c,f).

the experiment. In comparison, there was no overall reduction in cellular speed in the control cell population. Nuclear movement has been shown to be saltatory, with average speed as the product of movement frequency and magnitude (Danowski, Khodjakov et al. 2001; Umeshima, Hirano et al. 2007; Nichols, Carney et al. 2008). Therefore, the reduction in speed following rINGAP-treatment may have then been caused by either smaller saltatory motions and/or less frequent motions. In other words, when the rINGAP-treated hIPCs moved, they travelled shorter distances and/or they remained non-motile more often, resulting in the reduction in cellular speed. In order to more precisely evaluate the rINGAP effect on hIPCs in terms of migratory behavior, the time course imaging data was used to plot saltatory motion distances and frequencies over time (**figures 5-4c-f**). Saltatory behavior of hIPCs was confirmed with both large movements and non-motile periods. Prior to rINGAP addition both the control and rINGAP chambers demonstrated similar movement frequencies and magnitudes (**figures 5-4c,e**). However, following rINGAP addition the frequency and magnitude of saltatory motions decreased in comparison to the control (**figures 5-4d,f**). The percentage of non-motile observations increased from 30 to 45% following rINGAP-treatment, indicating fewer cellular motions as a result of rINGAP exposure (**figure 5-4i**). In comparison, control cells did not show a change in movement frequency over the 70 hours of the experiment (**figure 5-4i**).

Although it was concluded that rINGAP induced an increase in the frequency of stopped motions, it remained qualitative that rINGAP also reduced the magnitude of nuclear movements. To evaluate the magnitude of nuclear movements, the distribution of non-zero

measurements (motions > 0.5 μm) were logarithmically transformed before and after rINGAP-addition (**figures 5-4g,h**). In the rINGAP-treated chamber, the distribution of transformed speeds shifted left, indicating an increase in small motions and a reduction of larger motions (**figure 5-4h**), confirming rINGAP decreased the magnitude of the saltatory motions in addition to the frequency of non-motile periods. This shift had a significant ($p < 0.001$) overall decrease in mean log speed compared to no significant change in the control cell population (**figure 5-4j**). Since cell motility is driven by the actin cytoskeleton (Lambrechts, Van Troys et al. 2004), it is suggested that rINGAP disrupts the actin cytoskeleton, amongst a cascade of other cellular mechanisms which remain to be determined, resulting in the reduced motility of hIPCs.

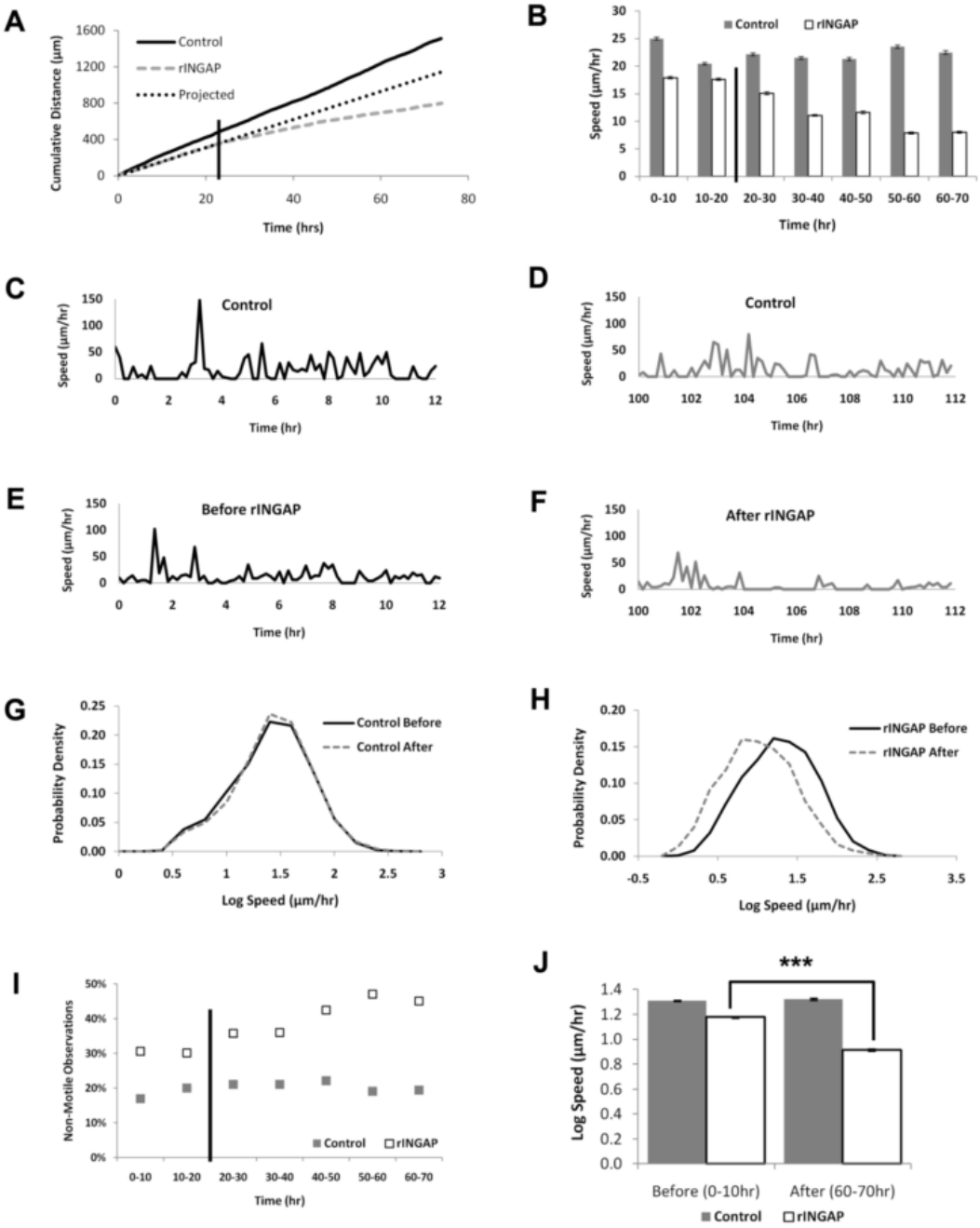

Figure 5-4: (a) Average cumulative distance plot of control versus rINGAP-treated cells. The dotted line represents the trend prior to rINGAP addition. Deviation from this line illustrates the immediacy of the rINGAP effect. (b) Average speeds over 10 hour intervals show a persistent loss of speed following rINGAP addition; standard error shown. (c,d,e,f) Velocity profiles of typical cells over 12hr periods show saltatory motion of nuclei. (d,f) Comparison of nuclei motions after rINGAP addition indicates rINGAP stops movement. (i) The proportion of measurements without movement was found to increase from 30 to 45% for rINGAP-treated cells. (g,h) The logarithmic transformation of the nuclear speed yielded a nuclear speed distribution diagram showing a reduction in the magnitude of nuclear motions that occurred after rINGAP addition. (j) The reduction in the mean log speed was statistically significant ($p < 0.001$) for rINGAP-treated cells. Vertical lines at 23hr indicate rINGAP addition (a,b,i).

Actin Binding Proteins are Reorganized in rINGAP-Treated hIPCs

Changes in nucleokinetic speed and cellular morphology were indicative of cytoskeletal effects on the hIPCs following rINGAP exposure. We performed a proteomic analysis using 2D Differential in Gel Electrophoresis (2D-DIGE) and identified several proteins responsive to rINGAP-treatment, including tropomyosin and caldesmon (manuscript in preparation). The effects on morphology and cell motility observed through the live-cell imaging led us to further investigate these two actin binding proteins (ABPs). Tropomyosin and caldesmon are involved in the organization and remodeling of the actin cytoskeleton in muscle and nonmuscle cells (Wang 2008). Specifically, they are both classified as actin "side-binders" because they stabilize F-actin (Wang 2008). The actin cytoskeleton maintains cell shape and its stability, is implicated in cell division, migration, endocytosis, apoptosis, vesicle trafficking, gene expression and differentiation (Mack, Somlyo et al. 2001; Pollard and Borisy 2003; Winder 2003; Albinsson, Nordstrom et al. 2004). ABPs are related to many, if not all of these cellular processes by controlling filament nucleation, elongation, severing, capping and depolymerization (Lee and Dominguez 2010). To evaluate the effect rINGAP had on the cytoskeleton, the localization of tropomyosin and caldesmon in hIPCs was investigated by immunofluorescence using antibodies specific for alpha and beta isoforms of tropomyosin and endogenous caldesmon (**figure 5-5**).

The control cells exhibited a more distinct fibrous-like localization of both tropomyosin and caldesmon throughout the cytoplasm compared to rINGAP-treated cells, indicative of both

proteins binding to the actin cytoskeleton in controls (**figure 5-5d,e**). The overlay image of the proteins in the controls demonstrates the co-localization of tropomyosin and caldesmon throughout the cytoplasm, consistent with a stable actin cytoskeleton and stress fibres, required for cell motility, changes in cell shape and the presence of focal adhesions (Abd-el-Basset, Ahmed et al. 1991; Tanaka, Watanabe et al. 1993). In addition, a strong co-localized signal was observed along the cell edges (**figure 5-5d**). Caldesmon was detected both in the cytoplasm and nucleus of control hIPCs. In comparison, rINGAP-treated hIPCs exhibited weak localization of caldesmon along the cell perimeters with a weaker distribution throughout the cytoplasm and a near-total loss of nuclear signal (**figure 5-5e**). The specific role(s) of caldesmon in the regulation of nuclear functions remain(s) unknown, however, the nuclear translocation of the protein coincides with the activation of the intranuclear protein kinase $p34^{cdc2}$, a regulator of G2/M transition, and the phosphorylation of caldesmon (Nurse 1990; Zheng, Weiden et al. 2007). Moreover, tropomyosin staining in rINGAP-treated hIPCs exhibited a loss of the distinct fibrous-like staining following rINGAP-treatment, consistent with tropomyosin dissociation from the actin filaments (**figure 5-5e**). Lastly, tropomyosin was redistributed into the perinuclear region of rINGAP-treated hIPCs. Although *in vitro* studies of caldesmon have commonly reported the protein as exclusively cytoplasmic, the novelty and validity of the caldesmon nuclear staining in control hIPCs can be supported since a recent study has provided evidence of the nuclear localization of caldesmon, implicating the protein in nuclear signaling and the regulation of cell proliferation (Zheng, Weiden et al. 2007). Of importance, to our knowledge no primary patient donor-derived cells or stem cells have been studied for caldesmon or tropomyosin localization in hIPCs.

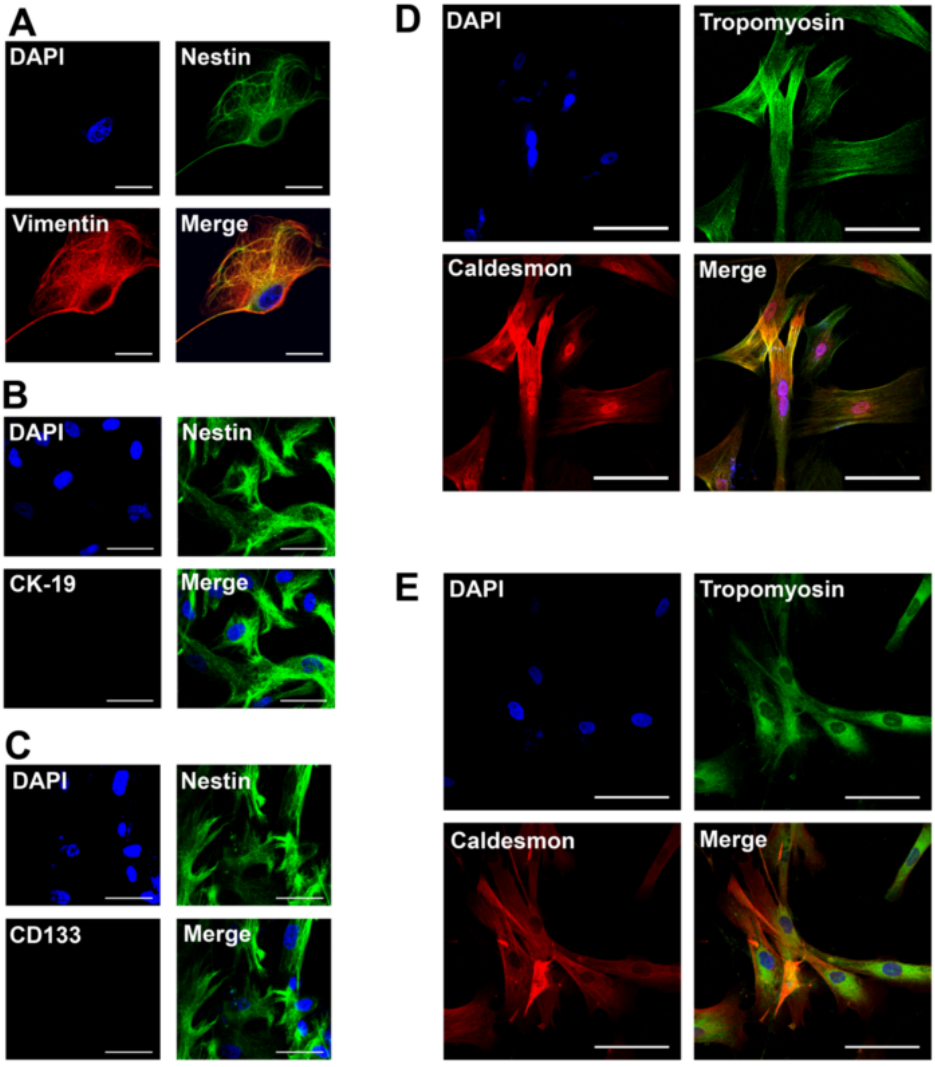

Figure 5-5: Immunocytochemistry of hIPCs at passage eight. (a) nestin^{+}, vimentin^{+} ; (b) nestin^{+}, CK19^{-} ; (c) nestin^{+}, CD133^{-} Expression and localization of (d) control and (e) rINGAP-treated tropomyosin and caldesmon proteins in hIPCs. (d) Control cells stained for tropomyosin and visualized with FITC (green) demonstrate a uniform distribution of tropomyosin throughout the cytoplasm and no nuclear localization. Control cells stained for caldesmon and visualized with Cy5 (red) also demonstrate a relatively uniform distribution of caldesmon throughout the cytoplasm as well as in the nuclei. DAPI staining (blue) shows the cellular nuclei. The merged image shows organized co-localization of tropomyosin and caldesmon throughout the cytoplasm (yellow) and localization of caldesmon in the nuclei (purple). (e) rINGAP-treated cells stained for tropomyosin and visualized with FITC (green) demonstrate a non-uniform perinuclear distribution of tropomyosin in the cytoplasm concentrated around the nuclei. rINGAP-treated cells stained for caldesmon antibody and visualized with Cy5 (red) demonstrate a relatively uniform distribution of caldesmon throughout the cytoplasm however no nuclear localization. DAPI staining (blue) shows the cellular nuclei. The merged image shows disorganized perinuclear staining of tropomyosin, moderate colocalization of tropomyosin and caldesmon throughout the cytoplasm and a loss of caldesmon in the nuclei (blue in comparison to purple). Scale bars represent 50µm (a-c) and 100µm (d,e).

5.7 Discussion

We investigated the response of hIPCs as a potential target of INGAP in this work. It was of interest to use long-term live-cell imaging to determine the duration and temporal correlation of any observed effects in relation to a previous proteomic analysis of hIPCs by our group which identified a potential perturbation of the actin cytoskeleton in response to rINGAP (manuscript in preparation). It was determined that expanded human islet-derived cells undergo cytoskeletal and nuclear motility changes upon rINGAP exposure. Investigation into the two parameters of migration, cell direction and speed, revealed hIPCs responded immediately to rINGAP with a decrease in cumulative distance travelled and average speed by more than 50% following rINGAP addition. rINGAP both decreased the magnitude of saltatory motions and increased the percentage of stationary instances, rendering 45% of the cells non-motile and decreasing the motility of the cells which remained motile.

We observed a loss in clearly defined nuclear features of hIPCs in response to rINGAP, rendering high resolution cell tracking very difficult or impossible under the given imaging conditions. This morphological change was often accompanied by cell rounding and retraction of the cytoplasm towards the nucleus and reduced cellular motility. Importantly, changes in cell morphology are commonly associated with mammalian cell differentiation, including MSCs (Rodriguez, Gonzalez et al. 2004). Immunocytochemistry of ABPs tropomyosin and caldesmon, exhibited pronounced perinuclear and extranuclear localization in rINGAP-treated cells, respectively, which confirms cytoskeletal reorganization. These

combined results suggest cell fate may be altered following rINGAP exposure, corresponding to the observed loss of adherence, the cytoplasmic retraction and the reduction in clearly defined nuclear features. To our knowledge, the subcellular localization of tropomyosin and caldesmon has not been previously studied in islet-derived cells, nor have the specific cellular functions of these proteins been fully identified and elucidated. Of importance, these proteins are known to play key roles in cell speed and motility through modulation of the actin cytoskeleton (Bach, Creed et al. 2009; Jiang, Huang et al. 2010), consistent with our live-cell imaging analysis.

Changes in tropomyosin expression have been correlated with tissue and organ differentiation during embryogenesis (Muthuchamy, Pajak et al. 1993; Clayton and Johnson 1998; Gunning, O'Neill et al. 2008). Furthermore, it has been proposed that tropomyosin regulates the transition of focal adhesions essential for directed cell movement (Bach, Creed et al. 2009). Therefore, the dissociation of tropomyosin from actin and its perinuclear localization in rINGAP-treated hIPCs supports the disruption of focal adhesions, consistent with decreased migration and speed. Additionally, intracellular sorting of tropomyosin has been associated with the retrograde translocation of organelles into the perinuclear area (Pelham, Lin et al. 1996), cell maturation in neuronal and epithelial cells (Gunning, Schevzov et al. 2005) and cell cycle regulation in fibroblast and epithelial cells (Percival, Thomas et al. 2000). Indeed, the observed changes in tropomyosin localization, further substantiates the potential effect of rINGAP on cell proliferation and fate. In addition, rINGAP-treated hIPCs revealed a weaker distribution of caldesmon throughout the

cytoplasm with the extranuclear translocation of the protein. The nuclear translocation of caldesmon corresponds with the activation of the intranuclear protein kinase $p34^{cdc2}$, and the phosphorylation of caldesmon (Nurse 1990; Zheng, Weiden et al. 2007). The phosphorylation of caldesmon by $p34^{cdc2}$ reduces its affinity for the actin cytoskeleton and allows for cytoskeletal rearrangements at the time of mitosis (Yamashiro, Yamakita et al. 1991). Caldesmon was reported to undergo intranuclear localization in proliferating cells (Zheng, Weiden et al. 2007), which supports the hypotheses that (1) non-rINGAP-treated hIPCs were proliferative; (2) extranuclear translocation of caldesmon in rINGAP-treated hIPCs is consistent with a loss of mitotic ability and proliferative potential.

Collectively, our studies indicate tropomyosin dissociates from the actin cytoskeleton and re-localizes in the perinuclear region, while caldesmon undergoes extranuclear translocation following rINGAP treatment. Furthermore, both findings are believed to contribute to the morphological and cell migration responses of rINGAP-treated hIPCs determined through live-cell imaging speed and tracking analyses. Based on the limited literature of tropomyosin perinuclear and caldesmon nuclear localization, it is hypothesized rINGAP involves the retrograde translocation of organelles into the perinuclear area (Pelham, Lin et al. 1996) of hIPCs, which may be related to cell maturation (Gunning, Schevzov et al. 2005) and cell cycle regulation (Percival, Thomas et al. 2000). Furthermore, rINGAP may activate the intranuclear protein kinase $p34^{cdc2}$, which phosphorylates caldesmon (Nurse 1990; Zheng, Weiden et al. 2007), triggering the extranuclear translation of caldesmon and the transition of hIPCs from a proliferative to differentiated state. These are previously unreported potential

mechanistic effects of rINGAP related to the cytoskeletal reorganization of hIPCs. These novel findings encourage further investigations into the role of ABPs and other proteins on the rINGAP mode of action on hIPCs.

MSCs and other cell types exhibit cytoskeletal changes during differentiation (Rodriguez, Gonzalez et al. 2004; Oh, Karlmark Raja et al. 2006; Yourek, Hussain et al. 2007), which is of noted significance to our reported cytoskeletal effects of rINGAP on hIPCs which have been previously characterized as pMSCs. In general, cytoskeletal reorganization and morphological changes are strongly associated with mammalian cell differentiation (Rodriguez, Gonzalez et al. 2004). Differentiating cells are also known to undergo states of motility and non-motility accompanied by the reorganization of F-actin (Abd-el-Basset, Ahmed et al. 1991). Furthermore, the reorganization and changes in expression levels of ABPs tropomyosin and caldesmon in differentiating astroglia cells has been observed (Abd-el-Basset, Ahmed et al. 1991). In human MSCs, imaging provides early clues for adipogenic or osteogenic outcomes during differentiation (Treiser, Yang et al. 2010). These fates can also be directly generated by the disruption of specific cytoskeletal elements. Specifically, disruption of actin filaments generates a strong preference for adipogenic differentiation in MSCs, while disruption of microtubules favours osteogenic differentiation (Kilian, Bugarija et al. 2010).

rINGAP induced cytoskeleton disruption in islet-derived cells may also be significant from an insulin-secretion perspective. It is well reported that the disruption of actin filaments can enhance glucose-induced insulin release from β-cells (Lacy, Klein et al. 1973; van Obberghen, Somers et al. 1973; Wang and Thurmond 2009). This may represent an accessory function of INGAP in supporting insulin homeostasis, although rINGAP-treated hIPCs did not stain for C-peptide (results not shown). hIPCs continued to express the stem cell marker vimentin after the 53 hours of rINGAP treatment, however with an observed reduction in intensity compared to control cells. As the statistical reliability of quantitative immunocytochemistry can be questioned, these results were not presented. However, the apparent reduction in vimentin expression, combined with morphological, nuclear motility and cytoskeletal reorganization of tropomyosin and caldesmon effects may indicate that hIPCs are poised for differentiation following exposure to rINGAP.

Expanded hIPCs may represent a useful mesenchymal stem cell population offering a large supply of cells for clinical diabetes applications. Although many exogenous growth factors have been explored for the proliferation and differentiation of hIPCs (Kutlu, Kayali et al. 2009; Sordi, Melzi et al. 2010), this work is the first to use live-cell imaging to investigate the cellular responses of rINGAP on hIPCs. We show that rINGAP decreases cell motility through reducing cell speed and directional persistence, induces a change in cellular morphology and rearranges the cytoskeleton in terms in ABPs tropomyosin and caldesmon. Due to the direct responses of expanded islet cells to rINGAP, we hypothesize that hIPCs play a role in the therapeutic mechanism of INGAP. It is acknowledged that the generation

of functional insulin secreting cells through *in vitro* culture and manipulation of hIPCs has not yet been achieved, however this work supports the incorporation of INGAP in future *in vitro* differentiation protocols and further characterization of hIPCs in culture using live-cell imaging techniques.

Acknowledgements:

The authors thank Devon Herman for database extraction and creation of rose plots, Ian Grzegorczyk for manual cell tracking, Darik Gamble for development of the cell tracking software, April Blaylock for development of the image acquisition system, Beatrice Assouline-Thomas for the production and purification of rINGAP and Professor Guy Guillemette for proof reading the manuscript. The Stem Cell Network of Canada and CIHR Nanomedicine provided financial funding for this research.

Chapter 6 Human Islet-Derived Progenitor Cells Treated with INGAP-PP

6.1 Preamble

This chapter extends the study of INGAP by evaluating the binding and the effects of the INGAP peptide, INGAP-PP, on hIPCs. The two previous chapters evaluated the effects of the recombinant form of INGAP (rINGAP) using proteomics, long-term live cell imaging and immunofluorescent staining. This chapter presents the study of INGAP-PP using fluorescent microscopy and flow cytometry analysis.

6.1.1 Objective

The main objective of this chapter was to evaluate the specificity of binding of INGAP-PP to hIPCs. hIPCs were exposed to either fluorescently labeled INGAP-PP or a scrambled fluorescent construct and imaged to determine if INGAP-PP bound specifically to islet-derived cells, relative to other non-pancreatic cell lines. Additionally, the phenotype of hIPCs exposed to INGAP-PP was analyzed and flow cytometry was utilized to evaluate INGAP-PPs effect on cell cycle.

6.1.2 Justification

The two previous chapters focused on the study of rINGAP, at the proteomic, behavioral and immunocytochemical levels. Although conclusive results were obtained which identified proteins perturbed from rINGAP exposure as well as phenotypic and migratory responses, the cellular specificity of INGAP was not confirmed. The specific mechanism of INGAP action, including cellular specificity and receptor, remain widely unknown. Using the

available fluorescent INGAP peptide and the scrambled peptide as a control, INGAPs binding to hIPCs was established. This confirmed the previous findings presented in chapters 4 and 5 which suggested that INGAP binds to hIPCs based on the observed cellular responses. All of these results combined, establishes previous unknown INGAP effects on hIPCs *in vitro*, which may prove to be clinically relevant in understanding the therapeutic potential of INGAP and hIPCs in the treatment of diabetes.

6.2 Publication Title and Authors

This research has not yet been submitted for publication. Additional live-cell imaging and flow cytometry analyses are being performed on hIPCs exposed to INGAP-PP which may provide sufficient clarification of the described nuclear phenomenon and verification of the data which indicated increased cellular granulation. With this supplementary data, firmer conclusions will be able to be drawn and the INGAP-PP analysis presented in this chapter will be complete for publication.

Title: INGAP-PP specifically binds and affects nuclear size of human islet-derived progenitor cells (hIPCs)

Erika Murray[1], Ilia Droujinine[1], Julien Verneau[1], Lawrence Rosenberg[2], Eric Jervis[1]
[1]Department of Chemical Engineering, University of Waterloo, Waterloo, Ontario, Canada; [2]Department of Surgery, McGill University, Montreal, Quebec, Canada

6.3 Overview

Islet neogenesis associated protein pentadecapeptide (INGAP-PP) expands beta-cell mass while reversing diabetes in rodents and increases endogenous insulin secretion in humans with diabetes. The mechanisms of INGAP-PP action, including a potential cellular receptor, remain to be identified. We studied the specificity of INGAP-PP binding and its morphological effects on human islet-derived progenitor cells (hIPCs) using a fluorescently-tagged form of the peptide and a scrambled construct. We show INGAP-PP binds specifically to hIPCs, and no binding was observed on two non-pancreatic derived cell lines. Furthermore, we report the observation of larger nuclei within 4.5 hours of hIPCs exposed to INGAP-PP compared to controls, which was dependent on the peptide sequence. Several mechanisms can be responsible for this nuclear phenomenon, such as the replication of the nuclear genome in the absence of cell division, termed endoreduplication. Additional copies of genetic material are characteristic of increased metabolic functions in terminally differentiated cells. To further explore this nuclear phenomenon, flow cytometry analysis on hIPCs treated with INGAP-PP was performed. One of the two analyses determined a larger proportion of cells with increased granularity, indicative of decreased proliferative potential which was previously suggested by our group in the study of rINGAP and hIPCs. These findings further support the hypothesis that hIPCs may be poised to differentiate following INGAP-PP exposure.

Key Words. Human islet-derived progenitor cell · Pancreatic mesenchymal stem cells · Islet neogenesis associated protein · Terminal differentiation · Ploidy

6.4 Introduction

Islet neogenesis associated protein (INGAP) is a 17 kDa protein that is involved in pancreatic islet neogenesis. A region of the protein consisting of 15 amino acids, termed INGAP pentadecapeptide (INGAP-PP), was identified to induce similar islet neogenesis effects as the full length protein (Rafaeloff, Pittenger et al. 1997). INGAP-PP has been shown to reverse diabetes in rodents (Rosenberg, Lipsett et al. 2004), expand beta-cell mass in normoglycemic rodents and dogs (Pittenger, Taylor-Fishwick et al. 2007), and most significantly to increase endogenous insulin secretion and improve glycemic control in humans with type 1 and type 2 diabetes (Dungan, Buse et al. 2009). Although there is substantial evidence indicating INGAP-PP holds therapeutic potential in the treatment of diabetes, an INGAP cellular receptor and its mechanisms of action remain unknown. Various groups have reported the outgrowth of mesenchymal cells following the *in vitro* expansion of islet cells (Gallo, Gambelli et al. 2007; Kutlu, Kayali et al. 2009; Russ, Ravassard et al. 2009). In particular, gene expression analysis of human pancreatic islets after *in vitro* expansion confirmed the expanded cells are highly comparable to other established mesenchymal stem cells (Kutlu, Kayali et al. 2009). Recently, it was determined that the expanding cells from pancreatic islet cultures are pancreatic mesenchymal stem cells (pMSCs), with the capacity to improve transplanted islet function (Sordi, Melzi et al. 2010). In the Sordi study, the expanded islet cells were confirmed to be pMSCs as they were able to differentiate along all three mesenchymal lineages, including: adipocytes, osteocytes and chondrocytes. It still remains to be established if all similar protocols which expand human islets in culture results in a population of pMSCs. Nevertheless, the exposure of extrinsic factors, such as INGAP, on

expanded islet-derived progenitor cells may induce insulin expression through differentiation.

In this study, we evaluated INGAP-PP binding and its morphological effects on human islet-derived progenitor cells (hIPCs). These cells stained positive for nestin^{+} and vimentin^{+} (mesenchymal markers) and negative for CK-19^{-} and CD133^{-} (epithelial markers) (**figure 5-5 a-c**). This suggested MSC phenotype; however the cells were not differentiated into all three mesenchymal lineages. Therefore, although the expanded islet cells may represent a pMSC population, MSC phenotype was not confirmed. We evaluated INGAP binding based on detected FAM (green fluorescent) punctate signal using labeled INGAP-PP, labeled scrambled INGAP-PP and three human cell lines, including hIPCs. Furthermore, we performed a fluorescence-activated cell sorting analysis (FACS) on hIPCs treated with INGAP-PP to analyze the effects of INGAP-PP on cell cycle. We show that INGAP-PP binds specifically to hIPCs, however we obtained inconclusive FACS results which could not confirm INGAP-PPs effect on granularity or cell cycle. Importantly, we report a significant and rapid increase in nuclear size following INGAP-PP exposure, suggestive of a change in the ploidy state of hIPCs exposed to INGAP.

6.5 Materials and Methods

hIPCs were derived from fresh human islets obtained from a non-diabetic adult cadaveric donor, approved by the Institutional Review Board of McGill University, Montréal, QC, as previously described (Jamal, Lipsett et al. 2005). Islets were plated in tissue culture-treated flasks at a density of 1 islet/mm^2, cultured in modified RPMI-1640 medium (Invitrogen,

Burlington, ON) with 10% FBS and incubated at 37ºC, 5% CO_2 and 95% humidified air for 15 days with complete media changes every 3 days. At day 15, the islets which had spread into monolayers were detached with 2.5 g/L trypsin (Invitrogen, Burlington, ON) and seeded as single cells at $1.2x10^4$ cells/cm^2, followed by subsequent passing at $4x10^3$ cells/cm^2 once 90% confluence was obtained. Human fetal neural stem cells (hfNSCs) were cultured according to a standard adherent culture protocol (Pollard, Yoshikawa et al. 2009) and human umbilical vein endothelial cells (HUVECs) were obtained from Lonza MD, USA and cultured according to the company's protocol. FAM-INGAP-PP and scrambled-FAM-INGAP-PP were synthesized and purified by Sheldon Biotech Centre, Montréal, QC and 5-FAM (Cedarlane Laboratories, Burlington, ON) was utilized as a fluorescent control.

Immunofluorescent Imaging and Analysis

The three constructs (5-FAM, FAM-INGAP-PP or scrambled-FAM-INGAP-PP) were supplemented into the media at 58 μM. All three cell types (hIPCs, HUVECs or hfNSCs) were seeded onto aminopropyl trimethoxy silane (APTS) glass treated imaging chambers at 90% confluency for 24 hours prior to being exposed to the various constructs for 4.5 hours the next day. Following exposure, the chambers were rinsed twice in PBS, fixed with 4% parafomaldehyde for 15 minutes, rinsed and nuclear stained using DAPI with antifade (Vector Laboratories Inc., Burlington, ON). The chambers were then replenished with PBS and imaged immediately on a laser scanning confocal microscope (Olympus FV1000).

FACS

Propidium iodide staining and analysis was carried out as previously described (Crissman, Mullaney et al. 1975; Nunez 2001), with minor modifications. Untreated, INGAP-PP treated or scrambled-INGAP-PP treated hIPCs were trypsinized, washed, and transferred to PBS. Three volumes of absolute ethanol were added drop wise while vortexing. Cells were fixed on ice for 45 minutes and stored at -20°C for no more than one week. After storage, cells were stained and RNA was digested in a solution containing 40µg/mL PI and 500 ng/mL RNase (DNase-free) for 30 min at 37°C. Flow cytometry analysis with doublet discrimination was then performed (Nunez 2001).

6.6 Results and Discussion

Immunofluorescent Imaging and Analysis

The physiological effects of INGAP-PP have been studied on rat and hamster islet cells, hamster ductal cells and mouse embryonic stem cells (Rafaeloff, Pittenger et al. 1997; Barbosa, Bordin et al. 2006; Francini, Del Zotto et al. 2009; Madrid, Del Zotto et al. 2009). Furthermore, INGAP-PP binding specificity has been investigated in hamsters (Borelli, Del Zotto et al. 2007) but the existence of a specific receptor remains elusive. To test whether INGAP-PP binds specifically to hIPCs, we subjected hIPCs, hfNSCs and HUVECs to media supplemented with FAM-INGAP-PP, scrambled-FAM-INGAP-PP or FAM, for 4.5 hours at 37^0C. When we evaluated the FAM signal using confocal microscopy, the FAM signal was only observed on hIPCs treated with FAM-INGAP-PP. Moreover, every hIPC observed ($n>10^4$) exhibited the punctate FAM-INGAP-PP signal (**figure 6-1a**), suggestive of bound receptor aggregation as reported for several other receptor-mediated signaling pathways

(Blumbach, Pancer et al. 1998; Sako, Minoghchi et al. 2000; Burke, Schooler et al. 2001). The punctate FAM-INGAP-PP cellular signal was completely absent on hfNSCs and HUVECs (**figures 6-1b and c**), indicating that INGAP-PP binding is somewhat cell-type specific with potential receptor expression restricted to hIPCs or other islet-derived cell type(s). Additionally, FAM signal was not detected on hIPCs exposed to the scrambled-FAM-INGAP-PP nor FAM (**figure 6-2**). This demonstrated that binding of INGAP-PP is dependent on the peptide sequence and independent of the attached FAM fluorescent label.

To further understand the binding of INGAP-PP, hIPCs were also imaged after 4.5 hours of FAM-INGAP-PP exposure at 4^{o}C (**figure 6-3a**). In comparison to hIPCs exposed to the peptide at 37^{o}C (**figures 6-1a, 6-3b, 6-4 and 6-5)**, the punctate FAM signal was near undetectable using identical sensitivity settings. This decrease in punctate signal is consistent with decreased binding, transport and cellular uptake at potential membrane binding sites, as previously observed at low temperatures (Goodrich and Morita 1977). All together, these results provide novel evidence that hIPCs exhibit specific INGAP surface binding and uptake mechanism(s), such as a cell surface receptor, whose expression may be restricted to islet derived progenitor cells.

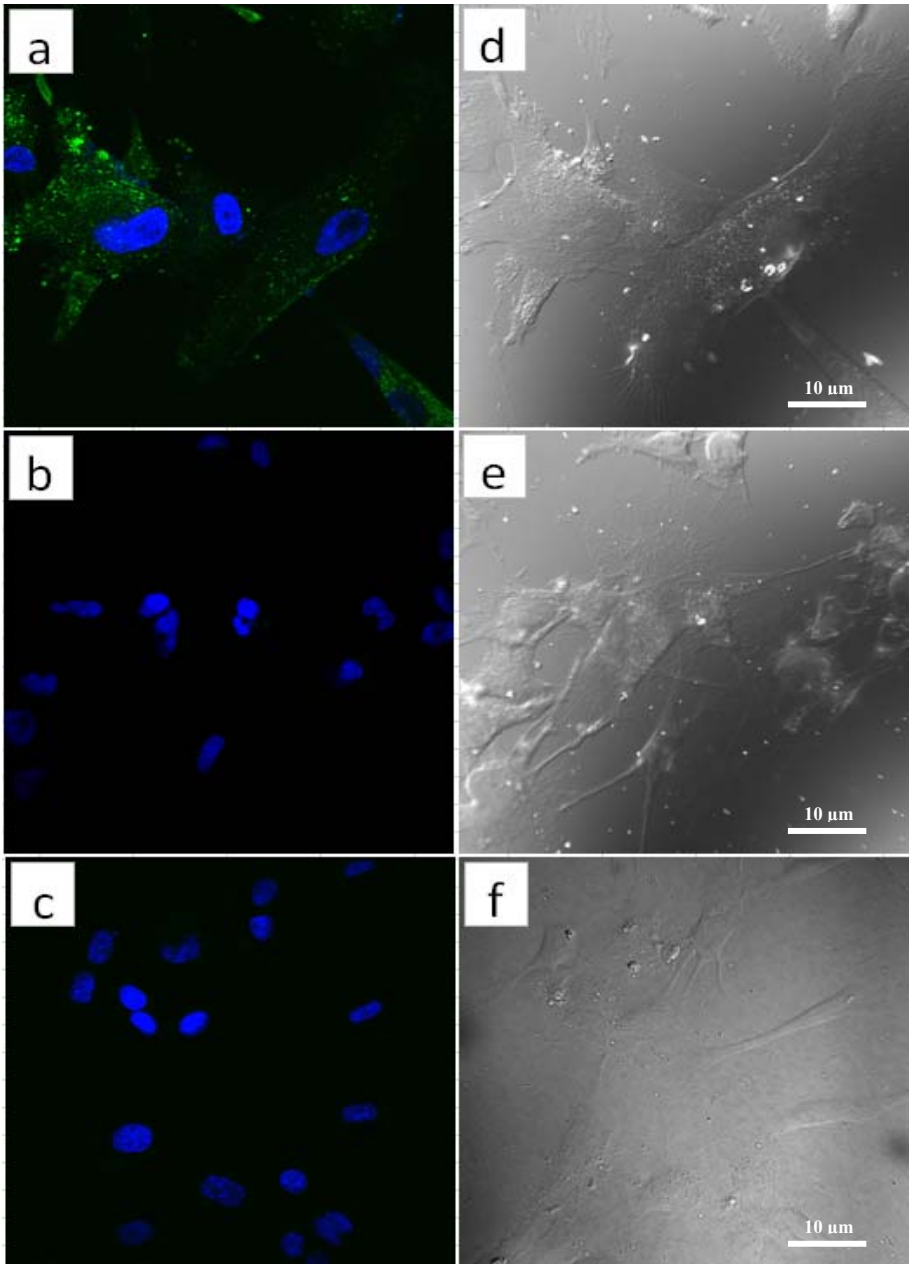

Figure 6-1: FAM-INGAP-PP treatment at 37ºC (a) hIPCs (b) hfNSCs (c) HUVECs were each incubated with 58 nM of FAM-INGAP-PP for 4.5 hours at 37ºC. Cells were rinsed twice in PBS, fixed with 4% parafomaldehyde for 15 minutes, rinsed and nuclear stained using DAPI. Shown are the confocal images of FITC excitation at 40X magnification. (d) hIPCs (e) hfNSCs (f) HUVECs are the bright field images.

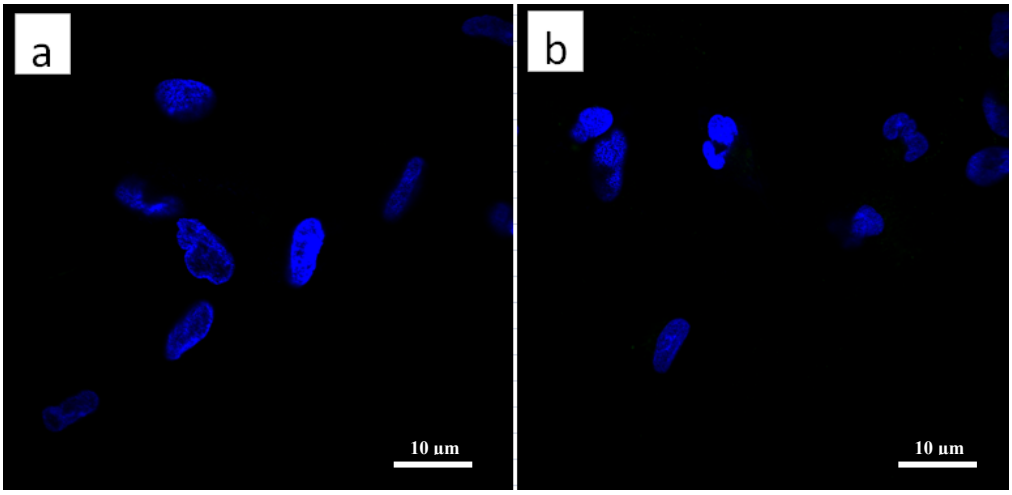

Figure 6-2: FAM and Scrambled-FAM-INGAP-PP hIPC treatment at 37ºC. hIPCs were incubated with 58 nM of (a) FAM or (b) Scrambled-FAM-INGAP-PP for 4.5 hours at 37ºC. Cells were rinsed twice in PBS, fixed with 4% parafomaldehyde for 15 minutes, rinsed and nuclear stained using DAPI. Shown are the confocal images of FITC excitation at 40X magnification.

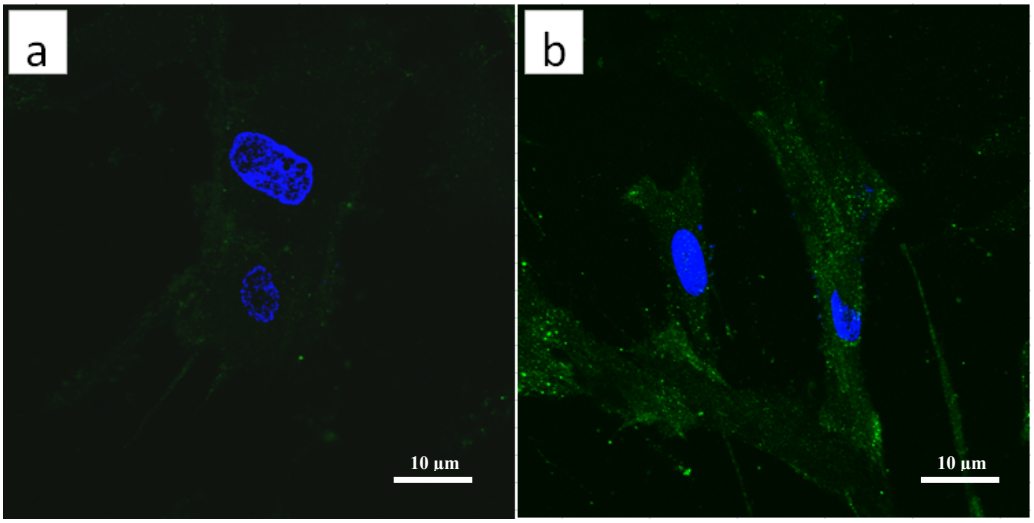

Figure 6-3: Comparison of FAM-INGAP-PP treatment at 4ºC versus 37 ºC. (a) hIPCs were incubated with 58 nM of FAM-INGAP-PP for 4.5 hours at 4ºC. (b) hIPCs were incubated with 58 nM of FAM-INGAP-PP for 4.5 hours at 37ºC. Cells were rinsed twice in PBS, fixed with 4% parafomaldehyde for 15 minutes, rinsed and nuclear stained using DAPI. Shown are the confocal images of FITC excitation at 40X magnification.

Following the demonstration of INGAP-PP binding specificity, cellular morphologies were examined 4.5 hours after FAM-INGAP-PP exposure at 37ºC. Overall, hIPCs treated with INGAP-PP presented large masses of cells with the loss of observed distinctive membranes. The most significant observation was that FAM-INGAP-PP exposed hIPCs had a significant increase in nuclear size. In particular, two distinct morphologies were identified, including hIPCs with oversized circular nuclear masses (**figure 6-4**), as well as hIPCs with oversized linear nuclear masses (**figure 6-5**). In the first case, the DNA staining revealed large nuclei with up to a seven times the nuclear perimeter found amongst other normally sized hIPC nuclei in the same field of view (**figure 6-4 a-d**). These large nuclei were either circular in shape (**figure 6-4 c,d**), appearing to be one extra-large nucleus, or several cells presented DNA staining which revealed among the extra-large nuclei the appearance of multiple smaller nucleus (**figure 6-4 a,b**). In the second case, hIPCs with oversized linear nuclear masses, there was the appearance of individual nuclei amongst the larger linear nuclear masses (**figure 6-5 a-d**). For example, in **figure 6-5c** there is the appearance of five nuclei within one large linear nuclear mass.

Neither of the observed nuclear morphologies have been previously reported in hIPCs. The increase in genetic material contained within an oversized nucleus has been hypothesized as a potentiator of metabolic function as cells differentiate (Ullah, Lee et al. 2009). In mammals, cell types known to be polyploid such as megakaryocytes (Ravid, Lu et al. 2002) and trophoblasts (Cross 2000) undergo a process called endoreduplication in which the genetic

material is duplicated but nuclear separation and cytokinesis do not follow (Edgar and Orr-Weaver 2001). This developmentally controlled event is a terminal differentiation point in the lineage hierarchy and these cells generally never re-enter mitosis (Lee, Davidson et al. 2009). Although hIPCs have never been reported to undergo endoreduplication, it is possible that the described extra-large nuclei appear from continuous DNA replication without nuclear separation and cytokinesis. This raises the interesting hypothesis that INGAP-PP may trigger endoreduplication and terminal differentiation of hIPCs *in vitro*, which to date has never been observed or reported.

As an alternative hypothesis to endoreduplication, the appearance of the extra-large nuclei may be explained from the mechanism of fusion, cellular and/or nuclear. The formation of multinucleated giant cells *in vitro* is known to occur from the cellular fusion of monocytes or macrophages during inflammatory response, however very little is known about the mechanism of fusion process or its role *in vivo* (Parwaresch, Kreipe et al. 1986; Chiozzi, Sanz et al. 1997; Most, Spotl et al. 1997; Gasser and Most 1999). Importantly, it is known that the formation of the multinucleated giant cells in culture is enhanced by various developmentally related cytokines (Enelow, Sullivan et al. 1992). In addition to cellular fusion, nuclear fusion may explain the observed extra-large hIPC nuclei following INGAP-PP exposure. Nuclear fusion following cell fusion has been described as rare, however it is known to occur between embryonic stem cells and bone marrow cell populations which contain hematopoietic stem cells, as well as with neural stem cells (Wurmser and Gage 2002). Of importance, thus far cell fusion has only been observed to occur *in vitro* and

between stem cell phenotypes. Therefore, if nuclear fusion is indeed the mechanism of the observed extra-large nuclei, the hIPCs likely represent a MSC population. However, it would remain unclear how relevant the observed INGAP-PP nuclear effect would be *in vivo*.

Finally, it has been reported that chemical disruption of cytoskeletal filaments alters nuclear morphology (Mazumder and Shivashankar 2010). The balance between microtubule pushing forces and actin-based pulling forces regulates nuclear shape (Mazumder and Shivashankar 2010), which raises a third mechanism; that INGAP-PP triggers cytoskeletal rearrangements in hIPCs leading to changes in nuclear morphology *in vitro*. Interestingly, the results presented in the previous chapter, Chapter 5, outlined the observed effects of rINGAP on hIPCs, which included the perturbation of the actin cytoskeleton and a near loss of nuclear features. However, these INGAP-PP results report enhanced nuclear features including the increase in size of the nuclei. Although we present evidence that both rINGAP and INGAP-PP alters the cytoskeleton of hIPCs following treatment, the observed nuclear effects are conflicting and opposing. The mechanisms of endoreduplication and fusion, would each involve cytoskeleton rearrangements. Therefore, cytoskeletal rearrangement may not be the primary mechanism responsible for the extra-large nuclei, however the cytoskeleton of hIPCs may be rearranged as a result of another principal nuclear mechanism, including endoreduplication or fusion.

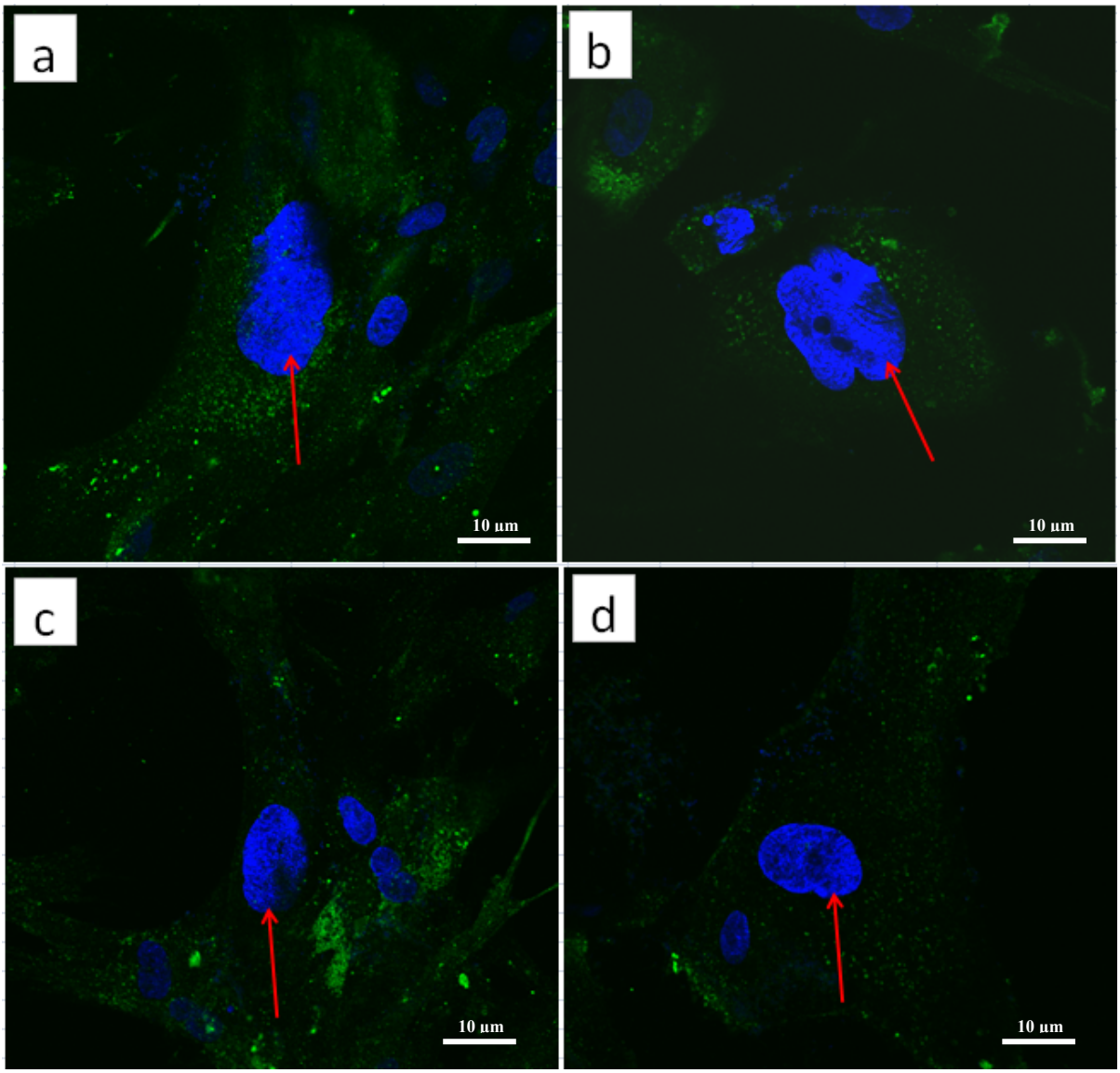

Figure 6-4: hIPCs treated with FAM-INGAP-PP at 37ºC with oversized circular nuclear masses (a-e). hIPCs were incubated with 58 nM of FAM-INGAP-PP for 4.5 hours at 37ºC. Cells were rinsed twice in PBS, fixed with 4% parafomaldehyde for 15 minutes, rinsed and nuclear stained using DAPI. Shown are the confocal images of FITC excitation at 40X magnification.

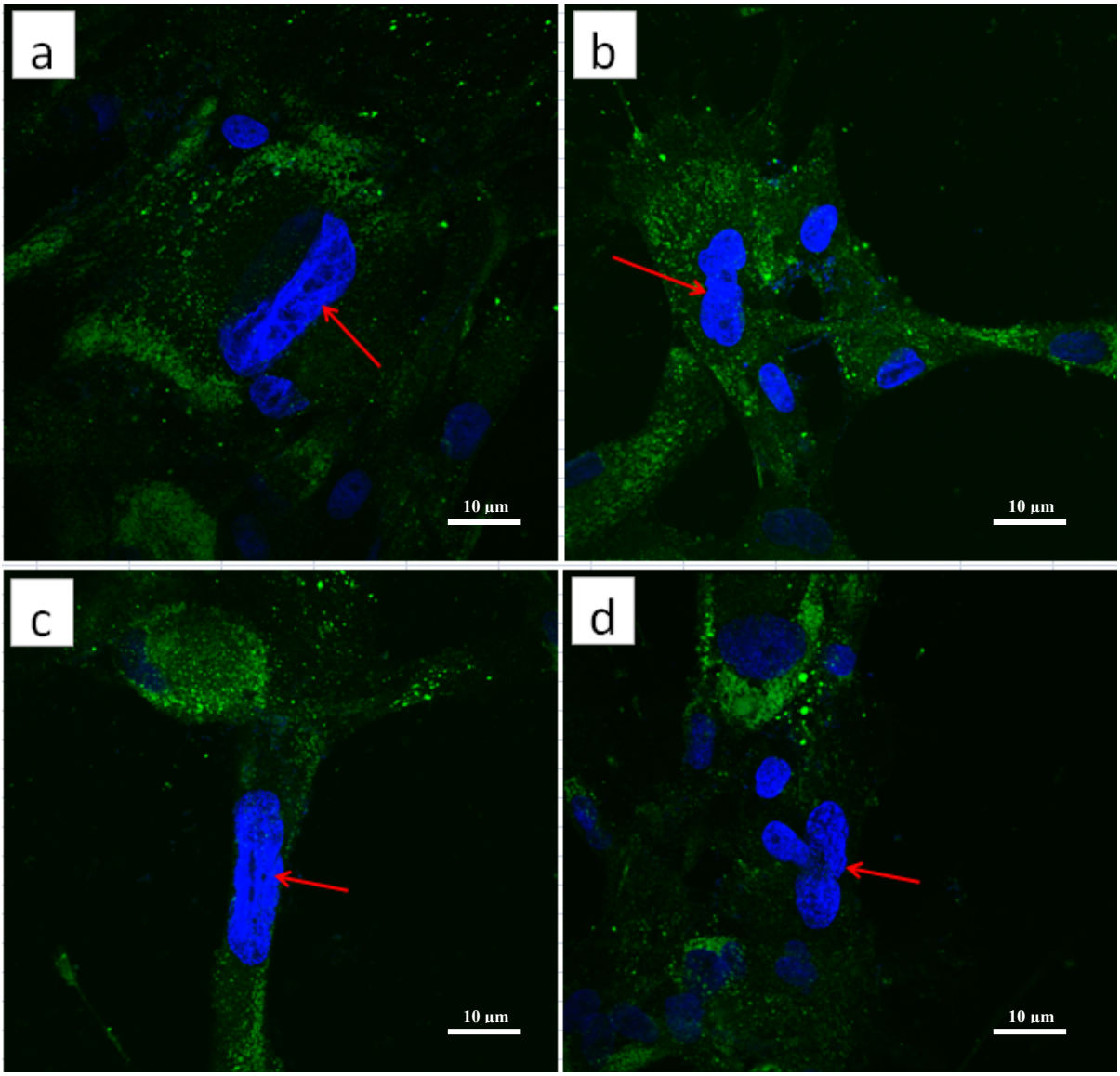

Figure 6-5: hIPCs treated with FAM-INGAP-PP at 37ºC with oversized linear nuclear masses (a-d). hIPCs were incubated with 58 nM of FAM-INGAP-PP for 4.5 hours at 37ºC. Cells were rinsed twice in PBS, fixed with 4% parafomaldehyde for 15 minutes, rinsed and nuclear stained using DAPI. Shown are the confocal images of FITC excitation at 40X magnification.

FACS

To further explore the observed nuclear phenomenon, flow cytometry analysis on hIPCs treated with INGAP-PP was performed. First, a FACS method for looking at cell cycle distributions was optimized using an assay on THP-1 monocytic cells provided by Dr. Maud Gorbet, Systems Design Engineering Department, University of Waterloo. In this assay, permeabilized cells were stained with a red-fluorescing DNA-binding dye, propidium iodide (PI; Nunez 2001). During optimization, several parameters were evaluated, including: cell concentration during fixation and PI staining, the duration of fixation, the fixation mode (adding cells dropwise to 70% (v/v) ethanol versus adding 100% ethanol drop wise to the cells, to a final ethanol concentration of 70%), storage conditions, gating, and voltage settings on the flow cytometer. **Figure 6-6** outlines the FACS optimization. Doublet discrimination gating was performed as per (Nunez 2001), and a valid cell cycle analysis was obtained (**figure 6-6a**). As well, it was confirmed that nocodazole treatment of THP-1 cells increased the proportion of cells with twice the DNA content (**figure 6-6b**). Finally, it was determined that a slow increase in ethanol concentration gave less variability in the forward scatter of THP-1 (**figure 6-6c**). Overall, it was found that the procedure outlined in section 1.5 Materials and Methods gave the best results for FACS analysis on THP-1 monocytic cells using the flow cytometer located in Dr. Maud Gorbet's laboratory. Therefore, these settings and fixation procedures were applied to the FACS analysis on hIPCs.

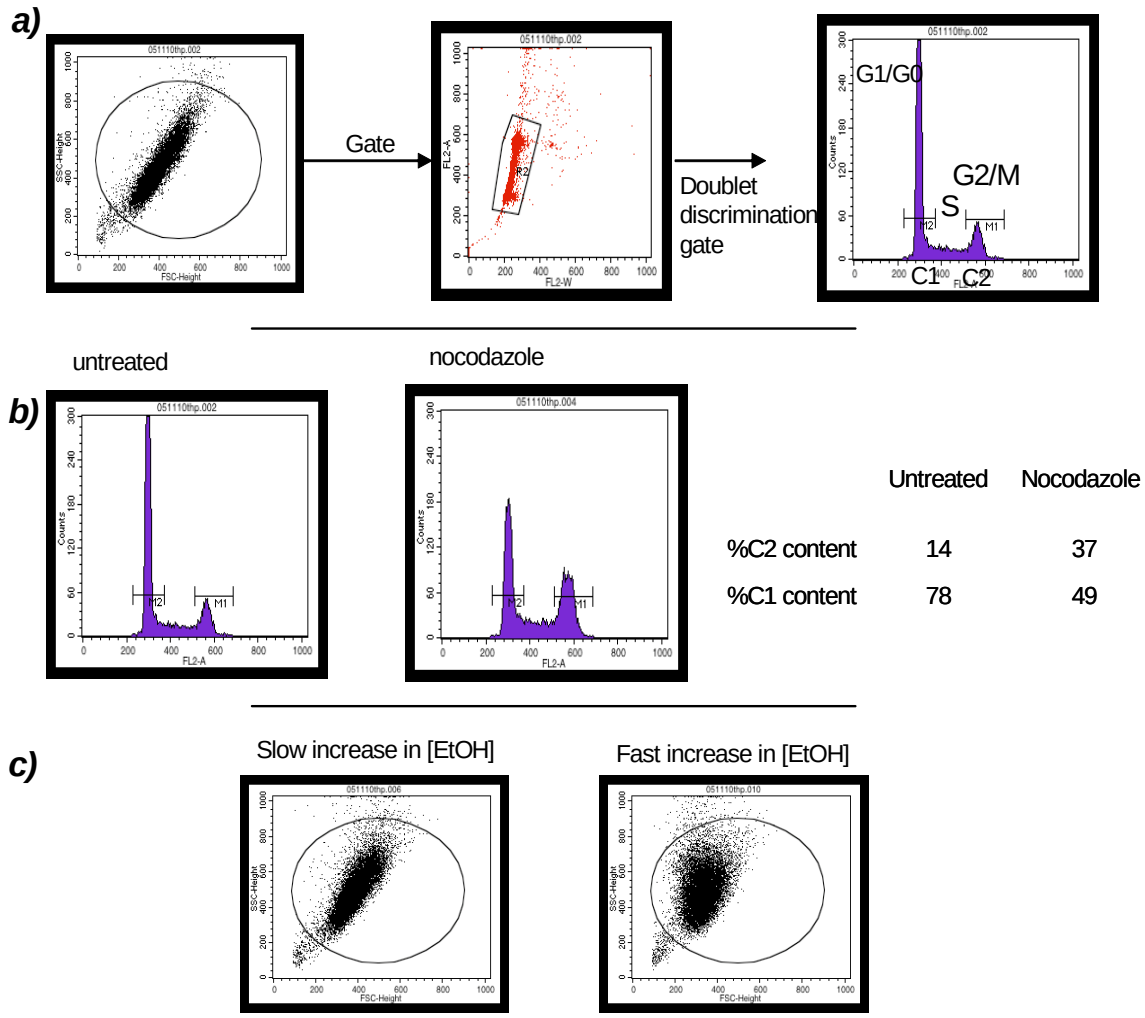

Figure 6-6: Optimization of propidium iodide (PI) cell cycle determination analysis by flow cytometry using THP-1 monocytes. (a) To select the population for analysis, events were gated based on forward and side scatter. Subsequently, a doublet discrimination gate was applied (Pi-signal area vs. width) and number of events versus PI-signal-area was plotted (Nunez 2001). (b) THP-1 cells were subjected to 100 ng/mL nocodazole for 18 hours and the percent of events with 2C DNA content increased. (c) Ethanol concentration was increased slowly during fixation. The variability in event forward scatter was less than when ethanol concentration was increased quickly.

Following FACS optimization, to determine whether INGAP-PP treatment resulted in changes to the nuclear organization and/or cell cycle of hIPCs, a FACS analysis was performed with INGAP-PP treated (14μM) and untreated hIPCs (**figure 6-7**). hIPCs exposed to INGAP-PP for approximately 2 days (44 hours) were found to have no significant difference between treated and untreated samples in terms of proportions of C1 (66% vs. 69%, respectively) and C2 (twice the DNA content of diploid cells; 28% vs. 25%) DNA content (**figure 6-7a top**). This suggested that since there were no significant differences in accumulation of DNA content between the C2 peaks, that endoreduplication may not be the mechanism responsible for the appearance of large hIPC nuclei (Edgar and Orr-Weaver, 2001). However, when PI-signal (FL2A) was plotted against side scatter (SSC-H), it appeared that the proportion of SSC-H^{HIGH} in INGAP-PP treated cells increased in C1 and C2 populations (**figure 6-7a bottom**). This suggested that following INGAP-PP treatment, there were a larger proportion of more granulated cells at both C1 and C2. Interestingly, following the INGAP-PP treatment at day 2 of the experiment, the INGAP-PP treated population had half the number of cells compared to the untreated hIPC population. It is possible that the decrease in PI^{LOW} SSC-H^{LOW} treated population (potentially small, recently divided cells), could indicate of decreased proliferative potential of hIPCs treated with INGAP-PP. This finding is consistent with effects of rINGAP on the cytoskeletal organization of hIPCs discussed in the previous chapter.

To confirm the initial FACS analysis which indicated a larger proportion of hIPCs with increased nuclear granularity, the INGAP treatment and FACS analysis was repeated

utilizing scrambled-INGAP-PP as an additional control. However, a similar effect on increased nuclear complexity was not observed (**figure 6-7b**). Treatment with an equivalent concentration and length of INGAP-PP did not produce the same effect found in the first analysis. Several possibilities could account for this inconsistency; however the only known difference between both experiments was the passage number of the hIPCs. The passage number of the hIPCs analyzed in the second trial (**figure 6-7b**) was 6. However, the first trial had a much higher passage number of 13. It is possible that these later passaged cells may have differing phenotypes in comparison to the early passage cells (Honczarenko, Le et al. 2006).

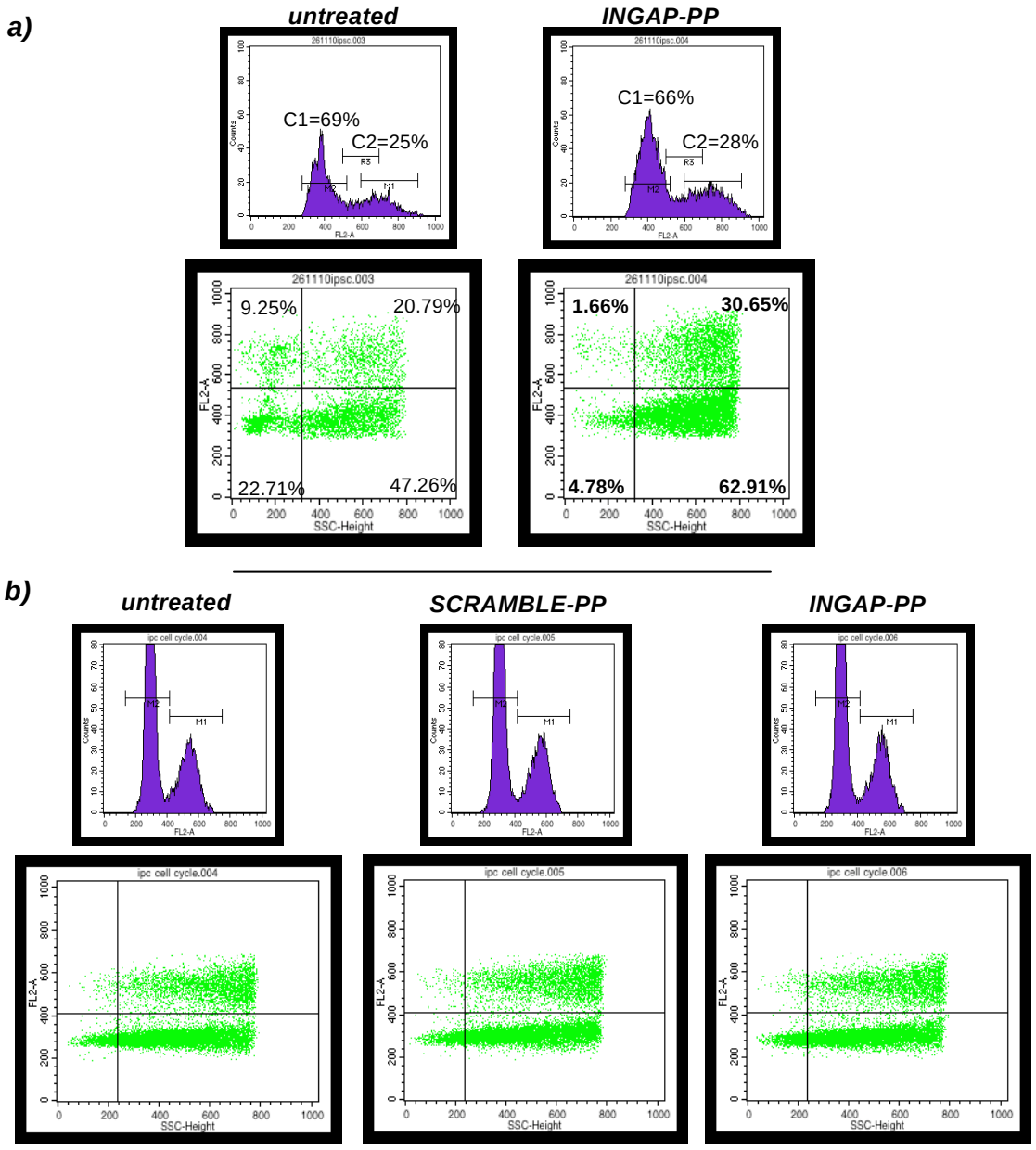

Figure 6-7. Cell cycle analysis of hIPCs following INGAP-PP treatment. Both histograms and dot plots are shown. hIPCs at 70-80% confluency were incubated with 14 µm of INGAP-PP in complete media. (a) First analysis with 44 hours of INGAP-PP treatment at passage 13. Demonstrated was a reduction in PI^{LOW} SSC^{LOW} population, consistent with the large nuclei presented above. (b) Second analysis with 46 hours of INGAP-PP treatment at passage 6. Scrambled-INGAP-PP was included as an additional control. There was no difference in cell cycle found between untreated, Scrambled-INGAP-PP or INGAP-PP treated hIPCs.

6.7 Conclusions

We evaluated INGAP-PP binding using fluorescently labeled INGAP-PP and a scrambled construct as a control. We show that INGAP-PP appeared to bind specifically to hIPCs and it did not bind to at least two other non-pancreatic-derived human cell lines. The most significant observation was the rapid appearance of hIPCs with oversized nuclei following FAM-INGAP-PP exposure. The nucleus is the most prominent cellular organelle. Its size and shape are indicative regulators of genome function. The increase in genetic material contained within an oversized nucleus has been suggested as a potentiator of metabolic function as cells differentiate (Ullah, Lee et al. 2009). The formation of multinucleated giant cells *in vitro* has also been reported in monocytes and macrophages (Most, Spotl et al. 1997; Gasser and Most 1999), however hIPCs with oversized or multinucleated cells has not been previously reported. Three mechanisms were presented and discussed as potential mechanisms of the observed large nuclei, including: endoreduplication, fusion and cytoskeletal rearrangement. However, the precise mechanism to elucidate this nuclear phenomenon remains to be determined.

Flow cytometry analysis on hIPCs treated with INGAP-PP was performed to further explore the observed nuclear change. One of the two analyses determined a larger proportion of cells with increased granularity, indicative of decreased proliferative potential which was previously suggested in the study of rINGAP and hIPCs (Chapter 5). Endoreduplication or the evasion of some parts of the S, G2, or M phases in the cell cycle was suggested to account for this phenomenon (Edgar and Orr-Weaver, 2001). Alternatively, nuclear fusion

may explain this observation, especially since this phenomena was only observed at higher cell densities, consistent with other nuclear fusion reports (Glick et al, 2010). Moreover, work presented in the previous chapter has shown that rINGAP treatment causes morphological alterations of hIPCs, including: cytoskeletal reorganization, decreased nuclear borders, and decreased cellular and nuclear motility. The unpacking of DNA and cytoskeleton rearrangement may also be occurring, perhaps representing an activated state of hIPCs, similar to lymphocytes upon antigen recognition (Mazumder and Shivashankar 2010).

In conclusion, the INGAP-PP analysis and results presented within this chapter indicate that INGAP-PP may specifically bind to hIPCs in a receptor-mediated fashion. It is proposed that INGAP-PP binding results in the rapid emergence of previously unreported extra-large hIPC nuclei. This phenomenon suggests increased metabolic activity and terminal differentiation of hIPCs following INGAP-PP exposure. However, the exact mechanism (endoreduplication, nuclear fusion, cytoskeletal rearrangement or otherwise) requires further investigation. Long term live-cell imaging and additional FACS analyses are currently being performed to further explain the rapid increase in nuclear size observed from hIPCs exposed to INGAP-PP. In particular, as both mechanisms should be observable in real-time, live-cell imaging is being utilized to confirm or rule out endoreduplication as well as fusion. Additionally, FACS analysis's are being repeated on later passage hIPCs to determine if the results of the first analysis which revealed a higher proportion of INGAP-PP treated hIPCs with increased complexity can be repeated. Although studies are still being performed, the results presented within this chapter further support the hypothesis presented from chapters four and five; that

hIPCs respond to INGAP exposure, undergoing cytoskeletal rearrangements and may be poised for differentiation.

Chapter 7 Human Islet-Derived Progenitor Cell Aggregates Treated with INGAP

7.1 Preamble

This chapter investigates a means to create islet like spherical structures from INGAP treated hIPCs. The three previous chapters evaluated the effects of the recombinant and peptide forms of INGAP, rINGAP and INGAP-PP, respectively. This chapter focuses on a potential method of engineering islets for transplantation using hIPCs and an INGAP treatment.

7.1.1 Objective

Engineering islets for *in vivo* transplantation would be the ultimate goal of this research. The main objective of this chapter is to extend the results of the previous three chapters, by presenting and evaluating a method to aggregate INGAP treated hIPCs. Specifically, hIPCs were treated with rINGAP or FAM-INGAP-PP and aggregated using an established method to create embryoid bodies. The aggregates were stained for insulin secretion and epithelial mesenchymal markers, as well the INGAP distribution within the spheroids was evaluated.

7.1.2 Justification

Pancreatic islet transplantation has proven to be successful in patients with type 1 diabetes, however there remains a large shortage of islet cells for transplantation. INGAP-PP enhances the secretion of insulin in animals and humans with diabetes, therefore tissue engineering islets *in vitro* from hIPCs exposed to INGAP may provide a large supply of islets for diabetic islet transplantation.

7.2 Introduction

The pancreas acts as both an endocrine gland, secreting vital hormones directly into the blood and as an exocrine gland by secreting and transporting digestive enzymes to the small intestine. The endocrine cells are disbursed throughout the organ in clusters, termed islets of Langerhans or islets. Islets are composed of four cells types, which together regulate blood glucose levels. They include, alpha, beta, delta and pancreatic polypeptide secreting cells, which produce the hormones glucagon, insulin, somatostatin and pancreatic polypeptide, respectively. Beta cells are the most prevalent cell type, comprising 65-85% of a pancreas. These cells are solely responsible for the secretion of insulin, the major hormone which maintains glucose homeostasis. Type I and type II diabetes are both characterized by the impairment of islet secretary function of the beta cells; therefore patients often require synthetic insulin injections. Unfortunately, long-term insulin therapy can ultimately lead to unstable blood glucose control, resulting in the risk of hypo- or hyperglycemic episodes. In attempts to achieve independence from insulin therapy, clinical trials have demonstrated promise of islet transplantation (Ryan, Lakey et al. 2001; Shapiro, Ryan et al. 2001). However, up to three islet transplants are needed to achieve insulin independence, as well as there is a frequent immune response to the transplanted islets (de Kort, de Koning et al. 2011). Besides the poor long-term results of islet transplantation, the availability of functional islet cells remains the primary obstacle to its widespread clinical application (Kodama, Kojima et al. 2009).

The results of the previous three chapters presented and analyzed the effects of INGAP on hIPCs. Specifically, hIPCs treated with rINGAP had 50% decrease in average nuclear speed,

a change in nuclear morphology and the differential translocation of two actin-binding proteins. Furthermore, the rapid emergence of larger nuclei in hIPCs exposed to INGAP-PP was reported. Based on these results which indicate that hIPCs *in vitro* respond to INGAP, combined with the fact that INGAP has been shown to promote islet neogenesis in animal diabetic models and to increase C-peptide secretion in humans with type 1 diabetes (Dungan, Buse et al. 2009; Madrid, Del Zotto et al. 2009), aggregating hIPCs treated with INGAP may provide a novel method for engineering transplantable islets.

Here, hIPCs were expanded, treated with rINGAP or FAM-INGAP-PP and aggregated to form islet like structures using an established method to create embryoid bodies. rINGAP treated aggregates appeared to have an increase in the nestin^{+} cells localized at the centre of the aggregates. This suggested that rINGAP in combination with aggregation promoted the multicelluar organization of the hIPCs and/or an epithelial-mesenchymal transition (EMT). Furthermore, when hIPCs were aggregated and treated with labeled FAM-INGAP-PP, the peptide signal was localized to the center of the aggregates. These results demonstrate that it is possible to create uniformly-sized and shaped hIPC 'islet-like' aggregates which appear to have a unique cellular organization and structure.

7.3 Methods

hIPCs were derived and cultured as previously described in section 5.5 Materials and Methods. After 3 or 8 passages, aggregates were created using the Aggrewell^{TM} technology ((Stem Cell Technologies, Canada; (Ungrin, Joshi et al. 2008)) (**figure 7-1**). In short, hIPCs were treated with 10 nM of rINGAP in complete media for 48 hours or not treated (controls

and INGAP-PP experiment). The cells were then trypsinized, washed, counted, and placed in 1.5 mLs of complete media to Aggrewell-400 plates which were previously prepared to remove bubbles by centrifugation at 2000*g* for 5 minutes. Once the cells were placed into the pre-spun plates, they were centrifuged at 100*g* for 3 minutes and incubated at 37°C, 100% humidity, and 5% CO_2 for 24 hours in the presence of 58 uM of FAM-INGAP-PP with media or just in complete media (controls and previously rINGAP treated). Following the 24 hours of incubation, the aggregates were extracted from the plates by pipette and placed in APTS-treated glass chambers to adhere overnight. The following day the aggregates were fixed in formaldehyde, stained with CK-19 and Nestin (rINGAP experiment), or C-peptide and phalloidin (FAM-INGAP-PP experiment) and DAPI. The chambers were imaged on an inverted microscope using DIC (Axiovert 200; Carl Zeiss MicroImaging GmbH, Berlin, Germany) or on a laser scanning confocal microscope (Olympus FV1000).

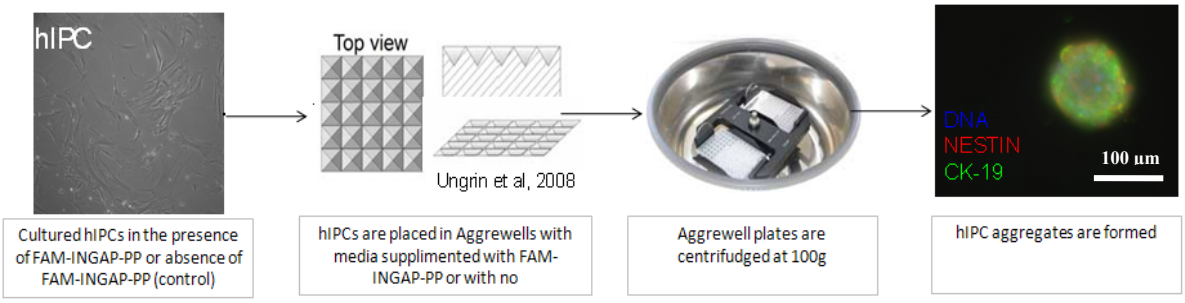

Figure 7-1: Generation of hIPC aggregates by the Aggrewell™ (Stem Cell Technologies) method. (a) hIPCs are cultured from expanded human islets as described above (b) hIPCs are placed into Aggrewells™ with 1.5 mLs of media supplemented with 58 µM FAM-INGAP-PP or just standard media. (c) The Aggrewell™ plate is centrifuged at 100g for 3 minutes to form hIPC aggregates. (d) The hIPC aggregates are removed, seeded into APTS glass-treated chambers to adhere and fluorescently imaged.

7.4 Results and Discussion

The Aggrewell^{TM} plate consists of small pyramidal wells and was designed to create embryoid bodies using cultured embryonic stem cells and centrifugation (Ungrin, Joshi et al. 2008). Since its commercialization, several groups have reported this method as superior to the previously established culture procedures due to the achieved uniform shape and size-control of the bodies achieved from the design (Bauwens, Peerani et al. 2008; Niebruegge, Bauwens et al. 2009; Gauvin and Khademhosseini 2011). In this study, the Aggrewell^{TM} technology was applied to hIPCs treated with INGAP in attempts to create insulin secreting islet like structures for transplantation. To our knowledge the Aggrewell^{TM} has not previously been employed to make islets using hIPCs.

Two different approaches of creating INGAP treated hIPC aggregates were evaluated. In the first experiment, the patient derived hIPCs were at passage 3 and half the cells were treated with rINGAP for 48 hours prior to aggregation. 48 hours of rINGAP treatment was performed based on the results presented in chapter 4, which revealed the largest proteomic response after 48 hours of rINGAP exposure. **Figures 7-2 a,c** show the aggregates following centrifugation and **figures 7-2 b,d** show the aggregates after 24 hours in the wells. Overall, there were no observable differences between the bright field images of the non-treated and rINGAP treated hIPCs neither in the Aggrewells^{TM} immediately after centrifugation nor after 24 hours (**figure 7-2**). Following the removal and adherence of the aggregates, they were nuclear stained with DAPI, as well as for mesenchymal and epithelial markers, nestin and

CK-19, respectively. **Figure 7-3** shows four fluorescent images of the hIPC aggregates formed using the Aggrewell^{TM} plates. The aggregates were relatively comparable in size with diameters ranging from 200-250 μm and were of a uniform spherical shape.

In comparison to the non-treated controls, the fluorescently stained rINGAP treated aggregates appeared to have an increase in nestin^{+} cells localized at the centre of the aggregates (**figure 7-3**). It is unknown if there was an increase in the number of nestin^{+} cells or if the rINGAP aggregates achieved greater organization of the two cells types which gave the appearance of an increase in the number of nestin^{+} cells. Several reasons could explain this observation, including: rINGAP in combination with aggregation promoted muticellular organization, rINGAP in combination with aggregation induced EMT of the epithelial cells to mesenchymal phenotype at the core of the aggregates, or, a fluorescent imaging artifact was observed. The aggregation in combination with rINGAP exposure could have promoted multicellular organization in which the CK-19^{+} cells were signaled to localize towards the outside of the aggregates and the nestin^{+} cells on the inside. This may have been achieved based on differential properties of these cells, such as deformability and cytoskeletal characteristics, or expression of differential complementary cell adhesion molecules, signaling factors and pathways (Ungrin, Joshi et al. 2008).

Alternatively, although widely disputed in the literature, an epithelial-to-mesenchymal transition could have occurred, in which a population of the epithelial (CK-19^{+} cells) were dedifferentiated into mesenchymal (nestin^{+}) cells. EMT has been shown to be critical in

embryogenesis, in which epithelial cells lose their mature characteristics (i.e. gap junctions) and acquire characteristics of mesenchymal cells (i.e. nestin and vimentin expression) (Vicovac and Aplin 1996). Studies have suggested that pancreatic beta-cells when cultured *in vitro* undergo EMT and dedifferentiate into hIPCs (Ozcan 2009; Russ, Ravassard et al. 2009; Joglekar and Hardikar 2010). Additionally, it has been shown that nestin$^+$ pMSCs are found to completely replace the non-proliferative highly apoptotic epithelial cells from expanded islets (Sordi, Melzi et al. 2010). Therefore, it is possible that rINGAP in combination with the aggregate formation, induced EMT or promoted apoptosis of the CK-19$^+$ cells. Lastly, it must be considered that since the fluorescent imaging was not performed using a confocal microscope, z-stacks of the aggregates were not evaluated. To conclusively examine the centers of the islet like structures confocal imaging must be performed. Therefore, it is possible that the observed difference in the nestin$^+$ rINGAP aggregate centres may actually be a fluorescent imaging artifact.

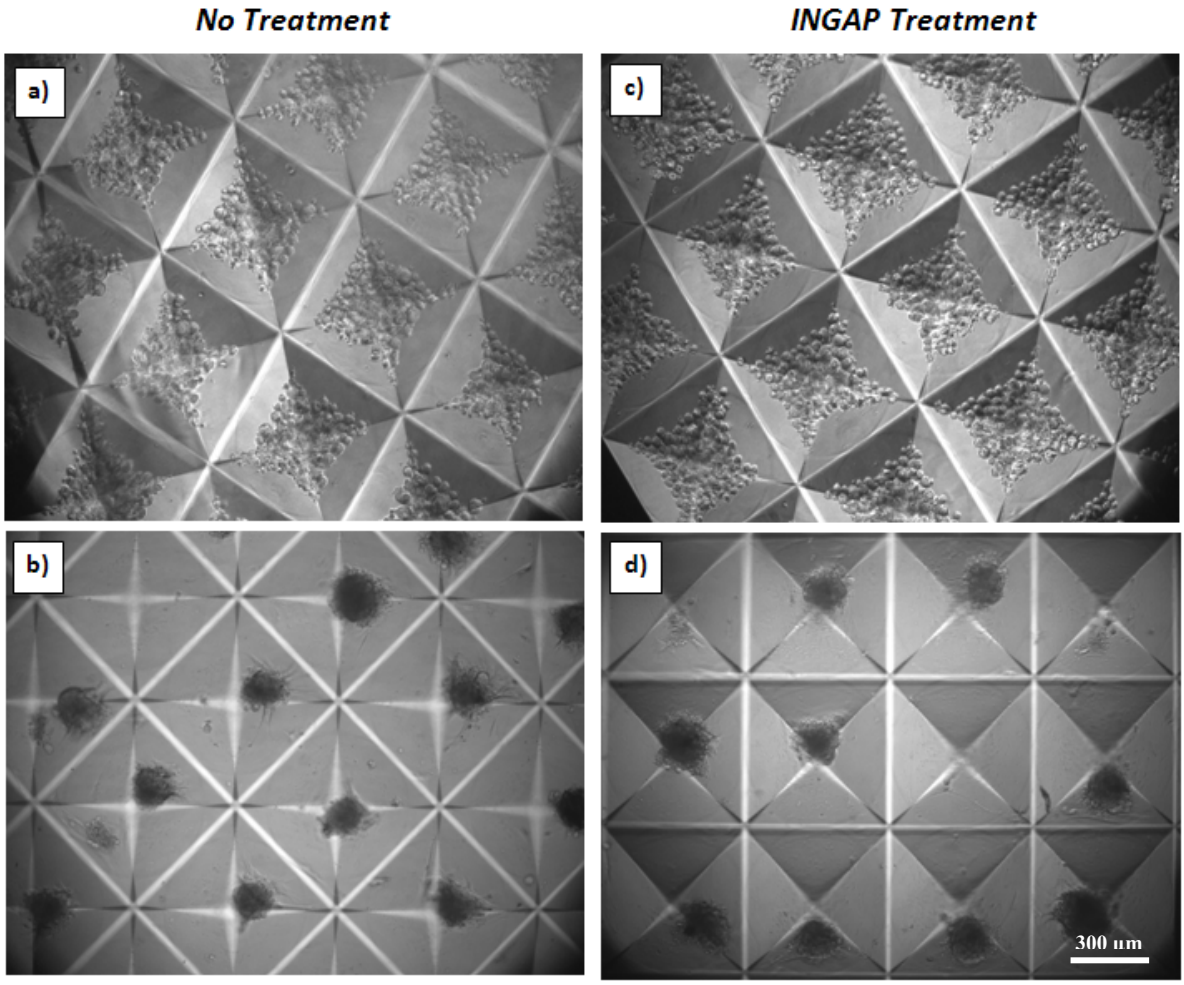

Figure 7-2: Bright field images at 5X magnification of hIPCs in the Aggrewells™ . (a) Non-treated hIPCs after 3 minutes of centrifugation at 100g. (b) Non-treated hIPCs shown in a) after 24 hours. (c) rINGAP treated hIPCs after 3 minutes of centrifugation at 100g. (d) rINGAP treated hIPCs shown in d) after 24 hours.

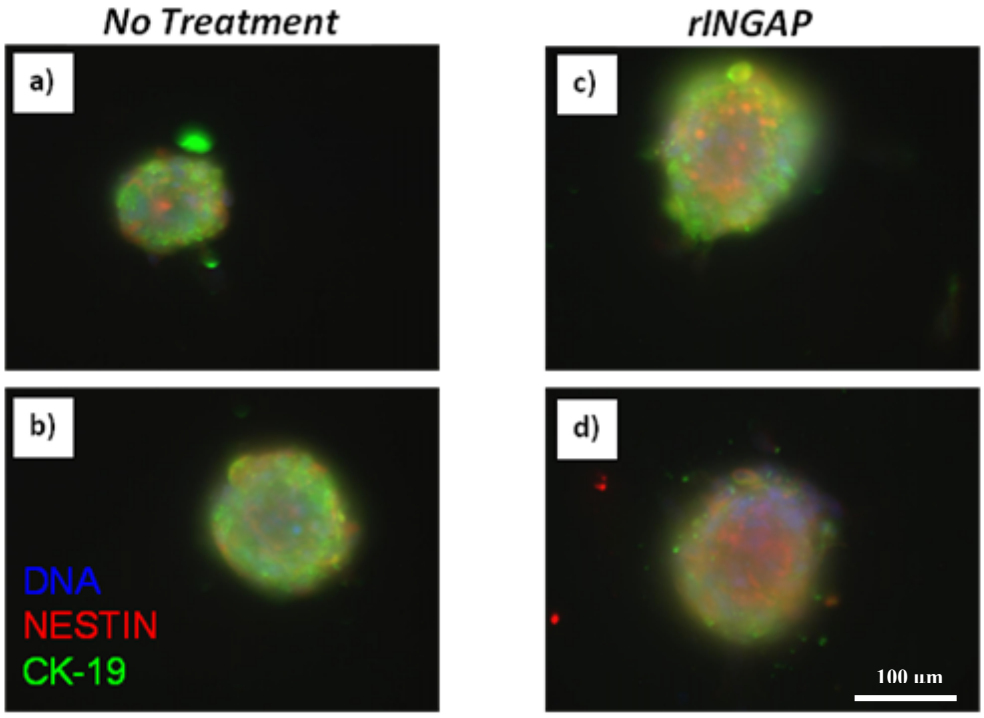

Figure 7-3: rINGAP aggregates at 10X magnification. (a,b) Non-treated hIPCs after immunostaining for DNA, Nestin and CK-19. (c,d) rINGAP-treated hIPCs after immunostaining for DNA, Nestin and CK-19.

To further understand the effect of INGAP and aggregation on the islet derived cells, in the second experiment labeled INGAP-PP was evaluated. hIPCs at passage 8, in comparison to the first experiment in which the hIPCs were at passage 3, were exposed to INGAP-PP upon aggregation. Immediately prior to aggregation, the media in the hIPC wells was supplemented with 58 µM of FAM-INGAP-PP. This concentration and strategy was performed based on the results presented in chapter 5, which revealed an increase in nuclear size following FAM-INGAP-PP exposure. In this experiment, the aggregates were not stained for CK-19 and nestin because at this passage number the cells stained nestin^{+},

vimentin^{+}, CK-19^{-} and CD133^{-}, demonstrated in **figure 5-5 a,b,c**. This was consistent with the report that nestin^{+} pMSCs are found to completely replace the non-proliferative highly apoptotic epithelial cells from expanded islets (Sordi, Melzi et al. 2010).

It was of interest to determine if any differences in the cytoskeletal structure of the aggregates could be observed and if INGAP was localizing centrally. Therefore, following FAM-INGAP-PP exposure and adherence, the hIPCs were stained for actin and DNA, using phalloidin and DAPI, respectively. **Figure 7-4** shows the FAM-INGAP-PP fluorescent images for three different z-positions (bottom, middle, top) and the corresponding bright field image of an adhered hIPC aggregate. The phalloidin staining did not penetrate through the cellular structures and was observed primarily on the edges of the hIPCs. Therefore, the cytoskeletal organization of the hIPCs within the aggregates was not observed. Overall, the most significant observation was the FAM signal was observed at the centre of the aggregates. The controls revealed no FAM signal (**figure 7-5**); therefore it is conclusive that the observed central signal was not an imaging artifact. However, it could be argued that the detected signal was free FAM or free FAM-INGAP-PP and not definitively FAM-INGAP-PP bound to the hIPCs. Although it is unclear why FAM-INGAP-PP would centrally localize, it is hypothesized that if a sub-population of the hIPCs bound/reacted to INGAP-PP they would potentially orientate according to their phenotype, similar to islets with beta cells located at the core.

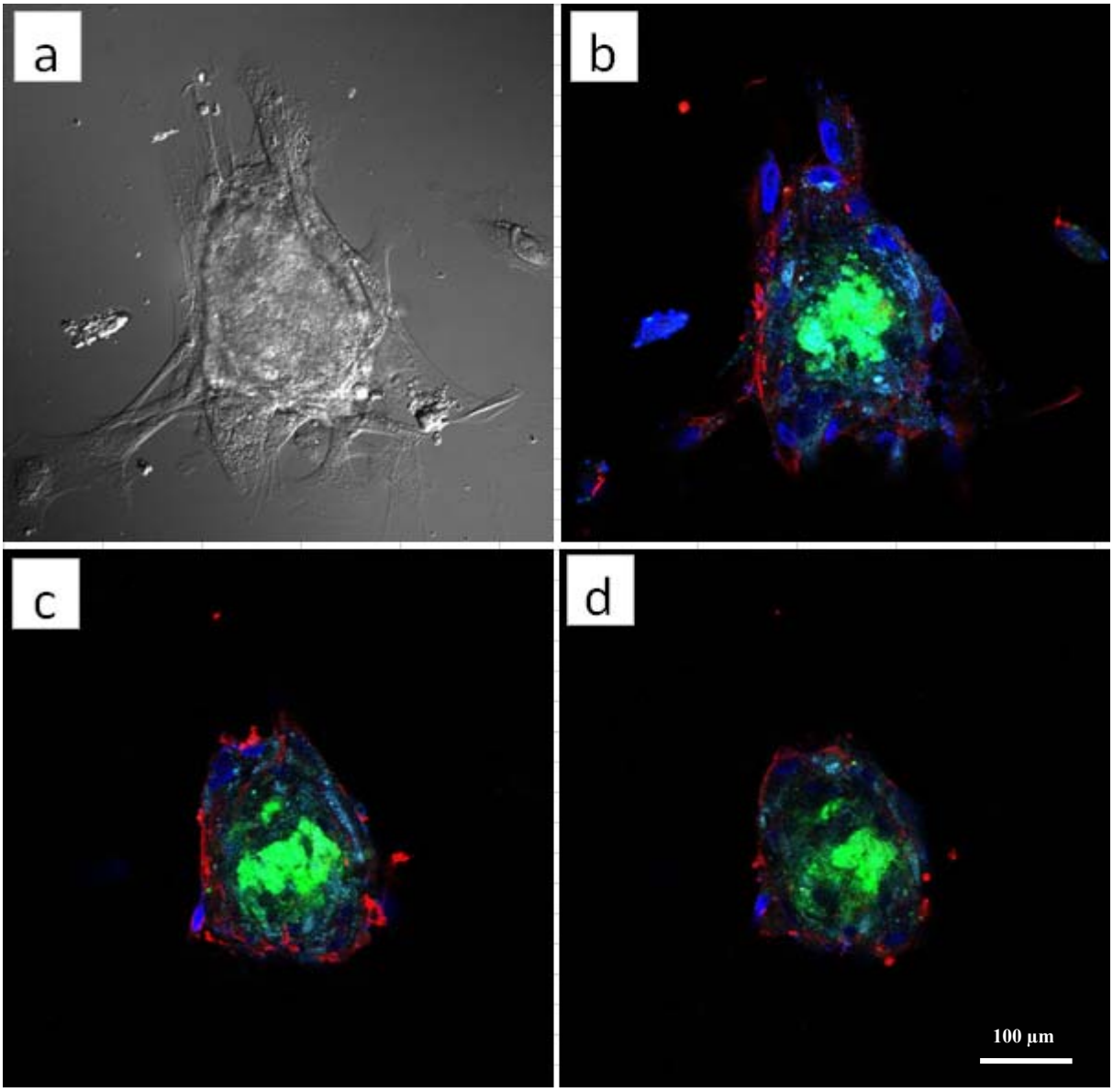

Figure 7-4: FAM-INGAP-PP treated hIPC aggregates at 20X magnification using confocal imaging. (a) Bright field image at z-bottom. (b) Fluorescent image of phalloidin and DAPI staining of aggregate shown in a) at z-bottom. (c) Fluorescent image of phalloidin and DAPI staining of aggregate shown in a) at z-middle (d) Fluorescent image of phalloidin and DAPI staining of aggregate shown in a) at z-top.

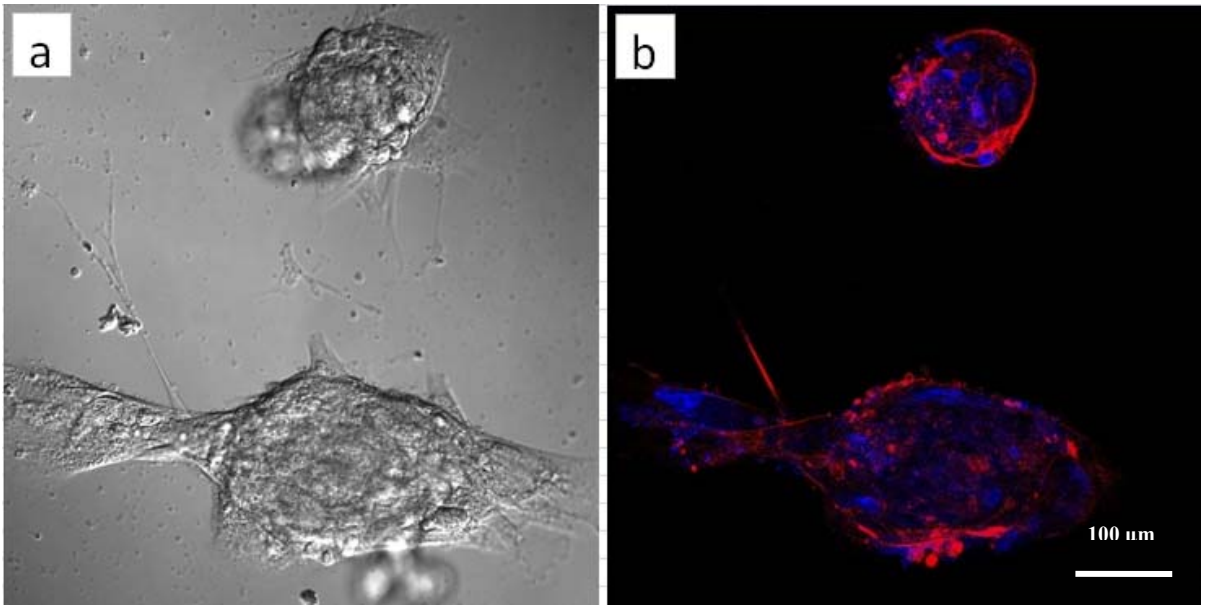

Figure 7-5: Untreated hIPC aggregates at 20X magnification using confocal imaging. (a) Bright field image at bottom. (b) Fluorescent image of phalloidin and DAPI staining of aggregates shown in a).

7.5 Conclusions

We evaluated a method originally designed to create embryoid bodies for feasibility of engineering organized islet-like structures from patient-derived expanded islet progenitor cells. The organized structure of an islet is perhaps key to its physiological functionality, consisting of β-cells throughout its core with the other endocrine cell types at and near its perimeter (Fernandes, King et al. 1997). It was of interest to evaluate if rINGAP or INGAP-PP induced phenotypic responses in the context of aggregated hIPCs. In summary, rINGAP treated aggregates appeared to have an increase in the nestin^{+} cells localized at the centre of the aggregates, which suggested rINGAP in combination with aggregation promoted the

multicelluar organization of the hIPCs. Furthermore, when hIPCs were aggregated and treated with FAM-INGAP-PP, the signal was localized at the center of the aggregates. These results demonstrate that it is possible to create uniformly-sized and shaped hIPC islet-like aggregates which appear to have increased cellular organization in the presence of INGAP.

In conclusion, the results presented in this chapter provide evidence that using the Aggrewells™ and INGAP treated hIPCs, allows for the creation of organized islet-derived hIPC structures. It must be acknowledged that under the two presented experimental conditions, neither rINGAP nor FAM-INGAP-PP aggregates stained positive for C-peptide (negative result not shown). Therefore, it remains unclear if the hIPC INGAP aggregates can be coaxed to secrete insulin. Furthermore, the nature of the cells present at the centre versus the periphery of the aggregates remains to be determined. Nevertheless, the application of the Aggrewell™ technology to generate islets should be investigated further to determine the validity of aggregating hIPCs treated with INGAP. Several factors should be considered in future trials, including, the length of time the hIPCs are in the Aggrewells™ and exposed to INGAP, the ideal passage number (early or late) and analyzing the effects of introducing additional factors or supporting cell types, such as endothelial cells (Hess, Li et al. 2003), must be performed. It will be of interest to examine these trials by immunocytochemistry for the expression of several proteins, including the proteins identified in the rINGAP DIGE analysis (chapter 4) and early insulin secretion transcription factors, such as PDX-1 and Ngn-3. Furthermore, the use of the scrambled peptide in combination with the FAM fluorophore as presented in chapter 6, would provide complete controls for a more detailed analysis.

Chapter 8 Conclusions and Future Work

This thesis presents findings from studying two cellular systems using a proteomics coupled with a long term live-cell imaging approach. The two cellular systems were:

1) Calmodulin (CaM) in the differentiation of a human glioblastoma cell line
2) Human islet-derived progenitor cells (hIPCs) treated with islet neogenesis associated protein (INGAP)

Review of the overall hypothesis:

> ***Live-cell imaging and proteomics can be collectively employed to systematically image and identify regulatory cellular changes, such as phenotypic variations and protein expression differences, which guide undifferentiated cells to different lineages; providing important information about the progression of cellular signaling at various stages of its development, having an impact in the fields of drug discovery and regenerative medicine.***

Two cellular systems were proposed based on practical considerations. Each system had potential challenges, including the unknown uptake efficiency of a cell penetrating peptide and the availability of human islet cells. To complete these investigations, affinity chromatography, DIGE, and long term live-cell imaging techniques were utilized. It was anticipated that the work of the first proposed CaM-mutant based cellular system would identify a new population of CaM binding proteins and that characterization of the CaM binding mediated cell signaling would be achieved through the use of a cell penetrating

peptide. As CaM is involved in various cellular processes, using the two non-conventionally combined methods was an attractive approach to advance the current understanding of the function of CaM protein interactions in cell division and differentiation. It was hypothesized that:

> ***Mutations to the calcium binding sites of CaM would identify a new sub-population of CaMBPs which bind to the CaM-mutant at high affinities and upon cellular delivery, the CaM-mutant would perturb critical signaling pathways involved in cellular function.***

Overall, the hypothesis of the first proposed cellular system was not confirmed. We initially performed affinity chromatography using columns coupled with a CaM-mutant and another with calcium-CaM. The columns were loaded with porcine brain extract and eluted to isolate calcium dependent and independent binding proteins. A limitation to this approach was the isolation of sufficient amounts of the CaM binding proteins to perform a subsequent proteomic analysis on the two protein populations. Using various packing and loading concentrations, the conditions required to elute protein quantities for DIGE were determined. Once the optimal coupling density and loading quantities were determined, the columns were re-loaded to obtain replicates for the DIGE analysis. DIGE achieves statistical inference through replication. Although DIGE is a very powerful proteomics technique, using three repeat column runs to represent replicates was a poor experimental design. Analysis of the elution profiles determined that the non-specific binding to the CaM column increased as the columns were re-used, introducing high variability between the runs and therefore between

the replicates. It was concluded that replication with N > 6 independent affinity chromatography packing and elution's in which the resin is coupled in batch would be required to reduce the variability between runs.

The second objective of the proposed experimental plan, the cellular uptake of CaM, overall, obtained inconclusive results. This work was premised on the cellular up-take of CaM using the HIV-derived TAT-binding domain, which had not previously been reported. The TAT-FITC construct which was to be used as a control to evaluate TAT cellular uptake, yielded a punctate cell staining pattern. This suggested that the TAT-FTIC construct was endocytosed into the cell cytoplasm, however it was inconclusive if TAT was indeed internalized or if TAT was simply bound to the cellular membrane. It was confirmed that there was no non-specific interactions between FITC and the human glioblastoma cells and therefore it was concluded that FITC is a suitable fluorophore to be utilized to label TAT for fluorescent cellular analysis. On the other hand, the TRITC fluorophore used to label CaM was unsuitable for cellular analysis due to the detected non-specific binding in the TRITC only control. Therefore, it was suggested that a different fluorophore be utilized to label CaM and recommended that the chosen fluorophore be evaluated for non-specific cellular interactions prior to the CaM constructs being labeled.

In conclusion, although inconclusive results were obtained from the study of the first proposed cellular system, it is possible with a large experimental design in which the column replicates are not obtained by re-using the columns, potentially new CaMBPs could be

identified and studied at the cellular level using the TAT cell penetrating peptide. No doubt there is great promise in elucidating a wide spectrum of CaM binding protein interactions using the proposed methods and purified CaM proteins. Unfortunately, time did not allow for such large scale experimental modifications and further analysis. However, there was valuable DIGE technique and experimental design knowledge obtained from studying the first cellular system.

It was anticipated that the work on the second proposed hIPC cellular system would determine the proteomic and phenotypic effects of INGAP on hIPCs. Specifically, it was hypothesized that by combing 2D DIGE and long term live-cell imaging:

1) **a subset of INGAPs mechanistic effects will be determined**
2) **INGAPs phenotypic effects will be observed**
3) **a clinically relevant understanding of INGAPs overall effects will be achieved**

hIPCs were cultured and long term live-cell imaging was performed while the cells were exposed to INGAP. After a proteomic DIGE analysis to determine if INGAP induced an effect, aggregates and single cells were characterized by immunofluorescence staining for markers of insulin, beta-cell maturation and proteins identified as significantly up-regulated or down-regulated in the DIGE analysis. This combined approach enabled isolation, separation and population comparisons of the hIPC proteins. A limitation to this approach was the inherent flask to flask variability within the same treatment group. Consequently, it

was determined that a flask sub-pooling design of experiments was required to perform a DIGE analysis with statistically valid protein detection. We identified for the first time a series of proteins which rINGAP altered expression. Specifically, the following proteins were identified: actin binding proteins caldesmon, transgelin, tropomyosin, and cofilin-1, heat shock protein 90 (HSP90), straitin, plasminogen activator inhibitor, annexin V, and alpha-enolase (glycolytic enzyme). These proteins and their related binding proteins form complex protein interaction networks which have been previously linked to diabetes, cell proliferation and cell differentiation (Imperatore, Hanson et al. 1998; Fogarty, Moczulski et al. 1999). Of the 13 proteins chosen for mass spectrometry analysis, 5 were cytoskeletal proteins (caldesmon, transgelin, tropomyosin, STRN and cofilin-1), involved in process formation, migration and differentiation. The identification of these proteins revealed major regulation of the hIPC cytoskeleton at 48 hours of rINGAP exposure. Overall, the temporal proteomic analysis suggests rINGAP perturbs and possibly reorganizes the hIPC cytoskeleton.

To evaluate if hIPCs were being differentiated towards insulin secreting islet-like cells following rINGAP treatment, a temporal mRNA analysis on islet genes was completed. The DIGE results demonstrated that rINGAP treatment changed the global protein expression levels of hIPCs at various treatment times, therefore the PCR analysis was performed at those same treatment times (24, 48 and 96 hours of rINGAP exposure). As well, the hIPCs were analyzed after 15 minutes and 1 hour of rINGAP treatment to evaluate immediate hIPC mRNA expression. Overall, it was determined that rINGAP exposure decreased the mRNA expression of the islet associated genes, glucagon, PPY and CK-19, while insulin expression

was unchanged or undetected. These results complement the DIGE analysis, as a similar trend was determined by DIGE with many of the protein changes having decreases in expression levels. Furthermore, at 96 hours of rINGAP exposure, most of the changes in expression levels were attenuated; that is the rINGAP hIPC expression levels were in the range of control mRNA and protein levels. It has been previously hypothesized that INGAP may act early in the islet cell induction cascade (Rafaeloff, Pittenger et al. 1997; Fleming and Rosenberg 2007). The early changes in mRNA profiling of hIPCs followed by the detected down-regulation of the actin-binding proteins following rINGAP treatment is consistent with this hypothesis. We have shown that rINGAP affects the hIPC cytoskeleton based on the down-regulation of five identified actin-binding proteins, as well as down-regulates three islet associated genes. These proteomic and mRNA results confirmed **hypothesis 1- a subset of INGAPs mechanistic effects will be determined.** Of relevance, cytoskeletal changes during mesenchymal differentiation have previously been reported (Rodriguez, Gonzalez et al. 2004; Yourek, Hussain et al. 2007; Hong, Chen et al. 2010). Therefore, rINGAP may act to suppress basal levels of PPY and glucagon endocrine hormones while reorganizing the hIPC cytoskeleton, possibly further poising hIPCs for differentiation.

To understand if INGAP induced any phonotypical effects through specific binding to hIPCs, live-cell imaging, FACS and immunofluorescent staining was performed. Live-cell imaging analysis revealed a greater than 50% decrease in average nuclear speed and a change in morphology of hIPCs exposed to rINGAP. Immunofluorescent labeling of two proteins which were identified through DIGE exhibited differential translocation in rINGAP-treated

cells. Furthermore, it was reported through imaging fluorescent INGAP-PP, that INGAP binds specifically to hIPCs and the rapid emergence of larger nuclei was observed. The large nuclei were suggestive of either increased ploidy following impaired nuclear separation after DNA duplication, the unpacking of DNA and/or changes in cytoskeletal organization or cellular/nuclear fusion. A FACS analysis was performed to evaluate cell cycle distributions and nuclear size. It was determined in one of the FACS experiments, a larger proportion of cells had increased granularity, indicative of decreased proliferative potential. All of these phenotypic findings, although not all understood at the mechanistic level, demonstrate that INGAP effects hIPCs *in vitro*, which confirmed **hypothesis 2 - INGAPs phenotypic effects will be observed**.

The data presented in this thesis establishes newly identified mechanistic and phenotypic effects of INGAP. It is acknowledged that the specific *in vivo* molecular mechanism(s) responsible for INGAP's islet regenerating effects in animals and humans remain unknown. Thus, **hypothesis 3 - A clinically relevant understanding of INGAPs overall effects will be determined,** was not fully established. However, taken together, this INGAP research will aid in further INGAP clinical developments and future investigations into the potential of hIPCs in relation to diabetes. Further work is necessary to determine possible mechanism(s) of hIPC differentiation into insulin-expressing β-like cells, in order to engineer islets for regenerative medicine applications. Future work should include parallel investigations into both rINGAP and INGAP-PPs effects on hIPCs, as well as on other pancreatic cell types, including pancreatic ductual cells. The DIGE analyses determined ten

proteins either up-regulated or down-regulated in response to rINGAP exposure, however only two of these proteins (caldesmon and tropomyosin) were evaluated using immunofluorescent staining. To further determine INGAPs effect on the perturbation of the actin cytoskeleton, the cellular distribution and localization of each protein identified in the DIGE analyses, specifically the actin binding proteins, is warranted for study. Supplemental to immunofluorescent staining, western blots on the 10 identified proteins would be valuable to support the results of the DIGE analyses. Furthermore, additional PCR analyses on the genes of the proteins identified would determine if INGAP has affects at the mRNA level as well as at the proteomic level. Moreover, earlier genes implicated in islet differentiation and the effects of complementary factors and cell types (e.g. endothelial cells) on hIPCs exposed to INGAP is recommended for future study.

References

Abd-el-Basset, E. M., I. Ahmed, et al. (1991). "Actin and actin-binding proteins in differentiating astroglia in tissue culture." J Neurosci Res **30**(1): 1-17.

Albinsson, S., I. Nordstrom, et al. (2004). "Stretch of the vascular wall induces smooth muscle differentiation by promoting actin polymerization." J Biol Chem **279**(33): 34849-34855.

Asoh, S., I. Ohsawa, et al. (2002). "Protection against ischemic brain injury by protein therapeutics." Proc Natl Acad Sci U S A **99**(26): 17107-17112.

Assinder, S. J., J. A. Stanton, et al. (2009). "Transgelin: an actin-binding protein and tumour suppressor." Int J Biochem Cell Biol **41**(3): 482-486.

Assouline-Thomas, B., A. Pilotte, et al. (2009). "Production and characterization of the recombinant Islet Neogenesis Associated Protein (rINGAP)." Protein Expr Purif **69**(1): 1-8.

Atouf, F., C. H. Park, et al. (2007). "No evidence for mouse pancreatic beta-cell epithelial-mesenchymal transition in vitro." Diabetes **56**(3): 699-702.

Aubry, S., F. Burlina, et al. (2009). "Cell-surface thiols affect cell entry of disulfide-conjugated peptides." FASEB J **23**(9): 2956-2967.

Axlund, S. D., J. R. Lambert, et al. (2010). "HOXC8 inhibits androgen receptor signaling in human prostate cancer cells by inhibiting SRC-3 recruitment to direct androgen target genes." Mol Cancer Res **8**(12): 1643-1655.

Bach, C. T., S. Creed, et al. (2009). "Tropomyosin isoform expression regulates the transition of adhesions to determine cell speed and direction." Mol Cell Biol **29**(6): 1506-1514.

Baharvand, H., H. Jafary, et al. (2006). "Generation of insulin-secreting cells from human embryonic stem cells." Dev Growth Differ **48**(5): 323-332.

Bar, Y., H. A. Russ, et al. (2008). "HES-1 is involved in adaptation of adult human beta-cells to proliferation in vitro." Diabetes **57**(9): 2413-2420.

Barbosa, H., S. Bordin, et al. (2006). "Islet Neogenesis Associated Protein (INGAP) modulates gene expression in cultured neonatal rat islets." Regul Pept **136**(1-3): 78-84.

Bartolome, F., N. de Las Cuevas, et al. (2007). "Impaired apoptosis in lymphoblasts from Alzheimer's disease patients: cross-talk of Ca2+/calmodulin and ERK1/2 signaling pathways." Cell Mol Life Sci **64**(11): 1437-1448.

Bauwens, C. L., R. Peerani, et al. (2008). "Control of human embryonic stem cell colony and aggregate size heterogeneity influences differentiation trajectories." Stem Cells **26**(9): 2300-2310.

Bennett, R. D., A. S. Mauer, et al. (2007). "Calmodulin-like protein increases filopodia-dependent cell motility via up-regulation of myosin-10." J Biol Chem **282**(5): 3205-3212.

Blumbach, B., Z. Pancer, et al. (1998). "The putative sponge aggregation receptor. Isolation and characterization of a molecule composed of scavenger receptor cysteine-rich domains and short consensus repeats." J Cell Sci **111 (Pt 17)**: 2635-2644.

Borelli, M. I., H. Del Zotto, et al. (2007). "Transcription, expression and tissue binding in vivo of INGAP and INGAP-related peptide in normal hamsters." Regul Pept **140**(3): 192-197.

Bouwens, L. and D. G. Pipeleers (1998). "Extra-insular beta cells associated with ductules are frequent in adult human pancreas." Diabetologia **41**(6): 629-633.

Brand, S. J., S. Tagerud, et al. (2002). "Pharmacological treatment of chronic diabetes by stimulating pancreatic beta-cell regeneration with systemic co-administration of EGF and gastrin." Pharmacol Toxicol **91**(6): 414-420.

Braun, A. P. and H. Schulman (1995). "The multifunctional calcium/calmodulin-dependent protein kinase: from form to function." Annu Rev Physiol **57**: 417-445.

Bregant, E., G. Renzone, et al. (2009). "Down-regulation of SM22/transgelin gene expression during H9c2 cells differentiation." Mol Cell Biochem **327**(1-2): 145-152.
Brennand, K., D. Huangfu, et al. (2007). "All beta cells contribute equally to islet growth and maintenance." PLoS Biol **5**(7): e163.
Bugatti, A., C. Urbinati, et al. (2007). "Heparin-mimicking sulfonic acid polymers as multitarget inhibitors of human immunodeficiency virus type 1 Tat and gp120 proteins." Antimicrob Agents Chemother **51**(7): 2337-2345.
Burke, P., K. Schooler, et al. (2001). "Regulation of epidermal growth factor receptor signaling by endocytosis and intracellular trafficking." Mol Biol Cell **12**(6): 1897-1910.
Butler, A. E., J. Janson, et al. (2003). "Beta-cell deficit and increased beta-cell apoptosis in humans with type 2 diabetes." Diabetes **52**(1): 102-110.
Cai, S. R., G. Xu, et al. (2006). "The kinetics and tissue distribution of protein transduction in mice." Eur J Pharm Sci **27**(4): 311-319.
Cao, G., W. Pei, et al. (2002). "In Vivo Delivery of a Bcl-xL Fusion Protein Containing the TAT Protein Transduction Domain Protects against Ischemic Brain Injury and Neuronal Apoptosis." J Neurosci **22**(13): 5423-5431.
Carlotti, F., A. Zaldumbide, et al. (2010). "Isolated human islets contain a distinct population of mesenchymal stem cells." Islets **2**(3): 164-173.
Caron, N. J., Y. Torrente, et al. (2001). "Intracellular delivery of a Tat-eGFP fusion protein into muscle cells." Mol Ther **3**(3): 310-318.
Chase, L. G., F. Ulloa-Montoya, et al. (2007). "Islet-derived fibroblast-like cells are not derived via epithelial-mesenchymal transition from Pdx-1 or insulin-positive cells." Diabetes **56**(1): 3-7.
Chiozzi, P., J. M. Sanz, et al. (1997). "Spontaneous cell fusion in macrophage cultures expressing high levels of the P2Z/P2X7 receptor." J Cell Biol **138**(3): 697-706.
Cho, W. C. (2007). "Proteomics technologies and challenges." Genomics Proteomics Bioinformatics **5**(2): 77-85.
Clapham, D. E. (1995). "Calcium signaling." Cell **80**(2): 259-268.
Clark, P. J. and F. C. Evans (1954). "Distance to Nearest Neighbor as a Measure of Spatial Relationships in Populations." Ecology **35**(4): 445-453.
Clayton, L. and M. H. Johnson (1998). "Tropomyosin in preimplantation mouse development: identification, expression, and organization during cell division and polarization." Exp Cell Res **238**(2): 450-464.
Colomer, J. and A. R. Means (2007). "Physiological roles of the Ca2+/CaM-dependent protein kinase cascade in health and disease." Subcell Biochem **45**: 169-214.
Conway, B. R., A. P. Maxwell, et al. (2004). "Association between variation in the actin-binding gene caldesmon and diabetic nephropathy in type 1 diabetes." Diabetes **53**(4): 1162-1165.
Cormier, S. A., M. A. Mello, et al. (2003). "Normal proliferation and differentiation of Hoxc-8 transgenic chondrocytes in vitro." BMC Dev Biol **3**: 4.
Crissman, H. A., P. F. Mullaney, et al. (1975). "Methods and applications of flow systems for analysis and sorting of mammalian cells." Methods Cell Biol **9**(0): 179-246.
Crivici, A. and M. Ikura (1995). "Molecular and structural basis of target recognition by calmodulin." Annu Rev Biophys Biomol Struct **24**: 85-116.
Cross, J. C. (2000). "Genetic insights into trophoblast differentiation and placental morphogenesis." Semin Cell Dev Biol **11**(2): 105-113.
Dabrowska, R., N. Kulikova, et al. (2004). "Nonmuscle caldesmon: its distribution and involvement in various cellular processes. Review article." Protoplasma **224**(1-2): 1-13.
Danowski, B. A., A. Khodjakov, et al. (2001). "Centrosome behavior in motile HGF-treated PtK2 cells expressing GFP-gamma tubulin." Cell Motil Cytoskeleton **50**(2): 59-68.

Davani, B., L. Ikonomou, et al. (2007). "Human islet-derived precursor cells are mesenchymal stromal cells that differentiate and mature to hormone-expressing cells in vivo." Stem Cells **25**(12): 3215-3222.
de Kort, H., E. J. de Koning, et al. (2011). "Islet transplantation in type 1 diabetes." BMJ **342**: d217.
Demou, Z. N. and L. V. McIntire (2002). "Fully automated three-dimensional tracking of cancer cells in collagen gels: determination of motility phenotypes at the cellular level." Cancer Res **62**(18): 5301-5307.
Dolphin, A. C. (2009). "Calcium channel diversity: multiple roles of calcium channel subunits." Curr Opin Neurobiol.
Dor, Y., J. Brown, et al. (2004). "Adult pancreatic beta-cells are formed by self-duplication rather than stem-cell differentiation." Nature **429**(6987): 41-46.
Duchardt, F., M. Fotin-Mleczek, et al. (2007). "A comprehensive model for the cellular uptake of cationic cell-penetrating peptides." Traffic **8**(7): 848-866.
Dungan, K. M., J. B. Buse, et al. (2009). "Effects of therapy in type 1 and type 2 diabetes mellitus with a peptide derived from islet neogenesis associated protein (INGAP)." Diabetes Metab Res Rev **25**(6): 558-565.
Earle, W. R. (1962). "Some morphologic variations of certain cells under controlled experimental conditions." Natl Cancer Inst Monogr **7**: 213-236.
Edgar, B. A. and T. L. Orr-Weaver (2001). "Endoreplication cell cycles: more for less." Cell **105**(3): 297-306.
Edlund, H. (2002). "Pancreatic organogenesis--developmental mechanisms and implications for therapy." Nat Rev Genet **3**(7): 524-532.
Enelow, R. I., G. W. Sullivan, et al. (1992). "Induction of multinucleated giant cell formation from in vitro culture of human monocytes with interleukin-3 and interferon-gamma: comparison with other stimulating factors." Am J Respir Cell Mol Biol **6**(1): 57-62.
Fackler, O. T. and R. Grosse (2008). "Cell motility through plasma membrane blebbing." J Cell Biol **181**(6): 879-884.
Fernandes, A., L. C. King, et al. (1997). "Differentiation of new insulin-producing cells is induced by injury in adult pancreatic islets." Endocrinology **138**(4): 1750-1762.
Fleming, A. and L. Rosenberg (2007). "Prospects and challenges for islet regeneration as a treatment for diabetes: a review of islet neogenesis associated protein." J Diabetes Sci Technol **1**(2): 231-244.
Fogarty, D. G., D. K. Moczulski, et al. (1999). "Evidence for a susceptibility locus for diabetic nephropathy (DN) on chromosome 7q in Caucasian families with type 2 diabetes." Diabetes **48**: A47-A47.
Fonseca, S. B., M. P. Pereira, et al. (2009). "Recent advances in the use of cell-penetrating peptides for medical and biological applications." Adv Drug Deliv Rev **61**(11): 953-964.
Francini, F., H. Del Zotto, et al. (2009). "Selective effect of INGAP-PP upon mouse embryonic stem cell differentiation toward islet cells." Regul Pept **153**(1-3): 43-48.
Frankel, A. D., D. S. Bredt, et al. (1988). "Tat protein from human immunodeficiency virus forms a metal-linked dimer." Science **240**(4848): 70-73.
Frankel, A. D. and C. O. Pabo (1988). "Cellular uptake of the tat protein from human immunodeficiency virus." Cell **55**(6): 1189-1193.
Froese, G. (1964). "The Distribution and Interdependence of Generation Times of Hela Cells." Exp Cell Res **35**: 415-419.
Gallo, R., F. Gambelli, et al. (2007). "Generation and expansion of multipotent mesenchymal progenitor cells from cultured human pancreatic islets." Cell Death Differ **14**(11): 1860-1871.

Gasser, A. and J. Most (1999). "Generation of multinucleated giant cells in vitro by culture of human monocytes with Mycobacterium bovis BCG in combination with cytokine-containing supernatants." Infect Immun **67**(1): 395-402.
Gauvin, R. and A. Khademhosseini (2011). "Microscale Technologies and Modular Approaches for Tissue Engineering: Moving toward the Fabrication of Complex Functional Structures." ACS Nano.
Gershengorn, M. C., A. A. Hardikar, et al. (2004). "Epithelial-to-mesenchymal transition generates proliferative human islet precursor cells." Science **306**(5705): 2261-2264.
Goodrich, T. D. and R. Y. Morita (1977). "Low temperature inhibition on binding, trasport, and incorporation of leucine, arginine, methionine, and histidine in Escherichia coli)." Z Allg Mikrobiol **17**(2): 91-97.
Gopalakrishna, R. and W. B. Anderson (1982). "Ca2+-induced hydrophobic site on calmodulin: application for purification of calmodulin by phenyl-Sepharose affinity chromatography." Biochem Biophys Res Commun **104**(2): 830-836.
Gump, J. M. and S. F. Dowdy (2007). "TAT transduction: the molecular mechanism and therapeutic prospects." Trends Mol Med **13**(10): 443-448.
Gunning, P., G. O'Neill, et al. (2008). "Tropomyosin-based regulation of the actin cytoskeleton in time and space." Physiol Rev **88**(1): 1-35.
Gunning, P. W., G. Schevzov, et al. (2005). "Tropomyosin isoforms: divining rods for actin cytoskeleton function." Trends Cell Biol **15**(6): 333-341.
Guz, Y., I. Nasir, et al. (2001). "Regeneration of pancreatic beta cells from intra-islet precursor cells in an experimental model of diabetes." Endocrinology **142**(11): 4956-4968.
Halban, P. A. (2004). "Cellular sources of new pancreatic beta cells and therapeutic implications for regenerative medicine." Nat Cell Biol **6**(11): 1021-1025.
Hayden-Martinez, K., L. P. Kane, et al. (2000). "Effects of a constitutively active form of calcineurin on T cell activation and thymic selection." J Immunol **165**(7): 3713-3721.
Hess, D., L. Li, et al. (2003). "Bone marrow-derived stem cells initiate pancreatic regeneration." Nat Biotechnol **21**(7): 763-770.
Hochberg, Y. and Y. Benjamini (1990). "More powerful procedures for multiple significance testing." Stat Med **9**(7): 811-818.
Honczarenko, M., Y. Le, et al. (2006). "Human bone marrow stromal cells express a distinct set of biologically functional chemokine receptors." Stem Cells **24**(4): 1030-1041.
Hong, D., H. X. Chen, et al. (2010). "Morphological and proteomic analysis of early stage of osteoblast differentiation in osteoblastic progenitor cells." Exp Cell Res **316**(14): 2291-2300.
Horgan, G. W. (2007). "Sample size and replication in 2D gel electrophoresis studies." J Proteome Res **6**(7): 2884-2887.
Houdusse, A., J. F. Gaucher, et al. (2006). "Crystal structure of apo-calmodulin bound to the first two IQ motifs of myosin V reveals essential recognition features." Proc Natl Acad Sci U S A **103**(51): 19326-19331.
Hsu, T. C. and D. S. Kellogg, Jr. (1960). "Mammalian chromosomes in vitro. XII. Experimental evolution of cell populations." J Natl Cancer Inst **24**: 1067-1093.
Ikebe, M. and S. Reardon (1988). "Binding of caldesmon to smooth muscle myosin." J Biol Chem **263**(7): 3055-3058.
Ikura, M. and J. B. Ames (2006). "Genetic polymorphism and protein conformational plasticity in the calmodulin superfamily: two ways to promote multifunctionality." Proc Natl Acad Sci U S A **103**(5): 1159-1164.

Imperatore, G., R. L. Hanson, et al. (1998). "Sib-pair linkage analysis for susceptibility genes for microvascular complications among Pima Indians with type 2 diabetes. Pima Diabetes Genes Group." Diabetes **47**(5): 821-830.
Issaq, H. and T. Veenstra (2008). "Two-dimensional polyacrylamide gel electrophoresis (2D-PAGE): advances and perspectives." Biotechniques **44**(5): 697-698, 700.
Jamal, A. M., M. Lipsett, et al. (2003). "Signals for death and differentiation: a two-step mechanism for in vitro transformation of adult islets of Langerhans to duct epithelial structures." Cell Death Differ **10**(9): 987-996.
Jamal, A. M., M. Lipsett, et al. (2005). "Morphogenetic plasticity of adult human pancreatic islets of Langerhans." Cell Death Differ **12**(7): 702-712.
Jamali, A. A., B. C. Emmerson, et al. (2005). "Fresh osteochondral allografts: results in the patellofemoral joint." Clin Orthop Relat Res(437): 176-185.
Jang, D. J., M. Guo, et al. (2007). "Proteomic and biochemical studies of calcium- and phosphorylation-dependent calmodulin complexes in Mammalian cells." J Proteome Res **6**(9): 3718-3728.
Jiang, Q., R. Huang, et al. (2010). "Caldesmon regulates the motility of vascular smooth muscle cells by modulating the actin cytoskeleton stability." J Biomed Sci **17**: 6.
Joglekar, M. V. and A. A. Hardikar (2010). "Epithelial-to-mesenchymal transition in pancreatic islet beta cells." Cell Cycle **9**(20): 4077-4079.
Joglekar, M. V., V. M. Joglekar, et al. (2009). "Human fetal pancreatic insulin-producing cells proliferate in vitro." J Endocrinol **201**(1): 27-36.
Jurado, L. A., P. S. Chockalingam, et al. (1999). "Apocalmodulin." Physiol Rev **79**(3): 661-682.
Kantawong, F., K. E. V. Burgess, et al. (2009). "Whole proteome analysis of osteoprogenitor differentiation induced by disordered nanotopography and mediated by ERK signalling." Biomaterials **30**(27): 4723-4731.
Karp, N. A., D. P. Kreil, et al. (2004). "Determining a significant change in protein expression with DeCyder during a pair-wise comparison using two-dimensional difference gel electrophoresis." Proteomics **4**(5): 1421-1432.
Karp, N. A. and K. S. Lilley (2009). "Investigating sample pooling strategies for DIGE experiments to address biological variability." Proteomics **9**(2): 388-397.
Karp, N. A., P. S. McCormick, et al. (2007). "Experimental and statistical considerations to avoid false conclusions in proteomics studies using differential in-gel electrophoresis." Mol Cell Proteomics **6**(8): 1354-1364.
Karp, N. A., M. Spencer, et al. (2005). "Impact of replicate types on proteomic expression analysis." J Proteome Res **4**(5): 1867-1871.
Kilian, K. A., B. Bugarija, et al. (2010). "Geometric cues for directing the differentiation of mesenchymal stem cells." Proc Natl Acad Sci U S A **107**(11): 4872-4877.
Kodama, S., K. Kojima, et al. (2009). "Engineering functional islets from cultured cells." Tissue Eng Part A **15**(11): 3321-3329.
Kramer, S. D. and H. Wunderli-Allenspach (2003). "No entry for TAT(44-57) into liposomes and intact MDCK cells: novel approach to study membrane permeation of cell-penetrating peptides." Biochim Biophys Acta **1609**(2): 161-169.
Kumarasuriyar, A., C. Dombrowski, et al. (2007). "A novel use of TAT-EGFP to validate techniques to alter osteosarcoma cell surface glycosaminoglycan expression." J Mol Histol **38**(5): 435-447.
Kutlu, B., A. G. Kayali, et al. (2009). "Meta-analysis of gene expression in human pancreatic islets after in vitro expansion." Physiol Genomics **39**(1): 72-81.

Lacy, P. E., N. J. Klein, et al. (1973). "Effect of cytochalasin B on the biphasic release of insulin in perifused rat islets." Endocrinology **92**(5): 1458-1468.
Lambrechts, A., M. Van Troys, et al. (2004). "The actin cytoskeleton in normal and pathological cell motility." Int J Biochem Cell Biol **36**(10): 1890-1909.
Lee, H. O., J. M. Davidson, et al. (2009). "Endoreplication: polyploidy with purpose." Genes Dev **23**(21): 2461-2477.
Lee, S. H. and R. Dominguez (2010). "Regulation of actin cytoskeleton dynamics in cells." Mol Cells **29**(4): 311-325.
Lewis, E. B. (1978). "A gene complex controlling segmentation in Drosophila." Nature **276**(5688): 565-570.
Li, C. J., R. Heim, et al. (1999). "Dynamic redistribution of calmodulin in HeLa cells during cell division as revealed by a GFP-calmodulin fusion protein technique." J Cell Sci **112 (Pt 10)**: 1567-1577.
Li, M., S. Li, et al. (2008). "Crystal structure of human transgelin." J Struct Biol **162**(2): 229-236.
Limback-Stokin, K., E. Korzus, et al. (2004). "Nuclear calcium/calmodulin regulates memory consolidation." J Neurosci **24**(48): 10858-10867.
Lin, J. J., R. D. Eppinga, et al. (2008). "Human tropomyosin isoforms in the regulation of cytoskeleton functions." Adv Exp Med Biol **644**: 201-222.
Lin, J. J., T. E. Hegmann, et al. (1988). "Differential localization of tropomyosin isoforms in cultured nonmuscle cells." J Cell Biol **107**(2): 563-572.
Lin, J. J., K. S. Warren, et al. (1997). "Tropomyosin isoforms in nonmuscle cells." Int Rev Cytol **170**: 1-38.
Lu, J., Y. P. Gu, et al. (2005). "Adult islets cultured in collagen gel transdifferentiate into duct-like cells." World J Gastroenterol **11**(22): 3426-3430.
Mack, C. P., A. V. Somlyo, et al. (2001). "Smooth muscle differentiation marker gene expression is regulated by RhoA-mediated actin polymerization." J Biol Chem **276**(1): 341-347.
Madrid, V., H. Del Zotto, et al. (2009). "Islet neogenesis-associated protein pentadecapeptide (INGAP-PP): mechanisms involved in its effect upon beta-cell mass and function." Regul Pept **157**(1-3): 25-31.
Mann, D. A. and A. D. Frankel (1991). "Endocytosis and targeting of exogenous HIV-1 Tat protein." EMBO J **10**(7): 1733-1739.
Mann, R. S. and G. Morata (2000). "The developmental and molecular biology of genes that subdivide the body of Drosophila." Annu Rev Cell Dev Biol **16**: 243-271.
Marouga, R., S. David, et al. (2005). "The development of the DIGE system: 2D fluorescence difference gel analysis technology." Anal Bioanal Chem **382**(3): 669-678.
Marston, S. B. (1989). "What is latch? New ideas about tonic contraction in smooth muscle." J Muscle Res Cell Motil **10**(2): 97-100.
Matsushita, M., K. Tomizawa, et al. (2001). "A high-efficiency protein transduction system demonstrating the role of PKA in long-lasting long-term potentiation." J Neurosci **21**(16): 6000-6007.
Mazumder, A. and G. V. Shivashankar (2010). "Emergence of a prestressed eukaryotic nucleus during cellular differentiation and development." J R Soc Interface **7 Suppl 3**: S321-330.
Montana, E., S. Bonner-Weir, et al. (1993). "Beta cell mass and growth after syngeneic islet cell transplantation in normal and streptozocin diabetic C57BL/6 mice." J Clin Invest **91**(3): 780-787.
Moogk, D., S. Hanley, et al. (2007). "Design and analysis of a long-term live-cell imaging chamber for tracking cellular dynamics within cultured human islets of Langerhans." Biotechnol Bioeng **97**(5): 1138-1147.

Morton, R. A., E. Geras-Raaka, et al. (2007). "Endocrine precursor cells from mouse islets are not generated by epithelial-to-mesenchymal transition of mature beta cells." Mol Cell Endocrinol **270**(1-2): 87-93.
Most, J., L. Spotl, et al. (1997). "Formation of multinucleated giant cells in vitro is dependent on the stage of monocyte to macrophage maturation." Blood **89**(2): 662-671.
Murray, K. D., C. M. Gall, et al. (1994). "Differential regulation of brain-derived neurotrophic factor and type II calcium/calmodulin-dependent protein kinase messenger RNA expression in Alzheimer's disease." Neuroscience **60**(1): 37-48.
Muthuchamy, M., L. Pajak, et al. (1993). "Developmental analysis of tropomyosin gene expression in embryonic stem cells and mouse embryos." Mol Cell Biol **13**(6): 3311-3323.
Mutskov, V., B. M. Raaka, et al. (2007). "The human insulin gene displays transcriptionally active epigenetic marks in islet-derived mesenchymal precursor cells in the absence of insulin expression." Stem Cells **25**(12): 3223-3233.
Nagahara, H., A. M. Vocero-Akbani, et al. (1998). "Transduction of full-length TAT fusion proteins into mammalian cells: TAT-p27Kip1 induces cell migration." Nat Med **4**(12): 1449-1452.
Nakase, I., A. Tadokoro, et al. (2007). "Interaction of arginine-rich peptides with membrane-associated proteoglycans is crucial for induction of actin organization and macropinocytosis." Biochemistry **46**(2): 492-501.
Nichols, A. J., L. H. Carney, et al. (2008). "Comparison of slow and fast neocortical neuron migration using a new in vitro model." BMC Neurosci **9**: 50.
Niebruegge, S., C. L. Bauwens, et al. (2009). "Generation of human embryonic stem cell-derived mesoderm and cardiac cells using size-specified aggregates in an oxygen-controlled bioreactor." Biotechnol Bioeng **102**(2): 493-507.
Nir, T., D. A. Melton, et al. (2007). "Recovery from diabetes in mice by beta cell regeneration." J Clin Invest **117**(9): 2553-2561.
Noguchi, H. (2009). "Pancreatic islet transplantation." World J Gastrointest Surg **1**(1): 16-20.
Nunez, R. (2001). "DNA measurement and cell cycle analysis by flow cytometry." Curr Issues Mol Biol **3**(3): 67-70.
Nurse, P. (1990). "Universal control mechanism regulating onset of M-phase." Nature **344**(6266): 503-508.
Oh-hora, M. and A. Rao (2008). "Calcium signaling in lymphocytes." Curr Opin Immunol **20**(3): 250-258.
Oh, J. E., K. Karlmark Raja, et al. (2006). "Cytoskeleton changes following differentiation of N1E-115 neuroblastoma cell line." Amino Acids **31**(3): 289-298.
Okamoto, F., H. Kajiya, et al. (2004). "Prostaglandin E2 activates outwardly rectifying Cl(-) channels via a cAMP-dependent pathway and reduces cell motility in rat osteoclasts." Am J Physiol Cell Physiol **287**(1): C114-124.
Oliver-Krasinski, J. M. and D. A. Stoffers (2008). "On the origin of the beta cell." Genes Dev **22**(15): 1998-2021.
Ozcan, S. (2009). "MiR-30 family and EMT in human fetal pancreatic islets." Islets **1**(3): 283-285.
Pai, S. Y., D. A. Fruman, et al. (1994). "Inhibition of calcineurin phosphatase activity in adult bone marrow transplant patients treated with cyclosporine A." Blood **84**(11): 3974-3979.
Parwaresch, M. R., H. Kreipe, et al. (1986). "Human macrophage hybrid forming spontaneous giant cells." Virchows Arch B Cell Pathol Incl Mol Pathol **51**(2): 89-96.
Pearson, J. C., D. Lemons, et al. (2005). "Modulating Hox gene functions during animal body patterning." Nat Rev Genet **6**(12): 893-904.
Peck, A. B., J. G. Cornelius, et al. (2002). "Generation of islets of Langerhans from adult pancreatic stem cells." J Hepatobiliary Pancreat Surg **9**(6): 704-709.

Pelham, R. J., Jr., J. J. Lin, et al. (1996). "A high molecular mass non-muscle tropomyosin isoform stimulates retrograde organelle transport." J Cell Sci **109 (Pt 5)**: 981-989.
Percival, J. M., G. Thomas, et al. (2000). "Sorting of tropomyosin isoforms in synchronised NIH 3T3 fibroblasts: evidence for distinct microfilament populations." Cell Motil Cytoskeleton **47**(3): 189-208.
Pittenger, G. L., D. A. Taylor-Fishwick, et al. (2007). "Intramuscular injection of islet neogenesis-associated protein peptide stimulates pancreatic islet neogenesis in healthy dogs." Pancreas **34**(1): 103-111.
Pittenger, G. L., A. I. Vinik, et al. (1992). "The partial isolation and characterization of ilotropin, a novel islet-specific growth factor." Adv Exp Med Biol **321**: 123-130; discussion 131-122.
Pollard, S. M., K. Yoshikawa, et al. (2009). "Glioma stem cell lines expanded in adherent culture have tumor-specific phenotypes and are suitable for chemical and genetic screens." Cell Stem Cell **4**(6): 568-580.
Pollard, T. D. and G. G. Borisy (2003). "Cellular motility driven by assembly and disassembly of actin filaments." Cell **112**(4): 453-465.
Poon, B., M. A. Chang, et al. (2007). "Vpr is required for efficient Nef expression from unintegrated human immunodeficiency virus type 1 DNA." J Virol **81**(19): 10515-10523.
Prasad, P. D., J. A. Stanton, et al. (2010). "Expression of the actin-associated protein transgelin (SM22) is decreased in prostate cancer." Cell Tissue Res **339**(2): 337-347.
Puricelli, L., E. Iori, et al. (2006). "Proteome analysis of cultured fibroblasts from type 1 diabetic patients and normal subjects." J Clin Endocrinol Metab **91**(9): 3507-3514.
Rabut, G. and J. Ellenberg (2004). "Automatic real-time three-dimensional cell tracking by fluorescence microscopy." J Microsc **216**(Pt 2): 131-137.
Rafaeloff, R., G. L. Pittenger, et al. (1997). "Cloning and sequencing of the pancreatic islet neogenesis associated protein (INGAP) gene and its expression in islet neogenesis in hamsters." J Clin Invest **99**(9): 2100-2109.
Ramunas, J., M. Illman, et al. (2006). "True monolayer cell culture in a confined 3D microenvironment enables lineage informatics." Cytometry A **69**(12): 1202-1211.
Ramunas, J., H. J. Montgomery, et al. (2007). "Real-time fluorescence tracking of dynamic transgene variegation in stem cells." Mol Ther **15**(4): 810-817.
Ravid, K., J. Lu, et al. (2002). "Roads to polyploidy: the megakaryocyte example." J Cell Physiol **190**(1): 7-20.
Richard, J. P., K. Melikov, et al. (2005). "Cellular uptake of unconjugated TAT peptide involves clathrin-dependent endocytosis and heparan sulfate receptors." J Biol Chem **280**(15): 15300-15306.
Richard, J. P., K. Melikov, et al. (2003). "Cell-penetrating peptides. A reevaluation of the mechanism of cellular uptake." J Biol Chem **278**(1): 585-590.
Roche, S., M. Provansal, et al. (2006). "Proteomics of primary mesenchymal stem cells." Regen Med **1**(4): 511-517.
Rodriguez, J. P., M. Gonzalez, et al. (2004). "Cytoskeletal organization of human mesenchymal stem cells (MSC) changes during their osteogenic differentiation." J Cell Biochem **93**(4): 721-731.
Rosenberg, L., M. Lipsett, et al. (2004). "A pentadecapeptide fragment of islet neogenesis-associated protein increases beta-cell mass and reverses diabetes in C57BL/6J mice." Ann Surg **240**(5): 875-884.
Rosenberg, L., A. I. Vinik, et al. (1996). "Islet-cell regeneration in the diabetic hamster pancreas with restoration of normoglycaemia can be induced by a local growth factor(s)." Diabetologia **39**(3): 256-262.

Rowlands, A. S., P. A. George, et al. (2008). "Directing osteogenic and myogenic differentiation of MSCs: interplay of stiffness and adhesive ligand presentation." Am J Physiol Cell Physiol **295**(4): C1037-1044.
Russ, H. A., P. Ravassard, et al. (2009). "Epithelial-mesenchymal transition in cells expanded in vitro from lineage-traced adult human pancreatic beta cells." PLoS One **4**(7): e6417.
Russ, R. D. and B. W. Tobin (1998). "Pancreatic islet transplantation, but not intensive insulin therapy, corrects the pulmonary vascular complications of streptozotocin diabetes." Can J Physiol Pharmacol **76**(4): 407-417.
Ryan, E. A., J. R. Lakey, et al. (2001). "Clinical outcomes and insulin secretion after islet transplantation with the Edmonton protocol." Diabetes **50**(4): 710-719.
Ryan, E. A., B. W. Paty, et al. (2005). "Five-year follow-up after clinical islet transplantation." Diabetes **54**(7): 2060-2069.
Sako, Y., S. Minoghchi, et al. (2000). "Single-molecule imaging of EGFR signalling on the surface of living cells." Nat Cell Biol **2**(3): 168-172.
Schmied, B. M., A. Ulrich, et al. (2001). "Transdifferentiation of human islet cells in a long-term culture." Pancreas **23**(2): 157-171.
Schmied, B. M., A. B. Ulrich, et al. (2000). "Alteration of the Langerhans islets in pancreatic cancer patients." Int J Pancreatol **28**(3): 187-197.
Schwarze, S. R., A. Ho, et al. (1999). "In vivo protein transduction: delivery of a biologically active protein into the mouse." Science **285**(5433): 1569-1572.
Seaberg, R. M., S. R. Smukler, et al. (2004). "Clonal identification of multipotent precursors from adult mouse pancreas that generate neural and pancreatic lineages." Nat Biotechnol **22**(9): 1115-1124.
Serup, P., O. D. Madsen, et al. (2001). "Islet and stem cell transplantation for treating diabetes." BMJ **322**(7277): 29-32.
Shamoon, H., H. Duffy, et al. (1993). "The Effect of Intensive Treatment of Diabetes on the Development and Progression of Long-Term Complications in Insulin-Dependent Diabetes-Mellitus." New England Journal of Medicine **329**(14): 977-986.
Shapiro, A. M., J. R. Lakey, et al. (2000). "Islet transplantation in seven patients with type 1 diabetes mellitus using a glucocorticoid-free immunosuppressive regimen." N Engl J Med **343**(4): 230-238.
Shapiro, A. M., E. A. Ryan, et al. (2001). "Clinical islet transplant--state of the art." Transplant Proc **33**(7-8): 3502-3503.
Shapland, C., J. J. Hsuan, et al. (1993). "Purification and properties of transgelin: a transformation and shape change sensitive actin-gelling protein." J Cell Biol **121**(5): 1065-1073.
Shields, J. M., K. Rogers-Graham, et al. (2002). "Loss of transgelin in breast and colon tumors and in RIE-1 cells by Ras deregulation of gene expression through Raf-independent pathways." J Biol Chem **277**(12): 9790-9799.
Shigeri, Y., A. Ishida, et al. (2008). "[Ca2+/calmodulin-dependent protein kinase signaling: regulatory mechanisms for switching on/off and their involvement in the pathogenesis of various diseases]." Tanpakushitsu Kakusan Koso **53**(11): 1360-1367.
Sienaert, I., N. Nadif Kasri, et al. (2002). "Localization and function of a calmodulin-apocalmodulin-binding domain in the N-terminal part of the type 1 inositol 1,4,5-trisphosphate receptor." Biochem J **365**(Pt 1): 269-277.
Silva, K. E., H. C. Barbosa, et al. (2008). "INGAP-PP up-regulates the expression of genes and proteins related to K+ ATP channels and ameliorates Ca2+ handling in cultured adult rat islets." Regul Pept **148**(1-3): 39-45.
Slack, J. M. (1995). "Developmental biology of the pancreas." Development **121**(6): 1569-1580.

Smith, C. W., K. Pritchard, et al. (1987). "The mechanism of Ca2+ regulation of vascular smooth muscle thin filaments by caldesmon and calmodulin." J Biol Chem **262**(1): 116-122.
Smith, L. (2006). "Proteomics: challenges and emerging technologies, EuroSciCon." Expert Rev Proteomics **3**(6): 573-577.
Sommerer, N., D. Centeno, et al. (2007). "Peptide mass fingerprinting: identification of proteins by MALDI-TOF." Methods Mol Biol **355**: 219-234.
Sordi, V., R. Melzi, et al. (2010). "Mesenchymal cells appearing in pancreatic tissue culture are bone marrow-derived stem cells with the capacity to improve transplanted islet function." Stem Cells **28**(1): 140-151.
Steffes, M. W., B. M. Chavers, et al. (2003). "Sustained effect of intensive treatment of type 1 diabetes mellitus on development and progression of diabetic nephropathy - The Epidemiology of Diabetes Interventions and Complications (EDIC) study." Jama-Journal of the American Medical Association **290**(16): 2159-2167.
Storey, J. D. and R. Tibshirani (2003). "Statistical significance for genomewide studies." Proc Natl Acad Sci U S A **100**(16): 9440-9445.
Suarez-Pinzon, W. L., J. R. Lakey, et al. (2005). "Combination therapy with epidermal growth factor and gastrin induces neogenesis of human islet {beta}-cells from pancreatic duct cells and an increase in functional {beta}-cell mass." J Clin Endocrinol Metab **90**(6): 3401-3409.
Suarez-Pinzon, W. L., Y. Yan, et al. (2005). "Combination therapy with epidermal growth factor and gastrin increases beta-cell mass and reverses hyperglycemia in diabetic NOD mice." Diabetes **54**(9): 2596-2601.
Suzuki, T., S. Futaki, et al. (2002). "Possible existence of common internalization mechanisms among arginine-rich peptides." J Biol Chem **277**(4): 2437-2443.
Takahashi, K., K. Tanabe, et al. (2007). "Induction of pluripotent stem cells from adult human fibroblasts by defined factors." Cell **131**(5): 861-872.
Tanaka, J., T. Watanabe, et al. (1993). "Morphological and biochemical analyses of contractile proteins (actin, myosin, caldesmon and tropomyosin) in normal and transformed cells." J Cell Sci **104 (Pt 2)**: 595-606.
Tateishi, K., J. He, et al. (2008). "Generation of insulin-secreting islet-like clusters from human skin fibroblasts." J Biol Chem **283**(46): 31601-31607.
Tourrel, C., D. Bailbe, et al. (2001). "Glucagon-like peptide-1 and exendin-4 stimulate beta-cell neogenesis in streptozotocin-treated newborn rats resulting in persistently improved glucose homeostasis at adult age." Diabetes **50**(7): 1562-1570.
Treiser, M. D., E. H. Yang, et al. (2010). "Cytoskeleton-based forecasting of stem cell lineage fates." Proc Natl Acad Sci U S A **107**(2): 610-615.
Tyagi, M., M. Rusnati, et al. (2001). "Internalization of HIV-1 tat requires cell surface heparan sulfate proteoglycans." J Biol Chem **276**(5): 3254-3261.
Ullah, Z., C. Y. Lee, et al. (2009). "Developmentally programmed endoreduplication in animals." Cell Cycle **8**(10): 1501-1509.
Umeshima, H., T. Hirano, et al. (2007). "Microtubule-based nuclear movement occurs independently of centrosome positioning in migrating neurons." Proc Natl Acad Sci U S A **104**(41): 16182-16187.
Ungrin, M. D., C. Joshi, et al. (2008). "Reproducible, ultra high-throughput formation of multicellular organization from single cell suspension-derived human embryonic stem cell aggregates." PLoS One **3**(2): e1565.
van Obberghen, E., G. Somers, et al. (1973). "Dynamics of insulin release and microtubular-microfilamentous system. I. Effect of cytochalasin B." J Clin Invest **52**(5): 1041-1051.

Vicovac, L. and J. D. Aplin (1996). "Epithelial-mesenchymal transition during trophoblast differentiation." Acta Anat (Basel) **156**(3): 202-216.
Violini, S., V. Sharma, et al. (2002). "Evidence for a plasma membrane-mediated permeability barrier to Tat basic domain in well-differentiated epithelial cells: lack of correlation with heparan sulfate." Biochemistry **41**(42): 12652-12661.
Vives, E. (2003). "Cellular uptake [correction of utake] of the Tat peptide: an endocytosis mechanism following ionic interactions." J Mol Recognit **16**(5): 265-271.
Vives, E., J. P. Richard, et al. (2003). "TAT peptide internalization: seeking the mechanism of entry." Curr Protein Pept Sci **4**(2): 125-132.
Vogel, H. J., R. D. Brokx, et al. (2002). "Calcium-binding proteins." Methods Mol Biol **172**: 3-20.
Wadia, J. S. and S. F. Dowdy (2005). "Transmembrane delivery of protein and peptide drugs by TAT-mediated transduction in the treatment of cancer." Adv Drug Deliv Rev **57**(4): 579-596.
Wadia, J. S., R. V. Stan, et al. (2004). "Transducible TAT-HA fusogenic peptide enhances escape of TAT-fusion proteins after lipid raft macropinocytosis." Nat Med **10**(3): 310-315.
Wang, C. L. (2008). "Caldesmon and the regulation of cytoskeletal functions." Adv Exp Med Biol **644**: 250-272.
Wang, Z. and D. C. Thurmond (2009). "Mechanisms of biphasic insulin-granule exocytosis - roles of the cytoskeleton, small GTPases and SNARE proteins." J Cell Sci **122**(Pt 7): 893-903.
Webb-Robertson, B. J. and W. R. Cannon (2007). "Current trends in computational inference from mass spectrometry-based proteomics." Brief Bioinform **8**(5): 304-317.
Weissmann, C. and R. Brandt (2008). "Mechanisms of neurodegenerative diseases: insights from live cell imaging." J Neurosci Res **86**(3): 504-511.
Weljie, A. M., A. P. Yamniuk, et al. (2003). "Protein conformational changes studied by diffusion NMR spectroscopy: application to helix-loop-helix calcium binding proteins." Protein Sci **12**(2): 228-236.
Wenisch, S., K. Trinkaus, et al. (2006). "Immunochemical, ultrastructural and electrophysiological investigations of bone-derived stem cells in the course of neuronal differentiation." Bone **38**(6): 911-921.
Wiesgigl, M. and J. Clos (2001). "Heat shock protein 90 homeostasis controls stage differentiation in Leishmania donovani." Mol Biol Cell **12**(11): 3307-3316.
Wilson, L. M., S. H. Wong, et al. (2009). "Insulin but not glucagon gene is silenced in human pancreas-derived mesenchymal stem cells." Stem Cells **27**(11): 2703-2711.
Winder, S. J. (2003). "Structural insights into actin-binding, branching and bundling proteins." Current Opinion in Cell Biology **15**(1): 14-22.
Worster, A. A., A. J. Nixon, et al. (2000). "Effect of transforming growth factor beta1 on chondrogenic differentiation of cultured equine mesenchymal stem cells." Am J Vet Res **61**(9): 1003-1010.
Wurmser, A. E. and F. H. Gage (2002). "Stem cells: cell fusion causes confusion." Nature **416**(6880): 485-487.
Xie, F., E. Goldys, et al. (2007). "Amplified protein sensing using deep purple fluorophores on homogeneous Au substrates." Biofactors **30**(4): 249-253.
Xu, G., H. Kaneto, et al. (2006). "GLP-1/exendin-4 facilitates beta-cell neogenesis in rat and human pancreatic ducts." Diabetes Res Clin Pract **73**(1): 107-110.
Xu, G., D. A. Stoffers, et al. (1999). "Exendin-4 stimulates both beta-cell replication and neogenesis, resulting in increased beta-cell mass and improved glucose tolerance in diabetic rats." Diabetes **48**(12): 2270-2276.
Xu, X., J. D'Hoker, et al. (2008). "Beta cells can be generated from endogenous progenitors in injured adult mouse pancreas." Cell **132**(2): 197-207.

Yamada, T., A. Hashiguchi, et al. (2000). "Function of 90-kDa heat shock protein in cellular differentiation of human embryonal carcinoma cells." In Vitro Cell Dev Biol Anim **36**(2): 139-146.

Yamashiro, S., Y. Yamakita, et al. (1991). "Phosphorylation of non-muscle caldesmon by p34cdc2 kinase during mitosis." Nature **349**(6305): 169-172.

Yamniuk, A. P. and H. J. Vogel (2004). "Calmodulin's flexibility allows for promiscuity in its interactions with target proteins and peptides." Mol Biotechnol **27**(1): 33-57.

Yezid, H., K. Konate, et al. (2009). "Mechanism for HIV-1 TAT insertion into the endosome membrane." J Biol Chem.

Yokouchi, K., Y. Numaguchi, et al. (2006). "l-Caldesmon regulates proliferation and migration of vascular smooth muscle cells and inhibits neointimal formation after angioplasty." Arterioscler Thromb Vasc Biol **26**(10): 2231-2237.

Yourek, G., M. A. Hussain, et al. (2007). "Cytoskeletal changes of mesenchymal stem cells during differentiation." ASAIO J **53**(2): 219-228.

Yuan, S., L. Rosenberg, et al. (1996). "Transdifferentiation of human islets to pancreatic ductal cells in collagen matrix culture." Differentiation **61**(1): 67-75.

Zheng, P. P., M. Weiden, et al. (2007). "Hela /-CaD undergoes a DNA replication-associated switch in localization from the cytoplasm to the nuclei of endothelial cells/endothelial progenitor cells in human tumor vasculature." Cancer Biol Ther **6**(6): 886-890.

Zhou, Q., J. Brown, et al. (2008). "In vivo reprogramming of adult pancreatic exocrine cells to beta-cells." Nature **455**(7213): 627-632.

Zulewski, H., E. J. Abraham, et al. (2001). "Multipotential nestin-positive stem cells isolated from adult pancreatic islets differentiate ex vivo into pancreatic endocrine, exocrine, and hepatic phenotypes." Diabetes **50**(3): 521-533.